



National Library
of Canada

Acquisitions and
Bibliographic Services Branch

395 Wellington Street
Ottawa, Ontario
K1A 0N4

Bibliothèque nationale
du Canada

Direction des acquisitions et
des services bibliographiques

395, rue Wellington
Ottawa (Ontario)
K1A 0N4

Number of copies

Number of copies

NOTICE

The quality of this microform is heavily dependent upon the quality of the original thesis submitted for microfilming. Every effort has been made to ensure the highest quality of reproduction possible.

If pages are missing, contact the university which granted the degree.

Some pages may have indistinct print especially if the original pages were typed with a poor typewriter ribbon or if the university sent us an inferior photocopy.

Reproduction in full or in part of this microform is governed by the Canadian Copyright Act, R.S.C. 1970, c. C-30, and subsequent amendments.

AVIS

La qualité de cette microforme dépend grandement de la qualité de la thèse soumise au microfilmage. Nous avons tout fait pour assurer une qualité supérieure de reproduction.

S'il manque des pages, veuillez communiquer avec l'université qui a conféré le grade.

La qualité d'impression de certaines pages peut laisser à désirer, surtout si les pages originales ont été dactylographiées à l'aide d'un ruban usé ou si l'université nous a fait parvenir une photocopie de qualité inférieure.

La reproduction, même partielle, de cette microforme est soumise à la Loi canadienne sur le droit d'auteur, SRC 1970, c. C-30, et ses amendements subséquents.

Canada

UNIVERSITY OF ALBERTA

**FINITE ELEMENT METHOD SOLUTIONS FOR EDDY CURRENT LOSSES IN
STEEL WELLBORE CASINGS**

BY



TRENT LOGA

**A THESIS SUBMITTED TO THE FACULTY OF GRADUATE STUDIES AND
RESEARCH IN PARTIAL FULFILLMENT OF THE REQUIREMENTS FOR THE
DEGREE OF MASTER OF SCIENCE**

DEPARTMENT OF ELECTRICAL ENGINEERING

EDMONTON, ALBERTA

SPRING 1994



National Library
of Canada

Acquisitions and
Bibliographic Services Branch

395 Wellington Street
Ottawa, Ontario
K1A 0N4

Bibliothèque nationale
du Canada

Direction des acquisitions et
des services bibliographiques

395, rue Wellington
Ottawa (Ontario)
K1A 0N4

Author: *[illegible]*

Title: *[illegible]*

The author has granted an irrevocable non-exclusive licence allowing the National Library of Canada to reproduce, loan, distribute or sell copies of his/her thesis by any means and in any form or format, making this thesis available to interested persons.

L'auteur a accordé une licence irrévocable et non exclusive permettant à la Bibliothèque nationale du Canada de reproduire, prêter, distribuer ou vendre des copies de sa thèse de quelque manière et sous quelque forme que ce soit pour mettre des exemplaires de cette thèse à la disposition des personnes intéressées.

The author retains ownership of the copyright in his/her thesis. Neither the thesis nor substantial extracts from it may be printed or otherwise reproduced without his/her permission.

L'auteur conserve la propriété du droit d'auteur qui protège sa thèse. Ni la thèse ni des extraits substantiels de celle-ci ne doivent être imprimés ou autrement reproduits sans son autorisation.

ISBN 0-612-11273-X

Canada

UNIVERSITY OF ALBERTA

RELEASE FORM

NAME OF AUTHOR: Trent Loga

TITLE OF THESIS: Finite Element Method Solutions For Eddy Current Losses In
Steel Wellbore Casings

DEGREE: Master of Science

YEAR THIS DEGREE GRANTED: 1994

Permission is hereby granted to the University of Alberta Library to reproduce single copies of this thesis and to lend or sell such copies for private, scholarly or scientific research purposes only.

The author reserves all other publication and other rights in association with the copyright in the thesis, and except as hereinbefore provided neither the thesis nor any substantial portion thereof may be printed or otherwise reproduced in any material form whatever without the author's prior written permission.

Trent Loga

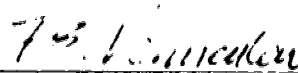
11830 - 37 Street
Edmonton, Alberta
Canada
T5W 2B8

DATE: April 19, 1994

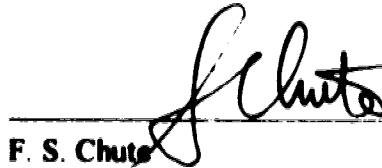
UNIVERSITY OF ALBERTA

FACULTY OF GRADUATE STUDIES AND RESEARCH

The undersigned certify that they have read, and recommended to the Faculty of Graduate Studies and Research for acceptance, a thesis entitled **FINITE ELEMENT METHOD SOLUTIONS FOR EDDY CURRENT LOSSES IN STEEL WELLBORE CASINGS** submitted by Trent Loga in partial fulfillment of the requirements for the degree of Master of Science.



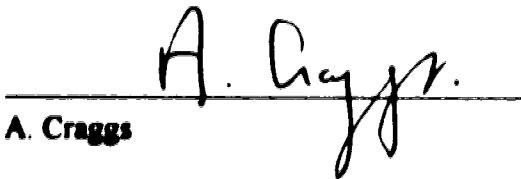
F. E. Vermeulen



F. S. Chute



C. R. James



A. Craggs

DATE: March 9, 1994

Dedication

This work is dedicated to my parents, Ellen and Raymond.

Abstract

One of the more promising methods for heating underground oil sand formations is to pass a low frequency alternating current through the formation and heat it resistively. Access to the oil sand formation is gained through a vertical wellbore. A low frequency alternating current travels from the power source on the surface, down the wellbore and into the sand embedded in the formation. Generally, the current is passed down the wellbore through one or more power cables which run along the entire length of the well.

The wellbore is lined with a carbon steel pipe for structural integrity. This pipe is called a wellbore *casing*. Eddy currents are induced in the metal casing by the magnetic fields associated with nearby power cables which carry an alternating current down the well. Note that this is similar to the situation where eddy currents are induced in pipe-type cables used in underground power transmission and distribution.

This thesis outlines a procedure for obtaining a two dimensional, numerical solution for the eddy current density induced in the wellbore casing. The eddy current problem is treated as a two dimensional boundary value problem. A partial differential equation which describes the electric field at any point in the domain of the problem is constructed from Maxwell's equations. The boundary value problem is then solved numerically using the finite element method. The resulting finite element solutions describe the electric field and current density in the metal casing.

In addition to the current density, numerical solutions are also obtained for the resistive losses in the casing due to the flow of eddy currents. These eddy current losses are calculated by numerically evaluating the integral from Poynting's theorem.

The main conclusion which can be drawn from this thesis is that accurate numerical solutions for the aforementioned eddy current problem may be obtained by using the finite element method provided that the magnetic field at the outer wall of the casing can be set to approximately zero.

Acknowledgement

I wish to thank my supervisors, Dr. F. E. Vermeulen and Dr. F. S. Chute, for their help, patience and support during the course of this study.

Table of Contents

	Page
CHAPTER 1. Introduction	1
1.1 A Description of the Problem: Eddy Current Losses in Steel Wellbore Casings	1
1.1.1 The General Problem of In-Situ Heavy Oil Recovery	1
1.1.2 An Introduction to Wellbore Electrical Losses	3
1.1.3 Eddy Current Losses	5
1.2 Solutions Published in the Literature	7
1.2.1 Review of Boundary Value Problem Solutions Derived From the Partial Differential Equation	7
1.2.1.1 Dwight's Solution	7
1.2.1.2 The Tegopoulos and Kriezis Solutions	8
1.2.1.3 The Solution of Kawasaki, Inami and Ishikawa	10
1.2.1.4 Other Solutions Utilizing the Partial Differential Equation	10
1.2.2 Review of Boundary Value Problem Solutions Derived From the Integral Equation	11
1.2.2.1 The Kriezis and Cangellaris Solution	11
1.2.2.2 The Poltz and Kuffel Solution	11
1.3 Method of Solution Used in This Thesis	12
1.3.1 Constructing the Boundary Value Problem	12
1.3.2 Solution of the Boundary Value Problem Using the Finite Element Method	12

1.3.3	Solution For a Problem With a Single Current Source.....	14
CHAPTER 2.	The Conditions Under Which the Magnetic Field at the Outer Wall of the Wellbore Casing is Approximately Zero	17
2.1	A Description of the Simple One Dimensional Boundary Value Problem	17
2.2	The Differential Equation for the Electric Field.....	18
2.3	The Differential Equation for the Magnetic Field	20
2.4	General Solutions For the Electric and Magnetic Fields	20
2.4.1	Simplification of the General Solutions in Region 2: Introduction of Large Argument Approximations for Hankel Functions.....	24
2.4.2	The Reflection Coefficient.....	25
2.5	Complete Solutions For the Electric and Magnetic Fields In Region 2.....	27
2.5.1	The Boundary Condition at $r = a$ in Region 2.....	27
2.5.2	The Boundary Conditions at $r = b$ in Region 2.....	29
2.5.2.1	The Exact Boundary Conditions at $r = b$	30
2.5.2.2	The Approximate Boundary Condition at $r = b$	31
2.5.3	Explicit Solution for $\Gamma_2(k_2, b)$ in Terms of $Z_2(k_2, b)$	32
2.5.4	The Final Solutions for the Electric and Magnetic Fields in the Wellbore Casing.....	33
2.6	Conditions Under Which $H_{\phi_2}(k_2, b) = 0$ Is an Acceptable Approximation For Exact Boundary Conditions	34
2.6.1	Conditions Under Which The Exact and Approximate Solutions Are In Close Agreement.....	34

2.6.1.1	Condition 1: The Wellbore Casing Is At Least Three Skin Depths Thick	34
2.6.1.2	Condition 2: $ Z_2(k,h) \gg \eta_2 $	37
2.6.2	Summary of Criteria Under Which $H_{\phi_2}(k,h) = 0$ Is an Acceptable Approximation	38
2.6.3	The Magnetic Shielding Ratio	39
2.6.3.1	Case 1: $l \gg l/\alpha$	40
2.6.3.2	Case 2: $ Z_2(k,h) \gg \eta_2 $	41
2.6.4	Magnetic Shielding Ratios For Typical Steel Wellbore Casings	43
2.6.5	The Minimum Magnetic Shielding Ratio For Which the Approximation $H_{\phi_2}(k,h) = 0$ Is Justified	45
2.7	The Effects of Attenuation and Reflection in Magnetic and Non-Magnetic Casings	48
2.8	Summary	48
CHAPTER 3. The Total Current and Power Dissipated in a Wellbore Casing Centered About a Single Power Cable		51
3.1	Eddy Current Density and the Total Current Induced in the Wellbore Casing	51
3.2	The Total Displacement Current Induced in Region 3	52
3.3	The Path of the Return Current	53
3.4	Power Dissipated in Casing by Eddy Currents	54
CHAPTER 4. A Finite Element Method Solution for the Electromagnetic Fields in a Steel Casing		56
4.1	Computing a Finite Element Method Solution Using UNAFEM II	56

4.1.1	Boundary Value Problems Solvable by UNAFEM II	57
4.1.2	UNAFEM II Input	57
4.2	A Finite Element Method Solution for a One Dimensional Boundary Value Problem	58
4.2.1	The Partial Differential Equation for Problem 1	59
4.2.2	Mapping the Domain of Problem 1 for UNAFEM II	60
4.2.3	Boundary Conditions	61
4.3	Comparison of FEM Solution with Analytic and Published Solutions	62
4.3.1	The Electric and Magnetic Fields	62
4.3.2	Eddy Current Density and Total Current Induced in the Casing	67
4.3.3	Resistive Power Loss In the Casing.....	69
4.3.4	Effective Casing Impedance	70
4.3.5	Conclusion.....	72
CHAPTER 5.	A Finite Element Method Solution For a Two Dimensional Boundary Value Problem.....	74
5.1	The Partial Differential Equation for Problem 2	76
5.2	Mapping the Domain of Problem 2 for UNAFEM II.....	78
5.3	Magnetic Field Boundary Conditions for Problem 2.....	78
5.3.1	The Magnetic Field Boundary Condition at the Surface of the Power Cable	79
5.3.2	The Magnetic Field Boundary Condition Along the Line of Symmetry of Problem 2	79

5.3.3	The Magnetic Field Boundary Condition Along the Outer Wall of the Wellbore Casing	79
5.4	UNAFEM II Boundary Conditions	80
5.4.1	The UNAFEM II Boundary Condition at the Surface of the Power Cable	82
5.4.2	The UNAFEM II Boundary Condition Along the Line of Symmetry of Problem 2	82
5.4.3	The UNAFEM II Boundary Condition at the Outer Wall of the Wellbore Casing	83
5.5	Comparison of the Finite Element Method Solutions with Published Solutions	84
5.5.1	The Finite Element Method Solution for Sample 1 of Problem 2	84
5.5.2	The Finite Element Method Solution for Sample 2 of Problem 2	90
5.5.3	The Finite Element Method Solution for Sample 3 of Problem 2	94
5.6	Discrepancies Between the Finite Element Method and Analytical Solutions	97
5.7	Conclusion	100
CHAPTER 6.	A Finite Element Method Solution For a Complex Two Dimensional Boundary Value Problem	101
6.1	A Description of Problem 3a	101
6.2	A Description of Problems 3b and 3c	102
6.3	The Method of Solution for a Multiple Cable Problem	104
6.3.1	The Superposition of the Single Cable Solutions	106

6.4	Modeling the Domains of Problems 3a, 3b and 3c for UNAFEM II	107
6.5	The Partial Differential Equation for the Single Cable Problem	108
6.6	The Boundary Condition at the Outer Wall of the Wellbore Casing.....	108
6.7	The Validity of the Approximation $\hat{H}_2 _{\rho=a} = 0$	109
6.8	The Boundary Condition at the Surface of the Power Cable and Along the Line of Azimuthal Symmetry	114
6.9	Finite Element Method Solutions for the Multi-Cable Problem Analyzed in Problem 3a.....	114
6.10	Finite Element Method Solutions for the Multi-Cable Problem Analyzed in Problem 3b.....	125
6.11	Finite Element Method Solutions for the Multi-Cable Problem Analyzed in Problem 3c.....	132
CHAPTER 7. Conclusion		139
7.1	The Finite Element Method and the Magnetic Field Boundary Condition at the Outer Wall of the Wellbore Casing	139
7.2	Proof That the Finite Element Method Can Yield Accurate Solutions for the Eddy Current Problem	140
7.3	Potential Areas of Further Investigation	142
Bibliography		144
Appendix I Errors and Inconsistencies In the Works of Tegopoulos and Kriezis Which Relate to the Eddy Current Distribution in Cylindrical Metal Shells of Infinite Length.....		147
A1.1	The Magnetic Vector Potential of an Infinitely Long Current Filament	148
A1.2	The Series Expansion of $\ln[r^2 + \rho^2 + 2\rho r \cos(\phi - \theta)]$	153

A1.3	Corrections to Equation (29) After Accounting for Errors In Its Original Derivation by Tegopoulos and Kriezis	153
A1.4	The Return Current	160
A1.5	The Expression For Eddy Current Loss In Reference [9]	162
Appendix 2	A Limitation of the Eddy Current Loss Formula of Kawasaki, Inami and Ishikawa	171
Appendix 3	Meshes Used to Model the Domain of Problem 2	173
Appendix 4	The General Solutions for $E_z(\rho,\theta)$, $H_\rho(\rho,\theta)$ and $H_\theta(\rho,\theta)$ in Region 2 of Problem 2.....	175
Appendix 5	Meshes Used to Model the Domains of Problems 3a, 3b and 3c	177

List of Tables

	Page
Table 2-1 A summary of the electromagnetic properties in each region of the boundary value problem illustrated in Figure 2-1.	23
Table 2-2. A summary of the general solutions for the electromagnetic fields in each region of the boundary value problem illustrated in Figure 2-1.	23
Table 2-3. Dimensions and electromagnetic properties for various samples of wellbore casings (adapted from Table 1 of Reference [3]).	44
Table 2-4. Magnetic shielding ratios for typical casing samples.	45
Table 4-1. FEM based numerical and analytical solutions for the total current induced in various wellbore casing samples.	68
Table 4-2. FEM based numerical and analytical solutions for the resistive power loss in various wellbore casing samples.	70
Table 4-3. FEM based numerical solutions and measured values for the effective impedance in various wellbore casing samples.	72
Table 5-1. Dimensions and electromagnetic properties for various samples of wellbore casings.	76
Table 5-2. Magnetic shielding ratios for the first five harmonics of $H_0(\rho, \theta)$ in casing samples 1 to 3.	98
Table 5-3. Magnetic shielding ratios for the first four harmonics of $H_{r_1}(\rho, \theta)$ in casing samples 1 to 3.	99
Table 6-1. The outer radii and thicknesses for each casing analyzed in problem 3a.	102
Table 6-2. The outer radii and thicknesses for each casing analyzed in problem 3b.	104
Table 6-3. The outer radii and thicknesses for each casing analyzed in problem 3c.	104
Table 6-4. A check of the approximation $\hat{H}_z _{\rho=a} = 0$ for casing samples 1 to 7 from problem 3a.	110

Table 6-5. A check of the approximation $\tilde{H}_1 \Big _{v, \delta} = 0$ for casing samples 1 to 5 from problem 3b.	112
Table 6-6. A check of the approximation $\tilde{H}_2 \Big _{v, \delta} = 0$ for casing samples 1 to 5 from problem 3c.	113

List of Figures

	Page
Figure 1-1. A simple schematic of low frequency electrical heating of an underground oil sand formation.....	2
Figure 1-2. Representations of various schemes for low frequency electrical heating of underground oil sand formations.....	3
Figure 1-3. A wellbore and power cable system; (a) three dimensional view, (b) two dimensional view.....	6
Figure 1-4. Radial cross section of conducting shell and current filament.....	9
Figure 1-5. Diagram of the general boundary value problem.....	12
Figure 1-6. Schematic showing the original boundary value problem is equivalent to the superposition of three smaller problems.....	13
Figure 1-7. Diagram of a boundary value problem with only a single current source present.....	14
Figure 2-1. A diagram of the one dimensional boundary value problem.....	18
Figure 2-2. Exact and approximate solutions for the electric and magnetic fields in the example in case 1.....	41
Figure 2-3. Exact and approximate solutions for the electric and magnetic fields in the example in case 2.....	43
Figure 2-4. Exact and approximate solutions for the electric and magnetic fields inside a wellbore casing with a magnetic shielding ratio magnitude $\ll 30$	46
Figure 2-5. Exact and approximate solutions for the electric and magnetic fields inside a wellbore casing with a magnetic shielding ratio magnitude $\cong 30$	47
Figure 4-1. A radial section of the domain of problem 1.....	60
Figure 4-2. FEM and analytical solutions for the electric and magnetic field intensities in wellbore casing sample #1.....	63
Figure 4-3. FEM and analytical solutions for the electric and magnetic field intensities in wellbore casing sample #2.....	63

Figure 4-4. FEM and analytical solutions for the electric and magnetic field intensities in wellbore casing sample #3.....	64
Figure 4-5. FEM and analytical solutions for the electric and magnetic field intensities in wellbore casing sample #4.....	64
Figure 4-6. FEM and analytical solutions for the electric and magnetic field intensities in wellbore casing sample #5.....	65
Figure 4-7. FEM and analytical solutions for the electric and magnetic field intensities in wellbore casing sample #6.....	65
Figure 4-8. FEM and analytical solutions for the electric and magnetic field intensities in wellbore casing sample #7.....	66
Figure 4-9. FEM and analytical solutions for the electric and magnetic field intensities in wellbore casing sample #8.....	66
Figure 4-10. A simplified diagram of the setup used by Stroemich et. al. to measure the effective impedance of a wellbore casing (adapted from Figure 5 of reference [3]).	71
Figure 5-1a. A diagram of problem 2.....	74
Figure 5-1b. The semicircular section of problem 2 in which the FEM solutions are computed	75
Figure 5-2. Contour plots of the current density in casing 1 of problem 2.....	86
Figure 5-3. Solutions for the current density in wellbore casing sample 1. The magnitude of the current density is plotted for; (a) $\rho = 0.100$ m, (b) $\rho = 0.106$ m and (c) $\rho = 0.112$ m.....	87
Figure 5-4. Solutions for the current density in wellbore casing sample 1. The phase of the current density is plotted for; (a) $\rho = 0.100$ m, (b) $\rho = 0.106$ m and (c) $\rho = 0.112$ m.....	88
Figure 5-5 Contour plots of the current density in casing 2 of problem 2.....	91
Figure 5-6. Solutions for the current density in wellbore casing sample 2. The magnitude of the current density is plotted for; (a) $\rho = 0.100$ m, (b) $\rho = 0.106$ m and (c) $\rho = 0.112$ m.....	92
Figure 5-7. Solutions for the current density in wellbore casing sample 2. The phase of the current density is plotted for; (a) $\rho = 0.100$ m, (b) $\rho = 0.106$ m and (c) $\rho = 0.112$ m.....	93

Figure 5-8	Contour plots of the current density in casing 3 of problem 2	95
Figure 5-9.	Solutions for the magnitude of the current density in wellbore casing sample 3	96
Figure 5-10.	Solutions for the phase of the current density in the wellbore casing of sample 3	96
Figure 6-1a.	A diagram of problem 3a	101
Figure 6-1b.	A diagram of problems 3b and 3c	103
Figure 6-2.	A simple example of the superposition of the single cable solutions	107
Figure 6-3	Real and imaginary components of the electric field intensity [V/m] in casing 1 of problem 3a	115
Figure 6-4	Contour plots of the current density in casing 1 of problem 3a	117
Figure 6-5	Contour plots of the current density in casing 2 of problem 3a	118
Figure 6-6	Contour plots of the current density in casing 3 of problem 3a	119
Figure 6-7	Contour plots of the current density in casing 4 of problem 3a	120
Figure 6-8	Contour plots of the current density in casing 5 of problem 3a	121
Figure 6-9	Contour plots of the current density in casing 6 of problem 3a	122
Figure 6-10	Contour plots of the current density in casing 7 of problem 3a	123
Figure 6-11.	Eddy current loss in wellbore casings of various thicknesses for problem 3a	124
Figure 6-12	Contour plots of the current density in casing 1 of problem 3b	126
Figure 6-13	Contour plots of the current density in casing 2 of problem 3b	127
Figure 6-14	Contour plots of the current density in casing 3 of problem 3b	128
Figure 6-15	Contour plots of the current density in casing 4 of problem 3b	129

Figure 6-16	Contour plots of the current density in casing 5 of problem 3b.....	130
Figure 6-17	Eddy current loss in wellbore casings of various thicknesses for problem 3b.....	131
Figure 6-18	Contour plots of the current density in casing 1 of problem 3c.....	133
Figure 6-19	Contour plots of the current density in casing 2 of problem 3c.....	134
Figure 6-20	Contour plots of the current density in casing 3 of problem 3c.....	135
Figure 6-21	Contour plots of the current density in casing 4 of problem 3c.....	136
Figure 6-22	Contour plots of the current density in casing 5 of problem 3c.....	137
Figure 6-23	Eddy current loss in wellbore casings of various thicknesses for problem 3c.....	138
Figure A1-1	An infinitely long current filament in unbounded space.....	148
Figure A1-2	A partial cross section of an infinitely long cylindrical shell and current filament.....	149
Figure A3-1	The mesh used to model the domain of problem 2 with casing sample 1.....	173
Figure A3-2	The mesh used to model the domain of problem 2 with casing sample 2.....	174
Figure A3-3	The mesh used to model the domain of problem 2 with casing sample 3.....	174
Figure A5-1	The mesh used to model the domain of problem 3a with casing sample 1.....	177
Figure A5-2	The mesh used to model the domain of problem 3a with casing sample 2.....	178
Figure A5-3	The mesh used to model the domain of problem 3a with casing sample 3.....	178

Figure A5-4	The mesh used to model the domain of problem 3a with casing sample 4	179
Figure A5-5	The mesh used to model the domain of problem 3a with casing sample 5	179
Figure A5-6	The mesh used to model the domain of problem 3a with casing sample 6	180
Figure A5-7	The mesh used to model the domain of problem 3a with casing sample 7	180
Figure A5-8	The mesh used to model the domain of problem 3b with casing sample	181
Figure A5-9	The mesh used to model the domain of problem 3b with casing sample 2	181
Figure A5-10	The mesh used to model the domain of problem 3b with casing sample 3	182
Figure A5-11	The mesh used to model the domain of problem 3b with casing sample 4	182
Figure A5-12	The mesh used to model the domain of problem 3a with casing sample 5	183
Figure A5-13	The mesh used to model the domain of problem 3c with casing sample 1	183
Figure A5-14	The mesh used to model the domain of problem 3c with casing sample 2	184
Figure A5-15	The mesh used to model the domain of problem 3c with casing sample 3	184
Figure A5-16	The mesh used to model the domain of problem 3c with casing sample 4	185
Figure A5-17	The mesh used to model the domain of problem 3c with casing sample 5	185

List of Symbols

a	Inner radius of a wellbore casing
\hat{a}	A unit vector parallel to a coordinate axis
\vec{B}_N	Magnetic flux density in region N of the problem domain
b	Outer radius of a wellbore casing
d	Radial distance of a power cable from the center of a wellbore casing
\vec{E}_N	Electric field (strength or intensity) in region N of the problem domain
E_{2+}, E_{2-}	Arbitrary constants in the general solution of the electric field in region 2
\vec{D}_N	Electric flux density in region N of the problem domain
f	Frequency
\vec{H}_N	Magnetic field (strength or intensity) in region N of the problem domain
$H_n^{(1)}, H_n^{(2)}$	Hankel functions of the first and second kind of order n
I	Phasor current in a power cable
I_{casing}	Total current induced in the wellbore casing
I_3	Total displacement current in region 3
j	$\sqrt{-1}$
\vec{J}_N	Current density in region N of the problem domain
k_N	Wave number in region N of the problem domain
\hat{n}	A unit vector, normal to a boundary
P_{loss}	Power loss (i.e., eddy current loss) in the wellbore casing
r	Radial coordinate in the cylindrical coordinate system
r_c, r_{cable}	Radius of a power cable
z	Longitudinal coordinate in the cylindrical coordinate system
Z_N	Wave impedance in region N of the problem domain

Z_N^*	Wave Impedance of the m th field harmonic in region N of the problem domain
α	Attenuation factor (the imaginary component of the wave number, k)
β	Phase constant (the real component of the wave number, k)
Γ_N	The reflection coefficient in region N of the problem domain
δ	Skin depth or $1/\alpha$
ϵ_N	Permittivity in region N of the problem domain
ϵ_0	Permittivity of free space
η_N	Intrinsic impedance in region N of the problem domain
θ	Azimuthal coordinate in the $\rho - \theta$ system of polar coordinates
μ_N	Permeability in region N of the problem domain
μ_0	Permeability of free space
μ_r	Relative permeability
ρ	Resistivity
ρ	Radial coordinate in the $\rho - \theta$ system of polar coordinates
σ_N	Conductivity in region N of the problem domain
ϕ	Azimuthal coordinate in the cylindrical coordinate system
ω	Radian or angular frequency
\angle	Argument of a complex number (i.e., $\angle\theta \Leftrightarrow e^{j\theta}$)

1

CHAPTER 1

INTRODUCTION

1.1 A Description of the Problem: Eddy Current Losses in Steel Wellbore Casings

1.1.1 The General Problem of In-situ Heavy Oil Recovery

Approximately 88% of oil sand deposits in Alberta are located at depths between 75 m and 750 m [1]. At these depths, recovery by conventional strip mining techniques is not feasible. Instead, in-situ recovery methods utilizing vertical and horizontal drilling techniques are used. Unfortunately, the bitumen in the oil sand deposits is extremely viscous and cannot be pumped to the surface using conventional methods.

This problem can be overcome by heating the oil sand reservoir [1]. An increase in temperature will lower the viscosity of the bitumen in the deposit. This enables the bitumen to be more easily extracted using conventional techniques.

One method for heating oil sand formations is with electromagnetic energy. Several methods of applying electromagnetic energy have been investigated [1,2]. One of the more common techniques is to pass a low frequency electrical current through the formation and heat it resistively. A simple example of this is shown in Figure 1-1.

Referring to the diagram in Figure 1-1, a well is drilled from the surface into an oil sand formation below. An electrode is then embedded in the formation. A power source on the surface is connected to the electrode via power cables which run along the entire length of the well. An alternating current travels from the power source on the surface, down the wellbore and into the electrode embedded in the formation. From there the current passes through the formation and returns to the surface, completing the circuit.

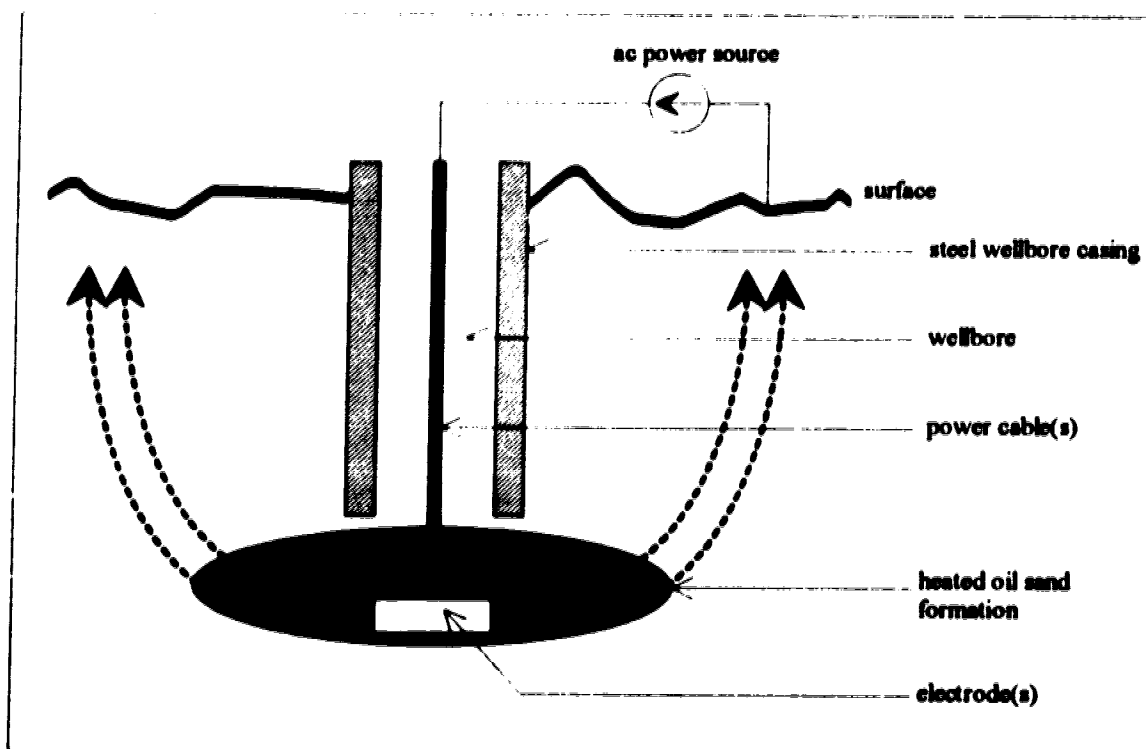


Figure 1-1. A simple schematic of low frequency electrical heating of an underground oil sand formation.

Three-phase or multi-phase power may also be used at the well. Often this achieves a more uniform heating of the formation. For example, in Figure 1-2(a) there are three electrodes embedded in the formation. The electrodes are connected to a three phase power source at the surface. The phase of the potential difference between each electrode differs by $\pm 120^\circ$. In the formation, current flows between the electrodes of differing phase. This results in a more uniform current distribution (compared to that of a single phase system) and consequently a more uniform heating of the formation.

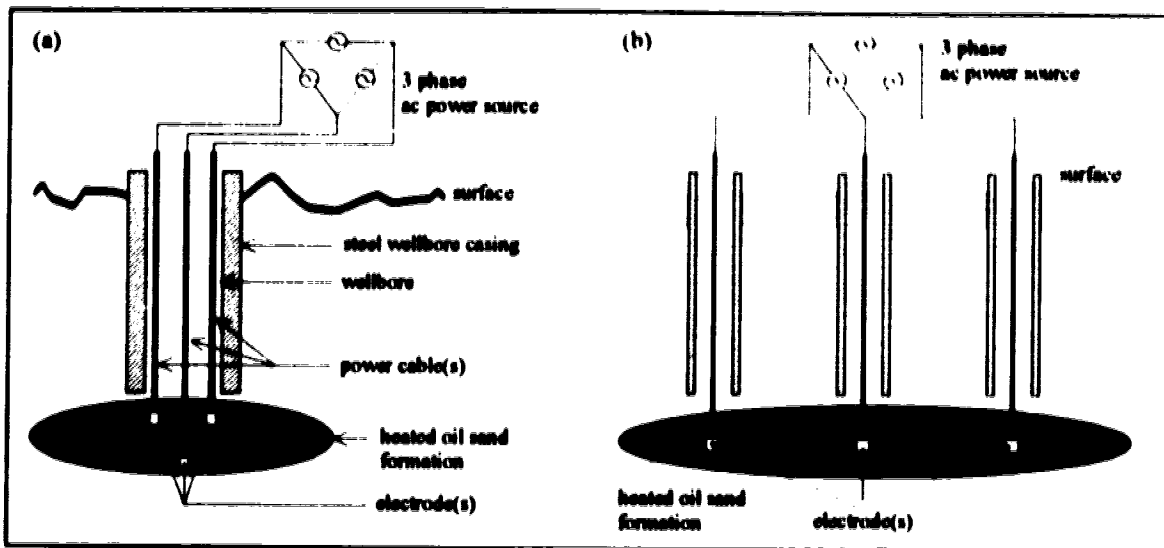


Figure 1-2. Representations of various schemes for low frequency electrical heating of underground oil sand formations.

Another variation of this method utilizes two or more wells. As shown in Figure 1-2(b), each well has a single electrode operating at a different phase. Current flows between the electrodes, heating the intervening oil sand formation.

1.1.2 An Introduction to Wellbore Electrical Losses

While the aforementioned methods of electromagnetic heating have proven effective [2], there are certain engineering aspects that need refinement. One particular problem is the electrical power losses that occur along the wellbore [3], specifically in the proximity of the power cable.

It is vital to determine the fraction of input power actually delivered to the oil sand formation below ground. This allows for accurate analysis of the heating of the formation. It also measures the efficiency of power delivery from source to formation. Hence there is a need to evaluate the electrical power lost in transmitting the current from the source on the surface to the formation underground [3].

There are three types of electrical losses that occur along the wellbore. The first, and most obvious, is the loss which occurs in the power cable itself. The copper conductors in the cable have a large, but not infinite conductivity. Consequently, there is a small amount of resistive loss that occurs when current is passed through the conductors.

The remaining two types of wellbore losses are somewhat less conspicuous, though just as significant. These losses are the result of a magnetic field, created by an alternating current flowing in the power cable, interacting with the surrounding wellbore casing. A wellbore casing is essentially a carbon steel pipe that lines the wall of the hole. It is vital to the structural integrity of the well.

The magnetic field from the power cable produces two types of losses in the steel casing [3]. First, because the casing is ferromagnetic, hysteresis loss occurs. Second, the magnetic field from the power cable induces eddy currents in the steel casing, resulting in a resistive power loss. This is also referred to as eddy current loss.

Together, these three losses determine what fraction of input power from the surface is lost before reaching the underground oil sand formation. Each type of loss is evaluated differently.

Data concerning the resistive losses in power cables is generally available from the cable manufacturer. Cable losses will not be discussed here in any great detail.

For hysteresis and eddy current losses, it is possible to measure these quantities experimentally. However, analytical or numerical solutions would be preferable for rapid analysis of many different configurations. The most straightforward non-experimental solution would be to apply Maxwell's equations and analytically or numerically solve for the electromagnetic fields in the casing.

There is one major drawback to the analytical or semi-analytical approach; it is extremely difficult to obtain a solution when the relationship between the magnetic flux density, \vec{B} and the magnetic field intensity, \vec{H} is not linear. In most materials, \vec{B} and \vec{H} are related by a constant magnetic permeability, μ . However, in ferromagnetic materials, such as steel, the relationship between \vec{B} and \vec{H} can be highly non-linear and as a result μ is no longer a constant. This is especially true if the \vec{H} field is strong enough to cause the steel to become magnetically saturated.

Alternatively, if the steel does not experience magnetic saturation, then a linear relation between \vec{B} and \vec{H} appears to be a good approximation. Thus, if μ is constant, the eddy current losses may still be solved using any number of analytical or numerical techniques. The resulting solution, while still ignoring hysteresis effects, would be valid for describing

the eddy current losses in the wellbore casing. This assertion is based on a comparison of published experimental results with results based on the linear approximation [4].

1.1.3 Eddy Current Losses

One of the goals of this work is to find a means of obtaining numerical values for the eddy current losses in steel wellbore casings. This presupposes finding a means of obtaining numerical values for the current density or electric field induced in steel wellbore casings.

As mentioned earlier, it is possible to obtain values for the electric field in a wellbore casing by applying Maxwell's equations and then solving them analytically or numerically. A constant permeability greatly simplifies the application of Maxwell's equations to the problem. The eddy current problem may further be simplified by reducing the dimensions of the problem from three to two.

Consider the problem viewed in three dimensions as illustrated in Figure 1-3(a). Three power cables, each carrying a different current, are arranged in arbitrary positions inside a wellbore casing. Because the currents in the power cables are oscillating at a frequency of 60 Hz (or less), transmission line effects along the cables will be negligible. Therefore the magnitudes and phases of the currents in the cables will not change significantly along the length of the wellbore (i.e. along the $\pm z$ direction). Consequently there will be little variation in the electromagnetic fields along the length of the well, except at the ends of the casing. For regions along the wellbore where end effects are negligible, the actual problem may be approximated by assuming both the cables and the casing are infinitely long. This eliminates any field dependence on the z coordinate. The problem becomes two dimensional, as shown in Figure 1-3(b), with dependence on the r and ϕ coordinates only.

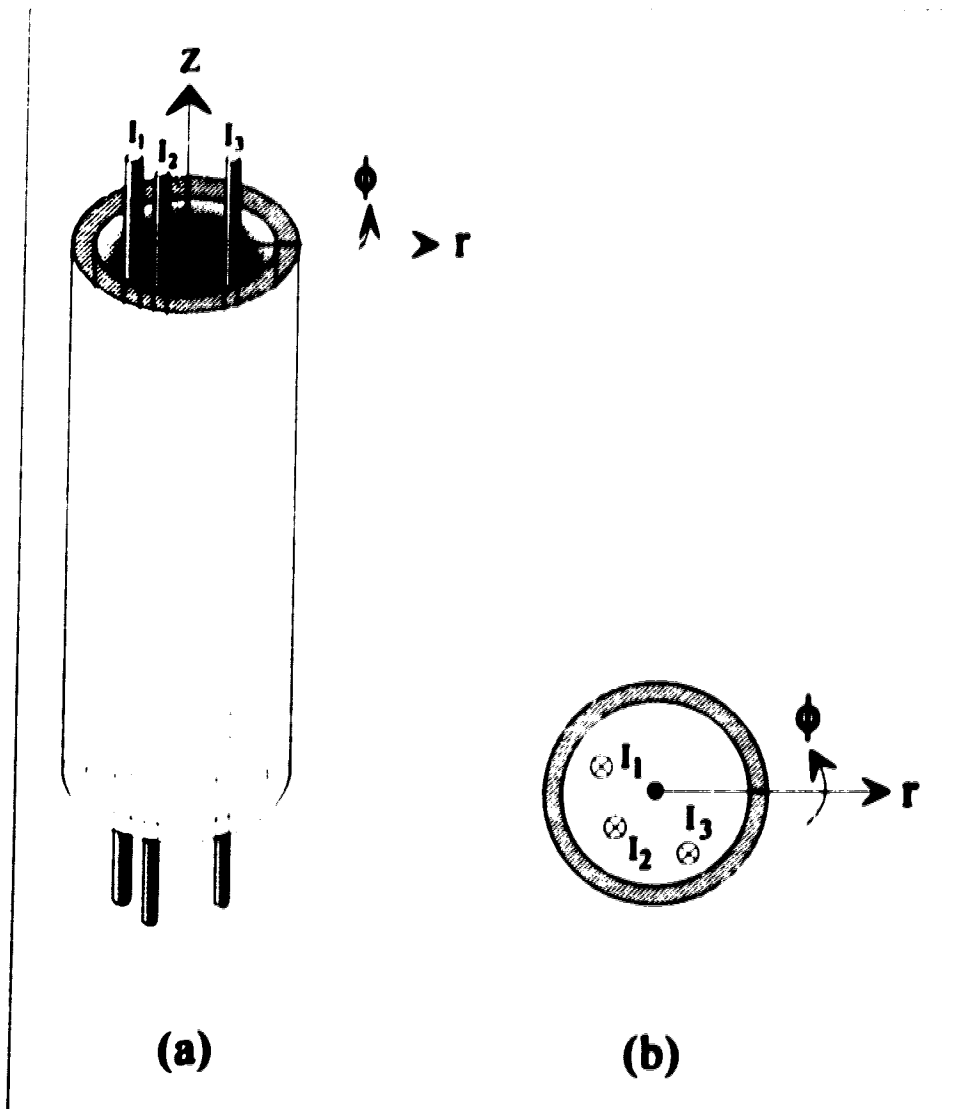


Figure 1-3. A wellbore and power cable system; (a) three dimensional view, (b) two dimensional view.

As a result of the above simplifications, the problem to be solved in this thesis may be stated as follows. Inside a steel wellbore casing is an arbitrary number of power cables, each carrying a low frequency current at a different phase. The cables are arranged in arbitrary positions inside the casing. The steel casing has a constant relative permeability. Given these conditions, the first objective is to find a solution for the electric field or corresponding current density induced in the wellbore casing. The solution for the electric field or current density need only be a function of coordinates r and ϕ . After obtaining a solution for the electric field or current density, that solution is used to calculate a numerical value for the eddy current loss in the wellbore casing.

Variations of the above problem have been considered in the published literature for many years. In fact, an almost identical problem exists in the field of power engineering, specifically in the area of underground power delivery systems. These systems often rely on what is known as pipe-type cable for transmission and distribution lines. A standard pipe-type cable consists of three power cables placed inside a metal pipe [5]. Three cables are used for three phase power. The pipe is generally made of high grade carbon steel. Hence the basic structure of pipe-type cable is virtually identical to the wellbore casing and cable arrangement. Consequently, much of the research on eddy current losses in pipe-type cable systems is directly applicable to the analysis of similar losses in the wellbore casings.

1.2 Solutions Published in the Literature

Over the years, various solutions to the eddy current loss problem have been published. Nearly all the solutions use the following basic procedure:

1. Using techniques for solving boundary value problems, obtain an analytic or numerical solution for the eddy currents induced in a metal, annular cylinder as a result of nearby current sources.
2. Apply Poynting's theorem to determine the losses in the metal cylinder which result from the flow of eddy currents.

Solving the boundary value problem is the main obstacle in this procedure. Methods of solving the boundary value problem fall into two main categories [5]:

1. Construct a partial differential equation from Maxwell's equations and solve it analytically or numerically.
2. Construct an integral equation from Maxwell's equations and solve it numerically.

1.2.1 Review of Boundary Value Problem Solutions Derived From the Partial Differential Equation

1.2.1.1 Dwight's Solution

One of the early studies of the eddy current problem was accomplished by H. B. Dwight. Dwight obtained an analytic expression [6,7] for the eddy current density

in a very thin tube produced by a filamentary current inside the tube. For a current I oscillating at a frequency f , Dwight's expression for the current density $J(\phi)$ in the tube is

$$J(\phi) = \frac{I}{2\pi a t} \left[1 + \sum_{n=1}^{\infty} \frac{s^n}{a^n} \cdot \frac{2jI^2}{(n + jI^2)} \cdot \cos(n\phi) \right], \quad (1.1)$$

where

a = average of the inner and outer radii of the tube

s = radial distance of the filament from the center of the tube

t = thickness of the tube

$$I = \frac{2\pi f \cdot \mu_0 \cdot a \cdot t}{2\rho}$$

Note that because the tube is very thin, there is assumed to be no radial variation in current density. The tube is assumed to have a permeability μ_0 and a resistivity ρ [$\Omega \cdot m$].

1.2.1.2 The Tegopoulos and Kriezis Solution

For thick metal tubes where the current density *does* vary with radial distance from the center of the tube, a solution is available from the works of Tegopoulos and Kriezis. The solution is fairly detailed, although unfortunately, several algebraic errors occur in its derivation and are carried through to the final expression for current density.

Tegopoulos and Kriezis undertook an extensive study of the eddy currents produced in a cylindrical metal shell by an axial current located inside the shell [8,9]. As illustrated in Figure 1-4, the problem is analyzed in two dimensions; both the shell and the conductor which carries the excitation current are assumed to be of infinite length in the axial direction.

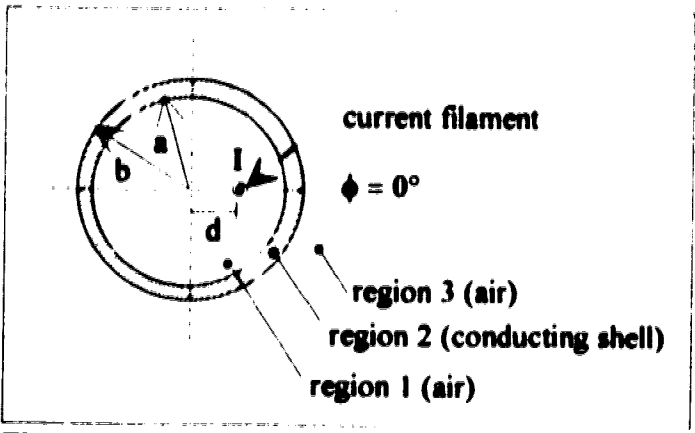


Figure 1-4. Radial cross section of conducting shell and current filament.

The excitation current is represented by a filament carrying a current 'I' located inside the shell. Tegopoulos and Kriezis assume that *all* the current in this filament returns to its source via the conducting shell; however, this assumption is incorrect. In appendix I of this thesis it is demonstrated that *only a portion* of the filamentary current returns to its source via the metal shell.

The shell (region 2) is assumed to have a magnetic permeability μ_0 and a resistivity ρ [$\Omega \cdot m$]. Regions 1 and 3 are assumed to have the electrical characteristics of free space. Displacement currents are neglected because of the low frequencies involved.

The partial differential equations constructed by Tegopoulos and Kriezis for this problem are

$$\nabla^2 \vec{\lambda} = 0 \quad \text{(in regions 1 and 3)}$$

and

$$\nabla^2 \vec{\lambda} = \frac{\mu}{\rho} \frac{\partial \vec{\lambda}}{\partial t} \quad \text{(in region 2),}$$

where $\vec{\lambda}$ is the magnetic vector potential at any point in space and μ and ρ are the permeability and resistivity of the shell. In regions 1 and 3, the vector potential and magnetic fields are assumed to be static. Solving for $\vec{\lambda}$ in the above equations with the appropriate boundary conditions will lead to a solution for the eddy current distribution in the shell, since $\vec{J} = -1/\rho \cdot \partial \vec{\lambda} / \partial t$ [8]. The resulting solution is given by equation (29) in reference [9]. Equation (29) is a rather complicated expression involving an infinite series of modified Bessel functions of the first and second kind. Again, it should be pointed out that equation (29) is somewhat in error because of several minor algebraic mistakes which

occur in its derivation. These errors are discussed in appendix 1. Also in appendix 1, equation (29) is rederived after correcting for the mistakes in the derivation in the original papers (references [8] and [9]). This corrected version of equation (29) will be used as a comparison with numerical solutions for eddy current density computed in chapter 5 of this thesis.

1.2.1.3 The Solution of Kawasaki, Inami and Ishikawa

Kawasaki, Inami and Ishikawa expanded on the work of Tegopoulos and Kriezis by adapting the solution derived by Tegopoulos and Kriezis to problems where *multiple* current filaments are present inside the shell [10]. They further eliminated the restriction that the shell have a relative permeability of unity. Note that the errors in the original Tegopoulos and Kriezis papers were *not* carried over into the work of Kawasaki et al.

The net eddy current distribution was found by superimposing the effects of each individual current filament. The resultant solution for the current density in the shell was, again, an expression involving an infinite series of modified Bessel Functions of the first and second kind [10].

After obtaining the solution for current density, Kawasaki et al. then used Poynting's theorem to derive an expression for the resistive power loss in the shell due to the flow of eddy currents. Experiments conducted by Kawasaki et al. seem to indicate their expression for eddy current loss gives results within 10% of measured values [10]. Note that their experiments focused only on situations where the filaments (i.e., power cables) in the shell carried a balanced, three phase current.

Although Kawasaki et al. maintain that their solution is valid for any configuration of current filaments inside the shell, a closer examination of their solution reveals it is only correct for a *balanced*, multi-phase system of current filaments. This assertion is discussed in appendix 2 of this thesis.

1.2.1.4 Other Solutions Utilizing the Partial Differential Equation

Emanuel and Doepken [11] and later Sikora, Purczynski, Palka and Gratkowski [12] both published solutions to the eddy current problem based on a two dimensional model which was slightly different from that of Kawasaki et al. Instead of representing the

power cables by current filaments, the current sources in the interior region of the shell were written in terms of a Fourier series expansion with respect to the ϕ coordinate. Otherwise, the method of solution used by Emanuel et al. and Sikora et al. was the same as that used by Tegopoulos and Kriezis.

1.2.2 Review of Boundary Value Problem Solutions Derived From the Integral Equation

1.2.2.1 The Kriezis and Cangellaris Solution

Using the same two dimensional model as Tegopoulos and Kriezis (see Figure 1-4), Kriezis and Cangellaris constructed an integral equation [13] to describe the magnetic vector potential A_z at any point P in Figure 1-4. The integral equation solved by Kriezis and Cangellaris is of the form

$$A_z(P) = A_{z_0}(P) - \frac{j\omega\mu\sigma}{4\pi} \int_V \frac{A_z(Q)}{|r_P - r_Q|} dv, \quad (1.3)$$

where μ and σ are the permeability and conductivity of the shell and ω is the angular frequency of the source. P is any point in space and Q is any point inside the volume of the metal shell. A numerical solution for the integral equation was obtained using the *method of moments* [13, 14].

1.2.2.2 The Peltz and Kuffel Solution

The integral equation technique was also used by Peltz and Kuffel who undertook an investigation of the eddy current problem in pipe-type cables [4,15,16]. Using the "method of images", Peltz and Kuffel constructed an integral equation to describe the current density produced by multiple current sources in the interior of a steel pipe. The method of images forced Peltz and Kuffel to make the assumption that the magnetic properties of the pipe extend to infinity in the radial direction. Nevertheless, their solutions for various examples do give results which closely agree with values calculated using the solution of Kawasaki et al. [4].

1.3 Method of Solution Used In This Thesis

1.3.1 Constructing The Boundary Value Problem

The approach to the boundary value problem in this work will be to construct a partial differential equation from Maxwell's equations which describes the electric field intensity at any point in the problem domain. The most general case of the boundary value problem to be solved is illustrated in Figure 1-5.

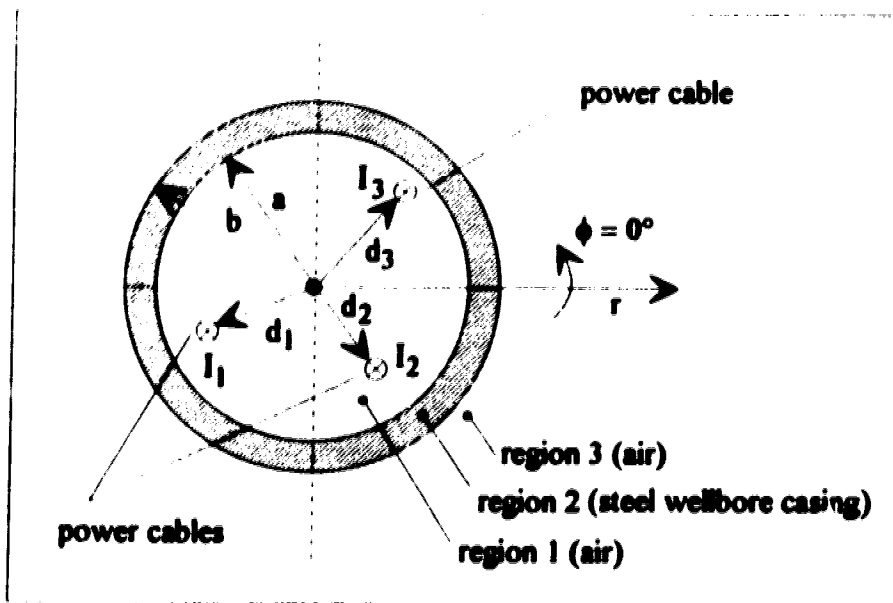


Figure 1-5. Diagram of the general boundary value problem.

The general case shown in Figure 1-5 may be divided into 3 regions. Region 1 is an air filled region inside the wellbore casing. Region 2 is the wellbore casing itself. Region 3 is an air filled region, beyond the casing, which extends to infinity in the radial direction. In region 1 is an arbitrary number of power cables, each carrying a 60 Hz current at a different phase. The cables are arranged in arbitrary positions inside the casing. The steel casing has a constant relative permeability, though it need not be unity.

1.3.2 Solution of the Boundary Value Problem using the Finite Element Method

Once the partial differential equation has been constructed, the *finite element method* (FEM) will be used to solve the boundary value problem. The finite element method can provide a numerical solution for the electromagnetic fields and consequently the eddy

currents in the steel casing. By solving the boundary value problem numerically with the finite element method, complex configurations may be analyzed with relative ease. For the general problem illustrated in Figure 1-5, the procedure for finding a solution for the eddy current loss in the wellbore casing is outlined below.

1. Consider the current in each power cable as an individual source. Superposition is invoked to help solve this problem numerically in the same manner it was used by Dwight [7] and Kawasaki et al. [10] to solve the problem analytically. The original problem is divided into series of smaller boundary value problems where only one current source is present in each problem. This is illustrated schematically in Figure 1-6.

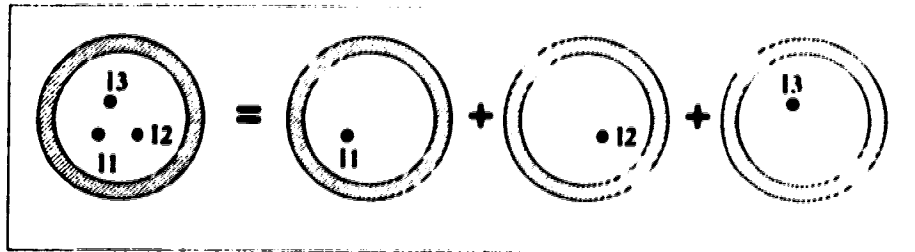


Figure 1-6. The original boundary value problem is equivalent to the superposition of three smaller problems.

Note that the boundary conditions at the outer wall of the casing in the original problem equals the sum of the corresponding boundary conditions in the three smaller problems.

2. Obtain a finite element method solution for the electric field \vec{E} produced by each individual current source in the casing.
3. Superimpose the electric field solutions from all of the smaller problems to get the total electric field, \vec{E}_{tot} , in the original problem.
4. Recognize that the eddy current density in the casing is $\sigma\vec{E}_{tot}$. Use Poynting's theorem and numerical integration to obtain the power dissipated in the casing by the flow of eddy currents, $\sigma\vec{E}_{tot}$.

Initially, it might seem more efficient to simply obtain a single finite element method solution which includes all the current sources in the original problem. However, this approach introduces two additional complications which are difficult to overcome. These

will be explained in detail in chapter 6. Overall, the method outlined above is the less troublesome approach.

1.3.3 Solution For a Problem With a Single Current Source

In the procedure outlined in the previous section, completion of step 2 is the main obstacle. To solve the single current source problem with the finite element method, both the partial differential equation and boundary conditions describing the problem must be known. A diagram of the boundary value problem consisting of a single power cable inside a steel casing is shown in Figure 1-7.

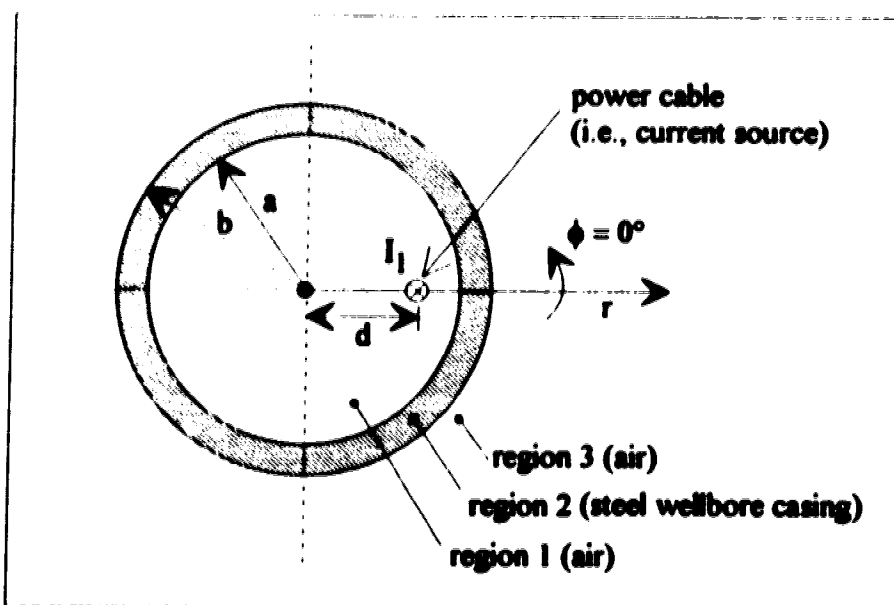


Figure 1-7. Diagram of a boundary value problem with only a single current source present.

The partial differential equation may be constructed from Maxwell's equations. One minor complication is that the electromagnetic properties (σ and μ) of region 2 differ from those of regions 1 and 3. As a result, the partial differential equation for region 2 will be slightly different from the equation for regions 1 and 3.

The boundary conditions for the eddy current problem shown in Figure 1-7 are as follows. First, at the interface between regions 1 and 2 and regions 2 and 3, the condition is that tangential \vec{E} and \vec{H} fields must be equal on either side of the interface. These are

typical boundary conditions for tangential electromagnetic fields at the interface of differing media. The remaining boundary conditions are summarized below:

1. In region 1, at the surface of the power cable, the electric and magnetic fields will be dependent on the current flowing in the power cable. This will be discussed in more detail in the next chapter.
2. In region 3, all fields must go to zero as r goes to infinity.

The second boundary condition poses a problem for the finite element method. Any finite element solution requires that the domain of the problem be defined by a grid or a mesh. Each section or "element" of the mesh produces a system of algebraic equations. This problem has an infinite domain because region 3 extends to infinity in the radial direction. Since an infinite number of elements is obviously out of the question, other options must be considered, if possible. In fact there are three basic approaches to dealing with an infinite domain [17].

The first approach is to use an *infinite element*. This is an element which covers a sector of the domain from a finite radius out to infinity [17]. The second approach is to use the finite element method in conjunction with a technique known as the *boundary element method*. The finite element method would provide a solution for an arbitrarily large but finite section of the problem domain. The boundary element method would provide a solution for the remaining portion of the domain. Note that for the boundary element method, only the boundary of the problem domain needs to be mapped onto a mesh.

In theory there is no reason why either of these two approaches could not be used. In practice however, the actual computer program used in this investigation is unable to implement either of these alternatives.

A third option for dealing with the infinite domain exists if it is known that the solution to the problem exhibits some sort of exponential decay for large arguments (i.e., $e^{-r} \rightarrow 0$ for large r). In this case, the domain need only be modeled out to a point where the contribution to the solution from the remaining portion of the infinite domain is insignificant. At this point a zero boundary condition is substituted for the actual boundary condition. Exactly how far out the domain is modeled is completely arbitrary. The error introduced can be made arbitrarily small by extending the domain further

towards infinity. The accuracy of the approximation may be judged by examining the convergence of the solution as the size of the domain is increased.

To use this technique it is highly recommended to have some idea of how the solution behaves before it is formally solved. This allows for an intelligent guess as to how much of the infinite domain need be modeled. *It is one of the central objectives of this thesis to show that, for the eddy current problem, the problem domain need only be modeled as far as the outer wall of the wellbore casing, and further that, at the outer wall, the magnetic field can be taken as approximately zero.* The validity of these assumptions is critically important to the accuracy of the resulting finite element solution. The full justification for these assumptions will be presented in the next chapter, but essentially the zero boundary condition is a good approximation if either of the following two criteria are satisfied:

1. The casing is at least three skin depths thick.
2. The wave impedance at the outer wall of the casing is much greater than the *intrinsic* impedance of the steel casing.

Consequently, for situations where either of the above two criteria are satisfied, the finite element method may be employed to obtain reasonably accurate solutions for eddy current losses.

CHAPTER 2

The Conditions Under Which The Magnetic Field At the Outer Wall of the Wellbore Casing Is Approximately Zero

The main objective of this chapter is to determine the conditions under which it is appropriate to apply the boundary condition $\vec{H} = 0$ to the boundary representing the outer surface of the casing. As mentioned in the introduction, $\vec{H} = 0$ is only an approximate boundary condition for the magnetic field at the outer wall of the casing. When using the finite element method to solve the boundary value problem, the approximate boundary condition is necessary to accommodate the infinite domain of the problem.

In order to determine when the approximate boundary condition is valid, two analytical solutions will be obtained for the electromagnetic fields induced in the wellbore casing by a single power cable. One solution will be obtained using the exact boundary conditions for the magnetic (and electric) fields at the outer wall of the casing. The other solution will be derived using the approximate boundary condition for the magnetic field at the outer wall: $\vec{H} = 0$. It will be shown that the two solutions are very similar under one or both of the following circumstances:

1. The steel casing is at least three skin depths thick.
2. The *wave impedance* at the outer wall of the steel casing is much greater than the *intrinsic impedance* of the casing.

If either of these criteria are met, then $\vec{H} = 0$ is a good approximation for the magnetic field boundary condition at the outer wall of the casing. As an aside, note that the second criterion in no way guarantees that $\vec{E} \cong 0$ at the outer wall of the casing.

2.1 A Description of the Simple One Dimensional Boundary Value Problem

Figure 2-1 is a cross sectional view of a wellbore casing centered about a power cable. This casing and cable assembly constitutes the boundary value problem to be analyzed in this chapter. Note that the analysis of the boundary value problem is greatly simplified by placing the power cable at the center of the wellbore casing. Solutions to the problem are then no longer dependent on the ϕ coordinate and are a function of only one variable,

namely r . Thus the boundary value problem is essentially reduced to a one dimensional problem

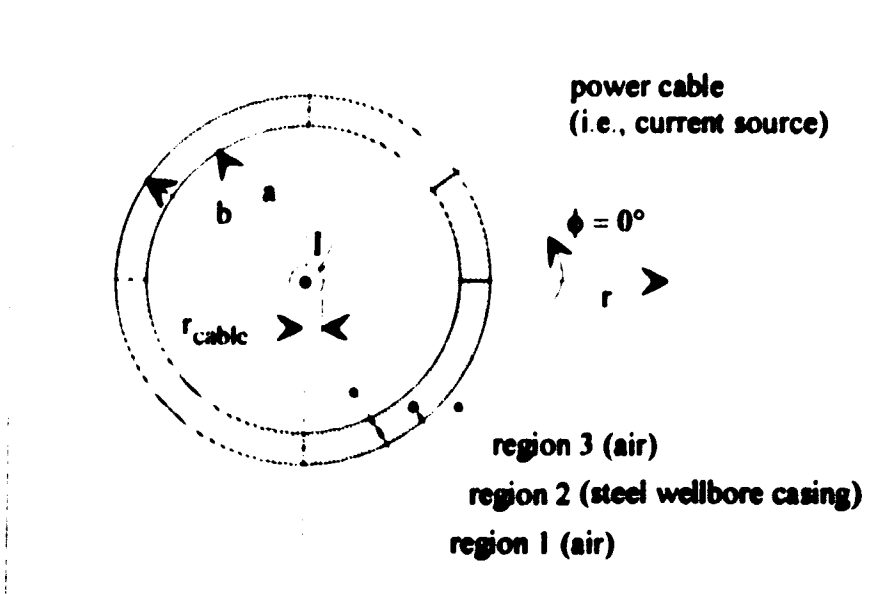


Figure 2-1. A diagram of the one dimensional boundary value problem.

Referring to Figure 2-1, 'I' is the total current that flows through the power cable. Region 1 is an air filled gap between the cable and the casing. Region 2 is the steel wellbore casing itself. Note that the terms *region 2* and *wellbore casing* are synonymous in further discussions. Region 3 is free space, extending to infinity in the radial direction.

2.2 The Differential Equation For the Electric Field

From Maxwell's Equations, the differential equation describing the electric field in an arbitrary region N of Figure 2-1 may be constructed as shown below.

$$\nabla \times \vec{E}_N = -j\omega\mu_N \vec{H}_N \quad (2.1)$$

$$\nabla \times \vec{H}_N = (\sigma_N + j\omega\epsilon_N) \vec{E}_N \quad (2.2)$$

Substituting (2.1) into (2.2) yields

$$\nabla \times \nabla \times \vec{E}_N = -j\omega\mu_N(\sigma_N + j\omega\epsilon_N)\vec{E}_N. \quad (2.3)$$

Equation (2.3) is simply the wave equation.

As previously mentioned, there are several approximations which are applied to this problem. The effects of these are summarized below.

1. $\frac{\partial}{\partial z} = 0$ since it is assumed the casing and cable are infinitely long.
2. $\frac{\partial}{\partial \phi} = 0$ since there is no dependence on the ϕ coordinate in the Figure 2-1.
3. The magnetic permeability, μ , is constant in region 2 (the steel casing).

Furthermore, while the z-directed current in the power cable is a source of the E_{z_N} and H_{ϕ_N} field components, there is no current source present which can sustain the E_{ϕ_N} and H_{z_N} field components. Consequently, the E_{ϕ_N} and H_{z_N} field components are identically zero. While this may not seem intuitively obvious, it may be verified by assuming E_{ϕ_N} and H_{z_N} are not zero and then solving the boundary value problem. The result is the same; namely $E_{\phi_N} = 0$ and $H_{z_N} = 0$.

Using the above approximations, (2.3) may now be written more explicitly as

$$-\left(\frac{\partial^2 E_{z_N}}{\partial r^2} + \frac{1}{r}\frac{\partial E_{z_N}}{\partial r}\right)\mathbf{a}_z = -j\omega\mu_N(\sigma_N + j\omega\epsilon_N)\vec{E}_N. \quad (2.4)$$

From (2.4), a scalar equation may be written for each vector component of the electric field.

$$E_{z_N} = 0 \quad (2.5a)$$

$$E_{\phi_N} = 0 \quad (2.5b)$$

$$\frac{\partial^2 E_{z_N}}{\partial r^2} + \frac{1}{r}\frac{\partial E_{z_N}}{\partial r} + k_N^2 E_{z_N} = 0, \quad (2.5c)$$

where k_N is the wave number, $k_N = \sqrt{-j\omega\mu_N(\sigma_N + j\omega\epsilon_N)}$.

2.3 The Differential Equation For the Magnetic Field

From (2.1), a differential equation for the magnetic field in an arbitrary region N of Figure 2-1 may be obtained.

$$\nabla \times \vec{E}_N = -j\omega\mu_N \vec{H}_N \quad (2.6a)$$

$$\begin{aligned} \nabla \times (E_{z_N} \hat{a}_z) &= -j\omega\mu_N \vec{H}_N \\ \hat{a}_\phi \left(-\frac{\partial E_{z_N}}{\partial r} \right) &= -j\omega\mu_N \vec{H}_N \end{aligned} \quad (2.6b)$$

From (2.6b), the following scalar differential equation may be extracted.

$$\frac{\partial(E_{z_N})}{\partial r} = j\omega\mu_N H_{\phi_N}. \quad (2.6c)$$

Once the general solution for E_{z_N} is known, it may be substituted into (2.6c) to obtain the general solutions for H_{ϕ_N} .

2.4 General Solutions For the Electric and Magnetic Fields

The differential equation of (2.5c) is an example of Bessel's equation. The general solution to Bessel's equation is a combination of linearly independent *Bessel functions*. Because there are several distinct varieties of Bessel functions there are several different forms of the general solution for Bessel's equation.

The most common form of solution for the differential equation in (2.5c) is

$$E_{z_N}(k_N r) = AJ_0(k_N r) + BY_0(k_N r). \quad (2.7)$$

$J_0(k_N r)$ is a zeroth order Bessel function of the first kind. Similarly, $Y_0(k_N r)$ is a zeroth order Bessel function of the second kind, also known as a Neumann function. A and B are arbitrary constants. Physically, $J_0(k_N r)$ and $Y_0(k_N r)$ represent *standing cylindrical waves* [18]. This is similar to the representation of standing plane waves by the sine and cosine functions in a rectangular geometry.

Another form of the solution for (2.5c) is

$$E_{z_n}(k_N r) = E_{z_+} H_0^{(2)}(k_N r) + E_{z_-} H_0^{(1)}(k_N r). \quad (2.8)$$

$H_0^{(1)}(k_N r)$ and $H_0^{(2)}(k_N r)$ are zeroth order Hankel functions of the first and second kind. E_{z_+} and E_{z_-} are arbitrary constants. Physically, $H_0^{(1)}(k_N r)$ and $H_0^{(2)}(k_N r)$ represent *traveling* cylindrical waves [18]. This is similar to the representation of traveling plane waves by the $e^{jk_N r}$ and $e^{-jk_N r}$ functions.

There is yet another form of the solution for (2.5c), which is somewhat useful when the region of interest is a good conductor. For good conductors, $\sigma_N \gg \omega \epsilon_N$. When this is true, the wave number k_N may be approximated by the expression $k_N \cong \sqrt{-j\omega\mu_N\sigma_N}$.

The general solution for (2.5c) may then be written as

$$E_{z_n}(k_N r) = A I_0(j^1 \sqrt{\omega\mu_N\sigma_N} r) + B K_0(j^1 \sqrt{\omega\mu_N\sigma_N} r) \quad (2.9a)$$

or

$$E_{z_n}(k_N r) = A \left[\text{ber}(\sqrt{\omega\mu_N\sigma_N} r) + j \cdot \text{bei}(\sqrt{\omega\mu_N\sigma_N} r) \right] \\ + B \left[\text{ker}(\sqrt{\omega\mu_N\sigma_N} r) + j \cdot \text{kei}(\sqrt{\omega\mu_N\sigma_N} r) \right]. \quad (2.9b)$$

A and B are arbitrary constants. The advantage of (2.9b) over (2.7) and (2.8) is that the arguments of the ber, bei, ker and kei functions are real. Tabulated values for the ber, bei, ker and kei functions are available from several sources. Tabulated values for Bessel and Hankel functions with complex arguments are not generally available.

The general solution for the magnetic field, H_{ϕ_n} , may be found by substituting any of the above general solutions for E_{z_n} into (2.6c). Substituting (2.7) into (2.6c) yields

$$H_{\phi_n}(k_N r) = \frac{-A}{j\eta_N} J_1(k_N r) - \frac{B}{j\eta_N} Y_1(k_N r), \quad (2.10)$$

where $\eta_N = \sqrt{\frac{j\omega\mu_N}{\sigma_N + j\omega\epsilon_N}}$. The quantity η_N is the *intrinsic impedance* of the material in region N.

Substituting (2.8) into (2.6c) yields

$$H_{\phi_N}(k_N r) = \frac{-E_0}{j\eta_N} H_1^{(2)}(k_N r) + \frac{-E_0}{j\eta_N} H_1^{(1)}(k_N r). \quad (2.11)$$

Finally, substituting (2.9b) into (2.6c) yields

$$H_{\phi_N}(k_N r) = \frac{A}{j \cdot \sqrt{\frac{j\omega\mu_N}{\sigma_N}}} \left[\text{ber}_1(\sqrt{\omega\mu_N\sigma_N} r) + j \cdot \text{bei}_1(\sqrt{\omega\mu_N\sigma_N} r) \right] \\ + \frac{B}{j \cdot \sqrt{\frac{j\omega\mu_N}{\sigma_N}}} \left[\text{ker}_1(\sqrt{\omega\mu_N\sigma_N} r) + j \cdot \text{kei}_1(\sqrt{\omega\mu_N\sigma_N} r) \right]. \quad (2.12)$$

While all of the above general solutions are valid, further analysis relies heavily on the application of *transmission line* concepts to the propagation of uniform cylindrical waves. For cylindrical waves, transmission line concepts need to be defined in terms of inward and outward traveling waves. Consequently, the best form of the general solutions to use in this analysis would be the Hankel function solutions, (2.8) and (2.11).

A summary of the electromagnetic properties for each region of the boundary value problem is presented in Table 2-1. The general solutions for the electric and magnetic fields in each region of the problem are presented in Table 2-2.

Table 2-1 A summary of the electromagnetic properties in each region of the boundary value problem illustrated in Figure 2-1.

Region	Media	Material Properties	Intrinsic Impedance	Wave Number
1	air	$\epsilon_1 = \epsilon_0$ $\mu_1 = \mu_0$ $\sigma_1 = 0$	$\eta_1 \cong 377\Omega$	$k_1 = \omega \sqrt{\mu_0 \epsilon_0}$
2	steel	$\epsilon_2 = \epsilon_0$ $\mu_2 = \mu_{steel}$ $\sigma_2 = \sigma_{steel}$	$\eta_2 = \sqrt{\frac{j\omega\mu_2}{\sigma_2 + j\omega\epsilon_2}}$ $\eta_2 \cong \sqrt{\frac{j\omega\mu_2}{\sigma_2}}$ if $\sigma_2 \gg \omega\epsilon_2$	$k_2 = \sqrt{-j\omega\mu_2(\sigma_2 + j\omega\epsilon_2)}$ $k_2 \cong \sqrt{-j\omega\mu_2\sigma_2}$ if $\sigma_2 \gg \omega\epsilon_2$
3	air	$\epsilon_3 = \epsilon_0$ $\mu_3 = \mu_0$ $\sigma_3 = 0$	$\eta_3 \cong 377\Omega$	$k_3 = \omega \sqrt{\mu_0 \epsilon_0}$

Table 2-2. A summary of the general solutions for the electromagnetic fields in each region of the boundary value problem illustrated in Figure 2-1.

Region 1	$E_z(k_1, r) = E_1 \cdot H_0^{(2)}(k_1, r) + E_1 \cdot H_0^{(1)}(k_1, r)$ (2.13a)
	$H_\theta(k_1, r) = \frac{-E_1}{j\eta_1} H_1^{(2)}(k_1, r) - \frac{E_1}{j\eta_1} H_1^{(1)}(k_1, r)$ (2.13b)
Region 2	$E_z(k_2, r) = E_2 \cdot H_0^{(2)}(k_2, r) + E_2 \cdot H_0^{(1)}(k_2, r)$ (2.14a)
	$H_\theta(k_2, r) = \frac{-E_2}{j\eta_2} H_1^{(2)}(k_2, r) - \frac{E_2}{j\eta_2} H_1^{(1)}(k_2, r)$ (2.14b)
Region 3	$E_z(k_3, r) = E_3 \cdot H_0^{(2)}(k_3, r) + E_3 \cdot H_0^{(1)}(k_3, r)$ (2.15a)
	$H_\theta(k_3, r) = \frac{-E_3}{j\eta_3} H_1^{(2)}(k_3, r) - \frac{E_3}{j\eta_3} H_1^{(1)}(k_3, r)$ (2.15b)

2.4.1 Simplification of the General Solutions in Region 2: Introduction of Large Argument Approximations for Hankel Functions.

Before continuing, an approximation for the general solutions in region 2 is introduced into the analysis. Recall from Table 2-2 that the general solutions for the electric and magnetic fields of this problem are composed of Hankel functions. If any of these Hankel functions possess arguments which are sufficiently "large", then the actual Hankel function may be approximated by one of the following asymptotic formulae.

$$H_0^{(1)}(z) \cong \sqrt{\frac{2}{\pi z}} \cdot \sqrt{-j} \cdot e^{\mu} \quad (2.16a)$$

$$H_1^{(1)}(z) \cong \sqrt{\frac{2}{\pi z}} \cdot \frac{\sqrt{-j}}{j} \cdot e^{\mu} \quad (2.16b)$$

$$H_0^{(2)}(z) \cong \sqrt{\frac{2}{\pi z}} \cdot \sqrt{j} \cdot e^{-\mu} \quad (2.16c)$$

$$H_1^{(2)}(z) \cong \sqrt{\frac{2}{\pi z}} \cdot j\sqrt{j} \cdot e^{-\mu} \quad (2.16d)$$

Because the asymptotic formulae are based on exponential functions, complicated expressions involving Hankel functions become more manageable when the asymptotic approximations are introduced. The above asymptotic formulae are particularly relevant to (2.14a) and (2.14b), the general solutions for the electric and magnetic fields in region 2 of the problem (the steel wellbore casing).

The Hankel functions in (2.14a) and (2.14b) all have the term $k_2 r$ as their argument. Due to the electrical properties and physical dimensions of the casing, the argument $k_2 r$ is typically $\gg 1$. Recall from Table 2-1 that $k_2 = \sqrt{-j\omega\mu_2(\sigma_2 + j\omega\epsilon_2)}$. The permeability of the steel casing, μ_2 , is rarely less than $40\mu_0$. The conductivity of the steel casing, σ_2 , is rarely less than 10^6 [S/m]. Therefore at 60 Hz, the magnitude of k_2 is typically 135 or greater. The inner radius of the wellbore casing, a , may vary from 0.05 to 0.50 meters or more. Therefore the magnitude of $k_2 r$ ranges from 7 to 70 and possible much higher, depending on μ_2 and σ_2 .

Thus for general solutions (2.14a) and (2.14b), where the arguments of the Hankel functions are "large", the Hankel functions may be replaced by the appropriate asymptotic formulae. The substitution of the asymptotic formulae from (2.16) into (2.14a) and (2.14b) results in the following expressions:

$$E_{z_1}(k_2, r) = E_{2_1} \sqrt{\frac{2}{\pi k_2 r}} \cdot \sqrt{j} \cdot e^{-k_2 r} + E_{2_2} \sqrt{\frac{2}{\pi k_2 r}} \cdot \sqrt{-j} \cdot e^{k_2 r} \quad (2.17a)$$

$$= E_{2_1} \sqrt{\frac{2}{\pi k_2 r}} \sqrt{j} e^{-k_2 r} \left[1 + \frac{E_{2_2}}{E_{2_1}} \cdot \frac{1}{j} \cdot e^{2k_2 r} \right] \quad (2.17b)$$

$$H_{\theta_1}(k_2, r) = \frac{-E_{2_1}}{\eta_2} \sqrt{\frac{2}{\pi k_2 r}} \cdot \sqrt{j} \cdot e^{-k_2 r} + \frac{E_{2_2}}{\eta_2} \sqrt{\frac{2}{\pi k_2 r}} \cdot \sqrt{-j} \cdot e^{k_2 r} \quad (2.18a)$$

$$= \frac{-E_{2_1}}{\eta_2} \sqrt{\frac{2}{\pi k_2 r}} \cdot \sqrt{j} \cdot e^{-k_2 r} \left[1 - \frac{E_{2_2}}{E_{2_1}} \cdot \frac{1}{j} \cdot e^{2k_2 r} \right] \quad (2.18b)$$

Expressions (2.17) and (2.18) are accurate approximations of the general solutions for the electric and magnetic fields in the steel wellbore casing. Subsequent analysis will utilize these approximate general solutions. Continued use of the original expressions containing the actual Hankel functions would result in unwieldy and unnecessarily complicated solutions for the unknown coefficients E_{2_1} and E_{2_2} .

2.4.2 The Reflection Coefficient

The term E_{2_2}/E_{2_1} in (2.17b) and (2.18b) has physical significance. It is directly related to the *reflection coefficient* at the outer wall of the wellbore casing. This is the ratio of the reflected portion of the electric field to incident portion of the field at the boundary between regions 2 and 3.

In general, the reflection coefficient in region N is defined as the ratio of the inward traveling wave to the outward traveling wave. Recall equation (2.8), the Hankel function general solution for the electric field in an arbitrary region N of Figure 2-1. In (2.8), the $H_n^{(2)}(r)$ function takes on the properties of an outward traveling wave while the $H_n^{(1)}(r)$ function acts as an inward traveling wave. Therefore, the reflection coefficient at any point in region N may be expressed as

$$\Gamma_N(r) = \frac{E_{-}}{E_{+}} \cdot \frac{H_0^{(1)}(k_N r)}{H_0^{(2)}(k_N r)}. \quad (2.19)$$

For region 2, where the arguments of the Hankel functions are "large", the expression for the reflection coefficient may be simplified by introducing the asymptotic approximations for the Hankel functions. Substituting (2.16) into (2.19) yields

$$\Gamma_2(k_2 r) = \frac{E_{2-}}{E_{2+}} \cdot \frac{1}{j} \cdot e^{j2k_2 r}. \quad (2.20)$$

At $r = b$, the outer wall of the casing, the reflection coefficient is given by

$$\Gamma_2(k_2 b) = \frac{E_{2-}}{E_{2+}} \cdot \frac{1}{j} \cdot e^{j2k_2 b}. \quad (2.21)$$

Rearranging (2.21) to specify E_{2-}/E_{2+} in terms of the reflection coefficient at $r = b$ yields:

$$\frac{E_{2-}}{E_{2+}} = j \cdot \Gamma_2(k_2 b) \cdot e^{-j2k_2 b}. \quad (2.22)$$

The general solutions for the electromagnetic fields in the wellbore casing may be expressed in terms of the reflection coefficient at $r = b$. Substituting (2.22) into (2.17b) and (2.18b) yields

$$E_{z_2}(k_2, r) = E_{z_2} \cdot \sqrt{\frac{2}{\pi k_2 r}} \cdot \sqrt{j} \cdot e^{-k_2 r} \left[1 + \Gamma_2(k_2, b) \cdot e^{j2k_2(r-b)} \right] \quad (2.23)$$

and

$$H_{\phi_2}(k_2, r) = \frac{-E_{z_2}}{\eta_2} \cdot \sqrt{\frac{2}{\pi k_2 r}} \cdot \sqrt{j} \cdot e^{-k_2 r} \left[1 - \Gamma_2(k_2, b) \cdot e^{j2k_2(r-b)} \right] \quad (2.24)$$

2.5 Complete Solutions For the Electric and Magnetic Fields In Region 2

Equations (2.23) and (2.24) are still only general solutions for the electromagnetic fields in region 2. To obtain complete solutions for the electromagnetic fields in the wellbore casing, it is necessary to express the unknown constants E_{z_2} and $\Gamma_2(k_2, b)$ in terms of the available boundary conditions. These boundary conditions are discussed in sections 2.5.1 and 2.5.2.

2.5.1 The Boundary Condition at $r = a$ in Region 2

The boundary condition at the inner wall of the wellbore casing, at $r = a$, is

$$H_{\phi_2}(k_2, a) = \frac{I}{2\pi a} \quad \text{B.C. (1)}$$

This boundary condition is somewhat of an approximation. A more rigorous boundary condition would be

$$H_{\phi_2}(k_2, a) = \frac{I}{2\pi a} + j\omega\epsilon_0 \int_0^{2\pi} \int_{r_{\text{casing}}}^a E_{z_2}(k_2, r) r dr d\phi \quad (2.25)$$

However, the second term in (2.25) is many orders of magnitude smaller than the first because the frequencies dealt with here are ≤ 60 Hz and the distance between r_{casing} and a is electrically very small. As a result, boundary condition (1) may be considered nearly exact. Note that the approximation in boundary condition (1) allows for explicit solutions of E_{z_2} and $\Gamma_2(k_2, b)$ without having to solve for E_{z_1} and E_{ϕ_1} . This greatly reduces the

amount of computation involved in the solution. Furthermore, the electromagnetic fields in region 1 are of little importance for this problem.

By applying boundary condition (1) to equation (2.24), the unknown constant $E_{2,}$ can be expressed in terms of the current in the power cable and $\Gamma_2(k_2b)$. Equation (2.24) is the general solution for the magnetic field in region 2. According to boundary condition (1), the magnetic field in region 2 at $r=a$ is $I/2\pi a$. Setting $r=a$ in (2.24) and substituting this expression into boundary condition (1) yields

$$\frac{I}{2\pi a} = \frac{-E_{2,}}{\eta_2} \cdot \sqrt{\frac{2}{\pi k_2 a}} \cdot \sqrt{j} \cdot e^{-k_2 a} [1 - \Gamma_2(k_2 b) \cdot e^{j2k_2(a-b)}]. \quad (2.26)$$

Rearranging (2.26) yields the following expression for $E_{2,}$:

$$E_{2,} = -\eta_2 \cdot \frac{I}{2\pi a} \cdot \sqrt{\frac{\pi k_2 a}{2}} \cdot \frac{1}{\sqrt{j} e^{-k_2 a} [1 - \Gamma_2(k_2 b) \cdot e^{j2k_2(a-b)}]}. \quad (2.27)$$

Substituting the expression for $E_{2,}$ from (2.27) into the general solution for the electric field from (2.23) yields

$$\begin{aligned} E_{z_1}(k_2 r) &= -\eta_2 \cdot \frac{I}{2\pi\sqrt{a}} \cdot \frac{1}{\sqrt{r}} \cdot \frac{e^{-k_2 r} [1 + \Gamma_2(k_2 b) \cdot e^{j2k_2(r-b)}]}{e^{-k_2 a} [1 - \Gamma_2(k_2 b) \cdot e^{j2k_2(a-b)}]} \\ &= -\eta_2 \cdot \frac{I}{2\pi\sqrt{a}} \cdot \frac{1}{\sqrt{r}} \cdot \frac{[e^{k_2(b-r)} + \Gamma_2(k_2 b) \cdot e^{-k_2(b-r)}]}{[e^{k_2(b-a)} - \Gamma_2(k_2 b) \cdot e^{-k_2(b-a)}]}. \end{aligned} \quad (2.28)$$

Similarly, substituting the expression for $E_{2,}$ from (2.27) into the general solution for the magnetic field from (2.24) yields

$$\begin{aligned} H_{\phi_1}(k_2 r) &= \frac{I}{2\pi\sqrt{a}} \cdot \frac{1}{\sqrt{r}} \cdot \frac{e^{-k_2 r} [1 - \Gamma_2(k_2 b) \cdot e^{j2k_2(r-b)}]}{e^{-k_2 a} [1 - \Gamma_2(k_2 b) \cdot e^{j2k_2(a-b)}]} \\ &= \frac{I}{2\pi\sqrt{a}} \cdot \frac{1}{\sqrt{r}} \cdot \frac{[e^{k_2(b-r)} - \Gamma_2(k_2 b) \cdot e^{-k_2(b-r)}]}{[e^{k_2(b-a)} - \Gamma_2(k_2 b) \cdot e^{-k_2(b-a)}]}. \end{aligned} \quad (2.29)$$

2.5.2 The Boundary Conditions at $r = b$ in Region 2

As was done for the boundary condition at $r = a$, the boundary conditions at $r = b$ could be defined in terms of the electromagnetic fields at $r = b$, namely $E_{z_2}(k_2, b)$ and $H_{\phi_2}(k_2, b)$. However, it is also possible, and in fact preferable, to define the boundary condition at $r = b$ in terms of the *wave impedance* at $r = b$.

Impedance is a parameter commonly used in the analysis of transmission lines. However, impedance concepts may also be used to analyze the behavior of uniform, transverse electromagnetic waves at the boundary between two electrically dissimilar regions, provided that the direction of propagation is normal to the boundary [19].

In general, the wave impedance in an arbitrary region N of Figure 2-1 is defined as

$$Z_N(k_N r) = -\frac{E_{z_N}(k_N r)}{H_{\phi_N}(k_N r)}. \quad (2.30)$$

This is the ratio of the total electric field to the total magnetic field at any point in region N. The negative sign ensures that if the real part of Z_N is positive, power flow is in the outward radial direction.

The wave impedance in region 2 at $r = b$ is

$$Z_2(k_2, b) = -\frac{E_{z_2}(k_2, b)}{H_{\phi_2}(k_2, b)}. \quad (2.31)$$

Obviously, the explicit value for $Z_2(k_2, b)$ is dependent on the boundary conditions for the electromagnetic fields at $r = b$. As mentioned at the beginning of this chapter, two sets of boundary conditions (exact and approximate) are imposed on the electromagnetic fields at $r = b$. This results in two distinct solutions for the electric and magnetic fields in the casing. The exact and approximate boundary conditions and their effects on $Z_2(k_2, b)$ are discussed in sections 2.5.2.1 and 2.5.2.2.

2.5.2.1 The Exact Boundary Conditions at $r = b$

At the interface between region 2 and region 3, the following boundary conditions must be satisfied.

$$E_{z_2}(k,b) = E_{z_1}(k,b). \quad \text{B.C. (2a)}$$

$$H_{\phi_2}(k,b) = H_{\phi_1}(k,b). \quad \text{B.C. (2b)}$$

These are general boundary conditions for tangential fields at the boundary between two electrically dissimilar media, in this case steel and air.

Using the definition of wave impedance from (2.30) and boundary conditions (2a) and (2b), the following statement can be made about the continuity of the wave impedance at $r = b$:

$$Z_2(k,b) = Z_1(k,b). \quad \text{B.C. (2c)}$$

Now recall (2.15a) and (2.15b), the general solutions for the electromagnetic fields in region 3. The following two boundary conditions are imposed on the electromagnetic fields at the outer boundary of region 3. Since region 3 extends radially out to infinity,

$$E_{z_3}(k,r) \rightarrow 0 \text{ as } r \rightarrow \infty \quad \text{B.C. (3)}$$

and
$$H_{\phi_3}(k,r) \rightarrow 0 \text{ as } r \rightarrow \infty. \quad \text{B.C. (4)}$$

In other words, the electromagnetic fields in region 3 must approach zero as r approaches infinity. The functions $H_0^{(1)}(k,r)$ and $H_1^{(1)}(k,r)$ approach infinity as r approaches infinity. Consequently the general solutions for the electric and magnetic fields in region 3 immediately reduce from (2.15a) and (2.15b) to

$$E_{z_3}(k,r) = E_{z_3} H_0^{(2)}(k,r) \quad (2.32a)$$

$$H_{\phi_3}(k,r) = \frac{-E_{z_3}}{j\eta_3} H_1^{(2)}(k,r). \quad (2.32b)$$

The coefficient E_{z_3} associated with $H_0^{(1)}(k,r)$ and $H_1^{(1)}(k,r)$ in (2.15a) and (2.15b) is identically zero.

The new general solutions for the electromagnetic fields in region 3 may be used to obtain an explicit expression for $Z_1(k, b)$. Substituting the general solutions for $E_z(k, r)$ and $H_\phi(k, r)$ from (2.32a) and (2.32b) into (2.30) yields

$$Z_1(k, b) = j\eta_3 \frac{H_0^{(2)}(k, b)}{H_1^{(2)}(k, b)}. \quad (2.33)$$

Note that according to (2.33), the only information required to specify $Z_1(k, b)$ is the intrinsic impedance in region 3 and the outer radius of the wellbore casing, b . Since both η_3 and b are known quantities, $Z_1(k, b)$ can be explicitly defined at the start of this problem.

Finally, since $Z_2(k, b) = Z_1(k, b)$ from boundary condition (2c), the *exact* boundary condition for $Z_2(k, b)$ can be stated explicitly as

$$Z_2(k, b) = j\eta_3 \frac{H_0^{(2)}(k, b)}{H_1^{(2)}(k, b)}. \quad (2.34)$$

2.5.2.2 The Approximate Boundary Condition at $r = b$

An alternate boundary condition for the magnetic field at $r = b$ is $H_\phi(k, b) = 0$. This boundary condition is not physically realizable and hence only an approximation, although depending on the circumstances it may be a very good one. Later in this chapter a general rule will be derived to help decide when the use of the approximate boundary condition is appropriate.

The approximation is based on two phenomena which affect the magnetic field in the steel casing. First, because steel is a lossy material, the incident wave in the magnetic field decays exponentially as it propagates outward through the casing. If the casing is at least three skin depths thick, then the magnitude of the field will be almost negligible at the outer wall of the casing. Secondly, if the wave impedance at the outer wall of the casing is much greater than the *intrinsic* impedance of the casing, then most of the magnetic field at the outer wall is reflected back into the casing and very little is transmitted into region 3. This is analogous to the behavior of current at the end of an open circuited transmission line, i.e., the interface between regions 2 and 3 is the equivalent of an open circuit.

It is possible to interpret the approximate boundary condition for the magnetic field in terms of the wave impedance at the outer wall of the steel casing. According to (2.31), the impedance at $r = b$ should approach infinity as the magnetic field goes to zero; i.e.,

$$Z_2(k_2, b) = -\frac{E_{z_1}(k_2, b)}{H_{\phi_1}(k_2, b)}$$

$$Z_2(k_2, b) \rightarrow -\infty \text{ as } H_{\phi_1}(k_2, b) \rightarrow 0,$$

with the understanding that $k_{z_1}(k_2, b) \neq 0$. Thus, if $H_{\phi_1}(k_2, b) = 0$, the boundary condition for $Z_2(k_2, b)$ is

$$Z_2(k_2, b) = -\infty. \quad (2.35)$$

2.5.3 Explicit Solution for $\Gamma_2(k_2, b)$ in Terms of $Z_2(k_2, b)$

Having explicitly defined exact and approximate boundary conditions for $Z_2(k_2, b)$, the next step is to express the unknown constant $\Gamma_2(k_2, b)$ in terms of $Z_2(k_2, b)$. The term $Z_2(k_2, b)$ will be carried along with the understanding that the exact or approximate expression for $Z_2(k_2, b)$ may be substituted into the analysis at any time.

An expression for the wave impedance at any point in region 2 may be obtained by substituting the general solutions for the electric and magnetic fields from (2.28) and (2.29) into (2.30). This yields

$$Z_2(k_2, r) = \eta_2 \frac{\left[1 + \Gamma_2(k_2, b) \cdot e^{j2k_2(r-b)} \right]}{\left[1 - \Gamma_2(k_2, b) \cdot e^{j2k_2(r-b)} \right]}. \quad (2.36)$$

By rearranging (2.36) and setting $r = b$, it is possible to express $\Gamma_2(k_2, b)$, the reflection coefficient at $r = b$, in terms of $Z_2(k_2, b)$. The resulting expression is shown below:

$$\Gamma_2(k_2, b) = \frac{Z_2(k_2, b) - \eta_2}{Z_2(k_2, b) + \eta_2}. \quad (2.37)$$

2.5.4 The Final Solutions for the Electric and Magnetic Fields in the Wellbore Casing

The solutions for the electric and magnetic fields in the wellbore casing are essentially given by equations (2.28) and (2.29). The $\Gamma_2(k_2, b)$ term in these solutions is given by the formula from (2.37):

$$\Gamma_2(k_2, b) = \frac{Z_2(k_2, b) - \eta_2}{Z_2(k_2, b) + \eta_2}.$$

Recall from the beginning of this chapter it was stated that *two* analytic solutions for the electromagnetic fields in the wellbore casing are to be derived. One solution, the exact solution, is derived using the exact value $Z_2(k_2, b)$. Similarly, an approximate solution is derived using the approximate value for $Z_2(k_2, b)$.

$Z_2(k_2, b)$ in the exact solution is given by (2.34):

$$Z_2(k_2, b) = j\eta_1 \frac{H_0^{(2)}(k_2, b)}{H_1^{(2)}(k_2, b)}.$$

$Z_2(k_2, b)$ in the approximate solution is given by (2.35):

$$Z_2(k_2, b) = -\infty.$$

Substituting $Z_2(k_2, b) = -\infty$ into the expression for $\Gamma_2(k_2, b)$ from (2.37) yields $\Gamma_2(k_2, b) = 1$. In turn, substituting $\Gamma_2(k_2, b) = 1$ into (2.28) and (2.29) yields the following approximate solutions for the electric and magnetic fields in the wellbore casing:

$$\tilde{E}_z(k_2, r) = -\eta_2 \cdot \frac{I}{2\pi\sqrt{a}} \cdot \frac{1}{\sqrt{r}} \cdot \left[\frac{e^{\mu_2(b-r)} + e^{-\mu_2(b-r)}}{e^{\mu_2(b-a)} - e^{-\mu_2(b-a)}} \right] \quad (2.38)$$

$$\text{and} \quad \tilde{H}_\phi(k_2, r) = \frac{I}{2\pi\sqrt{a}} \cdot \frac{1}{\sqrt{r}} \cdot \left[\frac{e^{\mu_2(b-r)} - e^{-\mu_2(b-r)}}{e^{\mu_2(b-a)} - e^{-\mu_2(b-a)}} \right]. \quad (2.39)$$

The \sim associated with $\tilde{E}_z(k_2, r)$ and $\tilde{H}_\phi(k_2, r)$ merely denotes that these solutions are based on the approximate boundary condition.

2.6 Conditions Under Which $H_{\phi}(k_2, b) = 0$ Is an Acceptable Approximation For Exact Boundary Conditions

As stated earlier, the main objective of this chapter is to determine the conditions under which it is acceptable to use the approximation $H_{\phi}(k_2, b) = 0$ as a boundary condition. It is important to know when this approximate boundary condition is valid because it will be used exclusively in *finite element* solutions of boundary value problems in upcoming chapters. Obviously, the accuracy of the finite element solutions is dependent on the validity of the boundary condition used to derive them.

To determine when it is acceptable to use the approximation $H_{\phi}(k_2, b) = 0$, consider the exact and approximate solutions for the electromagnetic fields in the steel wellbore casing. Both sets of solutions are derived from the same differential equations. When the exact and approximate solutions are in close agreement with each other, then the approximation $H_{\phi}(k_2, b) = 0$ is valid. $H_{\phi}(k_2, b) = 0$ should then be an acceptable substitute for the exact boundary conditions at $r = b$.

2.6.1 Conditions Under Which The Exact and Approximate Solutions Are In Close Agreement

There are two conditions under which the exact and approximate solutions for the electromagnetic fields may be considered to be reasonably close. These are discussed in the next two sections.

2.6.1.1 Condition 1: The Wellbore Casing Is At Least Three Skin Depths Thick

If the thickness of the wellbore casing, $(b - a)$, is at least three skin depths, then the exact and approximate solutions will closely agree with each other. Essentially, as the casing thickness becomes very large, both the exact and approximate solutions reduce to the same asymptotic expression. In general then, the thicker the casing, the better the agreement between the two sets of solutions.

The physical explanation for the equivalence of the exact and approximate solutions is as follows. The steel wellbore casing is highly lossy. If the casing is several skin depths

thick, incident electromagnetic waves originating at the inner wall of the casing will have decayed significantly by the time they reach the outer wall of the casing.

At the outer wall, some of the electromagnetic field is reflected back into the casing. As the reflected waves travel back towards the inner wall, they continue to attenuate. Compared to the magnitudes of the incident waves, the reflected waves are extremely small. Thus the effects of the reflected waves can be neglected everywhere except near the outer wall where they are still relatively unattenuated and comparable in magnitude to the incident waves. Wherever the reflected waves can be neglected, the exact and approximate solutions are in close agreement.

Near the outer wall, the reflected waves cannot be neglected and the exact and approximate solutions will diverge. However, because magnitudes of both the exact and approximate solutions near the outer wall are negligibly small compared to their respective maximums, the discrepancy between the solutions near the outer wall is not important.

Mathematically, the explanation for the equivalence of the two sets of solutions is as follows. From (2.28), the expression for the electric field based on the exact boundary conditions at $r = b$ is

$$E_z(k_2 r) = -\eta_2 \cdot \frac{I}{2\pi\sqrt{a}} \cdot \frac{1}{\sqrt{r}} \cdot \left[\frac{e^{jk_2(b-r)} + \Gamma_2(k_2 b) \cdot e^{-jk_2(b-r)}}{e^{jk_2(b-a)} - \Gamma_2(k_2 b) \cdot e^{-jk_2(b-a)}} \right]$$

The propagation constant jk_2 in (2.28) may be written in terms of an attenuation constant, α , and a phase constant, β . In other words, $jk_2 = \alpha + j\beta$, where α and β are real numbers. Substituting $jk_2 = \alpha + j\beta$ into (2.28) yields

$$E_z(k_2 r) = -\eta_2 \cdot \frac{I}{2\pi\sqrt{a}} \cdot \frac{1}{\sqrt{r}} \cdot \left[\frac{e^{(\alpha + j\beta)(b-r)} + \Gamma_2(k_2 b) \cdot e^{-(\alpha + j\beta)(b-r)}}{e^{(\alpha + j\beta)(b-a)} - \Gamma_2(k_2 b) \cdot e^{-(\alpha + j\beta)(b-a)}} \right] \quad (2.40)$$

If $(b-a)$, the casing thickness, is at least three times greater than $1/\alpha$ (the skin depth) then the second term in the denominator may be neglected since its magnitude is e^{-6} times smaller than the first. Thus, (2.40) becomes

$$E_{z_1}(k_2, r) \cong -\eta_2 \cdot \frac{I}{2\pi\sqrt{a}} \cdot \frac{1}{\sqrt{r}} \cdot \left[e^{-\alpha(r-a)} e^{-j\beta(r-a)} + \Gamma_2(k_2, b) \cdot e^{-\alpha(2b-a-r)} e^{-j\beta(2b-a-r)} \right]. \quad (2.41)$$

The above substitutions and approximations may also be applied to (2.38), the approximate solution for the electric field. Thus, $\tilde{E}_{z_1}(k_2, r)$ from (2.38) reduces to

$$\tilde{E}_{z_1}(k_2, r) \cong -\eta_2 \cdot \frac{I}{2\pi\sqrt{a}} \cdot \frac{1}{\sqrt{r}} \cdot \left(e^{-\alpha(r-a)} e^{-j\beta(r-a)} + e^{-\alpha(2b-a-r)} e^{-j\beta(2b-a-r)} \right). \quad (2.42)$$

Notice the similarity between (2.41) and (2.42). The only difference is the coefficient $\Gamma_2(k_2, b)$ in the second term inside the parentheses in (2.41). However, the second term in (2.41) and the second term (2.42) *both* become negligible as r approaches a ; consequently the closer r is to a , the closer the agreement between $E_{z_1}(k_2, r)$ and $\tilde{E}_{z_1}(k_2, r)$. This is also true for $H_{\phi_1}(k_2, r)$ and $\tilde{H}_{\phi_1}(k_2, r)$.

In other words, as the second terms in (2.41) and (2.42) become negligible (with respect to the first terms), *both* the exact and approximate solutions for the electric field reduce to

$$\left. \begin{array}{l} E_{z_1}(k_2, r) \\ \text{and} \\ \tilde{E}_{z_1}(k_2, r) \end{array} \right\} \cong -\eta_2 \cdot \frac{I}{2\pi\sqrt{a}} \cdot \frac{1}{\sqrt{r}} \cdot e^{-\alpha(r-a)} e^{-j\beta(r-a)}.$$

Likewise, *both* the exact and approximate solutions for the magnetic field in the wellbore casing reduce to

$$\left. \begin{array}{l} H_{\phi_1}(k_2, r) \\ \text{and} \\ \tilde{H}_{\phi_1}(k_2, r) \end{array} \right\} \cong \frac{I}{2\pi\sqrt{a}} \cdot \frac{1}{\sqrt{r}} \cdot e^{-\alpha(r-a)} e^{-j\beta(r-a)}.$$

However, as r approaches b , the second terms inside the parentheses in both (2.41) and (2.42) *cannot* be neglected. As a result, $E_{z_1}(k_2, b) \cong \tilde{E}_{z_1}(k_2, b)$ is no longer valid unless $\Gamma_2(k_2, b) \cong 1$. On the other hand, at $r = b$ both the exact and approximate solutions are only about 5% (e^{-3}) of their maximum value. Thus near the outer wall, where the

solutions begin to significantly diverge, both the exact and approximate fields are negligibly small compared to their respective maximums. In this region, the discrepancy between the two solutions can be considered irrelevant.

2.6.1.2 Condition 2: $|Z_2(k,b)| \gg |\eta_2|$

If the wave impedance at the outer wall of the casing is much greater than the *intrinsic* impedance of the casing then the exact and approximate solutions for the electromagnetic fields in the casing will be in close agreement. This is demonstrated as follows.

From (2.28), the solution for the electric field based on the exact boundary conditions is

$$E_{z_1}(k_1, r) = -\eta_2 \cdot \frac{I}{2\pi\sqrt{a}} \cdot \frac{1}{\sqrt{r}} \cdot \left[\frac{e^{\mu_1(b-r)} + \Gamma_2(k,b) \cdot e^{-\mu_1(b-r)}}{e^{\mu_1(b-a)} - \Gamma_2(k,b) \cdot e^{-\mu_1(b-a)}} \right]$$

If $|Z_2(k,b)| \gg |\eta_2|$ then, from (2.37), $\Gamma_2(k,b)$ in the above solution is approximately unity. The exact solution for the electric field can then be rewritten as

$$E_{z_1}(k_1, r) \cong -\eta_2 \cdot \frac{I}{2\pi\sqrt{a}} \cdot \frac{1}{\sqrt{r}} \cdot \frac{e^{\mu_1(b-r)} + e^{-\mu_1(b-r)}}{e^{\mu_1(b-a)} - e^{-\mu_1(b-a)}}$$

The expression on the right hand side of the above equation is identical to the approximate solution for the electric field from (2.38). Thus, if $|Z_2(k,b)| \gg |\eta_2|$ then $\Gamma_2(k,b) \cong 1$ and as a result $E_{z_1}(k_1, r) \cong \tilde{E}_{z_1}(k_1, r)$. It may also be shown that $H_{\phi_1}(k_1, r) \cong \tilde{H}_{\phi_1}(k_1, r)$ by applying the same condition, $\Gamma_2(k,b) \cong 1$, to (2.29) and comparing it with (2.39).

With regard to the magnetic field at $r = b$, the reflected portion of the field is essentially 180° out of phase with the incident field. Thus from (2.29), it can be seen that when $\Gamma_2(k,b) \cong 1$ the magnetic field at the outer wall of the casing is approximately zero. This is true *regardless of the amount of attenuation* experienced by the electromagnetic field in the casing. The casing might be only a fraction of a skin depth thick, yet the magnetic field at $r = b$ will still be negligible if $\Gamma_2(k,b) \cong 1$.

The physical interpretation of $\Gamma_2(k,b) \cong 1$ is that nearly all of the incident electromagnetic field at the outer wall of the casing is reflected back into the casing. As

mentioned earlier, this is highly analogous to the behavior of voltage and current along an open circuited transmission line, i.e., the interface between regions 2 and 3 is the equivalent of an open circuit.

2.6.2 Summary of Criteria Under Which $H_{\phi_1}(k_2b) = 0$ Is an Acceptable Approximation

To reiterate, if

1. the wellbore casing is at least three skin depths thick or
2. the *wave impedance* at the outer wall of the steel casing is much greater than the *intrinsic impedance* of the casing,

then the exact and approximate solutions for the electromagnetic fields are in close agreement with each other. Consequently, if *either* of the above criteria is satisfied then $H_{\phi_1}(k_2b) = 0$ is indeed a valid approximation and should then be an acceptable substitute for the exact boundary conditions at $r = b$.

The above two criteria are useful for judging whether or not $H_{\phi_1}(k_2b) = 0$ is an acceptable boundary condition for boundary value problems similar to the one studied in this chapter. The fact that the casing thickness and the reflection coefficient can be calculated at the start of a problem allows for an immediate assessment of the validity of the $H_{\phi_1}(k_2b) = 0$ approximation.

There are two limitations to the above criteria. First, with regard to the condition $|Z_2(k_2b)| \gg |\eta_2|$, the degree to which $|Z_2(k_2b)|$ needs to be greater than $|\eta_2|$ is somewhat subjective. Secondly, there are many boundary value problems in which the exact and approximate field solutions closely agree with each other despite the fact that neither of the above criteria are apparently satisfied. This is because the individual effects of attenuation and reflection are cumulative and together they bring about the convergence of the two solutions. This occurs even if the effect of attenuation or the effect of reflection is, by itself, insufficient to cause the exact and approximate solutions to agree. In all instances, a combination of attenuation and reflection affects the problem.

The above limitations on the criteria for judging the convergence of the exact and approximate solutions may be overcome by introducing a new quantity: the *magnetic shielding ratio*. This ratio can give an assessment of the combined effects of attenuation and reflection. The magnetic shielding ratio and its role in determining the validity of the $H_{\phi_1}(k_2, b) = 0$ approximation will be discussed in detail in the next section.

2.6.3 The Magnetic Shielding Ratio

For the boundary value problem discussed in this chapter, a quick and effective method of gauging how well the exact and approximate solutions agree with one another is to examine the magnetic shielding ratio. The magnetic shielding ratio is defined as the ratio of the magnetic field at the inner wall of the wellbore casing to the field at the outer wall. An expression for this ratio is obtained as follows. From (2.29), the *exact* solution for the magnetic field in the casing is

$$H_{\phi_1}(k_2, r) = \frac{I}{2\pi\sqrt{a}} \cdot \frac{1}{\sqrt{r}} \cdot \frac{\left[e^{k_2(b-r)} - \Gamma_2(k_2, b) \cdot e^{-k_2(b-r)} \right]}{\left[e^{k_2(b-a)} - \Gamma_2(k_2, b) \cdot e^{-k_2(b-a)} \right]}.$$

Given that $jk_2 = \alpha + j\beta$ and $\Gamma_2(k_2, b) = [Z_2(k_2, b) - \eta_2] / [Z_2(k_2, b) + \eta_2]$, the magnetic shielding ratio is written as

$$\frac{H_{\phi_1}(k_2, a)}{H_{\phi_1}(k_2, b)} = \frac{1}{2} \sqrt{\frac{b}{a}} \left\{ \frac{Z_2(k_2, b)}{\eta_2} (e^{\alpha a} e^{j\beta a} - e^{-\alpha a} e^{-j\beta a}) + (e^{\alpha a} e^{j\beta a} + e^{-\alpha a} e^{-j\beta a}) \right\}, \quad (2.43)$$

where

$t = (b - a)$, the thickness of the casing

$$Z_2(k_2, b) = j\eta_1 \frac{H_0^{(2)}(k_2, b)}{H_1^{(2)}(k_2, b)}.$$

The ratio in (2.43) is large if either $e^{\alpha a}$ is large or if the quotient $Z_2(k_2, b)/\eta_2$ is large. These two possibilities correspond to the criteria discussed in section 2.6.2. The ratio in (2.43) is also large if, from the combined effects of attenuation and reflection, the *product* of $e^{\alpha a}$ and $Z_2(k_2, b)/\eta_2$ is large.

To demonstrate the relationship between large shielding ratios and the convergence of the exact and approximate solutions, consider the following two cases:

2.6.3.1 Case 1: $t \gg 1/\alpha$

If a wellbore casing thickness t is many times greater than $1/\alpha$ (the skin depth) then the magnetic shielding ratio in (2.43) reduces to

$$\frac{H_{\theta_1}(k_1 a)}{H_{\theta_1}(k_1 b)} \cong \frac{1}{2} \sqrt{\frac{b}{a}} \cdot e^{\omega} e^{j\beta t} \left\{ \frac{Z_2(k_2 b)}{\eta_2} + 1 \right\}. \quad (2.44)$$

Note that even if $|Z_2(k_2 b)|$ is not greater than $|\eta_2|$, the magnitude of the shielding ratio expression in (2.44) will still be large due to the effect of attenuation.

Consider the following example. A power cable carrying a 100 A current at 60 Hz is located at the center of a wellbore casing, as shown in Figure 2-1. The wellbore casing has a relative permeability of 200 and conductivity of 5×10^6 S/m. The inner radius of the casing, a , is 10 mm while the outer radius, b , is 21 mm.

From Table 2-1, the propagation constant, jk_2 , at 60 Hz is $486.7 + j486.7$. Therefore $\alpha = 486.7$ and the skin depth of the casing is approximately 2.1 mm. Therefore the thickness of the casing is approximately five skin depths. Using the definition of η_2 from Table 2-1, the intrinsic impedance of the wellbore casing is found to be $9.73 \times 10^{-3} + j9.73 \times 10^{-3} \Omega$. Using the expression for $Z_2(k_2 b)$ from (2.34) and the values for k_2 and η_2 from Table 2-1, the magnitude of $Z_2(k_2 b)$ is found to be $1.75 \times 10^{-4} \Omega$. Thus, the magnitude of the quotient $Z_2(k_2 b)/\eta_2$ is 1.27.

From (2.43), the magnitude of magnetic shielding ratio in this example is 327.8. The approximate expression for the shielding ratio from (2.44) yields an almost identical value. The relatively large shielding ratio may be attributed almost exclusively to the effect of attenuation. The fact that $|Z_2(k_2 b)|$ is *not* much greater than $|\eta_2|$ indicates that the reflection of the electromagnetic field at the outer wall of the casing does not play a major role in the convergence of the exact and approximate field solutions. In fact the reflection coefficient at $r = b$ in this example is only 0.38.

Since the magnetic shielding ratio is large, the exact and approximate electromagnetic field solutions in this example should be in close agreement. To confirm this assumption, the exact and approximate solutions for the electric and magnetic fields are plotted below in Figure 2-2.

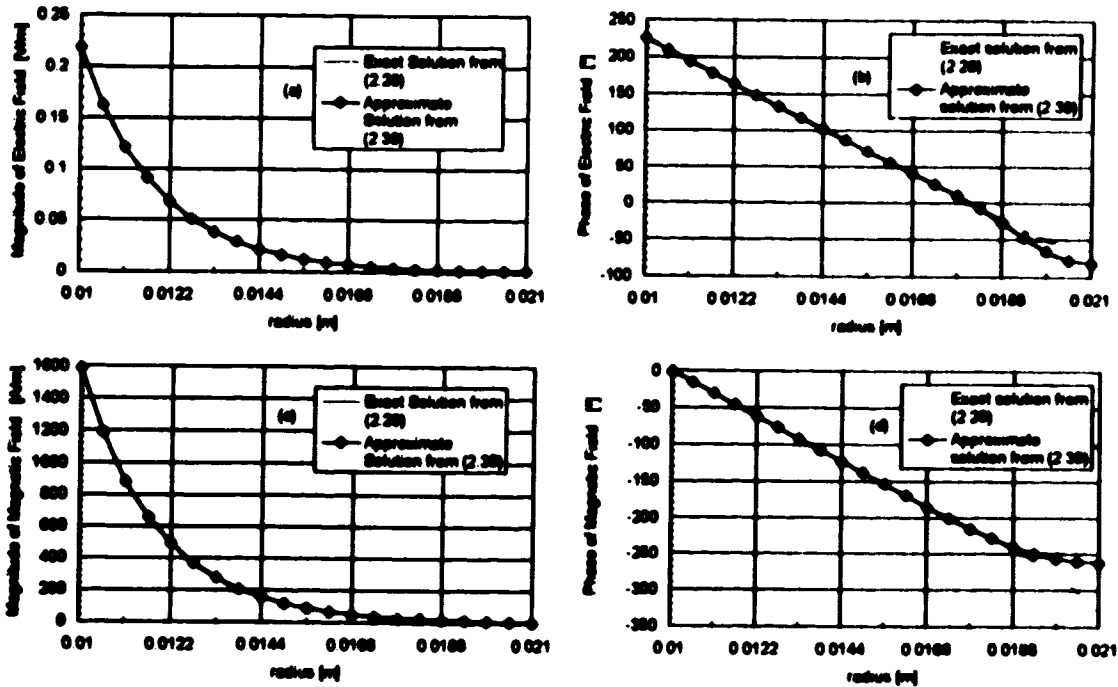


Figure 2-2. Exact and approximate solutions for the electric and magnetic fields in the example in case 1.

2.6.3.2 Case 2: $|Z_2(k_2 b)| \gg |\eta_2|$

With regards to the expression for magnetic shielding in (2.43), if the magnitude of $Z_2(k_2 b)$ is much greater than the magnitude of η_2 then (2.43) reduces to

$$\frac{H_{\phi_1}(k_2 a)}{H_{\phi_1}(k_2 b)} \cong \frac{1}{2} \sqrt{\frac{b}{a}} \frac{Z_2(k_2 b)}{\eta_2} (e^{u_2} e^{-u_1} - e^{-u_2} e^{-u_1}). \quad (2.45)$$

Note that even if the thickness of the casing is much less than one skin depth, the magnitude of the shielding ratio will still be large due to the near total reflection of the electromagnetic field at the outer wall of the casing.

Consider the following example. Once again, a power cable carrying a 100 A current at 60 Hz is located at the center of a wellbore casing, as shown in Figure 2-1. The wellbore casing has a relative permeability of unity and conductivity of 5×10^6 S/m. The inner radius of the casing, a , is 1.730 m while the outer radius, b , is 1.736 m.

From Table 2-1, the propagation constant, jk_2 , at 60 Hz is $34.4 + j34.4$. Therefore $\alpha = 34.4$ and the skin depth of the casing is approximately 29 mm. Therefore the thickness of the casing is approximately 20% of the skin depth. From the definitions of η_2 , η_1 , and k_1 in Table 2-1 and the expression for $Z_2(k_2, b)$ from (2.34), the magnitude of the quotient $Z_2(k_2, b)/\eta_2$ is approximately 1120. The magnitude of the reflection coefficient at $r = b$ is more than 0.998.

From (2.43), the magnitude of magnetic shielding ratio is 327.5. The approximate expression for the shielding ratio from (2.45) yields a value of 327.3. The relatively large shielding ratio is almost exclusively due to the near total reflection of the electromagnetic field at the outer wall of the casing. The effect of attenuation on the magnetic shielding ratio is minimal.

As with the previous example in case 1, the large magnetic shielding ratio in this example should indicate the close agreement between the exact and approximate field solutions. To confirm this assumption, the exact and approximate solutions for the electric and magnetic fields in this example are plotted in Figure 2-3.

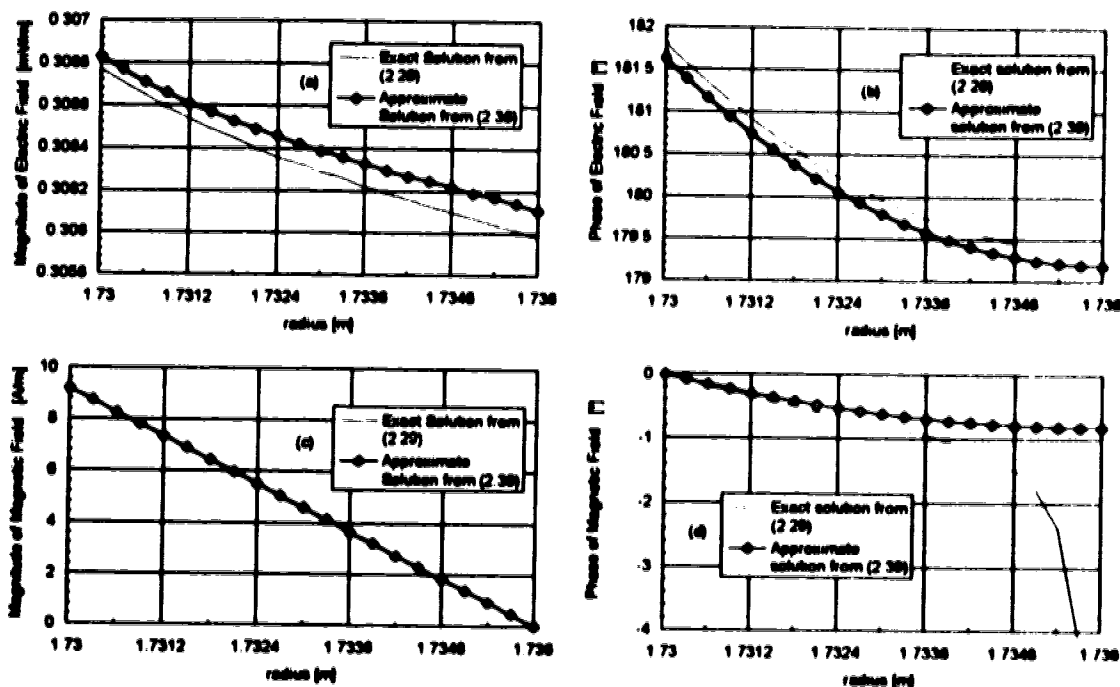


Figure 2-3. Exact and approximate solutions for the electric and magnetic fields in the example in case 2.

In the examples of case 1 and case 2, the exact and approximate solutions are in close agreement despite the fact that the dominant physical process at work in each example is very different. Also, based on results from the above examples, it is clear that a sufficiently large magnetic shielding ratio is a good indication that the exact and approximate field solutions are in close agreement. Consequently, a sufficiently large shielding ratio is also a good indication that the approximation $H_{\phi}(k_2 b) = 0$ is valid. Exactly how large is “sufficiently large” remains to be determined.

2.6.4 Magnetic Shielding Ratios For Typical Steel Wellbore Casings

Some of the casing dimensions and properties in the two examples from the previous section are not indicative of typical casings parameters. Generally, steel casings have an outer radius no greater than 200 mm and are less than 15 mm thick. The relative magnetic permeability of most steel casings is less than 150.

Dimensions and electromagnetic properties which are more representative of typical wellbore casings are available from the paper by Stroemich, Vermeulen, Chute and Sumbar [3]. Included in this paper are measurements of casing dimensions as well as the conductivities and relative permeabilities for several samples of wellbore casings. These measurements are presented here in Table 2-3.

Table 2-3. Dimensions and electromagnetic properties for various samples of wellbore casings (adapted from Table 1 of Reference [3]).

Sample #	Pipe type	Inner radius 'a' [mm]	Outer radius 'b' [mm]	Region 2 μ_r	σ_2 [S/m]
1	J-55	31.31	36.83	94	4.83×10^6
2	J-55	63.95	69.98	125	4.90×10^6
3	J-55	102.74	110.11	90	4.29×10^6
4	K-55	52.20	57.34	87	4.59×10^6
5	K-55	63.12	70.36	85	4.37×10^6
6	K-55	103.25	110.36	90	4.63×10^6
7	L-80	61.60	70.23	61	4.69×10^6
8	L-80	80.77	89.41	48	3.85×10^6

By using the definitions of η_2 , η_1 , k_2 and k_1 from Table 2-1 and the expression for $Z_2(k_2, b)$ from (2.34), the magnetic shielding ratio can be calculated for each casing sample in Table 2-3. The shielding ratios are calculated using (2.43) and are presented in Table 2-4, along with the ratios of casing thickness to skin depth and the ratios of $|Z_2(k_2, b)|$ to $|\eta_2|$.

Table 2-4. Magnetic shielding ratios for typical casing samples

Sample #	$\frac{\text{casing thickness}}{\text{skin depth}}$	$\frac{ Z_1(k,b) }{ \eta_2 }$	$\frac{ H_{\phi_1}(k,a) }{ H_{\phi_1}(k,b) }$
1	1.8	3.1	21.0
2	2.3	5.0	30.1
3	2.2	8.4	44.2
4	1.6	4.8	14.6
5	2.2	5.7	29.6
6	2.2	8.7	46.0
7	2.2	7.0	39.3
8	1.8	8.9	31.8

2.6.5 The Minimum Magnetic Shielding Ratio For Which the Approximation $H_{\phi_1}(k,b) = 0$ Is Justified

As mentioned earlier, a sufficiently large magnetic shielding ratio is a good indication that the approximation $H_{\phi_1}(k,b) = 0$ is valid. However, there still remains the question as to what is a “sufficiently large” shielding ratio. The intent of this section is to demonstrate that a magnetic shielding ratio of approximately 30 is the minimum shielding ratio for which the approximation $H_{\phi_1}(k,b) = 0$ is justified. The decision to set the minimum acceptable shielding ratio at 30 is based on empirical data presented in this section and later chapters.

It has already been demonstrated in the two examples from sections 2.6.3.1 and 2.6.3.2 that a magnetic shielding ratio much greater than 30 is evidence that $H_{\phi_1}(k,b) = 0$ is a valid approximation. Consider two more examples where the relationship between the magnetic shielding ratio and the $H_{\phi_1}(k,b) = 0$ approximation is explored.

In the first example, a power cable carrying a 25 A current at 60 Hz is located at the center of a wellbore casing, as shown in Figure 2-1. The wellbore casing has a relative permeability of 40 and a conductivity of 10^6 S/m. The inner radius of the casing, a , is 0.085 m while the outer radius, b , is 0.090 m. According to the formula from (2.43), the wellbore casing in this example has a magnetic shielding ratio magnitude of 3.9. As a result of such a low shielding ratio, relatively poor agreement between the exact and approximate solutions is to be expected; furthermore, $H_{\phi}(k, b) = 0$ is likely to be a poor approximation for the magnetic field boundary condition at $r = b$. To confirm these expectations, the exact and approximate solutions for the electric and magnetic fields are plotted below in Figure 2-4.

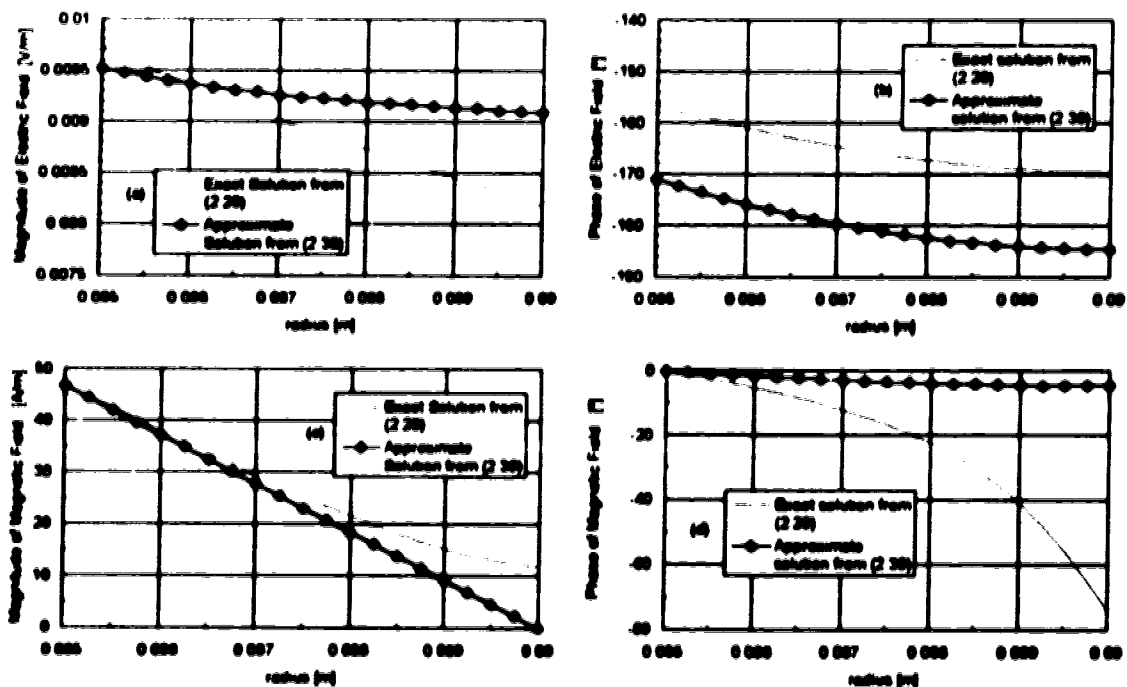


Figure 2-4. Exact and approximate solutions for the electric and magnetic fields inside a wellbore casing with a magnetic shielding ratio magnitude $\ll 30$.

In a second example, a power cable carrying a 25 A current at 60 Hz is again located at the center of a wellbore casing, as shown in Figure 2-1. The parameters of the wellbore casing are those of sample 2 in Table 2-3. The magnitude of the magnetic shielding ratio for this casing is 30.1. This example illustrates the degree of convergence between the exact and approximate field solutions and the validity of the $H_{\phi}(k,b) = 0$ approximation when the magnitude of the shielding ratio is close to 30. The exact and approximate solutions for the electric and magnetic fields are plotted below in Figure 2-5.

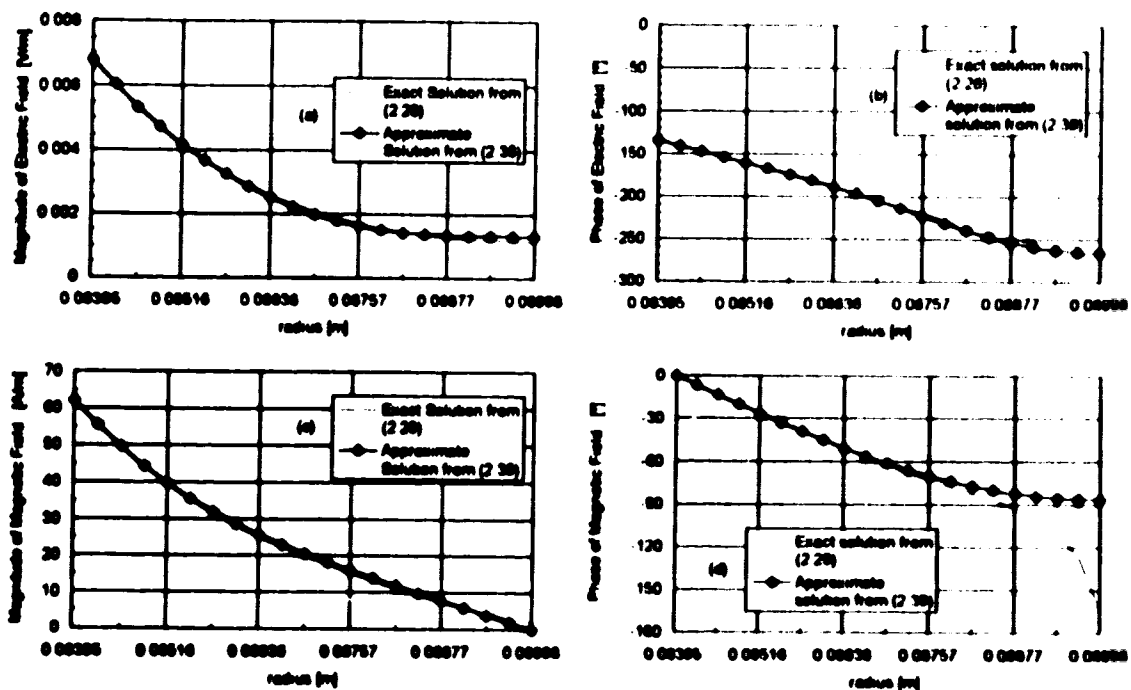


Figure 2-5. Exact and approximate solutions for the electric and magnetic fields inside a wellbore casing with a magnetic shielding ratio magnitude ≈ 30 .

On the basis of Figure 2-5, as well as comparisons of exact and approximate solutions to be presented later in chapter 4, the following statement is made: *for boundary value problems described by Figure 2-1, a convenient guideline for deciding if $H_{\phi}(k,b) = 0$ is a valid boundary condition is to check whether the magnitude of the magnetic shielding ratio is greater than 30. Admittedly, this guideline is relatively crude; however, it will be seen in later chapters that a magnetic shielding ratio > 30 does indeed give adequate indication that the approximation $H_{\phi}(k,b) = 0$ is valid.*

2.7 The Effects of Attenuation and Reflection in Magnetic and Non-Magnetic Casings

Although a large magnetic shielding ratio usually arises due to a combination of attenuation and reflection effects, there are certain circumstances where one effect is more pronounced than the other. For example, in casings constructed of a magnetic material such as steel, large shielding ratios are primarily due to the *attenuation* of electromagnetic waves within the casing. Conversely, in casings constructed of a non-magnetic material such as copper or aluminum, large shielding ratios are primarily due to the *reflection* of electromagnetic waves at the outer wall of the casing.

The relative permeability of ferromagnetic wellbore casings generally range from 50 to 150 or higher. Thus the relative permeability of ferromagnetic casings is at least 50 times that of non-magnetic casings. Given that skin depth is proportional to $1/\sqrt{\mu}$, ferromagnetic casings will have skin depths at least 7 times smaller than those for non-magnetic casings, which have a relative permeability of unity. Consequently, electromagnetic waves propagating through a magnetic casing will experience a much higher degree of attenuation than waves propagating through a non-magnetic casing of similar dimensions and electrical conductivity. Conversely, the degree of reflection experienced by electromagnetic waves in magnetic casings is generally less than that experienced by waves in non-magnetic casings. This is because the ratio of $|Z_2(k,b)/\eta_2|$ is $\sqrt{\mu_{relative}}$ times smaller for magnetic casings than for non-magnetic casings, since η_2 is proportional to $\sqrt{\mu}$.

2.8 Summary

Much of this chapter has been devoted to solving for the electromagnetic fields induced inside the wellbore casing illustrated in Figure 2-1. This problem is viewed from the perspective of uniform, cylindrical electromagnetic waves propagating radially through the wellbore casing. The solutions for the electric and magnetic fields in the casing are expressed in terms of the wave impedance at the outer wall of the casing, $Z_2(k,b)$, and the reflection coefficient at the outer wall, $\Gamma_2(k,b)$. Parameters such as wave impedance and reflection coefficients are normally used in the analysis of transmission line and waveguide problems; for the problem in this chapter, however, they have been adapted for use in analyzing the propagation of uniform, cylindrical waves in linear, homogeneous media.

The solution for the electric field in the wellbore casing is given by the expression from (2.28):

$$E_{z_2}(k_2, r) = -\eta_2 \cdot \frac{I}{2\pi\sqrt{a}} \cdot \frac{1}{\sqrt{r}} \cdot \left[\frac{e^{\mu_2(h-r)} + \Gamma_2(k_2, h) \cdot e^{-\mu_2(h-r)}}{e^{\mu_2(h-a)} - \Gamma_2(k_2, h) \cdot e^{-\mu_2(h-a)}} \right],$$

where

$$\Gamma_2(k_2, h) = \frac{Z_2(k_2, h) - \eta_2}{Z_2(k_2, h) + \eta_2}$$

and

$$Z_2(k_2, h) = j\eta_1 \frac{H_0^{(2)}(k_1, h)}{H_1^{(2)}(k_1, h)}$$

Similarly, the solution for the magnetic field in the wellbore casing is given by the expression from (2.29):

$$H_{\phi_2}(k_2, r) = \frac{I}{2\pi\sqrt{a}} \cdot \frac{1}{\sqrt{r}} \cdot \left[\frac{e^{\mu_2(h-r)} - \Gamma_2(k_2, h) \cdot e^{-\mu_2(h-r)}}{e^{\mu_2(h-a)} - \Gamma_2(k_2, h) \cdot e^{-\mu_2(h-a)}} \right]$$

The analytical solutions derived in this chapter for the electric and magnetic fields in the wellbore casing will be used to verify the accuracy of *finite element method* solutions in later chapters. Because the finite element method solutions in this thesis are based on an approximate boundary condition for the magnetic field at the outer wall of the casing, it is important to know when this approximate boundary condition is valid. In fact, the main objective of this chapter has been to determine the conditions under which it is appropriate to substitute the approximate boundary condition, $H_{\phi_2}(k_2, h) = 0$, for the exact boundary conditions at the outer wall of the wellbore casing.

A convenient, though somewhat crude, guideline for deciding if $H_{\phi}(k_2 h) = 0$ is a valid boundary condition is to check whether the magnitude of the magnetic shielding ratio for a given casing is greater than 30. The formula for the magnetic shielding ratio is given in (2.43). This ratio is dependent upon two physical processes which affect electromagnetic waves within the wellbore casing: the attenuation of the waves as they propagate through the casing and the reflection of the waves at the outer wall of the casing. In circumstances where the casing thickness is much greater than one skin depth or the reflection coefficient at the outer wall of the casing is close to unity, then the magnetic shielding ratio for the casing will be very large; consequently $H_{\phi}(k_2 h) = 0$ will be an excellent approximation for the magnetic field at the outer wall of the casing.

CHAPTER 3

The Total Current and Power Dissipated in a Wellbore Casing Centered About a Single Power Cable

Consider the boundary value problem illustrated in Figure 2-1. Having obtained an expression for the electric field in the steel casing, it is a relatively simple matter to determine the eddy current density and the total current induced in the casing. In addition, it is possible to derive an expression for the power dissipated in the casing due to the flow of eddy currents. The analytical expressions derived in this chapter will be used in the following chapter to verify the accuracy of finite element solutions for the total current and resistive power dissipated in the wellbore casing illustrated in Figure 2-1

3.1 Eddy Current Density and the Total Current Induced in the Wellbore Casing

From Ohm's law, the eddy current density in the steel casing, $\vec{J}_2(r)$, is simply the electric field in the casing multiplied by the conductivity of the steel casing. Therefore,

$$\vec{J}_2(r) = \sigma_2 \vec{E}_2(r). \quad (3.1)$$

Substituting (2.14a), the general solution for the electric field in region 2, into (3.1) yields

$$\begin{aligned} \vec{J}_2(r) &= \sigma_2 E_{z_2}(k_2 r) \hat{a}_z \\ &= \sigma_2 [K_2 H_0^{(2)}(k_2 r) + K_2' H_0^{(1)}(k_2 r)] \hat{a}_z. \end{aligned} \quad (3.2)$$

To obtain the total current in the steel casing, it is simply a matter of integrating the eddy current density over the cross sectional area of the casing.

$$\begin{aligned} I_{\text{casing}} &= \int_0^{2\pi} \int_a^b J_2(r) r dr d\phi \\ &= \int_0^{2\pi} \int_a^b J_2(r) r dr d\phi. \end{aligned} \quad (3.3)$$

Referring to Figure 2-1, a and b are the inner and outer radii of the wellbore casing. Substituting the expression for $J_2(r)$ from (3.2) into (3.3) and integrating yields the total current induced the steel casing:

$$I_{casing} = E_2 \cdot \frac{2\pi\sigma}{k_2} \left(\left[b H_1^{(2)}(k_2 b) - a H_1^{(2)}(k_2 a) \right] + \frac{E_2}{E_2} \left[b H_1^{(1)}(k_2 b) - a H_1^{(1)}(k_2 a) \right] \right). \quad (3.4)$$

Next, the asymptotic formulae from (2.16), the expression for E_2 / E_2 , from (2.22) and the expression for E_2 , from (2.27) are all substituted into (3.4); this yields a final expression for the total current induced in the casing:

$$I_{steel} = -I \left(1 - \sqrt{\frac{b}{a}} \frac{[1 - \Gamma_2(k_2 b)]}{[e^{\mu_2(b-a)} - \Gamma_2(k_2 b) \cdot e^{-\mu_2(b-a)}]} \right). \quad (3.5)$$

3.2 The Total Displacement Current Induced in Region 3

As an aside, the current induced in region 3 can also be calculated. Since region 3 is virtually lossless, the current in region 3 is almost completely in the form of displacement current. This displacement current is calculated from the integral

$$I_3 = \int_0^{2\pi} \int_b^{\infty} j\omega\epsilon_3 E_3(k, r) r dr d\phi. \quad (3.6)$$

Substituting (2.32a), the general solution for the electric field in region 3, into (3.6) yields

$$I_3 = j\omega\epsilon_3 E_3 \int_0^{2\pi} \int_b^{\infty} H_0^{(2)}(k, r) r dr d\phi. \quad (3.7)$$

Evaluating the integral in (3.7) yields

$$I_3 = 2\pi \cdot j\omega\epsilon_3 \cdot E_3 \cdot \int_b^{\infty} \frac{r}{k_3} H_1^{(2)}(k, r). \quad (3.8)$$

If region 3 is even slightly lossy, then (3.8) reduces to

$$\begin{aligned} I_3 &= 2\pi \cdot j\omega\epsilon_1 \cdot E_{z_1} \left[0 - \frac{h}{k_1} H_1^{(2)}(k_1, h) \right] \\ &= -2\pi h \frac{j\omega\epsilon_1}{k_1} E_{z_1} H_1^{(2)}(k_1, h). \end{aligned} \quad (3.9)$$

The single unknown constant E_{z_1} in (3.9) can be easily calculated as follows. From boundary condition (2b),

$$H_{\theta_1}(k_1, h) = H_{\theta_2}(k_2, h).$$

From (2.32b), the magnetic field in region 3 at $r = h$ is

$$H_{\theta_1}(k_1, h) = \frac{-E_{z_1}}{j\eta_1} H_1^{(2)}(k_1, h) \quad (3.10)$$

and from (2.29), the magnetic field in region 2 at $r = h$ is

$$H_{\theta_2}(k_2, h) = \frac{I}{2\pi\sqrt{a}} \cdot \frac{1}{\sqrt{h}} \cdot \frac{[1 - \Gamma_2(k_2, h)]}{[e^{\mu_2(h-a)} - \Gamma_2(k_2, h) \cdot e^{-\mu_2(h-a)}]} \quad (3.11)$$

Substituting (3.10) and (3.11) into boundary condition (2b) and solving for E_{z_1} yields

$$E_{z_1} = \frac{-j\eta_1}{H_1^{(2)}(k_1, h)} \frac{I}{2\pi\sqrt{a}} \cdot \frac{1}{\sqrt{h}} \cdot \frac{[1 - \Gamma_2(k_2, h)]}{[e^{\mu_2(h-a)} - \Gamma_2(k_2, h) \cdot e^{-\mu_2(h-a)}]} \quad (3.12)$$

Finally, substituting the above expression for E_{z_1} into (3.9) yields a final expression for the total displacement current in region 3:

$$I_3 = -I \sqrt{\frac{h}{a}} \frac{[1 - \Gamma_2(k_2, h)]}{[e^{\mu_2(h-a)} - \Gamma_2(k_2, h) \cdot e^{-\mu_2(h-a)}]} \quad (3.13)$$

3.3 The Path of the Return Current

In the description of the boundary value problem illustrated in Figure 2-1, no mention was made of the path by which the current in the central cable returns to its source. In fact, there are no prior assumptions regarding the path of the return current in this

problem, although the path can be influenced by phenomena which affect the propagation of electromagnetic waves in the wellbore casing, such as attenuation and reflection.

For example, if $\Gamma_2(k, b) = 1$ then, according to equation (3.5), the total current induced in the casing is equal in magnitude and 180° out of phase with the current in the center power cable; also, the total displacement current outside the casing is zero, according to equation (3.13). In other words, if $\Gamma_2(k, b) = 1$ then the path of the return current is confined entirely inside the casing.

As an aside, the statement $\Gamma_2(k, b) = 1$ is equivalent to the boundary condition $H_{\phi_2}(k, b) = 0$. This was discussed in section 2.5.2.2. Recall that $H_{\phi_2}(k, b) = 0$ results in $Z_2(k, b) = -\infty$. This, in turn, results in $\Gamma_2(k, b) = 1$ according to equation (2.37).

In actual situations where $|\Gamma_2(k, b)| < 1$, a displacement current does exist in region 3 and constitutes a portion of the return current. The conduction current in the wellbore casing and the displacement current in region 3 constitute the total return current in the problem. This is apparent when the solution for I_{casing} from (3.5) is added to the solution for I_3 from (3.13): $I_{\text{casing}} + I_3 = -I$.

In circumstances where the thickness of the casing is much greater than one skin depth, most of the return current is again confined to the wellbore casing. This conclusion is apparent if one considers the effect of the exponential term $e^{\beta_2(b-a)}$ in (3.5) and (3.13) when the magnitude of $e^{\beta_2(b-a)}$ becomes very large.

3.4 Power Dissipated in Casing by Eddy Currents

The power dissipated in the casing due to resistive heating by the flow of eddy currents can be calculated from Poynting's theorem. The resistive power loss in the casing may be found by evaluating

$$\begin{aligned} P_{\text{loss}} &= \frac{\sigma_2}{2} \int_{\text{Volume}} |\mathbf{E}_2|^2 dV \\ &= \frac{\sigma_2}{2} \int_0^{2\pi} \int_a^b \int_{-l}^l |E_{z_2}(k, r)|^2 dz r dr d\phi, \end{aligned} \quad (3.14)$$

where σ_2 is the conductivity of the steel, $E_{z_2}(k, r)$ is the electric field in the steel casing, 'a' and 'b' are the inner and outer radii of the casing and l is the length of the casing.

Substituting (2.28), the solution for the electric field in region 2, into (3.14) yields

$$\begin{aligned}
 P_{\text{loss}} &= \frac{\sigma_2}{2} \int_0^{2\pi} \int_0^h \int_0^a \left| -\eta_2 \cdot \frac{l}{2\pi\sqrt{a}} \cdot \frac{1}{\sqrt{r}} \cdot \frac{\left[e^{\alpha(b-r)} e^{j\beta(b-r)} + \Gamma_2(k_2, h) \cdot e^{-\alpha(b-r)} e^{-j\beta(b-r)} \right]}{\left[e^{\alpha(b-a)} e^{j\beta(b-a)} - \Gamma_2(k_2, h) \cdot e^{-\alpha(b-a)} e^{-j\beta(b-a)} \right]} \right|^2 dz r dr d\phi \\
 &= \sigma_2 \pi l \int_0^a \left| -\eta_2 \cdot \frac{l}{2\pi\sqrt{a}} \cdot \frac{1}{\sqrt{r}} \cdot \frac{\left[e^{\alpha(b-r)} e^{j\beta(b-r)} + \Gamma_2(k_2, h) \cdot e^{-\alpha(b-r)} e^{-j\beta(b-r)} \right]}{\left[e^{\alpha(b-a)} e^{j\beta(b-a)} - \Gamma_2(k_2, h) \cdot e^{-\alpha(b-a)} e^{-j\beta(b-a)} \right]} \right|^2 r dr. \quad (3.15)
 \end{aligned}$$

Evaluating the integral of (3.15) yields

$$P_{\text{loss}} = \sigma_2 l \frac{|\eta_2 l|^2}{4\pi a} \frac{\left(\frac{1}{2\alpha} \left[|\Gamma_2(k_2, h)|^2 - 1 \right] + \frac{1}{2\alpha} \left[e^{2\alpha} - |\Gamma_2(k_2, h)|^2 e^{-2\alpha} \right] + \frac{1}{\beta} \cdot \text{Im}\{\Gamma_2(k_2, h)\} - \frac{1}{\beta} \cdot \left[\cos(2\beta h) \cdot \text{Im}\{\Gamma_2(k_2, h)\} - \sin(2\beta h) \cdot \text{Re}\{\Gamma_2(k_2, h)\} \right] \right)}{\left| e^{\alpha} e^{j\beta} - \Gamma_2(k_2, h) \cdot e^{-\alpha} e^{-j\beta} \right|^2}, \quad (3.16)$$

where α and β , the attenuation and phase constants, are obtained from the propagation constant, $jk_2 = \alpha + j\beta$. Dividing both sides of (3.16) by the length of the casing, l , yields the power dissipated per unit length of casing.

CHAPTER 4

A Finite Element Method Solution For the Electromagnetic Fields in a Steel Casing

As discussed in the introduction, the *finite element method* (FEM) is a numerical method for solving boundary value problems. An in-depth discussion of the theory behind the finite element method is somewhat beyond the scope of this work. It should suffice to say that the finite element method is an accepted numerical method, capable of solving many types of boundary value problems.

The emphasis of this chapter is on the *solutions* obtained from the finite element method rather than the finite element method itself. Once the dimensions, physical properties and boundary conditions of the problem are assigned numerical values, a FEM solution may be computed which will yield the electric and magnetic field intensities in the wellbore casing. This FEM solution can be compared with the analytic solution derived in chapter 2 for simple problems where the power cable is at the center of the casing. For problems where the cable is positioned off center or if multiple cables are present, the FEM solution may be compared with solutions published in the literature.

4.1 Computing a Finite Element Method Solution Using UNAFEM II

For problems of even moderate complexity, a vast amount of numerical work is usually required to obtain a FEM solution. Consequently, computers are a virtual necessity when dealing with most problems. In fact, with only minor changes to the code, a single computer program can be adapted to solve a variety of boundary value problems using the finite element method. Only data concerning the boundary conditions, the differential equation and the domain specific to each problem would need to be changed.

The computer program to be used in this work for calculating FEM solutions is the UNAFEM II program. UNAFEM II is based on an earlier program known simply as UNAFEM which was written by W. J. Denkmann and D.S. Burnett at AT&T Laboratories. The code for UNAFEM was published as an instructional aid in the text *Finite Element Analysis* by D. S. Burnett. Later, this code was modified by E. Sumbur at the University of Alberta for use in solving electromagnetic boundary value problems and renamed UNAFEM II.

4.1.1 Boundary Value Problems Solvable by UNAFEM II

UNAFEM II can compute a FEM solution for any boundary value problem provided it meets the following requirements:

1. The partial differential equation for the boundary value problem must be of the form given in (4.1):

$$-\frac{\partial}{\partial x} \left\{ \alpha_x(x,y) \frac{\partial U(x,y)}{\partial x} \right\} - \frac{\partial}{\partial y} \left\{ \alpha_y(x,y) \frac{\partial U(x,y)}{\partial y} \right\} + \beta(x,y)U(x,y) = 0. \quad (4.1)$$

This is the actual differential equation which is solved by UNAFEM II. The coefficients $\alpha_x(x,y)$, $\alpha_y(x,y)$ and $\beta(x,y)$ must also be written in the following form:

$$C(x,y) = c_1 + c_2x + c_3x^2 + c_4y + c_5y^2 + c_6xy + c_7 \frac{1}{x}, \quad (4.1a)$$

where c_1, c_2, \dots, c_7 are complex numerical constants. Note that $U(x,y)$ is *NOT* restricted to the form of equation (4.1a). Also note there is no $1/y$ term in (4.1a). If the coefficients $\alpha_x(x,y)$, $\alpha_y(x,y)$ and $\beta(x,y)$ cannot be written in the form of (4.1a) then the problem cannot be solved by UNAFEM II.

2. The appropriate boundary conditions of the boundary value problem must be known. The boundary conditions may be either Dirichlet or Neumann. In other words, values for either U or $-\alpha_x \cdot \partial U / \partial x$ and $-\alpha_y \cdot \partial U / \partial y$ must be known at the boundaries of the problem.

4.1.2 UNAFEM II Input

UNAFEM II requires the following input to compute a FEM solution:

1. UNAFEM II requires the constants c_1, c_2, \dots, c_7 , as defined in (4.1a), for each of the coefficients α_x , α_y , and β in the partial differential equation (4.1). If the boundary value problem is composed of several regions with different material properties, each region will have a different set of constants. To obtain all the necessary constants, the partial differential equation for the problem is written in the same form as (4.1). Then, the constants c_1, c_2, \dots, c_7 are extracted from the factors in the equation which correspond to α_x , α_y , and β .

2. UNAFEM II requires the coordinates for each node in the mesh that models the problem domain. For one dimensional problems, the domain is simply divided into a series of line segments. For two dimensional problems, the domain is mapped out by a grid or mesh composed of triangular or rectangular elements.
3. UNAFEM II requires the boundary conditions of the problem. The value of a given boundary condition is specified at discrete points (i.e., nodes) which coincide with the location of the boundary condition. The boundary condition must be in terms of either $U(x,y)$ or the sum of $-\alpha_x \partial U / \partial x \hat{a}_x \cdot \hat{n}$ and $-\alpha_y \partial U / \partial y \hat{a}_y \cdot \hat{n}$, where \hat{n} is a unit vector normal to the boundary in question. These are the Dirichlet and Neumann boundary conditions respectively.

4.2 A Finite Element Method Solution for a One Dimensional Boundary Value Problem

In chapter 2, an analytical solution was obtained for the electromagnetic fields in the simple, one dimensional boundary value problem illustrated in Figure 2-1. Henceforth, that simple, one dimensional boundary value problem illustrated in Figure 2-1 shall be referred to as problem 1. In this chapter, a FEM solution for the electromagnetic fields in problem 1 will be computed. The resulting FEM solution for the fields in the wellbore casing will be compared with the analytical solutions obtained in chapter 2.

To obtain a FEM solution for problem 1, numerical values must be assigned to the physical dimensions and electromagnetic properties of the problem. Referring to Figure 2-1, the radius of the power cable, r_{cable} , typically may vary from 5 mm to 30 mm. The dimensions a and b are determined by the inner and outer radii of the wellbore casing. Dimensions for several samples of wellbore casings are available from Table 2-3 in chapter 2.

The electromagnetic properties of regions 1 and 3 are those for free space, namely $\epsilon_{1,3} = \epsilon_0$, $\mu_{1,3} = \mu_0$ and $\sigma_{1,3} = 0$. The properties of region 2 are dependent on the wellbore casing. Properties for several samples of wellbore casings are, again, available from Table 2-3 in chapter 2. In general, there is considerable variation in conductivity and magnetic permeability between different types of casings. Even samples of the same type of casing may have widely varying electromagnetic properties.

In addition to physical dimensions and electromagnetic properties, the magnitude, phase and frequency of the current in the power cable must be specified. For the FEM solutions calculated in this chapter, the current in the power cable is approximately 25 A rms at a phase angle of 180° (i.e., the current flows in the -z direction, down the wellbore). The frequency of the current is 60 Hz.

The dimensions and properties of each casing sample listed in Table 2-3 will be substituted for the variables a , b , μ_2 , and σ_2 in problem 1. Thus, for each sample, a new FEM solution will be computed for the electromagnetic fields in problem 1. The decision to analyze casing samples from Table 2-3 will enable portions of the FEM solutions to be compared with experimental results published in reference [3] and with analytical solutions derived in chapters 2 and 3.

4.2.1 The Partial Differential Equation for Problem 1

The first step in obtaining a FEM solution for problem 1 is to write the governing partial differential equation for the problem and extract the constant coefficients required by UNAFEM II. From (2.4), the differential equation describing the electric field intensity in an arbitrary region N is

$$-\left(\frac{\partial^2 E_{zN}}{\partial r^2} + \frac{1}{r} \frac{\partial E_{zN}}{\partial r}\right) \mathbf{a}_r = -j\omega\mu_N (\sigma_N + j\omega\epsilon_N) \vec{E}_{zN}.$$

The above equation may be rewritten in same form as (4.1):

$$-\frac{\partial}{\partial r} \left(\frac{-r}{j\omega\mu_N} \cdot \frac{\partial E_{zN}}{\partial r} \right) + (-r[\sigma_N + j\omega\epsilon_N]) E_{zN} = 0. \quad (4.2)$$

Thus, the differential equation for the boundary value problem is now in the form which UNAFEM II uses to compute a FEM solution.

The terms in (4.2) which correspond to α_x , α_y , and β in (4.1) are

$$\alpha_x(x, y) \Rightarrow \frac{-r}{j\omega\mu_N}, \quad (4.2a)$$

$$\alpha_y(x, y) \Rightarrow 0, \quad (4.2b)$$

and
$$\beta(x, y) \Rightarrow -r[\sigma_N + j\omega\epsilon_N], \quad (4.2c)$$

where x corresponds to r and y corresponds to ϕ . Note that there is no actual ϕ dependence in equation (4.2) and therefore $\alpha_x(x, y)$ and $\beta(x, y)$ are technically functions of x (i.e., r) only. The constants c_1, c_2, \dots, c_7 , as defined in (4.1a), may be extracted from the coefficients in (4.2a-c). For $\alpha_x(x, y)$, the only non-zero constant is c_2 , which corresponds to $j/\omega\mu_N$. For $\alpha_y(x, y)$ all the constants are zero ($\alpha_y(x, y)$ does not exist in the one dimensional equation). For $\beta(x, y)$ the only non-zero constant is c_2 , which corresponds to $(-\sigma_N - j\omega\epsilon_N)$. Since σ_N and μ_N vary from region to region, the constants for α_x , and β will also vary from region to region.

4.2.2 Mapping the Domain of Problem I for UNAFEM II

Since problem I is a one dimensional azimuthally symmetric problem, the solution is a function of the r coordinate only. Therefore the domain of the problem need only be modeled in the radial direction at an arbitrary angle ϕ . This is shown below in Figure 4-1. A radial section of the domain is modeled from the surface of the power cable out to the outer wall of the wellbore casing. It is along this radial section that UNAFEM II will compute a solution for the electric and magnetic fields.

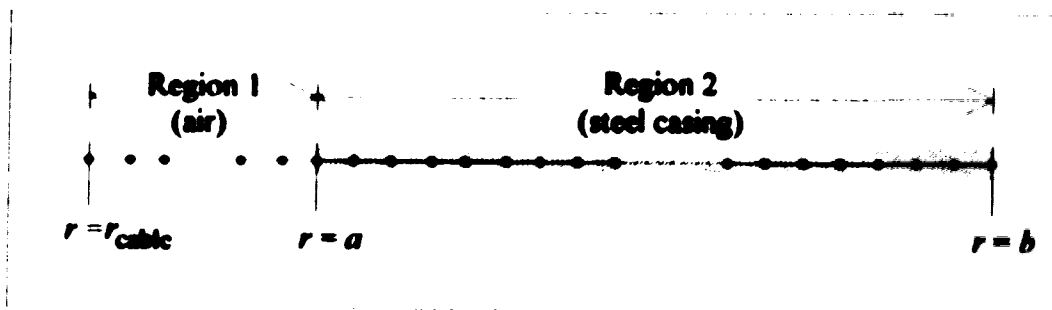


Figure 4-1. A radial section of the domain of problem I.

4.2.3 Boundary Conditions

To solve problem I using the finite element method, it was stated in the introduction that an approximate boundary condition, namely $H_{\phi_s}(k, h) = 0$, needs to be imposed at the outer wall of the casing. This avoids the problem of modeling the radially infinite region beyond the outer wall of the casing. In chapter 2 it was demonstrated that, in circumstances where the magnitude of the magnetic shielding ratio is greater than 30, a solution based on the approximate boundary condition will be nearly equal to a solution based on the exact boundary conditions.

The magnetic shielding ratios for the casings listed in Table 2-3 have already been calculated in chapter 2 and are available from Table 2-4. For samples 1 and 4, the magnetic shielding ratio magnitude is less than 30; in these instances $H_{\phi_s}(k, h) = 0$ is a poor approximation for the exact boundary conditions at $r = h$. The FEM solutions for the electromagnetic fields in these casing samples may differ considerably from the exact, analytical solutions.

A boundary condition is also required at the inner boundary of the domain of the problem, i.e., at the surface of the power cable in region I. Here the boundary condition is given by

$$H_{\phi_s}(k, r_{\text{cable}}) = \frac{I}{2\pi r_{\text{cable}}}. \quad (4.3)$$

This is essentially the same boundary condition that was used to derive the analytic solution in chapter 2, $H_{\phi_s}(k, a) = I/2\pi a$. The only difference between $H_{\phi_s}(k, r_{\text{cable}})$ and $H_{\phi_s}(k, a)$ is a small contribution to the magnetic field from the displacement current in region I. The magnetic field created by the displacement current in region I is negligible compared to the field generated by the conduction current in the power cable.

Recall that UNAFEM II can only interpret boundary conditions in terms of U or the component of $-\left[\alpha_x \partial U / \partial x \hat{a}_x + \alpha_y \partial U / \partial y \hat{a}_y\right]$ normal to the boundary in question. Therefore, to relate the magnetic field boundary conditions in problem I to UNAFEM II, a correspondence between $H_{\phi_s}(k, r)$ and U or $-\left[\alpha_x \partial U / \partial x \hat{a}_x + \alpha_y \partial U / \partial y \hat{a}_y\right] \cdot \hat{n} \Rightarrow r H_{\phi_s}$ must be established. In fact, it will now be shown that $-\left[\alpha_x \partial U / \partial x \hat{a}_x + \alpha_y \partial U / \partial y \hat{a}_y\right] \cdot \hat{n} \Rightarrow r H_{\phi_s}$,

Since $\alpha_y \partial U / \partial y = 0$ in this problem, $-\left[\alpha_x \partial U / \partial x \hat{a}_x + \alpha_y \partial U / \partial y \hat{a}_y\right]$ reduces to $-\alpha_x \partial U / \partial x \hat{a}_x$. By comparing the differential equation solved by UNAFEM II in (4.1) with the differential equation for problem I as written in (4.2), it is apparent that

$$-\alpha_x \partial U / \partial x \hat{a}_x \Rightarrow \frac{r}{j\omega\mu_2} \frac{\partial H_{z1}}{\partial r} \hat{a}_r \quad (4.4)$$

Furthermore, according to (2.6), the term on the right hand side of (4.4) may be rewritten as

$$-\alpha_x \partial U / \partial x \hat{a}_x \Rightarrow r H_{\phi}(r) \hat{a}_r \quad (4.5)$$

Finally, since \hat{a}_r is normal to both the boundary at the surface of the power cable in region I and the boundary at outer wall of the casing,

$$\begin{aligned} -\alpha_x \partial U / \partial x \hat{a}_x \cdot \hat{a}_r &\Rightarrow r H_{\phi}(r) \hat{a}_r \cdot \hat{a}_r \\ &\Rightarrow r H_{\phi}(r) \end{aligned} \quad (4.6)$$

Thus, the UNAFEM II boundary conditions at $r = r_{cable}$ and $r = b$ are

$$-\alpha_x \partial U / \partial x \hat{a}_x \cdot \hat{a}_r \Big|_{r=r_{cable}} \Rightarrow \frac{I}{2\pi} \quad (4.6a)$$

and
$$-\alpha_x \partial U / \partial x \hat{a}_x \cdot \hat{a}_r \Big|_{r=b} \Rightarrow 0. \quad (4.6b)$$

4.3 Comparison of FEM Solution with Analytic and Published Solutions

Having defined the inner and outer boundary conditions, as well as the material properties and dimensions of the problem, the data is conveyed to UNAFEM II and a numerical solution is generated.

4.3.1 The Electric and Magnetic Fields

The FEM solutions for $E_z(r)$ and $H_{\phi}(r)$ are plotted in Figures 4-2 to 4-9. Also shown for comparison are the exact analytical solutions for the electric and magnetic fields in the casing, as described by (2.28) and (2.29).

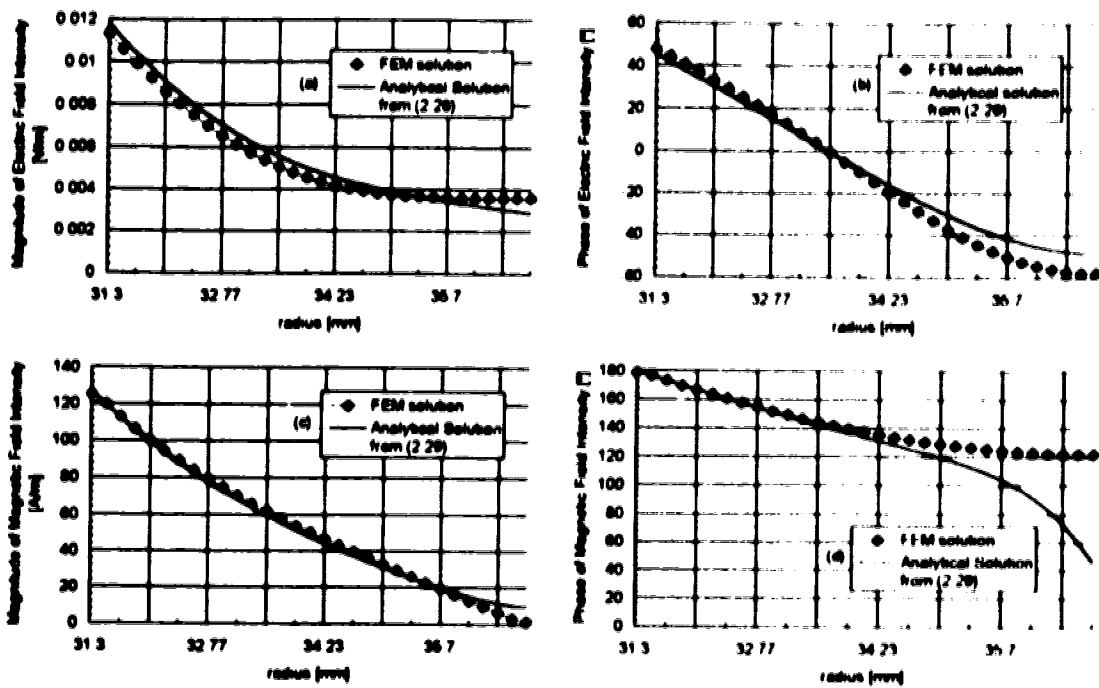


Figure 4-2. FEM and analytical solutions for the electric and magnetic field intensities in wellbore casing sample #1.

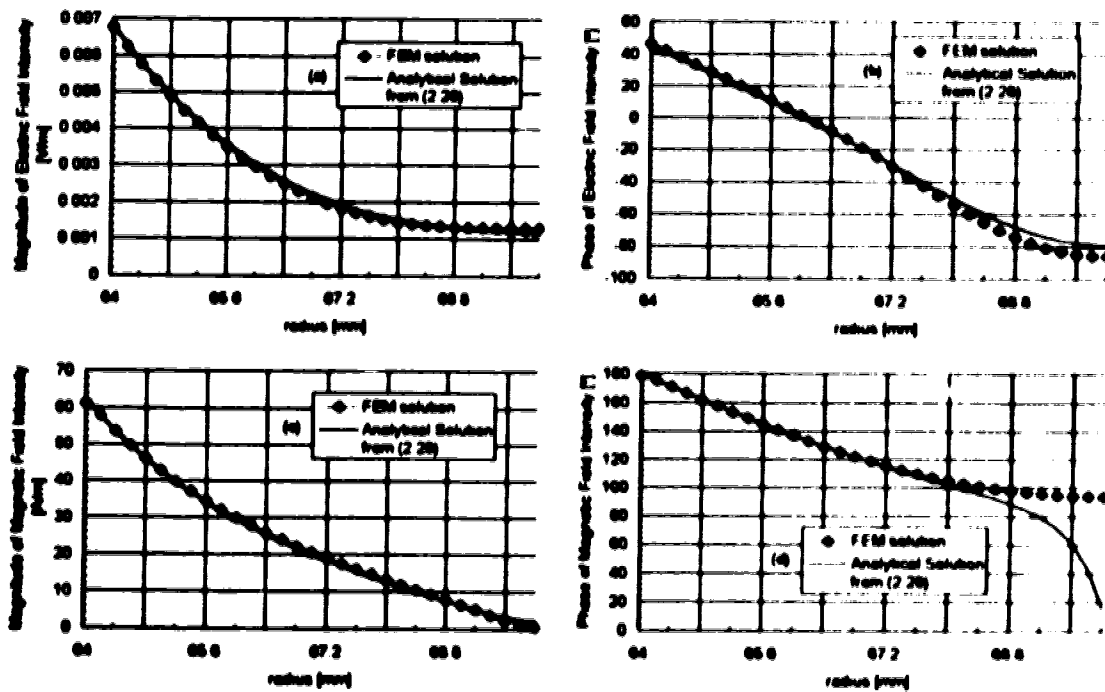


Figure 4-3. FEM and analytical solutions for the electric and magnetic field intensities in wellbore casing sample #2.

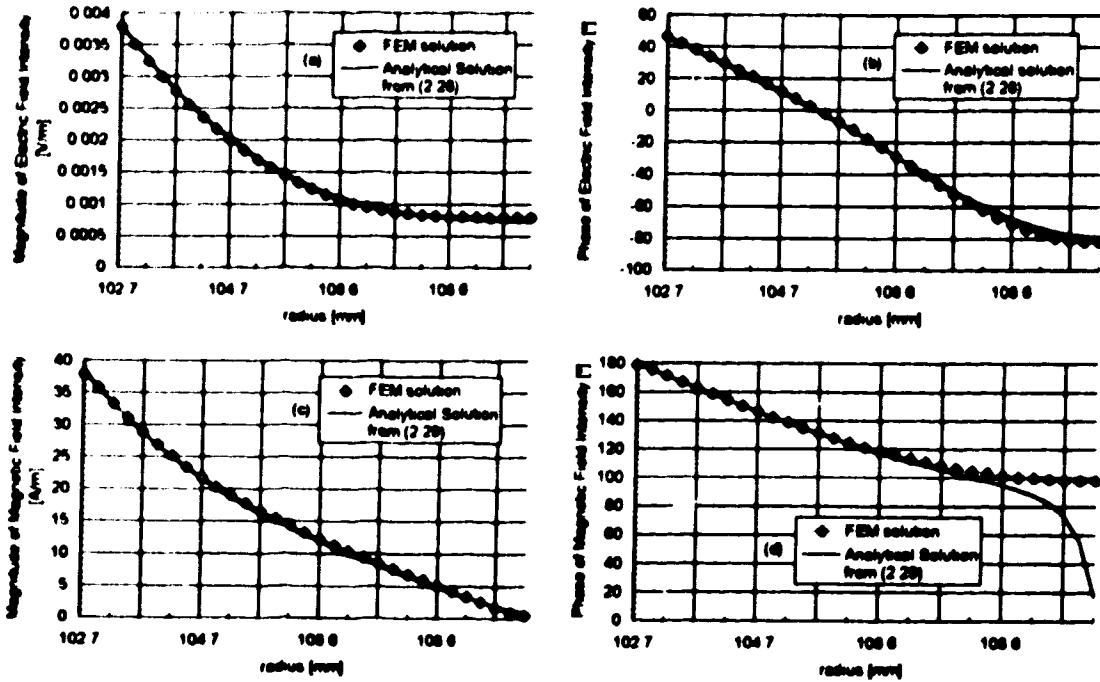


Figure 4-4. FEM and analytical solutions for the electric and magnetic field intensities in wellbore casing sample #3.

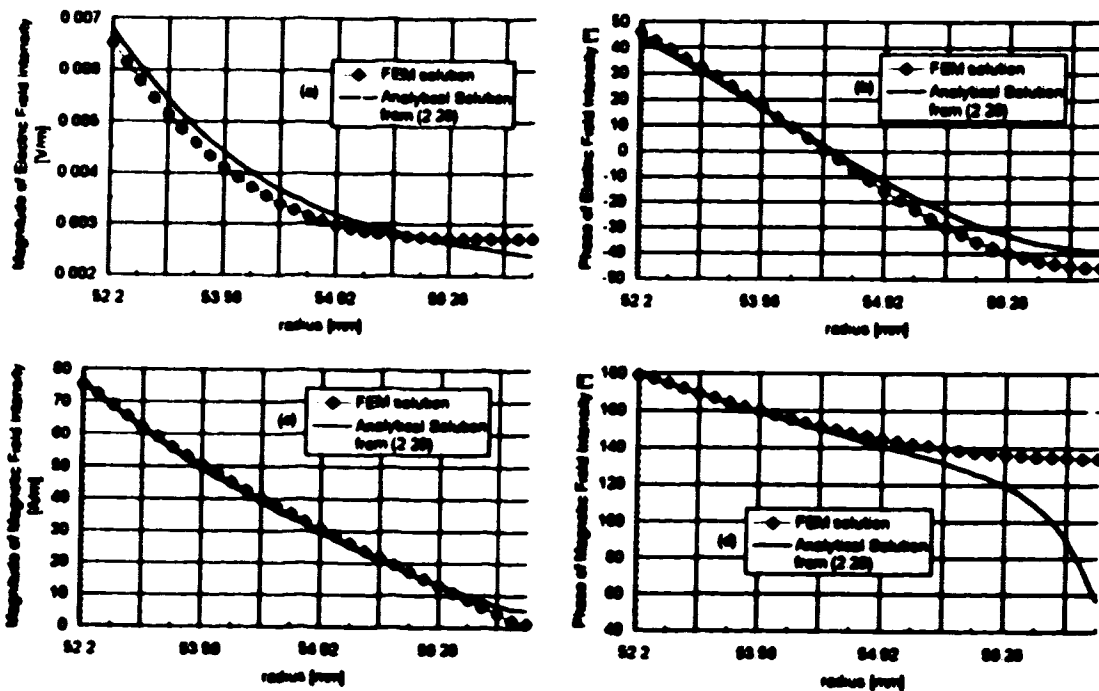


Figure 4-5. FEM and analytical solutions for the electric and magnetic field intensities in wellbore casing sample #4.

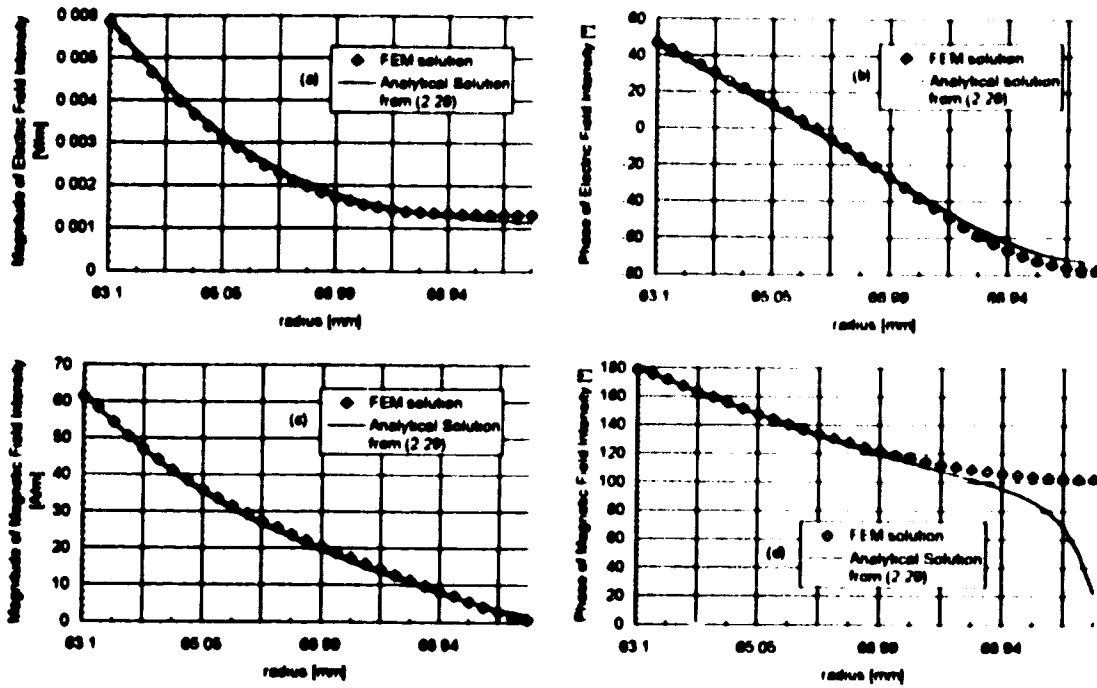


Figure 4-6. FEM and analytical solutions for the electric and magnetic field intensities in wellbore casing sample #5.

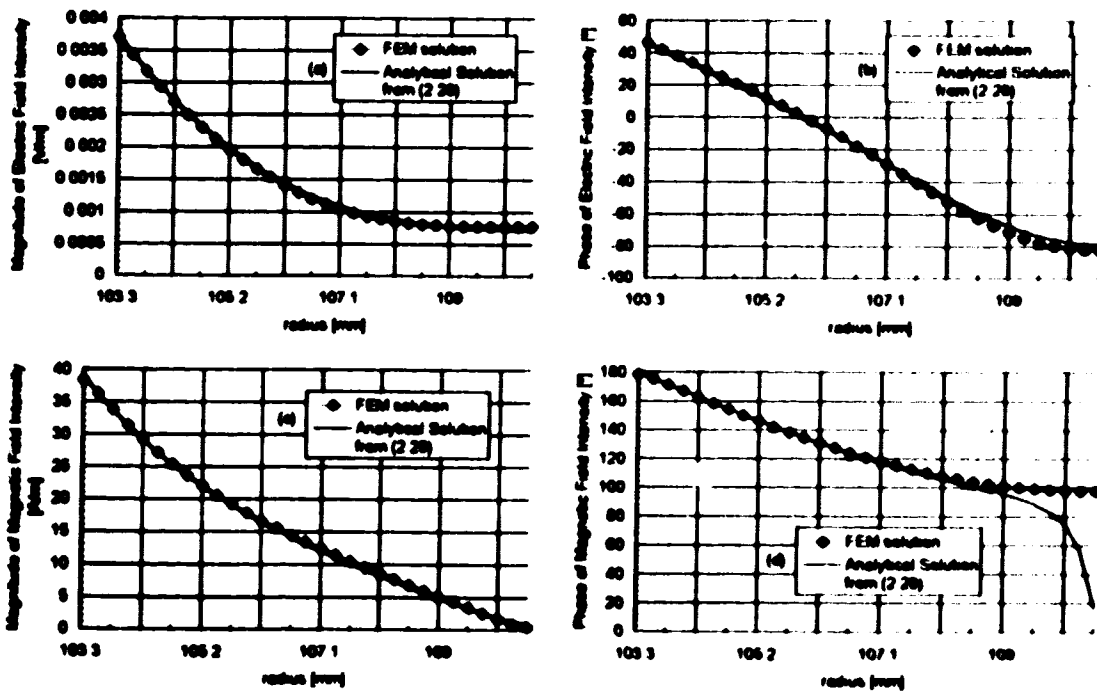


Figure 4-7. FEM and analytical solutions for the electric and magnetic field intensities in wellbore casing sample #6.

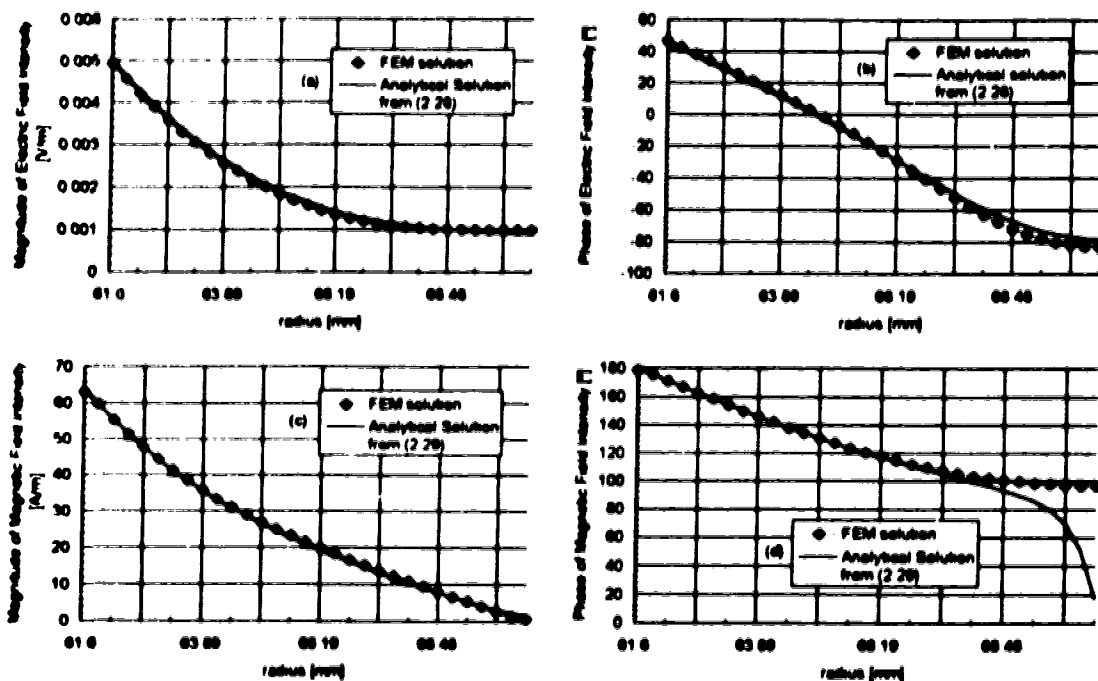


Figure 4-8. FEM and analytical solutions for the electric and magnetic field intensities in wellbore casing sample #7.

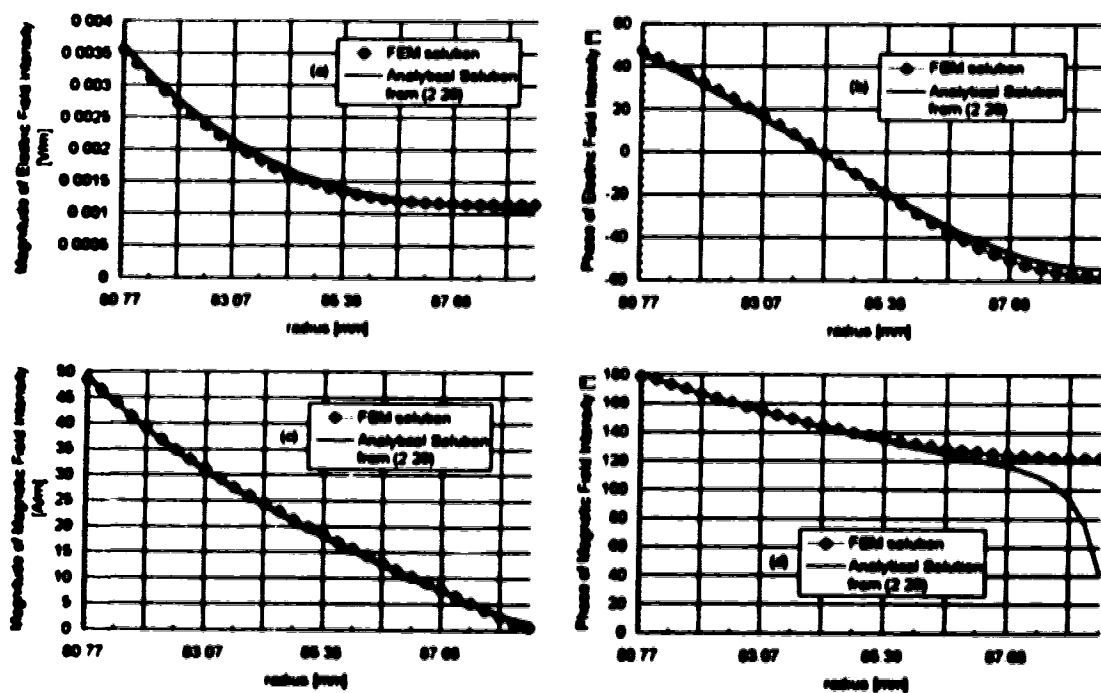


Figure 4-9. FEM and analytical solutions for the electric and magnetic field intensities in wellbore casing sample #8.

As demonstrated in Figures 4-2 to 4-9, the FEM solutions do, in general, agree with the analytical solutions. The main discrepancy is in the phase of the magnetic field in the casing. This may be attributed to the use of the approximate boundary condition, $H_\phi(k_2 b) = 0$, in the FEM solutions. Although the magnetic shielding ratio was greater than 30 for most of the casing samples, only an infinite shielding ratio will guarantee perfect agreement between the analytical and FEM solutions. In spite of this, the FEM solutions for $E_{z_1}(r)$ and $|H_\phi(r)|$ closely agree with the analytical solutions. Even for samples 1 and 4, where the approximate boundary condition $H_\phi(k_2 b) = 0$ could not be entirely justified, the FEM and analytic solutions are satisfactorily close.

4.3.2 Eddy Current Density and Total Current Induced in the Casing

The eddy current density in the wellbore casing is easily calculated from Ohm's law,

$$\begin{aligned} J_z(r) &= \sigma_2 \tilde{E}_z(r) \\ &= \sigma_2 E_{z_1}(r) \hat{a}_z \end{aligned} \quad (4.7)$$

The total current induced in the casing may be found by integrating the eddy current density over the cross sectional area of the casing.

$$\begin{aligned} I_{\text{casing}} &= \int_0^{2\pi} \int_a^b J_{z_1}(r) r dr d\phi \\ &= 2\pi \int_a^b J_{z_1}(r) r dr \end{aligned} \quad (4.8)$$

The integration in (4.8) is performed numerically because the FEM can only provide a numerical solution for the eddy current density. Using Simpson's rule, (4.8) becomes

$$I_{\text{casing}} \cong 2\pi \frac{h}{3} \left[f(r_0) + f(r_{2n}) + 2 \sum_{i=1}^{n-1} f(r_{2i}) + 4 \sum_{i=1}^n f(r_{2i-1}) \right], \quad (4.9)$$

where $f(r) = J_{z_1}(r) \cdot r$, $r_0 = a$, $r_i = a + i \cdot h$, and $h = (b - a)/2n$. The portion of the mesh used to model region 2, from $r = a$ to $r = b$, consists of 30 elements of equal size. Consequently $h = (b - a)/30$ or $n = 15$.

Applying (4.9) to the FEM solution for each casing sample yields values for I_{casing} . These are presented in Table 4-1. For comparison, the analytic solutions for I_{casing} from (3.5) are also included in the table.

Table 4-1 FEM based numerical and analytical solutions for the total current induced in various wellbore casing samples. I_{cable} is the current in the power cable in region 1 of problem 1. All current phasor magnitudes are rms values.

Casing sample #	I_{cable} [A]	FEM solution for I_{casing} [A]	Analytic solution for I_{casing} [A]	$\% \Delta I_{casing} $ ^a	$\Delta \angle I_{casing}$ ^b
1	25.0 $\angle 180^\circ$	24.9 $\angle -0.033^\circ$	26.6 $\angle 3.5^\circ$	-6.4	-3.5°
2	25.1 $\angle 180^\circ$	25.0 $\angle -0.053^\circ$	26.0 $\angle 0.57^\circ$	-3.8	-0.62°
3	24.9 $\angle 180^\circ$	25.0 $\angle -0.059^\circ$	25.5 $\angle 0.39^\circ$	-2.0	-0.45
4	25.0 $\angle 180^\circ$	24.8 $\angle -0.021^\circ$	26.1 $\angle 3.5^\circ$	-5.0	-3.5°
5	24.8 $\angle 180^\circ$	25.0 $\angle -0.063^\circ$	25.7 $\angle 0.79^\circ$	-2.7	-0.85°
6	25.4 $\angle 180^\circ$	25.4 $\angle -0.054^\circ$	26.0 $\angle 0.39^\circ$	-2.3	-0.44°
7	24.9 $\angle 180^\circ$	24.8 $\angle -0.052^\circ$	25.6 $\angle 0.48^\circ$	-3.1	-0.53°
8	25.0 $\angle 180^\circ$	25.0 $\angle -0.038^\circ$	25.7 $\angle 1.3^\circ$	-2.7	-1.3°

$$^a \ \% \Delta |I_{casing}| = \frac{|I_{casing}|_{FEM \ solution} - |I_{casing}|_{Analytic \ solution}}{|I_{casing}|_{Analytic \ solution}} \cdot 100$$

$$^b \ \Delta \angle I_{casing} = \{ \angle I_{casing} \}_{FEM \ solution} - \{ \angle I_{casing} \}_{Analytic \ solution}$$

Based on the results in Table 4-1, the numerical and analytical values for the induced currents are generally in good agreement. The largest differences in magnitude between the FEM based and analytical solutions for I_{casing} are for samples 1 and 4. Again recall that for these samples the approximate boundary condition used in the FEM solution was not completely justified.

The differences in phase angle between the FEM and analytical values for I_{casing} in Table 4-1 can also be attributed to the approximate boundary condition. Ideally, the FEM based solution should yield a value for I_{casing} equal to $-I_{cable}$ because the FEM solution

uses the approximate boundary condition which forces the return current to flow entirely within the casing. This situation was discussed in more detail in section 3.3.

4.3.3 Resistive Power Loss In the Casing

The power dissipated in the casing due to resistive heating by eddy currents can be calculated from Poynting's theorem. The resistive power loss in the casing may be found as follows:

$$\begin{aligned}
 P_{\text{loss}} &= \sigma_2 \int_{\text{Volume}} |\vec{E}_{z,\text{rms}}|^2 dV \\
 &= \sigma_2 \int_0^{2\pi} \int_a^b \int_0^l |E_{z,\text{rms}}(k,r)|^2 dz r dr d\phi \\
 &= \sigma_2 l 2\pi \int_a^b |E_{z,\text{rms}}(k,r)|^2 r dr.
 \end{aligned} \tag{4.10}$$

Again, the FEM can only provide a numerical solution for $E_z(r)$ and therefore, just as with the integral in (4.8), the integral in (4.10) is evaluated numerically. As before, Simpson's rule is used.

$$P_{\text{loss}} = \sigma_2 l 2\pi \frac{h}{3} \left[f(r_0) + f(r_{2n}) + 2 \sum_{i=1}^{n-1} f(r_{2i}) + 4 \sum_{i=1}^n f(r_{2i-1}) \right], \tag{4.11}$$

where $f(r) = |E_{z,\text{rms}}(k,r)|^2 r$, $r_0 = a$, $r_i = a + i \cdot h$, and $h = (b-a)/2n$. Just as with (4.9), $n=30$.

Applying (4.11) to the FEM solution for each casing sample yields values for P_{loss} . These are presented in Table 4-2. For comparison, the analytic solutions for P_{loss} from (3.16) and some measured values from Stroemich et. al. [3] are also included in the table.

Table 4-2 FEM based numerical and analytical solutions for the resistive power loss in various wellbore casing samples. I_{cable} is the current in the power cable in region I of problem I.

Casing sample #	I_{cable} [A]	FEM solution for $\frac{P_{loss}}{l}$ [W/m]	Analytical solution for $\frac{P_{loss}}{l}$ [W/m]	Measured $\frac{P_{loss}}{l}$ ^a [W/m]
1	25.0 $\angle 180^\circ$	0.190	0.205	0.24
2	25.1 $\angle 180^\circ$	0.116	0.119	not available
3	24.9 $\angle 180^\circ$	0.0650	0.0659	not available
4	25.0 $\angle 180^\circ$	0.112	0.120	0.12
5	24.8 $\angle 180^\circ$	0.0996	0.102	not available
6	25.4 $\angle 180^\circ$	0.0645	0.0656	not available
7	24.9 $\angle 180^\circ$	0.0835	0.0865	not available
8	25.0 $\angle 180^\circ$	0.0603	0.0627	not available

^a From Stroemich et. al [3].

In general, the numerical and analytical values for P_{loss}/l in Table 4-2 do agree. The largest difference between the FEM based and analytical solutions are, again, for samples 1 and 4. As mentioned previously, the approximate boundary condition used in the FEM solutions of these samples was not completely justified.

4.3.4 Effective Casing Impedance

Consider the schematic in Figure 4-10. This is a simplified representation of the setup used by Stroemich et al. [3] to measure the *effective impedance* of a casing sample. Note that effective impedance is not identical to either wave or intrinsic impedance, though it is related to these quantities.

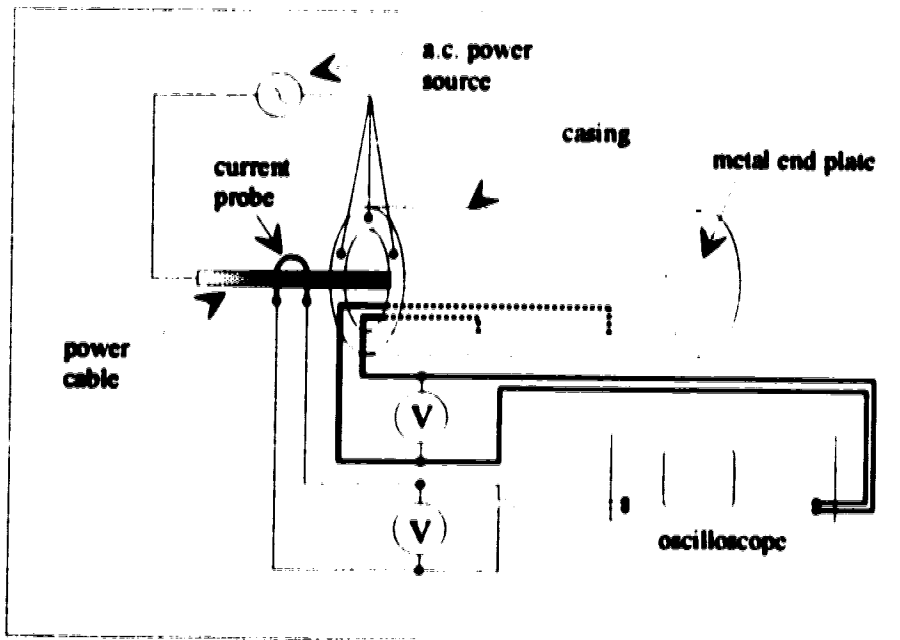


Figure 4-10. A simplified diagram of the setup used by Stroemich et. al. to measure the effective impedance of a wellbore casing (adapted from Figure 5 of reference [3]).

For the setup in Figure 4-10, effective impedance is *defined* as

$$Z_{\text{effective}} = \frac{V}{I} \quad [\Omega/\text{m}] \quad (4.12)$$

where V is the phasor voltage drop per unit length along the inner wall of the casing and I is the phasor current which flows through the power cable and returns to the source through the casing. Measured values for the effective impedance of several samples of wellbore casing are presented in Table 4-3.

A value for effective impedance may also be calculated from the FEM solution. The voltage drop along one meter at the inner wall of the casing is

$$V = 1[\text{m}] \cdot E_{z_1}(a) [\text{V}/\text{m}]. \quad (4.13)$$

Dividing this quantity by the current in the power cable, $-I_{\text{cable}}$, will yield the $Z_{\text{effective}}$ for the casing sample in question. These results are also presented in Table 4-3.

Table 4-3 FEM based numerical solutions and measured values for the effective impedance in various wellbore casing samples.

Casing sample #	I_{casing} [A]	FEM values for $E_{z_1}(a)$ [V/m]	FEM values for $Z_{effective}$ [Ω/m]	^a Experimental values for $Z_{effective}$ [Ω/m]	$\% \Delta$ $ Z_{effective} $ ^b	$\% \Delta$ $\angle Z_{effective}$ ^c
1	25.0 $\angle 180^\circ$	0.01135 $\angle 47.8^\circ$	$4.54 \times 10^{-4} \angle 47.8^\circ$	$4.49 \times 10^{-4} \angle 47.3^\circ$	1.1	1.1
2	25.1 $\angle 180^\circ$	0.00678 $\angle 46.7^\circ$	$2.70 \times 10^{-4} \angle 46.7^\circ$	$2.97 \times 10^{-4} \angle 45.7^\circ$	-9.1	2.1
3	24.9 $\angle 180^\circ$	0.00379 $\angle 46.7^\circ$	$1.52 \times 10^{-4} \angle 46.7^\circ$	$1.44 \times 10^{-4} \angle 45.4^\circ$	5.5	2.9
4	25.0 $\angle 180^\circ$	0.00653 $\angle 46.0^\circ$	$2.61 \times 10^{-4} \angle 46.0^\circ$	$2.79 \times 10^{-4} \angle 45.0^\circ$	-6.5	2.2
5	24.8 $\angle 180^\circ$	0.00586 $\angle 47.2^\circ$	$2.36 \times 10^{-4} \angle 47.2^\circ$	$2.28 \times 10^{-4} \angle 45.9^\circ$	3.5	2.8
6	25.4 $\angle 180^\circ$	0.00371 $\angle 46.7^\circ$	$1.46 \times 10^{-4} \angle 46.7^\circ$	$1.51 \times 10^{-4} \angle 47.0^\circ$	-3.3	-0.64
7	24.9 $\angle 180^\circ$	0.00495 $\angle 47.1^\circ$	$1.99 \times 10^{-4} \angle 47.1^\circ$	$1.93 \times 10^{-4} \angle 45.3^\circ$	3.1	4.0
8	25.0 $\angle 180^\circ$	0.00356 $\angle 47.3^\circ$	$1.42 \times 10^{-4} \angle 47.3^\circ$	$1.41 \times 10^{-4} \angle 47.0^\circ$	0.71	0.64

^a From Stroemich et. al [3].

$$^b \% \Delta |Z_{effective}| = \frac{|Z_{effective}|_{FEM \text{ solution}} - |Z_{effective}|_{Experimental}}{|Z_{effective}|_{Experimental}} \cdot 100$$

$$^c \% \Delta \angle Z_{effective} = \frac{\{\angle Z_{effective}\}_{FEM \text{ solution}} - \{\angle Z_{effective}\}_{Experimental}}{\{\angle Z_{effective}\}_{Experimental}} \cdot 100$$

The agreement between the experimentally measured values for $Z_{effective}$ and the values calculated using the FEM solution is remarkably good. From Table 4-3, the largest difference in magnitude is about 10% while the largest difference in phase angle is only 4%.

4.3.5 Conclusion

For problem 1 (the boundary value problem illustrated in Figure 2-1 of chapter 2) it is possible to obtain a reasonably accurate FEM solution for the electromagnetic fields in the wellbore casing using the approximation that $H_\phi(k, b) = 0$.

Furthermore, a reasonably accurate value for the resistive loss due to eddy currents in the casing may be obtained from the FEM solution for the electric field in the casing and

Poynting's theorem. Substituting discrete values for the electric field from the FEM solution into Poynting's theorem and then using Simpson's rule to numerically evaluate the integral will yield the power loss in the wellbore casing.

The accuracy of the FEM solutions presented in this section are dependent on the judicious use of the approximate boundary condition, $H_{\phi}(b) = 0$. This boundary condition allows for the radially infinite region 3 in problem 1 to be neglected when modeling the problem domain for the finite element method.

CHAPTER 5

A Finite Element Method Solution For a Two Dimensional Boundary Value Problem

Consider a new boundary value problem which, with one exception, is identical to that of problem 1. Instead of having the power cable positioned at the center of the wellbore casing, the new problem has the cable displaced a distance d from the center of the casing. A diagram of this new problem, problem 2, is illustrated below in Figure 5-1a

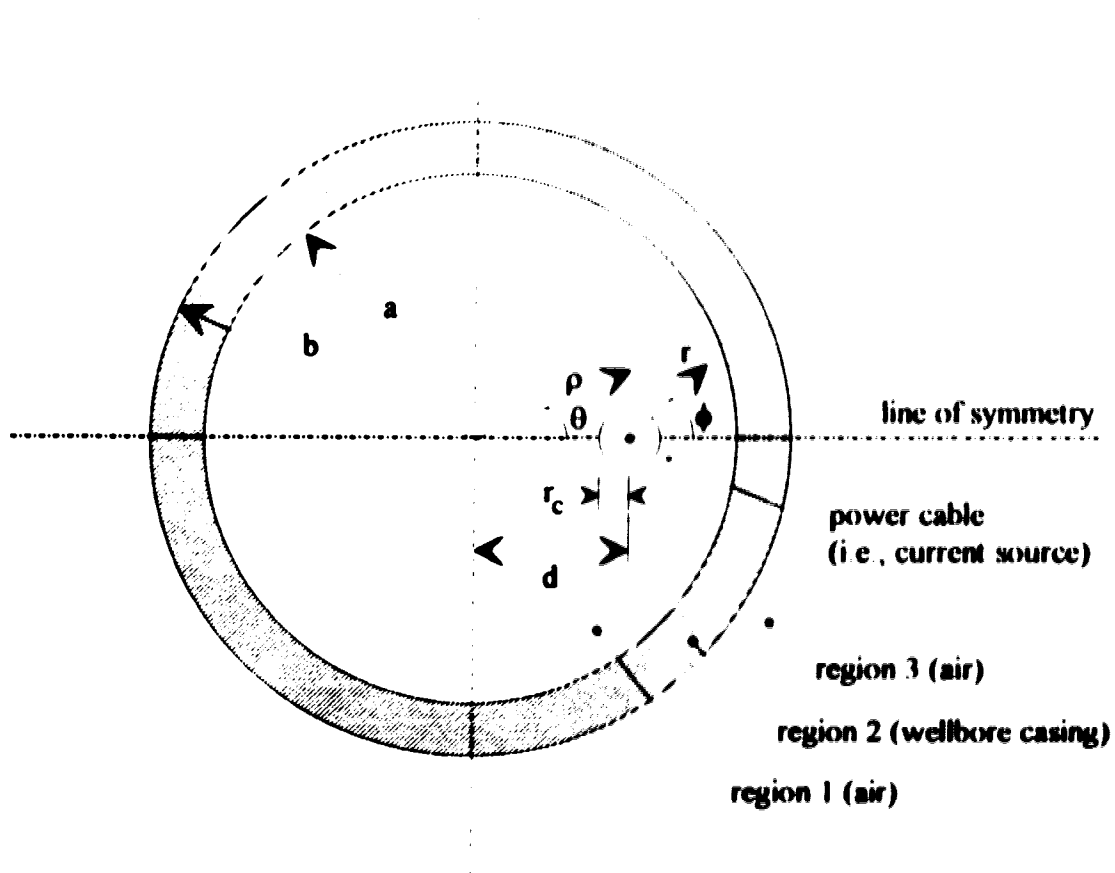


Figure 5-1a. A diagram of problem 2.

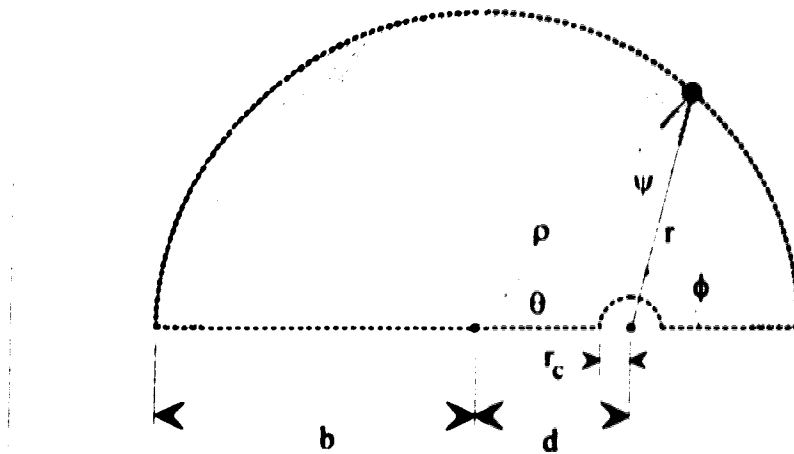


Figure 5-1b. The semicircular section of problem 2 for which the FEM solutions are computed.

As with problem 1, to obtain a FEM solution for problem 2, numerical values must be assigned to the physical dimensions and electromagnetic properties of the boundary value problem. As mentioned in the introduction, several solutions to the problem illustrated in Figure 5-1a have been published in the literature. By choosing physical dimensions and electromagnetic properties for problem 2 from examples published in the literature, the FEM solutions for problem 2 may be compared with the published solutions.

The first set of sample properties and dimensions for problem 2 is based on a numerical example included in both the papers of Tegopoulos and Kriezis [9] and Kriezis and Cangelaris [13]. The inner and outer radii of the wellbore casing, a and b , are 0.100 m and 0.112 m, respectively. The radial displacement, d , of the power cable is 0.090 m. The relative permeability of the casing is unity, implying that the casing is actually composed of a non-magnetic material. The conductivity of the casing is approximately 35.7×10^6 S/m. The magnitude and phase of the current in the power cable is $100 \angle 180^\circ$ A rms (i.e., the current flows in the $-z$ direction, down the well bore). The frequency of the current in the cable is 50 Hz. At 50 Hz, the casing has a skin depth of 11.9 mm.

A second numerical example is also included in the paper by Kriezis and Cangelaris [13]. It is identical to the previous example, except that the radial displacement of the power cable is 0.070 m. The values used in this example will serve as the second set of sample properties and dimensions for problem 2.

A third and final set of sample properties and dimensions will be applied to problem 2 in order that a FEM solution may be compared to a solution based on Dwight's formula from references [6] and [7]. As mentioned in the introduction, Dwight's formula is only valid when the casing thickness is much less than one skin depth and the casing material is non-magnetic. Recall that the second sample has a relative permeability of unity and a skin depth of 11.9 mm. By reducing the thickness of the casing in the second sample from 12 mm to 3 mm, it becomes possible to apply Dwight's formula. Thus a third set of sample parameters for problem 2 may be derived from the second sample by decreasing the casing thickness to approximately 25% of the skin depth.

The properties and dimensions for all three samples are summarized in Table 5-1. Note that in all cases, the properties of regions 1 and 3 are those of free space, namely $\epsilon_{1,3} = \epsilon_0$, $\mu_{1,3} = \mu_0$ and $\sigma_{1,3} = 0$.

Table 5-1. Dimensions and electromagnetic properties for various samples of wellbore casings.

Sample #	Inner radius 'a' [m]	Outer radius 'b' [m]	Displacement 'd' [m]	Region 2 μ_r	σ_c [S/m]
1	0.100	0.112	0.090	1	35.7×10^{-6}
2	0.100	0.112	0.070	1	35.7×10^{-6}
3	0.100	0.103	0.070	1	35.7×10^{-6}

5.1 The Partial Differential Equation for Problem 2

Notice there are two different systems of polar coordinates in Figure 5-1a, the diagram which describes problem 2. The r and ϕ coordinate system will be used to model the problem for UNAFEM II. The r and ϕ coordinate system is chosen over the ρ and θ system because the non-homogeneous boundary condition at the surface of the power cable is more easily described in terms of r and ϕ . Solutions for current density in the wellbore casings will be plotted using the ρ and θ coordinate system.

Problem 2 is a two dimensional problem since the electromagnetic fields are a function of ϕ as well as r . As a result, the simplification $\frac{\partial}{\partial z} = 0$ originally introduced in chapter 2 is

no longer valid. For problem 2, a new differential equation must be constructed. This new equation will take into account the ϕ dependence in the E_{z_N} and H_{ϕ_N} field components

Just as was done for the one dimensional boundary value problem in chapter 2, the following simplifications are made to the two dimensional problem illustrated in Figure 5-1a.

1. $\frac{\partial}{\partial z} = 0$ since it is assumed the casing and cable are infinitely long.
2. The magnetic permeability μ is constant in region 2 (the steel casing).
3. The E_{ϕ_N} and H_{z_N} field components are identically zero because there is no current source present which can sustain these components.

After applying the above simplifications to the basic wave equation in (2.3), the partial differential equation describing the electric field in an arbitrary region N of Figure 5-1a may be written as

$$-\frac{\partial}{\partial r} \left(\frac{-r}{j\omega\mu_N} \cdot \frac{\partial E_{z_N}}{\partial r} \right) - \frac{\partial}{\partial \phi} \left(\frac{-1}{j\omega\mu_N} \cdot \frac{1}{r} \cdot \frac{\partial E_{z_N}}{\partial \phi} \right) + (-r[\sigma_N + j\omega\epsilon_N])E_{z_N} = 0. \quad (5.1)$$

E_{z_N} is the only non-zero component of the electric field in problem 2.

The terms in (5.1) which correspond to the coefficients α_x , α_y and β in (4.1) are

$$\alpha_x(x, y) \Rightarrow \frac{-r}{j\omega\mu_N}, \quad (5.1a)$$

$$\alpha_y(x, y) \Rightarrow \frac{-1}{j\omega\mu_N} \cdot \frac{1}{r}, \quad (5.1b)$$

and
$$\beta(x, y) \Rightarrow -r[\sigma_N + j\omega\epsilon_N], \quad (5.1c)$$

where x corresponds to r and y corresponds to ϕ . The constants $c_1, c_2 \dots c_7$, as defined in (4.1a), may be extracted from the coefficients in (5.1a-c). For $\alpha_x(x, y)$ the only non-zero constant is c_2 , which corresponds to $j/\omega\mu_N$. For $\alpha_y(x, y)$ the only non-zero constant is c_7 , which corresponds to $j/\omega\mu_N$. For $\beta(x, y)$ the only non-zero constant is c_2 , which

corresponds to $(-\sigma_v - j\omega\epsilon_v)$. Since σ_v and μ_v vary from region to region, the constants will also vary from region to region

5.2 Mapping the Domain of Problem 2 for UNAFEM II

As with the one dimensional problem in the previous chapter, it is necessary to map the domain of problem 2 onto a mesh so that UNAFEM II may compute the FEM solution. It should be apparent from the diagram of problem 2 in Figure 5-1a that the solution to problem 2 will be symmetric about $\phi = 0$. Consequently, a FEM solution need only be computed for the semicircular region illustrated in Figure 5-1b. The domain of the problem is modeled by a semicircular mesh which extends azimuthally from $\theta = 0^\circ$ to $\theta = 180^\circ$ and radially from the surface of the power cable in region 1 to the outer wall of the wellbore casing in region 2. It is in this section of the domain that UNAFEM II will compute a FEM solution for the electric and magnetic fields. The meshes used to model the domain of problem 2 are included in appendix 3.

5.3 Magnetic Field Boundary Conditions for Problem 2

The dashed line in Figure 5-1b illustrates the boundary for that section of problem 2 where FEM solutions are to be computed. This boundary is essentially constructed of four segments. The first segment of the boundary coincides with the surface of the power cable; this is the arc described by $r = r_c$ from $\phi = 0^\circ$ to $\phi = 180^\circ$. The second segment is part of the line of symmetry which divides problem 2 into two semicircular sections, the second segment extends radially from $r = r_c$ to $\rho = b$ along an angle of $\phi = 180^\circ$. The third segment of the boundary coincides with the outer wall of the wellbore casing and is an arc described by $\rho = b$ from $\theta = 180^\circ$ to $\theta = 0^\circ$. The fourth and final segment of the boundary is again part of the line of symmetry which bisects problem 2, the fourth segment extends radially from $\rho = b$ to $r = r_c$ along an angle of $\phi = 0^\circ$.

Boundary conditions for the magnetic field will be used by UNAFEM II to help compute FEM solutions for the electromagnetic fields in problem 2. These boundary conditions are discussed in sections 5.3.1 to 5.3.3.

5.3.1 The Magnetic Field Boundary Condition at the Surface of the Power Cable

The magnetic field boundary condition at the surface of the power cable in problem 2 is

$$H_{\phi}(r_c, \phi) = \frac{I}{2\pi r_c} \quad (5.2)$$

Equation (5.2) is a close approximation for the ϕ component of the magnetic field at the surface of the power cable.

5.3.2 The Magnetic Field Boundary Condition Along the Line of Symmetry of Problem 2

Along the line of symmetry which divides problem 2 into two semicircular sections, the radial component of the magnetic field is exactly zero. This is apparent from the symmetry of the problem; $\partial F_{z_n} / \partial \phi = 0$ along the line of symmetry in Figure 5-1a and therefore $H_{r_n} = 0$ along the line of symmetry as well.

5.3.3 The Magnetic Field Boundary Condition Along the Outer Wall of the Wellbore Casing

For problem 1, the one dimensional boundary value problem considered in the last chapter, an approximate boundary condition for the magnetic field was used to compute a FEM solution. The approximate boundary condition was used instead of the exact boundary condition to avoid the problem of modeling region 3, the radially infinite region beyond the outer wall of the casing. The approximate boundary condition used in problem 1 was $H_{\phi_1}(k_2 b) = 0$ (i.e., the magnetic field at the outer wall of the wellbore casing is zero).

For problem 2, the magnetic field at the outer wall of the wellbore casing is also assumed to be zero. Thus, $\tilde{H}_2|_{r=b} = 0$ constitutes one of the boundary conditions to be used for computing FEM solutions for problem 2. Again, imposing the boundary condition $\tilde{H}_2|_{r=b} = 0$ avoids the problem of modeling the radially infinite region beyond the outer wall of the casing. The validity of this boundary condition will be discussed later in this chapter.

5.4 UNAFEM II Boundary Conditions

In order to use UNAFEM II to compute a FEM solution for problem 2, the boundary conditions for problem 2 must be rewritten in terms of the notation used in equation (4.1), the partial differential equation solved by UNAFEM II. Specifically, a boundary condition conveyed by UNAFEM II must correspond to one of the following quantities

1. U
2. $(-\alpha_x \hat{a}_x + (-\alpha_y \partial U / \partial y) \hat{a}_y) \cdot \hat{n}$, where \hat{n} is a unit vector normal to the boundary in question.

The function $U(x, y)$ corresponds to the electric field $E_z(r, \phi)$ in (5.1). The values for $U(x, y)$ (i.e., the electric field) at the boundaries of problem 2 are unknown. However, boundary conditions are available for the magnetic fields. Furthermore, these magnetic field boundary conditions can be shown to correspond to the terms $-\alpha_x \partial U / \partial x$ and $-\alpha_y \partial U / \partial y$. This relationship is demonstrated as follows.

By comparing the partial differential equation solved by UNAFEM II from (4.1) with the partial differential equation for problem 2 in (5.1), the following correspondences are obtained:

$$-\alpha_x(x, y) \frac{\partial U}{\partial x} \hat{a}_x \Rightarrow \frac{r}{j\omega\mu_N} \cdot \frac{\partial E_{zN}}{\partial r} \hat{a}_r, \quad (5.3a)$$

$$-\alpha_y(x, y) \frac{\partial U}{\partial y} \hat{a}_y \Rightarrow \frac{1}{j\omega\mu_N} \cdot \frac{1}{r} \cdot \frac{\partial E_{zN}}{\partial \phi} \hat{a}_\phi. \quad (5.3b)$$

The terms on the right hand side of (5.3a) and (5.3b) may be expressed in terms of $H_{\phi_N}(r, \phi)$ and $H_{r_N}(r, \phi)$ respectively. According to Maxwell's equations,

$$\nabla \times \vec{E}_N = -j\omega\mu_N \vec{H}_N. \quad (5.4)$$

Given that there exists only a z component of the electric field, (5.4) reduces to

$$\hat{a}_r \left(\frac{1}{r} \frac{\partial E_{zN}}{\partial \phi} \right) + \hat{a}_\phi \left(-\frac{\partial E_{zN}}{\partial r} \right) = -j\omega\mu_N \vec{H}_N. \quad (5.5)$$

From (5.5) a scalar differential equation may be extracted from each of the field components:

$$H_{r_n}(r, \phi) = \frac{-1}{j\omega\mu_N r} \frac{\partial E_{z_n}}{\partial \phi}, \quad (5.6a)$$

$$H_{\phi_n}(r, \phi) = \frac{1}{j\omega\mu_N} \frac{\partial E_{z_n}}{\partial r}. \quad (5.6b)$$

Substituting (5.6b) into (5.3a) and (5.6a) into (5.3b) yields the following relationships between the partial derivatives of $U(x, y)$ and the magnetic fields in problem 2:

$$-\alpha_x(x, y) \frac{\partial U(x, y)}{\partial x} \hat{\mathbf{a}}_x \Rightarrow r H_{\phi_n}(r, \phi) \hat{\mathbf{a}}_r, \quad (5.7)$$

$$-\alpha_y(x, y) \frac{\partial U(x, y)}{\partial y} \hat{\mathbf{a}}_y \Rightarrow -H_{r_n}(r, \phi) \hat{\mathbf{a}}_\phi. \quad (5.8)$$

At any point 'P' along the boundary of problem 2, the UNAFEM II boundary condition is the normal flux,

$$-\left(\hat{\mathbf{a}}_x \alpha_x \frac{\partial U}{\partial x} \Big|_P + \hat{\mathbf{a}}_y \alpha_y \frac{\partial U}{\partial y} \Big|_P \right) \cdot \hat{\mathbf{n}}, \quad (5.9)$$

where $\hat{\mathbf{n}}$ must be specified as a unit vector normal to the boundary. Substituting (5.7) and (5.8) into (5.9) yields a general expression for the boundary flux in terms of the magnetic field at any point 'P' on the boundary:

$$-\left(\hat{\mathbf{a}}_x \alpha_x \frac{\partial U}{\partial x} \Big|_P + \hat{\mathbf{a}}_y \alpha_y \frac{\partial U}{\partial y} \Big|_P \right) \cdot \hat{\mathbf{n}} \Rightarrow \left(\hat{\mathbf{a}}_r [r H_{\phi_n}]_P - \hat{\mathbf{a}}_\phi [H_{r_n}]_P \right) \cdot \hat{\mathbf{n}}. \quad (5.10)$$

5.4.1 The UNAFEM II Boundary Condition at the Surface of the Power Cable

As mentioned earlier, the semicircular arc $r = r_c$ describes that segment of the boundary of problem 2 which lies along the surface of the power cable. Furthermore, in the r and ϕ coordinate system, the unit vector $\hat{\mathbf{n}}_r$ is normal to the surface of the power cable. Using this information, the general UNAFEM II boundary condition from (5.10) can be rewritten specifically for this section of the boundary:

$$\begin{aligned} -\left(\hat{\mathbf{n}}_x \alpha_x \frac{\partial U}{\partial x}\bigg|_{r=r_c} + \hat{\mathbf{n}}_y \alpha_y \frac{\partial U}{\partial y}\bigg|_{r=r_c}\right) \cdot \hat{\mathbf{n}} &\Rightarrow (\hat{\mathbf{n}}_r H_{\phi}(r_c, \phi) - \hat{\mathbf{n}}_{\phi} H_r(r_c, \phi)) \cdot \hat{\mathbf{n}} \\ &\Rightarrow \hat{\mathbf{n}}_r \cdot \hat{\mathbf{n}}_r H_{\phi}(r_c, \phi) - \hat{\mathbf{n}}_{\phi} \cdot \hat{\mathbf{n}} H_r(r_c, \phi) \\ &\Rightarrow r_c H_{\phi}(r_c, \phi) \end{aligned} \quad (5.11)$$

Substituting the magnetic field boundary condition from (5.2) into the right hand side of (5.11) yields a value for the boundary condition at the surface of the power cable which can be related to UNAFEM II:

$$-\left(\hat{\mathbf{n}}_x \alpha_x \frac{\partial U}{\partial x}\bigg|_{r=r_c} + \hat{\mathbf{n}}_y \alpha_y \frac{\partial U}{\partial y}\bigg|_{r=r_c}\right) \cdot \hat{\mathbf{n}} \Rightarrow \frac{I}{2\pi} \quad (5.12)$$

5.4.2 The UNAFEM II Boundary Condition Along the Line of Symmetry of Problem 2

The line of symmetry in Figure 5-1a serves as part of the boundary for the semicircular section of problem 2 (illustrated in Figure 5-1b) where the FEM solutions are computed. The unit vector normal to this segment of the boundary is $\hat{\mathbf{n}}_{\phi}$. Along this segment of the boundary, the general UNAFEM II boundary condition of (5.10) reduces to

$$\begin{aligned} -\left(\hat{\mathbf{n}}_x \alpha_x \frac{\partial U}{\partial x}\bigg|_{\substack{\phi=0^\circ \text{ or} \\ \phi=180^\circ}} + \hat{\mathbf{n}}_y \alpha_y \frac{\partial U}{\partial y}\bigg|_{\substack{\phi=0^\circ \text{ or} \\ \phi=180^\circ}}\right) \cdot \hat{\mathbf{n}} &\Rightarrow (\hat{\mathbf{n}}_r [r H_{\phi, n}]_{\phi=0^\circ \text{ or} 180^\circ} - \hat{\mathbf{n}}_{\phi} [H_{r, n}]_{\phi=0^\circ \text{ or} 180^\circ}) \cdot \hat{\mathbf{n}} \\ &\Rightarrow \hat{\mathbf{n}}_r \cdot \hat{\mathbf{n}}_{\phi} [r H_{\phi, n}]_{\phi=0^\circ \text{ or} 180^\circ} - \hat{\mathbf{n}}_{\phi} \cdot \hat{\mathbf{n}}_{\phi} [H_{r, n}]_{\phi=0^\circ \text{ or} 180^\circ} \\ &\Rightarrow -[H_{r, n}]_{\phi=0^\circ \text{ or} 180^\circ} \end{aligned} \quad (5.13)$$

As discussed in section 5.3.2, $H_{r,\nu} = 0$ along the line of symmetry in Figure 5-1a (i.e., $H_{r,\nu}(r, 0^\circ) = 0$ and $H_{r,\nu}(r, 180^\circ) = 0$). As a result, the right hand side of (5.13) reduces to zero and the UNAFEM II boundary condition along the line of symmetry becomes

$$-\left(\hat{\mathbf{a}}_x \alpha_x \frac{\partial U}{\partial x} \Big|_{\phi=0^\circ, 180^\circ} + \hat{\mathbf{a}}_y \alpha_y \frac{\partial U}{\partial y} \Big|_{\phi=0^\circ, 180^\circ} \right) \cdot \hat{\mathbf{n}} \rightarrow 0. \quad (5.14)$$

5.4.3 The UNAFEM II Boundary Condition at the Outer Wall of the Wellbore Casing

The segment of the boundary of problem 2 which lies along the outer wall of the wellbore casing is described by the semicircular arc $\rho = b$. The unit vector $\hat{\mathbf{a}}_\rho$ is a unit vector normal to the outer wall of the wellbore casing. By equating $\hat{\mathbf{n}}$ with $\hat{\mathbf{a}}_\rho$, the general UNAFEM II boundary condition of (5.10) can be rewritten as

$$\begin{aligned} -\left(\hat{\mathbf{a}}_x \alpha_x \frac{\partial U}{\partial x} \Big|_{\rho=b} + \hat{\mathbf{a}}_y \alpha_y \frac{\partial U}{\partial y} \Big|_{\rho=b} \right) \cdot \hat{\mathbf{n}} &\Rightarrow \left(\hat{\mathbf{a}}_r [r H_{\phi_2}(r, \phi)]_{\rho=b} + \hat{\mathbf{a}}_\phi [-H_{r_2}(r, \phi)]_{\rho=b} \right) \cdot \hat{\mathbf{a}}_\rho \\ &\Rightarrow \begin{pmatrix} \hat{\mathbf{a}}_r \cdot \hat{\mathbf{a}}_\rho [r H_{\phi_2}(r, \phi)]_{\rho=b} + \\ \hat{\mathbf{a}}_\phi \cdot \hat{\mathbf{a}}_\rho [-H_{r_2}(r, \phi)]_{\rho=b} \end{pmatrix} \\ &\Rightarrow \begin{pmatrix} [\cos(\psi) r H_{\phi_2}(r, \phi)]_{\rho=b} + \\ [\sin(\psi) H_{r_2}(r, \phi)]_{\rho=b} \end{pmatrix}. \end{aligned} \quad (5.15)$$

The angle ψ is equal to $\phi - \theta$, as illustrated in Figure 5-1b.

Note that the r and ϕ components of the magnetic field along the outer wall of the casing may be written in terms of magnetic field components *which are normal and tangential to the casing*. In other words, the r and ϕ components of the magnetic field may be written in terms of ρ and θ components. The relations between field components at a given point along the boundary of problem 2 are

$$\begin{aligned} H_r &= H_\rho \cos(\psi) + H_\theta \sin(\psi) \\ H_\phi &= -H_\rho \sin(\psi) + H_\theta \cos(\psi). \end{aligned} \quad (5.16)$$

Substituting these relations for H_r and H_ϕ into (5.15) yields

$$\begin{aligned}
 -\left(\hat{\mathbf{a}}_x \alpha_x \frac{\partial U}{\partial x} \Big|_{\rho, \phi} + \hat{\mathbf{a}}_y \alpha_y \frac{\partial U}{\partial y} \Big|_{\rho, \phi}\right) \cdot \hat{\mathbf{n}} &\Rightarrow \left(\begin{array}{l} [\cos(\psi) r H_\phi(r, \phi)]_{\rho, \phi} \\ [\sin(\psi) H_r(r, \phi)]_{\rho, \phi} \end{array} \right) \\
 &\Rightarrow \left(\begin{array}{l} [-r H_\phi \sin(\psi) \cos(\psi) + r H_r \cos(\psi) \cos(\psi)]_{\rho, \phi} \\ [H_\phi \cos(\psi) \sin(\psi) + H_r \sin(\psi) \sin(\psi)]_{\rho, \phi} \end{array} \right) \\
 &\Rightarrow \left(\begin{array}{l} H_\phi [r \cos^2(\psi) + \sin^2(\psi)] \\ + H_r \cos(\psi) \sin(\psi) [1 - r] \end{array} \right)_{\rho, \phi} \quad (5.17)
 \end{aligned}$$

According to the boundary condition discussed in section 5.3.3, $\dot{H}_z|_{\rho, \phi} = 0$. Thus $H_\theta = 0$ and $H_\phi = 0$ at $\rho = b$. The right hand side of (5.17) therefore reduces to zero and the UNAFEM II boundary condition at the outer wall of the casing is simply

$$-\left(\hat{\mathbf{a}}_x \alpha_x \frac{\partial U}{\partial x} \Big|_{\rho, \phi} + \hat{\mathbf{a}}_y \alpha_y \frac{\partial U}{\partial y} \Big|_{\rho, \phi}\right) \cdot \hat{\mathbf{n}} = 0 \quad (5.18)$$

5.5 Comparison of the Finite Element Solutions with Published Solutions

After defining the boundary conditions, electromagnetic properties and dimensions for problem 2, the data is conveyed to UNAFEM II. A FEM solution is then computed for each set of sample parameters in Table 5-1. For each sample, the FEM solution for the electric field in the casing is multiplied by the conductivity of the casing to obtain a solution for the current density. The FEM based solution for the current density may then be compared with published solutions. In addition, by numerically evaluating the integral from Poynting's theorem using data from the FEM solution, a value for the resistive power loss in the casing may be obtained. This quantity may also be compared with published results.

5.5.1 The Finite Element Method Solution for Sample 1 of Problem 2

For sample 1, contour plots of the FEM solution for current density are shown in Figures 5-2a and 5-2b. In Figures 5-3 and 5-4, the accuracy of the FEM solution for current density is checked by comparing it with both an analytical solution and an integral equation solution.

The analytical solution is based on the solution derived by Tegopoulos and Kriezis in reference [9]. As mentioned in section 1.2.1.2, the original current density expression derived by Tegopoulos and Kriezis is incorrect due to several errors which occur in the derivation of the solution. In appendix 1 of this thesis, these errors are identified and corrected. The “revised” Tegopoulos and Kriezis solution for current density is given by equation (A1.24). This solution is comprised of a summation of an infinite series of Bessel functions. Numerical evaluation of the revised Tegopoulos and Kriezis solution (equation A1.24) was performed using Mathematica 2.1 [20]. The sum of the first 70 terms in equation (A1.24) yields values for current density which are accurate to at least four significant digits.

The integral equation solution is the solution obtained by Kriezis and Cangellaris in reference [13]. As discussed in the introduction, this is a numerical solution to the integral equation which describes the current density in problem 2. A plot of the solution for eddy current density is given in Figure 7 of reference [13].

Figures 5-3a to 5-3c are plots of $|J_{z_1}(0.100, \theta)|$, $|J_{z_1}(0.106, \theta)|$ and $|J_{z_1}(0.112, \theta)|$ respectively. Figures 5-4a to 5-4c are phase angle plots of $J_{z_1}(0.100, \theta)$, $J_{z_1}(0.106, \theta)$ and $J_{z_1}(0.112, \theta)$ respectively. Note that there were no values for phase angle published in reference [13].

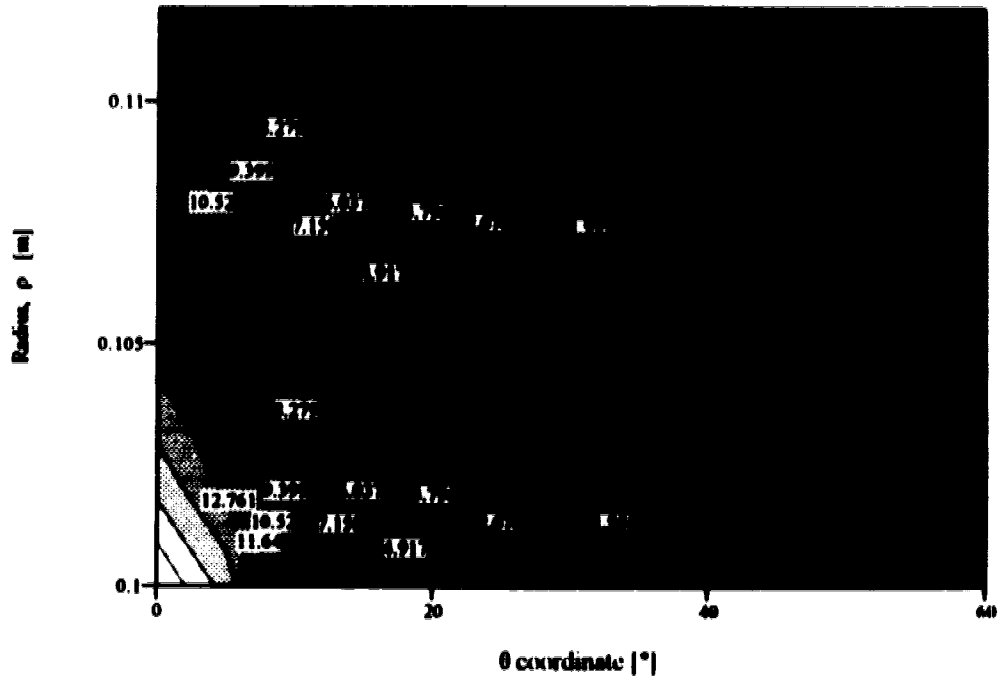


Figure 5-2a Contour plot of the magnitude of the current density [A/cm²] in the wellbore casing of sample 1.

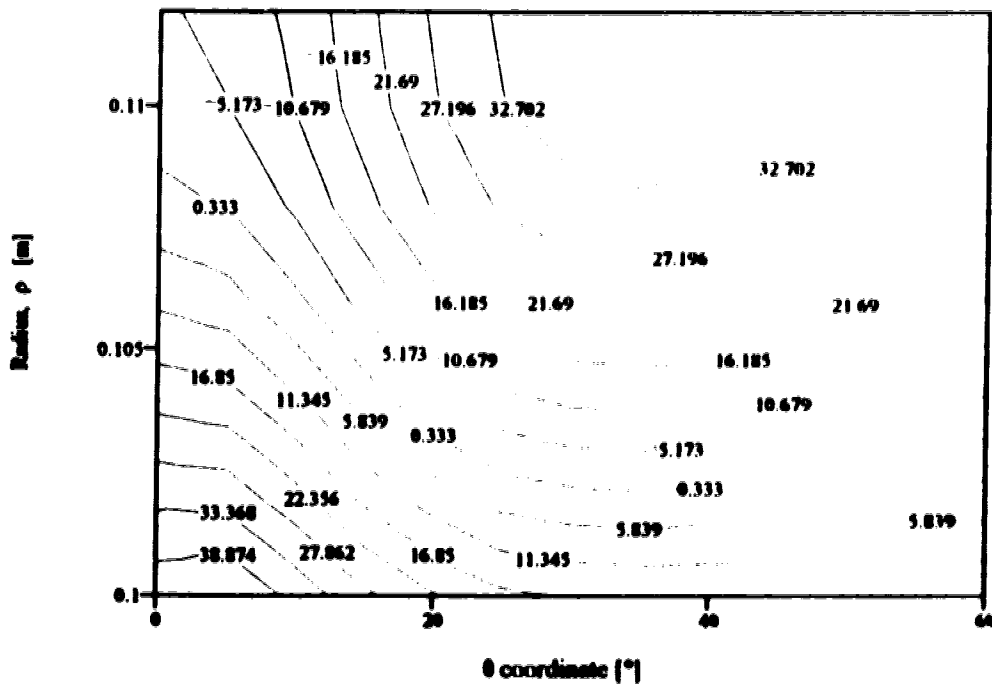


Figure 5-2b Contour plot of the phase of the current density [°] in the wellbore casing of sample 1.

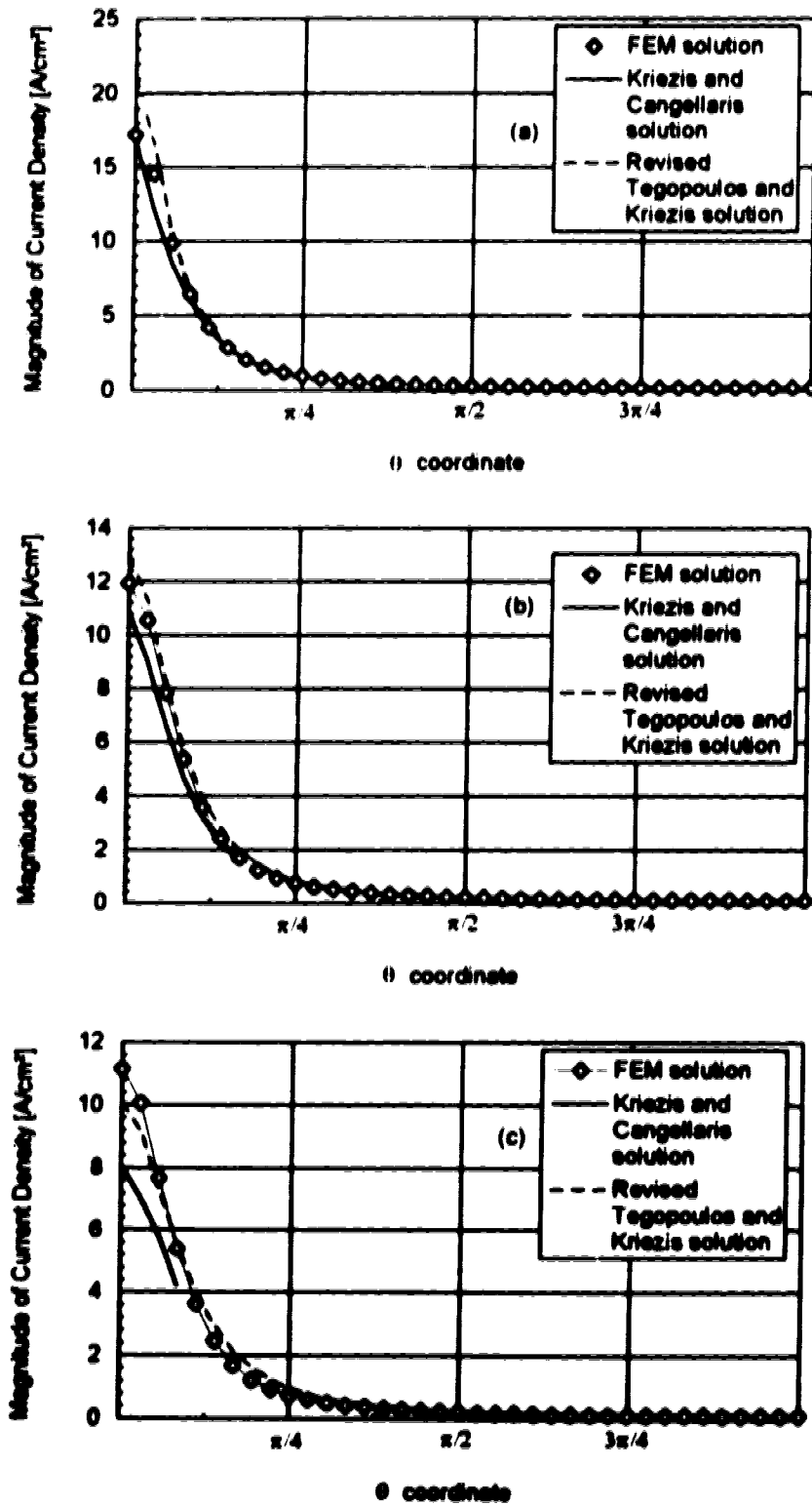


Figure 5-3. Solutions for the current density in wellbore casing sample 1. The magnitude of the current density is plotted for; (a) $\rho=0.100$ m, (b) $\rho=0.106$ m and (c) $\rho=0.112$ m.

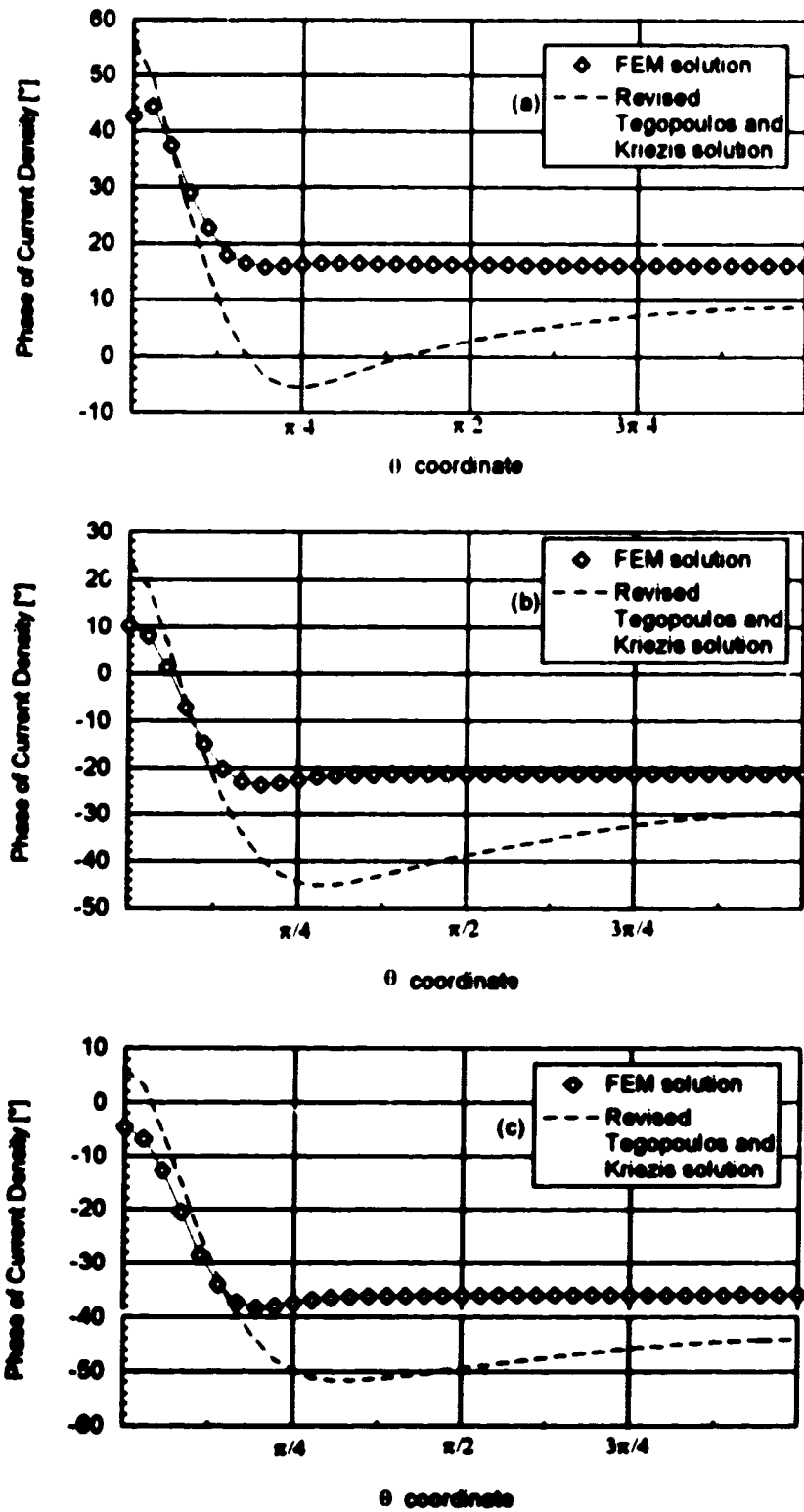


Figure 5-4. Solutions for the current density in wellbore casing sample 1. The phase of the current density is plotted for, (a) $\rho=0.100$ m, (b) $\rho=0.106$ m and (c) $\rho=0.112$ m.

It is apparent from Figure 5-3 that the FEM solution for the magnitude of the current density agrees reasonably well with the revised Tegopoulos and Kriezis solution and the Kriezis and Cangellaris solution. However, from Figure 5-4 there appears to be some discrepancy between the solutions for the phase angle. While the general shape of both curves is similar, the actual values differ by as much as 25°.

A comparison of solutions for the power loss in the wellbore casing is also possible. For the resistive power loss due to the flow of eddy currents, references [9] and [13] provide values for power loss per meter of casing.

In reference [9], Tegopoulos and Kriezis derive an expression for power loss based on their analytical solution for current density. However, as mentioned earlier, the Tegopoulos and Kriezis solution for current density is erroneous. Thus their expression for power loss is also flawed; this is discussed in detail in section A1.4. The revised Tegopoulos and Kriezis current density solution (equation A1.24) can be used to rederive the analytic expression for power loss. This leads to equation (A1.49). By evaluating (A1.49), the power loss in casing sample 1 is found to be 0.239 W/m.

A value for power loss in casing sample 1 is also available from reference [13]. This value is based on the integral equation solution for current density computed by Kriezis and Cangellaris. According to Figure 9 of reference [13], the power dissipated in casing sample 1 is 0.125 W/m. This is almost 50% smaller than the 0.239 W/m power loss obtained from equation (A1.49). This author is unable to explain the discrepancy.

To obtain a value for the power dissipated based on the FEM solution, $\sigma_2 |E_z(\rho, \theta)|^2$ is integrated numerically over the cross sectional area of the casing (values for $E_z(\rho, \theta)$ are those from the FEM solution). Since the integral is a function of ρ and θ , a double numerical integration must be performed. Using Simpson's rule twice to evaluate the double integral

$$2 \int_0^{\pi} \int_0^b \sigma_2 |E_z(\rho, \theta)|^2 d\rho d\theta \quad (5.19)$$

yields a value of 0.206 W/m for the power dissipated by the casing in sample 1. Thus, the FEM solution for power loss is about 15% smaller than the revised Tegopoulos and

Kriezis solution. However, the FEM solution appears to be approximately 40% larger than integral equation solution from Kriezis and Cangelaris

5.5.2 The Finite Element Method Solution for Sample 2 of Problem 2

For sample 2, contour plots of the FEM solution for current density are shown in Figures 5-5a and 5-5b. Also, as with sample 1, the FEM solution for current density in casing sample 2 may be plotted and compared with the revised Tegopoulos and Kriezis solution given by equation (A1.24) and the integral equation solution from reference [13].

Figures 5-6a to 5-6c are plots of $|J_{z_1}(0.100, \theta)|$, $|J_{z_1}(0.106, \theta)|$ and $|J_{z_1}(0.112, \theta)|$ respectively. Figures 5-7a to 5-7c are phase angle plots of $J_{z_1}(0.100, 0)$, $J_{z_1}(0.106, 0)$ and $J_{z_1}(0.112, 0)$ respectively.

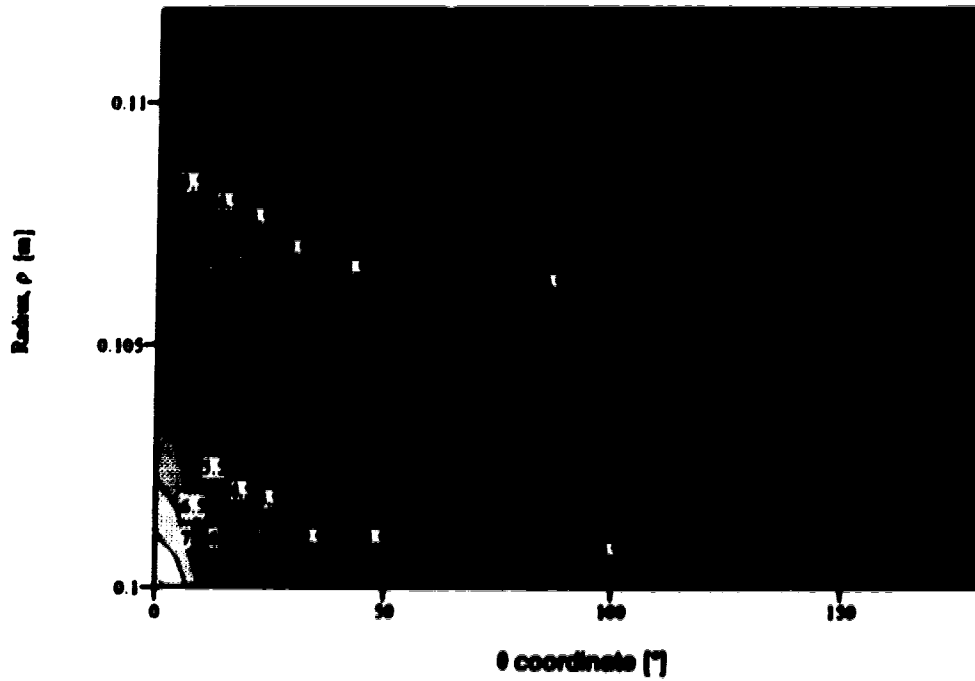


Figure 5-5a Contour plot of the magnitude of the current density [A/cm^2] in the wellbore casing of sample 2.

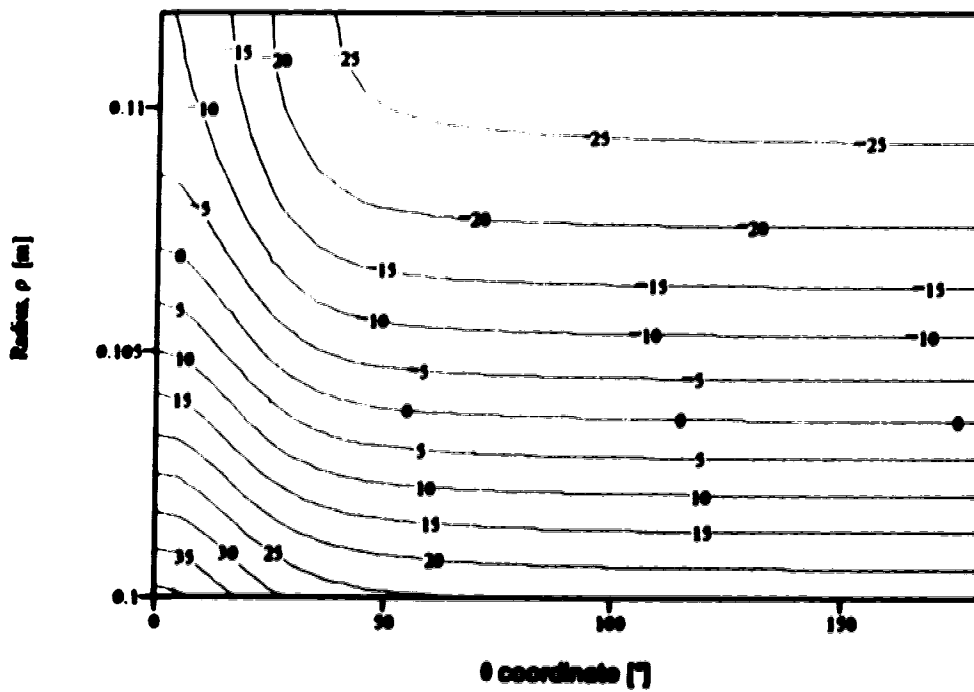


Figure 5-5b Contour plot of the phase of the current density [$^\circ$] in the wellbore casing of sample 2.

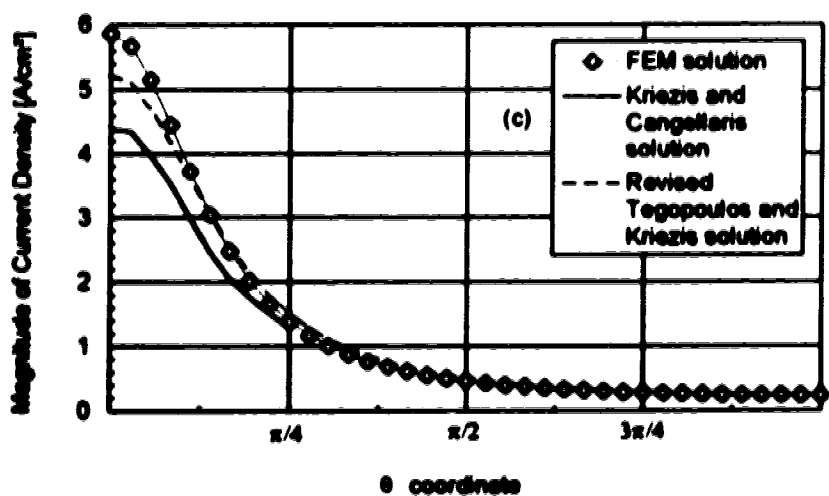
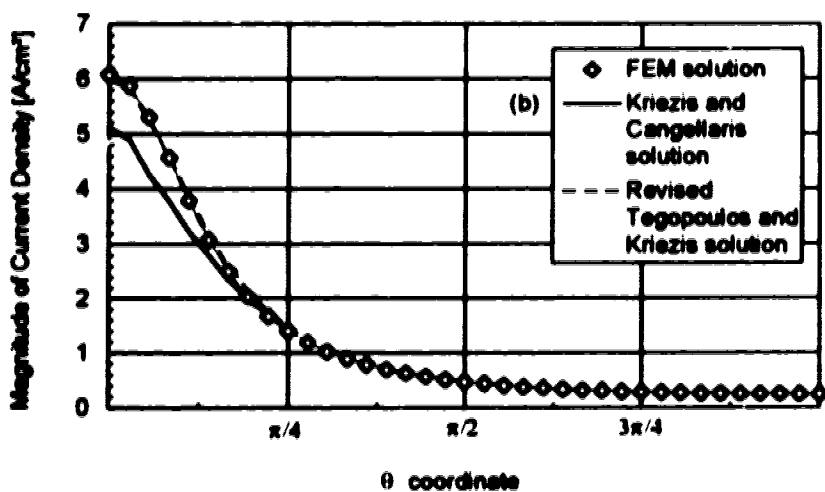
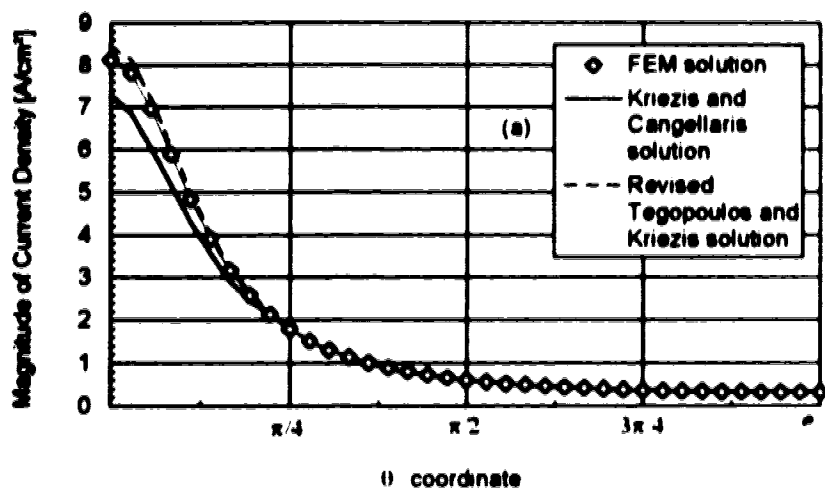


Figure 5-6. Solutions for the current density in wellbore casing sample 2. The magnitude of the current density is plotted for, (a) $\rho=0.100$ m, (b) $\rho=0.106$ m and (c) $\rho=0.112$ m.

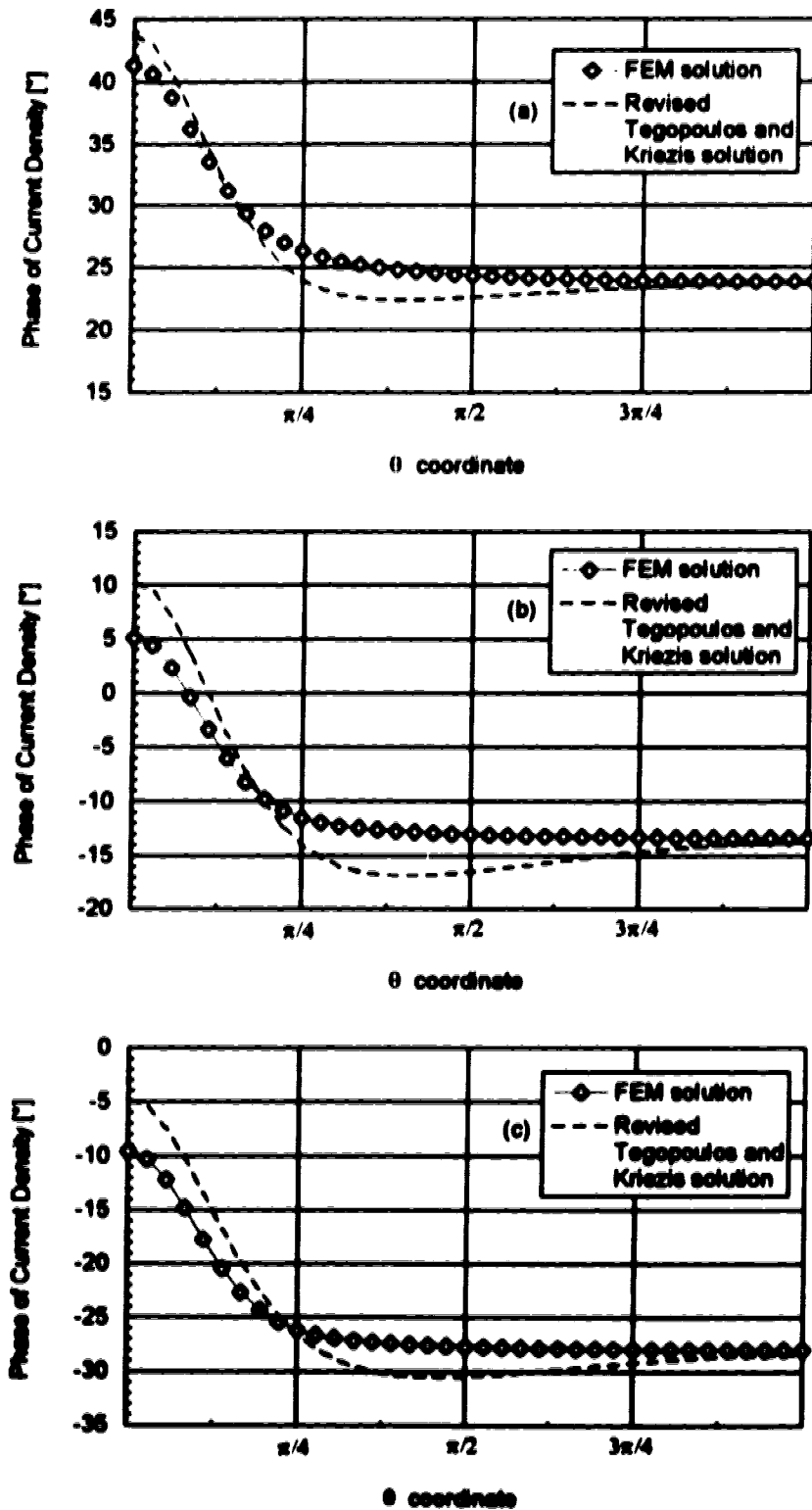


Figure 5-7. Solutions for the current density in wellbore casing sample 2. The phase of the current density is plotted for, (a) $\rho=0.100$ m, (b) $\rho=0.106$ m and (c) $\rho=0.112$ m.

According to Figures 5-6 and 5-7, it appears that the FEM solution for current density is in close agreement with the revised Tegopoulos and Kriezis solution and the Kriezis and Cangelaris solution.

As was done for sample 1, a value for the power loss per meter of casing is derived from the FEM solution. Using the discrete values for the electric field obtained from the FEM solution, the integral of (5.19) is evaluated numerically. The result yields a value of 0.101 W/m for the power dissipated in the casing of sample 2.

As a comparison, the value for the power loss obtained from evaluating (A1.49), the revised Tegopoulos and Kriezis solution, is 0.102 W/m. The power loss based on the solution to integral equation from Figure 9 of reference [13] is 0.081 W/m. Thus, the FEM solution for power loss is within 25% of the integral equation solution and within 1% of the revised Tegopoulos and Kriezis solution.

5.5.3 The Finite Element Method Solution for Sample 3 of Problem 2

For the third casing sample, contour plots of the FEM solution for current density are shown in Figures 5-8a and 5-8b. Also, the FEM solution for current density is again compared with the revised Tegopoulos and Kriezis solution given by equation (A1.24). In addition, because the thickness of the casing in sample 3 is only 25% of the skin depth, Dwight's solution from reference [7] is also included for comparison. Recall from the introduction that Dwight's formula (1.1) is based on the assumption that current density is constant with respect to r , which is essentially true when the casing is much thinner than one skin depth.

Figure 5-9 is a plot of the current density magnitude at the average radius of the casing in sample 3. Similarly, Figure 5-10 is a plot of the phase angle of the current density at the average radius of the casing.

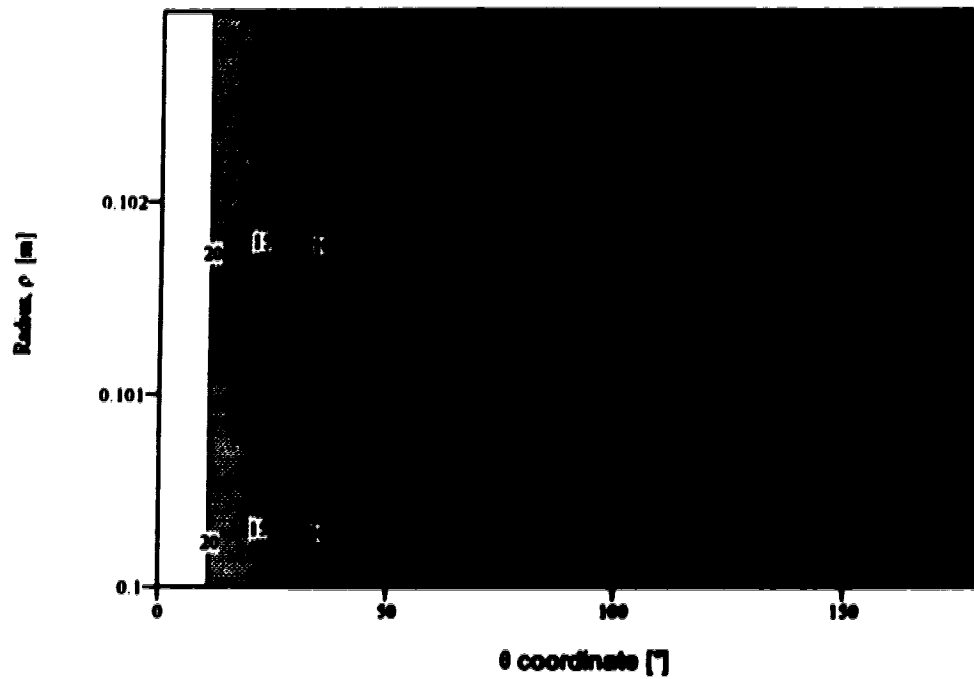


Figure 5-8a Contour plot of the magnitude of the current density [A/cm^2] in the wellbore casing of sample 3.

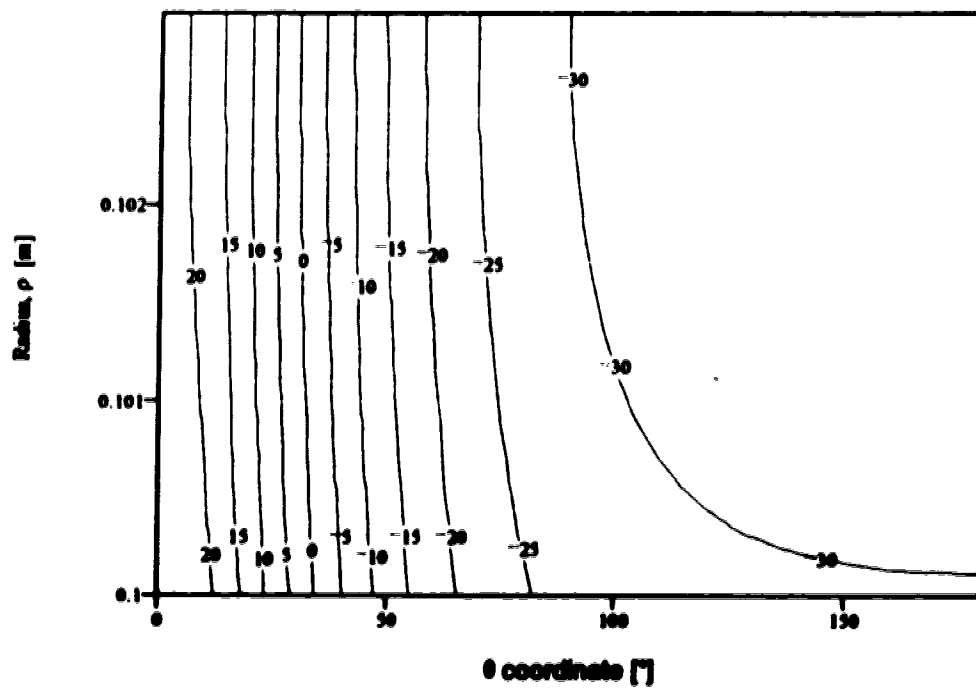


Figure 5-8b Contour plot of the phase of the current density [$^{\circ}$] in the wellbore casing of sample 3.

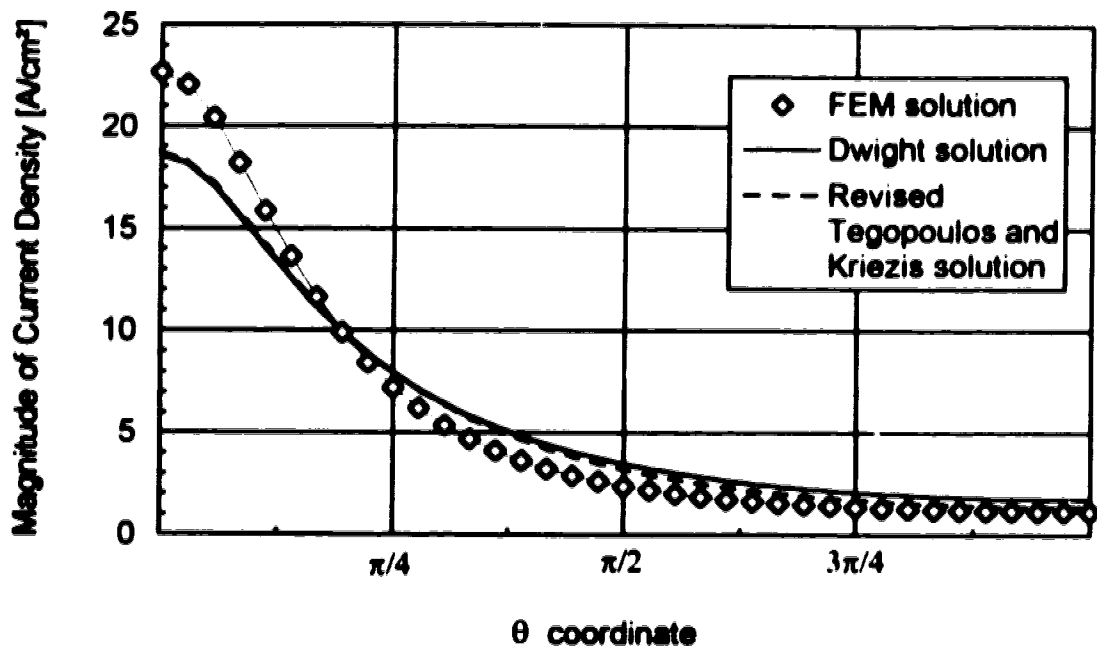


Figure 5-9. Solutions for the magnitude of the current density in wellbore casing sample 3.

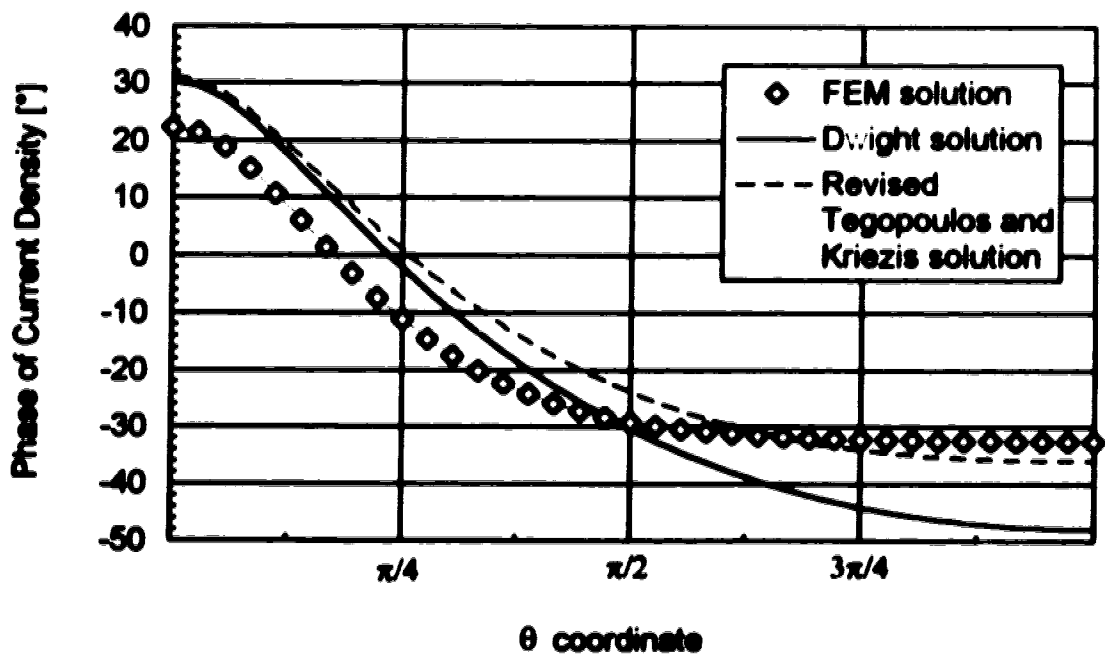


Figure 5-10. Solutions for the phase of the current density in the wellbore casing of sample 3.

From the current density plots in Figures 5-9 and 5-10, it appears that the agreement between the FEM solution and the two comparison solutions is somewhat mediocre. The greatest difference in magnitude between the FEM solution and the other two solutions occurs at $\theta = 0^\circ$; here the FEM solution is about 20% larger than either of the two comparison solutions. There also is some discrepancy between the phase angle solutions in Figure 5-10; the FEM solution differs from the other two solutions by as much as 15° at some points.

The power loss in casing sample 3 was calculated using discrete values for the electric field from the FEM solution and the integral from Poynting's theorem in (5.19). Numerically evaluating (5.19) yields a value for the power loss of 0.36 W/m. In comparison, the power loss obtained from evaluating (A1.49), the revised Tegopoulos and Kriezis solution, is 0.314 W/m.

A second comparison value for power loss can be obtained by substituting Dwight's formula for current density (1.1) into the integral derived from Poynting's theorem,

$$P_{\text{loss}} = \int_0^{2\pi} \int_{0.100}^{0.103} \frac{1}{\sigma} |J(\phi)|^2 r dr d\phi.$$

Evaluating the above integral yields

$$P_{\text{loss}} = \frac{1}{\sigma} \left| \frac{I}{2\pi a t} \right|^2 (a t) \left(2\pi + \pi \sum_{n=1}^{\infty} \left(\frac{s}{a} \right)^{2n} \left(\frac{2l^n}{(n^2 + l^2)} \right)^2 + \pi \sum_{n=1}^{\infty} \left(\frac{s}{a} \right)^{2n} \left(\frac{2nl^2}{(n^2 + l^2)} \right)^2 \right)$$

$$P_{\text{loss}} \cong 0.312 \text{ W/m}, \quad (5.20)$$

where a , t , s and l are as defined in equation (1.1) in chapter 1. Thus, the FEM solution for power loss is within 15% of both Dwight's value and the value from the revised Tegopoulos and Kriezis solution.

5.6 Discrepancies Between the Finite Element Method and Analytical Solutions

The discrepancies between the FEM and analytical solutions in this chapter can be attributed to the use of the approximate boundary condition, $\tilde{H}_2|_{\rho=b} = 0$, in the FEM solutions. Consider the general, analytical solution for $\tilde{H}_2(\rho, \theta)$ which is derived in appendix 4. $\tilde{H}_2(\rho, \theta)$ consists of two field components: $H_{\rho_2}(\rho, \theta)$ and $H_{\theta_2}(\rho, \theta)$. The

general solutions for $H_{\rho_1}(\rho, \theta)$ and $H_{\rho_2}(\rho, \theta)$, given by equations (A4.7) and (A4.8), consist of an infinite number of spatial harmonics with respect to the θ coordinate. *The approximate boundary condition, $\tilde{H}_z|_{\rho=b} = 0$, used for the FEM solution assumes that all the individual harmonics of the magnetic field are zero at the outer wall of the casing.*

For the three casing samples examined in problem 2, the criterion for judging whether $\tilde{H}_z|_{\rho=b} = 0$ is a valid approximation for the exact magnetic field boundary condition is as follows: if the magnetic shielding ratios for the first five spatial harmonics of $H_{\rho_1}(\rho, \theta)$ and $H_{\rho_2}(\rho, \theta)$ are greater than 30 then $\tilde{H}_z|_{\rho=b} = 0$ is a valid approximation. The decision to test only the first five harmonics may seem somewhat arbitrary. In general, the closer a power cable is to the inner wall of the casing, the greater the importance of the higher order harmonics. However, sample 1 of problem 2 can serve as an extreme test case. In sample 1, the power cable was offset from the center of the casing by 0.9 of the inner radius of the casing. In this instance over 80% of the power dissipated in the casing lies in the first five harmonics, according to the analytical expression for power loss from equation (A1.49). In instances where the cable is offset by more than 0.9 of the inner radius, higher order harmonics of $H_{\rho_1}(\rho, \theta)$ and $H_{\rho_2}(\rho, \theta)$ should be tested.

The shielding ratio formulae for individual harmonics of $H_{\rho_1}(\rho, \theta)$ and $H_{\rho_2}(\rho, \theta)$ are derived in appendix 4 and given by expressions (A4.9) and (A4.10), respectively. Note that the expression for the magnetic shielding ratio given by (2.43) in chapter 2 is actually the shielding ratio for the zeroth harmonic of H_{ρ_1} . The H_{ρ_1} and H_{ρ_2} magnetic shielding ratios for casing samples 1, 2 and 3 are presented in Tables 5-2 and 5-3.

Table 5-2. Magnetic shielding ratios for the first five harmonics of $H_{\rho_1}(\rho, \theta)$ in casing samples 1 to 3.

Sample	$\left \frac{H_{\rho_1}(a, \theta)_{n=0}}{H_{\rho_1}(b, \theta)_{n=0}} \right $	$\left \frac{H_{\rho_1}(a, \theta)_{n=1}}{H_{\rho_1}(b, \theta)_{n=1}} \right $	$\left \frac{H_{\rho_1}(a, \theta)_{n=2}}{H_{\rho_1}(b, \theta)_{n=2}} \right $	$\left \frac{H_{\rho_1}(a, \theta)_{n=3}}{H_{\rho_1}(b, \theta)_{n=3}} \right $	$\left \frac{H_{\rho_1}(a, \theta)_{n=4}}{H_{\rho_1}(b, \theta)_{n=4}} \right $
1	331.9	21.2	11.0	7.6	6.0
2	331.9	21.2	11.0	7.6	6.0
3	198.5	12.2	6.11	4.08	3.06

Table 5-3. Magnetic shielding ratios for the first four harmonics of $H_{\rho_2}(\rho, \theta)$ in casing samples 1 to 3.

Sample	$\left \frac{H_{\rho_2}(a, \theta)_{n=1}}{H_{\rho_2}(b, \theta)_{n=1}} \right $	$\left \frac{H_{\rho_2}(a, \theta)_{n=2}}{H_{\rho_2}(b, \theta)_{n=2}} \right $	$\left \frac{H_{\rho_2}(a, \theta)_{n=3}}{H_{\rho_2}(b, \theta)_{n=3}} \right $	$\left \frac{H_{\rho_2}(a, \theta)_{n=4}}{H_{\rho_2}(b, \theta)_{n=4}} \right $
1	1.65	1.77	1.89	2.00
2	1.65	1.77	1.89	2.00
3	1.08	1.11	1.14	1.17

On the basis of the data in Tables 5-2 and 5-3, the approximation $\tilde{H}_2|_{\rho=b} = 0$ is difficult to justify. For each of the three casing samples, only the zeroth harmonic of the H_0 shielding ratio is greater than 30. Thus, for the three casing samples, $\tilde{H}_2|_{\rho=b} = 0$ is a poor substitute for the exact magnetic field boundary condition at $\rho = b$. This explains the sometimes mediocre agreement between the FEM and analytical solutions of problem 2. For casing sample 3, which has the lowest shielding ratios, $\tilde{H}_2|_{\rho=b} = 0$ is a very poor approximation and as a result, the discrepancies between the FEM and analytic solutions for current density and power dissipated are particularly large.

Note that although casing samples 1 and 2 have identical shielding ratios, the approximation $\tilde{H}_2|_{\rho=b} = 0$ seems more valid for sample 2 than for sample 1 because the FEM and analytic solutions for sample 2 are in much closer agreement. This anomaly can be explained by comparing the power distribution in the spatial harmonics of the electromagnetic fields in samples 1 and 2. For both samples, the power in the $n=0$ harmonic is 0.04 W/m, according to the $n=0$ term from the analytic expression for power loss (A1.49). For sample 2, in which the total power dissipated is 0.10 W/m, the $n=0$ harmonic contains 40% of the total power. However for sample 1, in which the total power dissipated is 0.24 W/m, the $n=0$ harmonic contains only 17% of the total power.

In general, sample 2 has a greater percentage of total power in the lower spatial harmonics than does sample 1. This is because the power cable is located closer to the center of the casing in sample 2 than it is in sample 1. Therefore, even though the

magnetic shielding ratios in samples 1 and 2 are identical, the shielding ratios for the lower order harmonics are "weighted" more heavily in sample 2 than in sample 1. Since the lower order harmonics generally have larger shielding ratios, $\tilde{H}_z|_{\rho=a} = 0$ is a better approximation for sample 2 than for sample 1.

In a subsequent test, FEM and analytical solutions were obtained for a fourth casing sample where the approximate boundary condition, $\tilde{H}_z|_{\rho=a} = 0$, was justified. The casing sample was over four skin depths thick and as a result the shielding ratios for the first five harmonics of the magnetic field were all greater than 30. The agreement between the FEM and analytic solutions was excellent. This is further evidence that the differences between the FEM and analytical solutions for samples 1, 2 and 3 are due to the use of the approximate boundary condition.

5.7 Conclusion

For problem 2, the boundary value problem illustrated in Figure 5-1a, the FEM method can provide a reasonably accurate solution for the electric field in the wellbore casing, provided the approximate boundary condition, $\tilde{H}_z|_{\rho=a} = 0$, is valid. For the three casing samples examined in this chapter, the accuracy of the FEM solutions is generally good, although there are some instances where the analytic and FEM solutions for power loss differ by as much as 50%. The discrepancies between the FEM and analytical solutions may be attributed to the fact that the justification for the approximate boundary condition was relatively weak.

CHAPTER 6

A Finite Element Method Solution For a Complex Two Dimensional Boundary Value Problem

Expanding upon the boundary value problem posed in problem 2, consider a wellbore casing that encompasses multiple power cables. Each cable carries an alternating current at an arbitrary phase. The cables may be arranged in an arbitrary configuration inside the casing. Two possible configurations are considered in the following boundary value problems.

6.1 A Description of Problem 3a

Boundary value problem 3a is illustrated in Figure 6-1a. Three power cables are arranged in a triangular configuration as shown in the diagram. Each cable carries a 300 A rms current at a frequency of 50 Hz. The currents in the three power cables constitute a balanced, three phase system. The casing has a relative permeability of unity and a resistivity of $2 \times 10^{-8} \Omega \cdot \text{m}$. The skin depth of the casing is approximately 10 mm. Casings of various thicknesses will be examined. The properties and dimensions have been chosen to match the values used in an example from reference [10]. The solutions calculated in reference [10] by Kawasaki, Inami and Ishikawa will serve as a check for the FEM solutions of problem 3a.

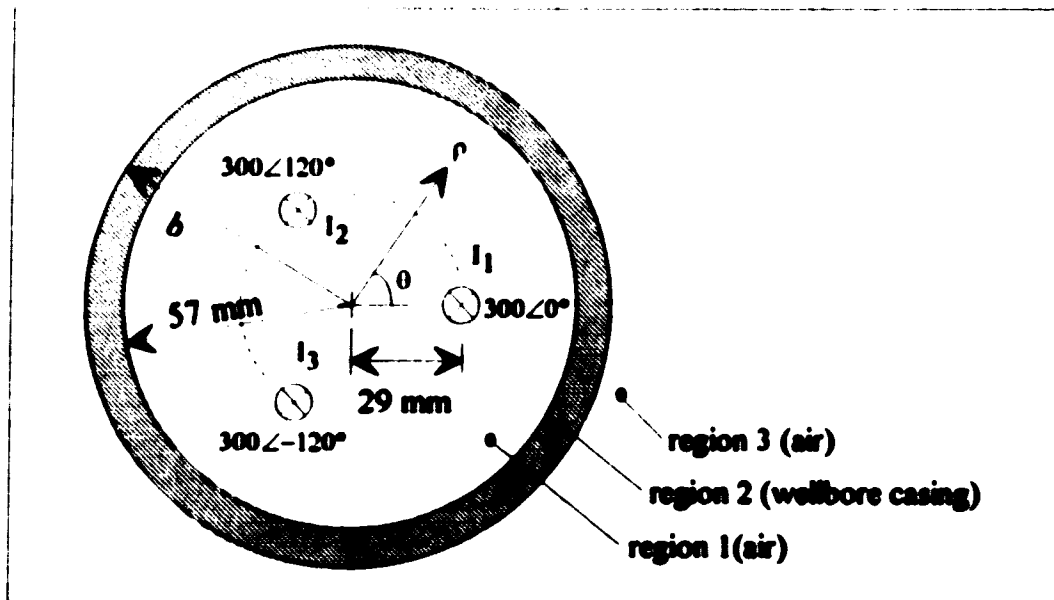


Figure 6-1a. A diagram of problem 3a

In Figure 6-1a, the outer radius of the wellbore casing is not specified. This is because different thicknesses of casings are to be considered. The inner radius for the casing is fixed at 57.3 mm. The outer radii and resultant thicknesses are listed in Table 6-1.

Table 6-1. The outer radii and thicknesses for each casing analyzed in problem 3a

Casing #	Outer radius 'h' [mm]	Casing thickness [mm]	<u>casing thickness</u> skin depth
1	59.3	2	0.2
2	61.3	4	0.4
3	63.3	6	0.6
4	65.3	8	0.8
5	67.3	10	1.0
6	69.3	12	1.2
7	71.3	14	1.4

6.2 A Description of Problems 3b and 3c

Boundary value problem 3b is also based on an example from reference [10]. Problem 3b is illustrated in Figure 6-1b. The three power cables inside the casing are arranged in what is referred to as a "cradle" configuration. Each cable carries a current of 1000 A rms at a frequency of 50 Hz. Once again, the currents in the power cables constitute a balanced, three phase system. The casing has a relative permeability of 200 and a resistivity of $20 \times 10^{-8} \Omega \cdot m$.

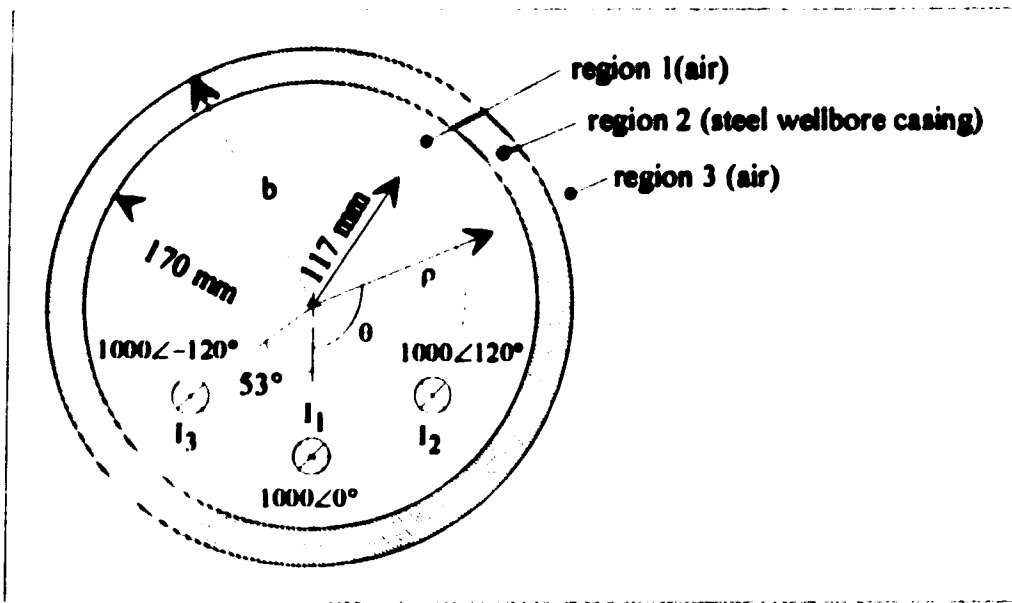


Figure 6-1b. A diagram of problems 3b and 3c

Boundary value problem 3c is basically identical to problem 3b. The only difference is the magnetic permeability of the wellbore casing. For problem 3c, the relative permeability of the casing is 700.

As with problem 3a, wellbore casings of various thicknesses are considered in problems 3b and 3c. The inner radius for each casing is fixed at 0.170 m. The outer radii are listed in Tables 6-2 and 6-3.

Table 6-2. The outer radii and thicknesses for each casing analyzed in problem 3b.

Casing sample #	Outer radius ' b ' [m]	Casing thickness Skin depth
1	0.17225	1
2	0.1745	2
3	0.17675	3
4	0.179	4
5	0.18125	5

Table 6-3. The outer radii and thicknesses for each casing analyzed in problem 3c.

Casing #	Outer radius ' b ' [m]	Casing thickness Skin depth
1	0.1712	1
2	0.1724	2
3	0.1736	3
4	0.1748	4
5	0.1760	5

6.3 The Method of Solution for a Multiple Cable Problem

Superposition is invoked to help solve this problem in the same manner it was used by Dwight [7] and Kawasaki et al. [10] to solve the problem analytically. Essentially, the multiple power cable problem is solved by breaking it down into a series of single cable problems. The single cable problem consists of only the casing and one cable. All other

cables are removed from the problem. A FEM solution is then obtained for the electromagnetic fields created by the current in the single cable. The process is repeated for all other cables until a FEM solution is obtained for each one. The individual solutions are then superimposed to produce a solution for the original problem, in which all the currents are present. *Note the individual solutions are superimposed with due regard to the azimuthal positions of the power cables in the original multi-cable problem.*

For problems examined in this chapter, the three power cables are all the same radial distance from the center of the casing. The magnitudes of the currents in all three cables are also the same. Therefore it is not strictly necessary to obtain a FEM solution for all three single cable problems of the multi-cable problem. Rather, a FEM solution need only be obtained for one of the single cable problems. The solutions for the other two *single cable problems* are then obtained by multiplying the available FEM solution by $e^{\pm j120^\circ}$ to account for the differing phases in the cable currents. However, for more general problems, where the individual power cables may be at different radial distances from the center of the casing, a separate FEM solution must be obtained for each single cable problem.

The method for solving a multi-cable problem is formally described as follows.

1. Subdivide the multiple cable problem into a series of single cable problems and map the domain of each single cable problem onto a mesh to be conveyed UNAFEM II. In some instances, the same mesh can be used for more than one of the single cable problems.
2. Write the partial differential equation for the single cable problem in a form that is solvable by UNAFEM II. Then, identify the numerical constants in the equation which UNAFEM II requires to compute a FEM solution.
3. Impose the approximate boundary condition $\hat{H}_z|_{r=a} = 0$ on the multi-cable boundary value problem. Because this boundary condition is homogeneous, $\hat{H}_z|_{r=a} = 0$ can also be imposed on each of the single cable problems.
4. Test the validity of the approximation $\hat{H}_z|_{r=a} = 0$ in the *single cable* problems. If $\hat{H}_z|_{r=a} = 0$ is a valid approximation in *all* of the single cable problems then $\hat{H}_z|_{r=a} = 0$ should be a good approximation in the multi-cable problem.

5. Define the boundary conditions for the magnetic field at the surface of the power cable, accounting for the magnitude and phase of the current carried by the cable. If the total current in a given power cable is essentially the same in both single and multi-cable problems, then the magnetic field *tangential to the surface of the cable* should be very similar in both the single and multi-cable problems.
6. Compute the FEM solution for the single cable problem using UNAFEM II.
7. Repeat steps 5 and 6 for each power cable present in the original problem.
8. Superimpose the single cable FEM solutions to obtain the total electric field *in the casing* of the original multi-cable problem. The single cable solutions must be superimposed with due regard to the azimuthal positions of the power cables in the original multi-cable problem (this step is detailed in section 6.3.1).

Note that it is also possible to compute a single FEM solution for a multiple cable problem where all currents are initially taken into account. This approach introduces two additional complications. First, the difficulty in designing a mesh to model the domain of the problem is increased. This is particularly true when attempting to represent the curved surface of small diameter cables with straight lines or quadratic curves.

The second complication arises when it becomes necessary to define the non-homogeneous boundary condition at the surface of the power cables. For a single cable problem, a local system of polar coordinates (r, ϕ) may be defined at the center of the cable and the boundary condition written simply as $H_{\phi}(r_{cable}, \phi) = I / 2\pi r_{cable}$. However, if more than one cable is present, then there is no alternative but to define the boundary conditions on the surfaces of the cables using a single, global coordinate system. This yields awkward and complicated expressions for the boundary conditions.

6.3.1 The Superposition of the Single Cable Solutions

In step 8 from section 6.3, it was stated that single cable FEM solutions are superimposed to obtain the solution for the electric field in a multi-cable problem. Moreover, the single cable solutions are superimposed with due regard to the azimuthal positions of the power cables in the original multi-cable problem. This process is explained in more detail in this section.

For each single cable problem, UNAFEM II computes numerical values for the electric field at discrete points in the domain of the single cable problem. These discrete points are at the *nodes* of the mesh which models the problem domain. It is the “nodal” values of the electric field from each of the single cable problems which are superimposed.

In this chapter, it is the electric field in region 2 (the wellbore casing) which is of primary interest. Therefore, only nodal values of the electric field from region 2 of the single cable problems will be superimposed. Consider the simple example illustrated schematically in Figure 6-2. The total electric field at node 1 in the original multi-cable problem is equal to the electric field at *node 5* in single cable problem #1 plus the electric field at *node 1* in single cable problem #2 plus the electric field at *node 15* in single cable problem #3. Similarly, the total electric field at node 2 in the original multi-cable problem is equal to the electric field at *node 6* in single cable problem #1 plus the electric field at *node 2* in single cable problem #2 plus the electric field at *node 16* in single cable problem #3. The total field at other nodes in the original problem is calculated in a like manner.

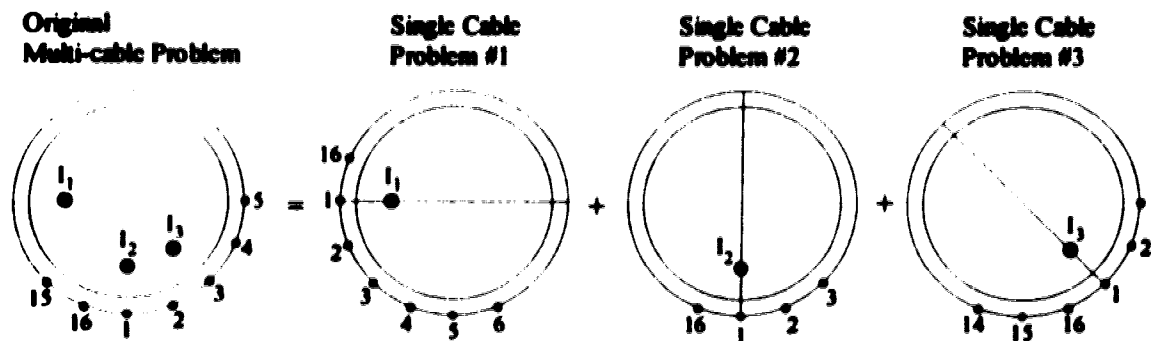


Figure 6-2. A simple example of the superposition of the single cable solutions.

6.4 Modeling the Domains of Problems 3a, 3b and 3c for UNAFEM II

As mentioned in section 6.3, a problem with multiple power cables is subdivided into a set of single cable problems. Note that the single cable problems are all essentially the same as problem 2 from the previous chapter. With only the casing and a single cable present, the domain of the problem is symmetric about $\phi = 0$. Thus, as with problem 2, the domain of the single cable problem need only be modeled by a semicircular mesh which extends radially from the surface of the power cable to the outer wall of the casing, and azimuthally from $\phi = 0^\circ$ to $\phi = 180^\circ$.

Thus for each single cable problem, a FEM solution will provide numerical values for the electric field (induced by a single cable) in the wellbore casing *at discrete points from* $\phi = 0^\circ$ *to* $\phi = 180^\circ$. However, prior to superimposing the single cable solutions, the solutions must be expanded to provide numerical values for the electric field at points *around the entire circumference of the wellbore casing* (not just from $\phi = 0^\circ$ to $\phi = 180^\circ$). This presents no real problem because the single cable problem has even azimuthal symmetry and therefore $\vec{E}_{\text{single cable}}(r, \phi) = \vec{E}_{\text{single cable}}(r, -\phi)$.

Based on Figure 6-1a and the casing dimensions given in Table 6-1, semicircular meshes are constructed to model each casing analyzed in problem 3a. Similarly, meshes are also constructed for each casing analyzed in problems 3b and 3c using Figure 6-3 and the casing dimensions given in Tables 6-2 and 6-3. These meshes are all included in appendix 5.

6.5 The Partial Differential Equation for the Single Cable Problem

The partial differential equation for the single cable problem is derived in section 5.1 and is given by equation (5.1). Section 5.1 also identifies the constants in the partial differential equation that are required by UNAFEM II to compute a FEM solution.

6.6 The Boundary Condition at the Outer Wall of the Wellbore Casing

For the single cable problem, the boundary condition on the magnetic field at the outer wall of the casing is given by the approximation $\vec{H}_2|_{\rho=b} = 0$. In terms of UNAFEM II notation, this boundary condition corresponds to

$$-\left(\hat{a}_x \alpha_x \frac{\partial U}{\partial x} \Big|_{\text{outer boundary}} + \hat{a}_y \alpha_y \frac{\partial U}{\partial y} \Big|_{\text{outer boundary}} \right) \cdot \hat{a} = 0. \quad (6.1)$$

Expression (6.1) is the UNAFEM II boundary condition at the outer wall of the casing. The relationships between UNAFEM II boundary conditions and magnetic field boundary conditions in the single cable problem were discussed in detail in sections 5.4 and 5.4.3.

6.7 The Validity of the Approximation $\bar{H}_2|_{\rho=b} = 0$

For each casing in the single cable problems constructed from multi-cable problems 3a, 3b and 3c, the validity of the approximation $\bar{H}_2|_{\rho=b} = 0$ is tested by examining the magnetic shielding ratios. As was discussed in section 5.6, if the magnetic shielding ratios for the first five harmonics of $H_{\rho_2}(\rho, \theta)$ and $H_{\theta_2}(\rho, \theta)$ are greater than 30 then $\bar{H}_2|_{\rho=b} = 0$ is a good approximation. In some cases where the shielding ratio for the *zeroth* harmonic is much greater than 30 but the shielding ratios for all other harmonics are less than 30, $\bar{H}_2|_{\rho=b} = 0$ may still be a satisfactory approximation.

Using the formulae from (A4.9) and (A4.10) and the data given in the sections 6.1 and 6.2, shielding ratios are calculated for each casing sample analyzed in problems 3a, 3b and 3c. The values for the shielding ratios and conclusions regarding the validity of the approximation $\bar{H}_2|_{\rho=b} = 0$ are presented in Tables 6-4, 6-5 and 6-6.

Table 6-4. A check of the approximation $\bar{H}_2|_{\rho=0} = 0$ for casing samples 1 to 7 from problem 3a.

	Casing #1	Casing #2	Casing #3	Casing #4	Casing #5	Casing #6	Casing #7
$\frac{H_{\rho_1}(a, \theta)_{n=0}}{H_{\rho_1}(b, \theta)_{n=0}}$	40.1	84.1	132.5	185.9	245.8	314.6	395.9
$\frac{H_{\rho_1}(a, \theta)_{n=1}}{H_{\rho_1}(b, \theta)_{n=1}}$	2.6	5.2	8.2	11.6	15.5	19.9	25.2
$\frac{H_{\rho_1}(a, \theta)_{n=2}}{H_{\rho_1}(b, \theta)_{n=2}}$	1.6	2.8	4.3	6.1	8.2	10.5	13.4
$\frac{H_{\rho_1}(a, \theta)_{n=3}}{H_{\rho_1}(b, \theta)_{n=3}}$	1.3	2.1	3.1	4.3	5.7	7.4	9.5
$\frac{H_{\rho_1}(a, \theta)_{n=4}}{H_{\rho_1}(b, \theta)_{n=4}}$	1.2	1.7	2.5	3.4	4.5	5.9	7.5
$\frac{H_{\rho_2}(a, \theta)_{n=1}}{H_{\rho_2}(b, \theta)_{n=1}}$	1.1	1.2	1.3	1.5	1.8	2.2	2.9
$\frac{H_{\rho_2}(a, \theta)_{n=2}}{H_{\rho_2}(b, \theta)_{n=2}}$	1.1	1.3	1.4	1.7	2.0	2.4	3.1
$\frac{H_{\rho_2}(a, \theta)_{n=3}}{H_{\rho_2}(b, \theta)_{n=3}}$	1.2	1.3	1.5	1.8	2.2	2.7	3.3
$\frac{H_{\rho_2}(a, \theta)_{n=4}}{H_{\rho_2}(b, \theta)_{n=4}}$	1.2	1.4	1.6	1.9	2.3	2.9	3.9
$\bar{H}_2 _{\rho=0}$ justified ?	----- Inconclusive -----						

For the casing samples in Table 6-4, the decision as to whether $\hat{H}_2|_{\rho=b} = 0$ is a justifiable approximation is inconclusive. Even though the shielding ratios for the zeroth harmonic of the H_0 , are the only shielding ratios greater than 30, it will be seen later that the FEM based solutions for the eddy current losses in casings 4 through 7 agree relatively well with corresponding analytical solutions.

Table 6-5. A check of the approximation $\tilde{H}_2|_{\rho=b} = 0$ for casing samples 1 to 5 from problem 3b.

	Casing #1	Casing #2	Casing #3	Casing #4	Casing #5
$\frac{ H_{\theta_1}(a, \theta)_{n=0} }{ H_{\theta_1}(b, \theta)_{n=0} }$	13.2	35.6	97.1	269.0	743.4
$\frac{ H_{\theta_1}(a, \theta)_{n=1} }{ H_{\theta_1}(b, \theta)_{n=1} }$	1.8	5.4	14.8	40.6	111.6
$\frac{ H_{\theta_1}(a, \theta)_{n=2} }{ H_{\theta_1}(b, \theta)_{n=2} }$	1.5	4.5	12.4	34.0	93.2
$\frac{ H_{\theta_1}(a, \theta)_{n=3} }{ H_{\theta_1}(b, \theta)_{n=3} }$	1.5	4.2	11.7	31.9	87.4
$\frac{ H_{\theta_1}(a, \theta)_{n=4} }{ H_{\theta_1}(b, \theta)_{n=4} }$	1.4	4.1	11.3	30.9	84.5
$\frac{ H_{\theta_2}(a, \theta)_{n=1} }{ H_{\theta_2}(b, \theta)_{n=1} }$	3.9	10.1	27.7	76.1	209.0
$\frac{ H_{\theta_2}(a, \theta)_{n=2} }{ H_{\theta_2}(b, \theta)_{n=2} }$	6.6	17.0	46.4	127.3	348.9
$\frac{ H_{\theta_2}(a, \theta)_{n=3} }{ H_{\theta_2}(b, \theta)_{n=3} }$	9.3	24.0	65.3	179.2	490.7
$\frac{ H_{\theta_2}(a, \theta)_{n=4} }{ H_{\theta_2}(b, \theta)_{n=4} }$	12.0	31.1	84.3	231.3	633.2
$\tilde{H}_2 _{\rho=b} = 0$ justified ?	no	inconclusive	inconclusive	yes	yes

Table 6-6. A check of the approximation $\bar{H}_2|_{p,b} = 0$ for casing samples 1 to 5 from problem 3c.

	Casing #1	Casing #2	Casing #3	Casing #4	Casing #5
$\frac{ H_{\theta_1}(a,\theta)_{n,0} }{ H_{\theta_1}(b,\theta)_{n,0} }$	7.4	20.0	54.2	148.5	406.4
$\frac{ H_{\theta_1}(a,\theta)_{n,1} }{ H_{\theta_1}(b,\theta)_{n,1} }$	1.6	4.5	12.3	33.6	91.5
$\frac{ H_{\theta_1}(a,\theta)_{n,2} }{ H_{\theta_1}(b,\theta)_{n,2} }$	1.4	4.1	11.2	30.4	82.7
$\frac{ H_{\theta_1}(a,\theta)_{n,3} }{ H_{\theta_1}(b,\theta)_{n,3} }$	1.4	3.9	10.8	29.4	79.9
$\frac{ H_{\theta_1}(a,\theta)_{n,4} }{ H_{\theta_1}(b,\theta)_{n,4} }$	1.4	3.9	10.6	28.9	78.5
$\frac{ H_{r_2}(a,\theta)_{n,1} }{ H_{r_2}(b,\theta)_{n,1} }$	6.2	15.9	43.1	117.6	320.4
$\frac{ H_{r_2}(a,\theta)_{n,2} }{ H_{r_2}(b,\theta)_{n,2} }$	11.3	28.9	78.0	212.8	579.4
$\frac{ H_{r_2}(a,\theta)_{n,3} }{ H_{r_2}(b,\theta)_{n,3} }$	16.3	42.0	113.1	308.5	839.7
$\frac{ H_{r_2}(a,\theta)_{n,4} }{ H_{r_2}(b,\theta)_{n,4} }$	21.4	55.1	148.2	404.3	1100.4
$\bar{H}_2 _{p,b} = 0$ justified?	no	inconclusive	inconclusive	yes	yes

6.8 The Boundary Conditions at the Surface of the Power Cable and Along the Line of Azimuthal Symmetry

For the single cable problem, the boundary condition for the magnetic field at the surface of the cable is closely approximated by

$$H_{\phi}(r_{cable}, \phi) = \frac{I}{2\pi r_{cable}} \quad (6.2)$$

This magnetic field boundary condition may be easily related to a UNAFEM II boundary condition using the relations derived in section 5.4.1. According to (5.12), the UNAFEM II boundary condition at the surface of the power cable is

$$-\left(\hat{\mathbf{n}}_x \alpha_x \frac{\partial U}{\partial x} \Big|_{\text{inner boundary}} + \hat{\mathbf{n}}_y \alpha_y \frac{\partial U}{\partial y} \Big|_{\text{inner boundary}} \right) \cdot \hat{\mathbf{n}} \Rightarrow \frac{I}{2\pi} \quad (6.3)$$

This is the same boundary condition applied to problem 2 in chapter 5

Along the line of azimuthal symmetry which bisects the single cable problem into two semicircular sections, $H_r = 0$. Again, this is the same boundary condition which was applied to problem 2 in chapter 5. The resultant UNAFEM II boundary conditions is

$$-\left(\hat{\mathbf{n}}_x \alpha_x \frac{\partial U}{\partial x} \Big|_{\phi = \frac{\pi}{2} \text{ or } \frac{3\pi}{2}} + \hat{\mathbf{n}}_y \alpha_y \frac{\partial U}{\partial y} \Big|_{\phi = \frac{\pi}{2} \text{ or } \frac{3\pi}{2}} \right) \cdot \hat{\mathbf{n}} \Rightarrow 0.$$

6.9 Finite Element Method Solutions for the Multi-Cable Problem Analyzed in Problem 3a

For *each* casing analyzed in problem 3a, three FEM solutions are computed using UNAFEM II. Each FEM solution yields a solution for that portion of the total electric field in problem 3a which can be attributed to the current in a *single* power cable. The three single cable solutions are superimposed to obtain the total electric field in a given casing. Note the single cable solutions are superimposed with due regard to the original, azimuthal positions of the power cables in problem 3a. For casing 1 of problem 3a, this process is illustrated below in Figure 6-3.

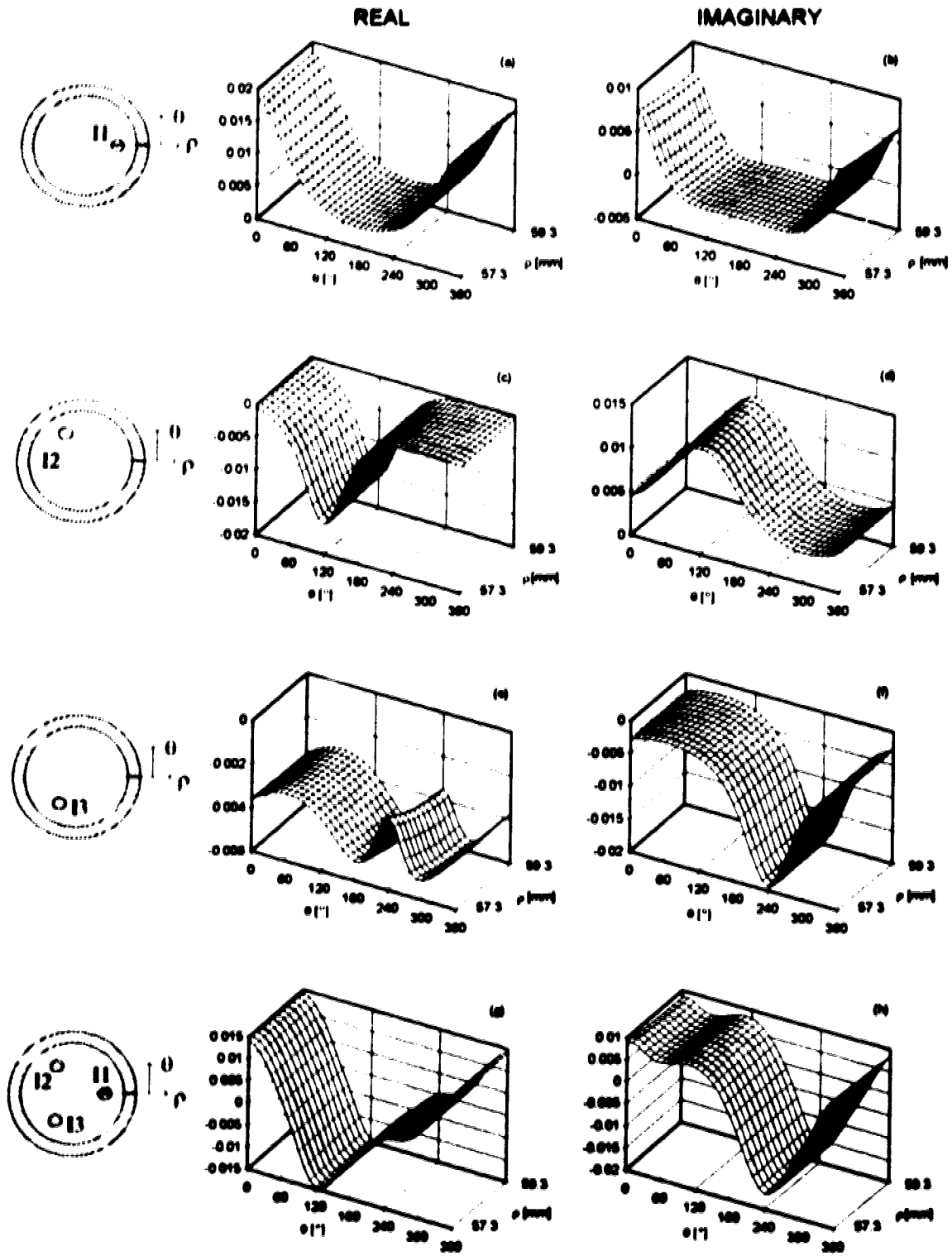


Figure 6-3 Real and imaginary components of the electric field intensity [V/m] in casing 1 of problem 3a.

Figures 6-3 (a), (c) and (e) are the single cable FEM solutions for the real components of the electric field in the wellbore casing. Similarly, Figures 6-3 (b), (d) and (f) are the single cable FEM solutions for the imaginary components of the electric field in the casing. Figures 6-3 (g) and (h) are, respectively, the sums of the individual real and imaginary solutions. Thus, Figures 6-3 (g) and (h) represent the total electric field induced in casing 1 by all three currents in problem 3a.

Contour plots of the FEM solutions for the current density (σE_z) in casings 1 through 7 of problem 3a are shown in Figures 6-4 to 6-10.

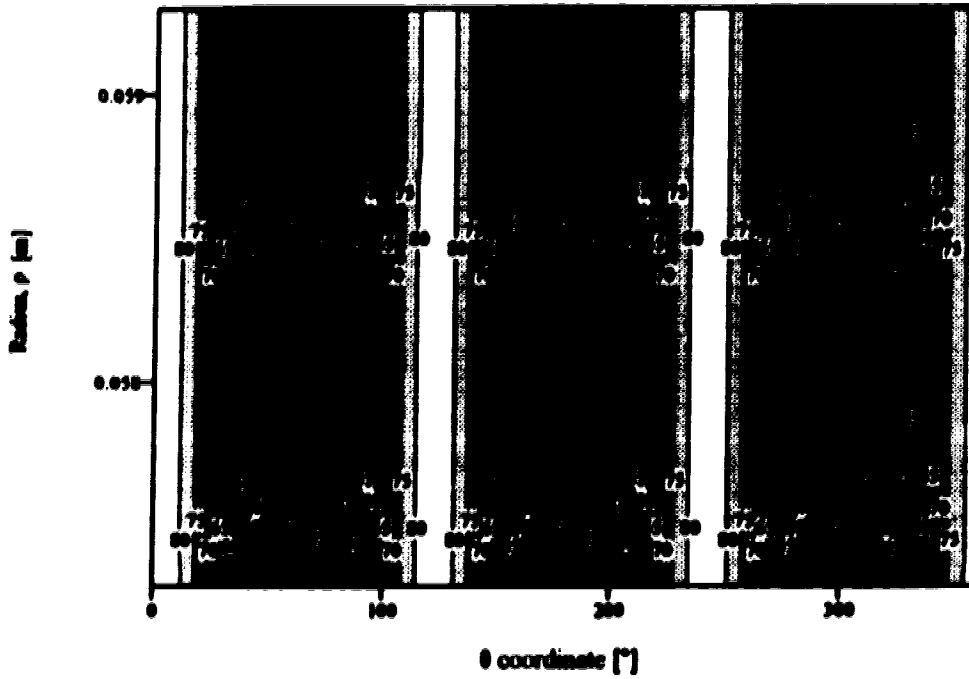


Figure 6-4a Contour plot of the magnitude of the current density [A/cm²] in wellbore casing #1.

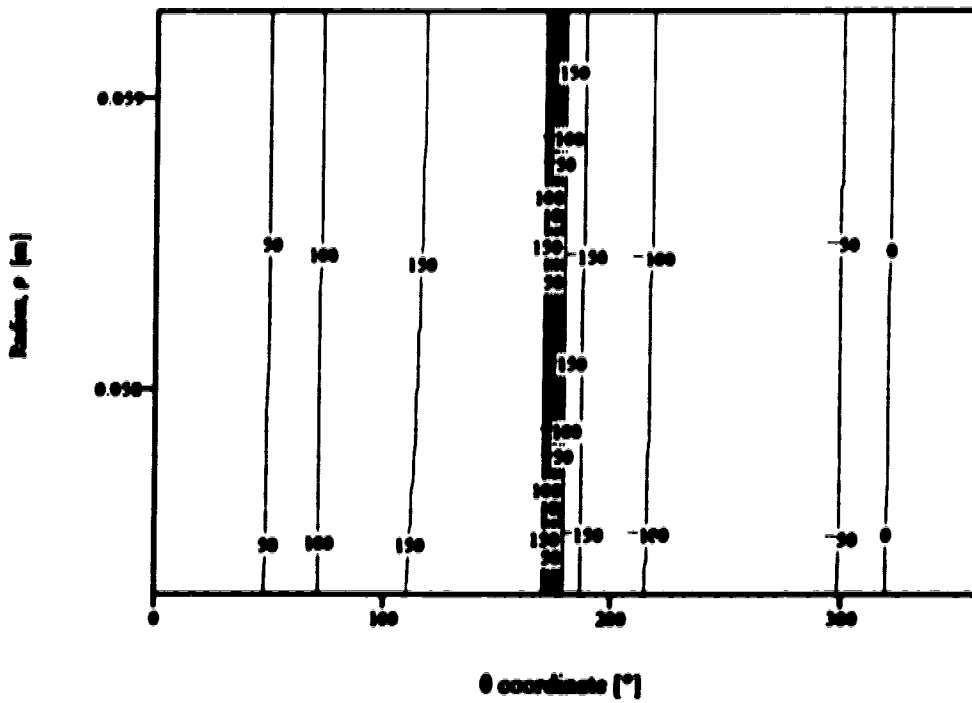


Figure 6-4b Contour plot of the phase of the current density [°] in wellbore casing #1.

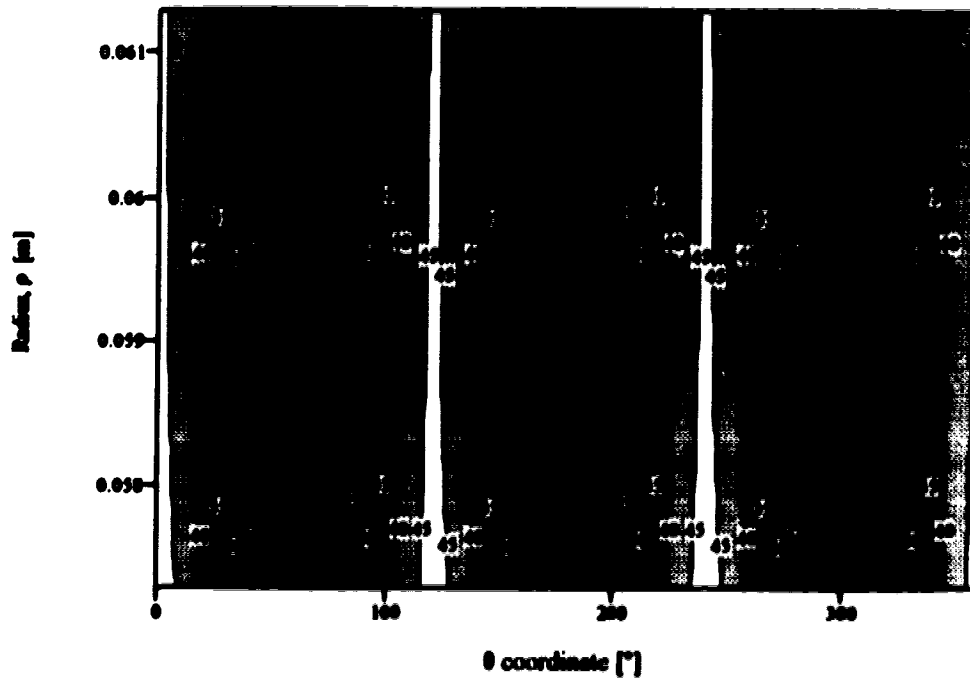


Figure 6-5a Contour plot of the magnitude of the current density [A/cm²] in wellbore casing 2.

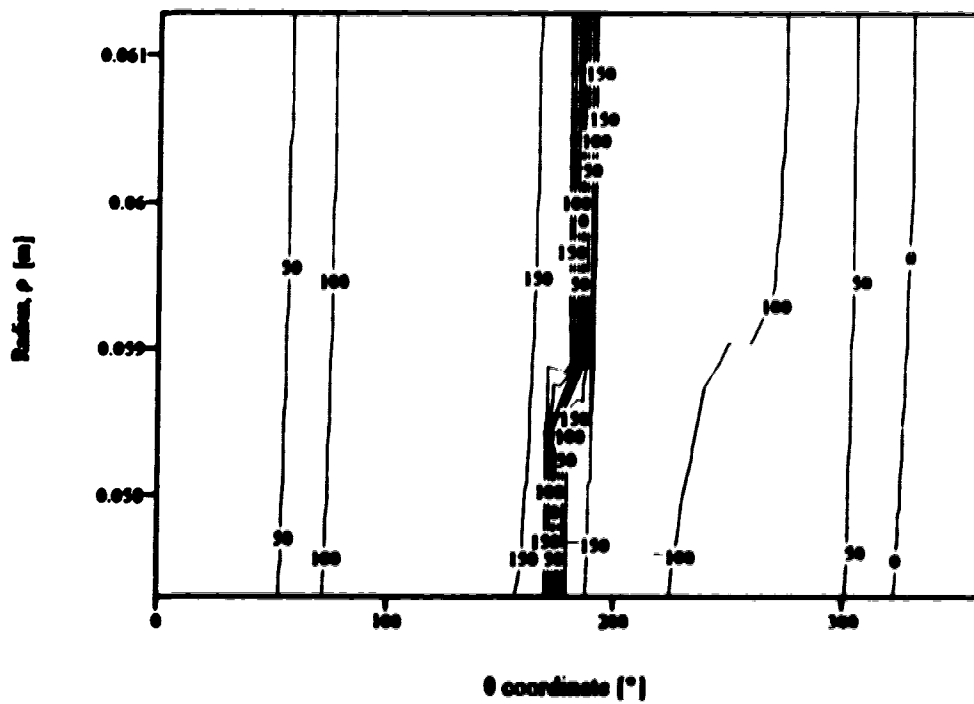


Figure 6-5b Contour plot of the phase of the current density [$^{\circ}$] in wellbore casing 2.

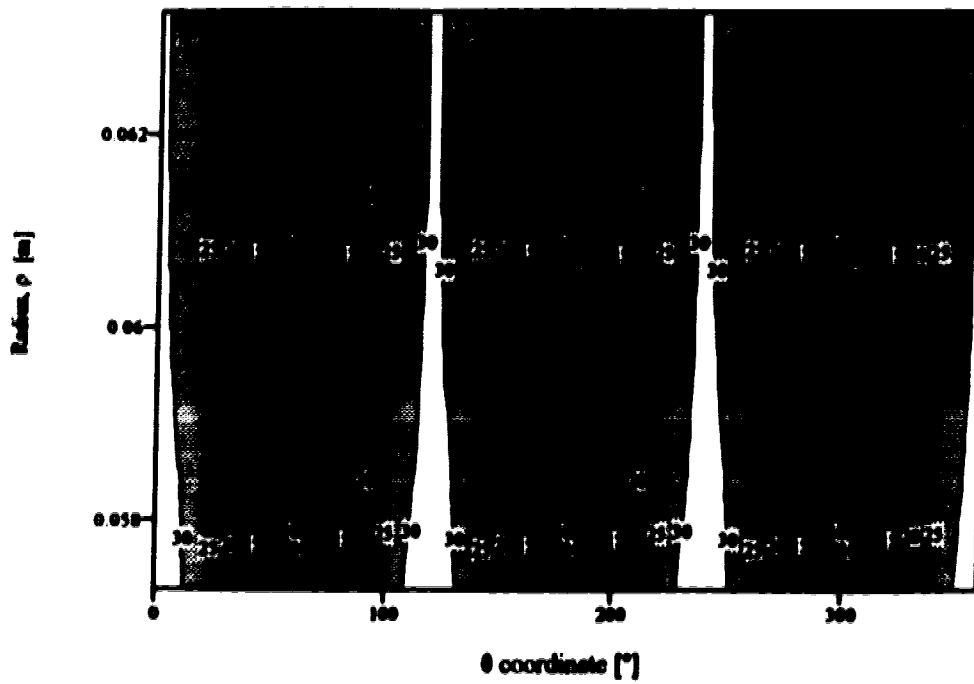


Figure 6-6a Contour plot of the magnitude of the current density [A/cm^2] in wellbore casing 3.

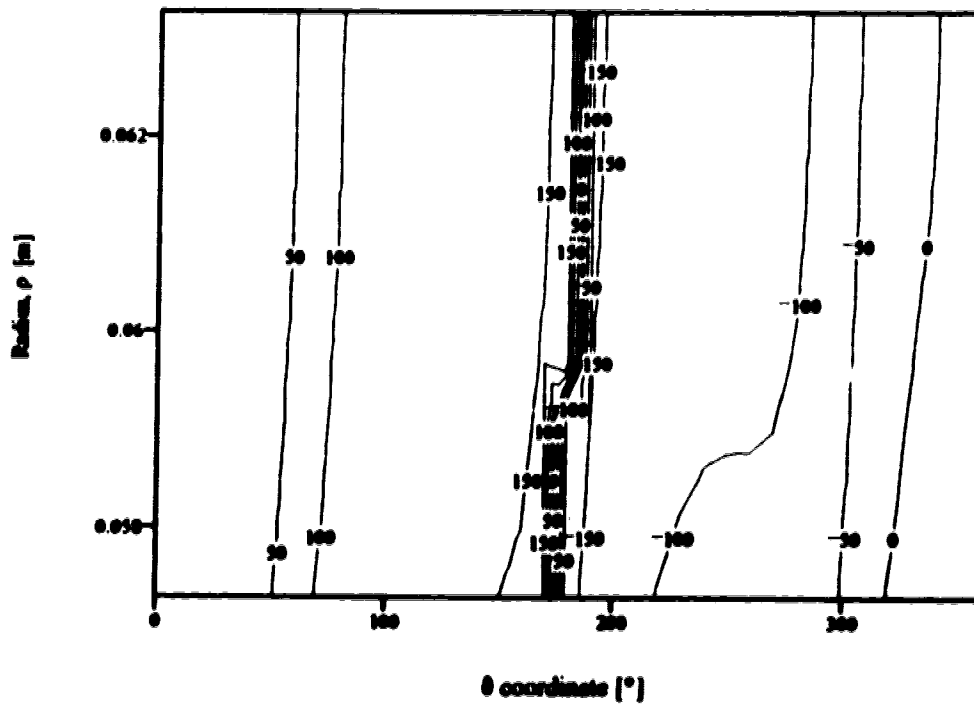


Figure 6-6b Contour plot of the phase of the current density [$^{\circ}$] in wellbore casing 3.

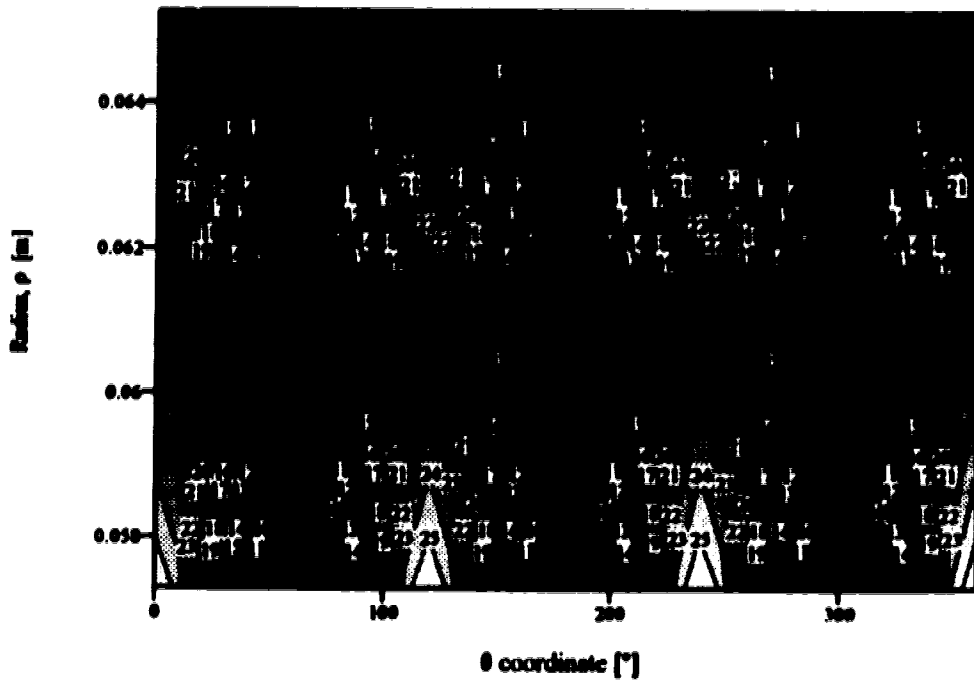


Figure 6-7a Contour plot of the magnitude of the current density [A/cm²] in wellbore casing 4.

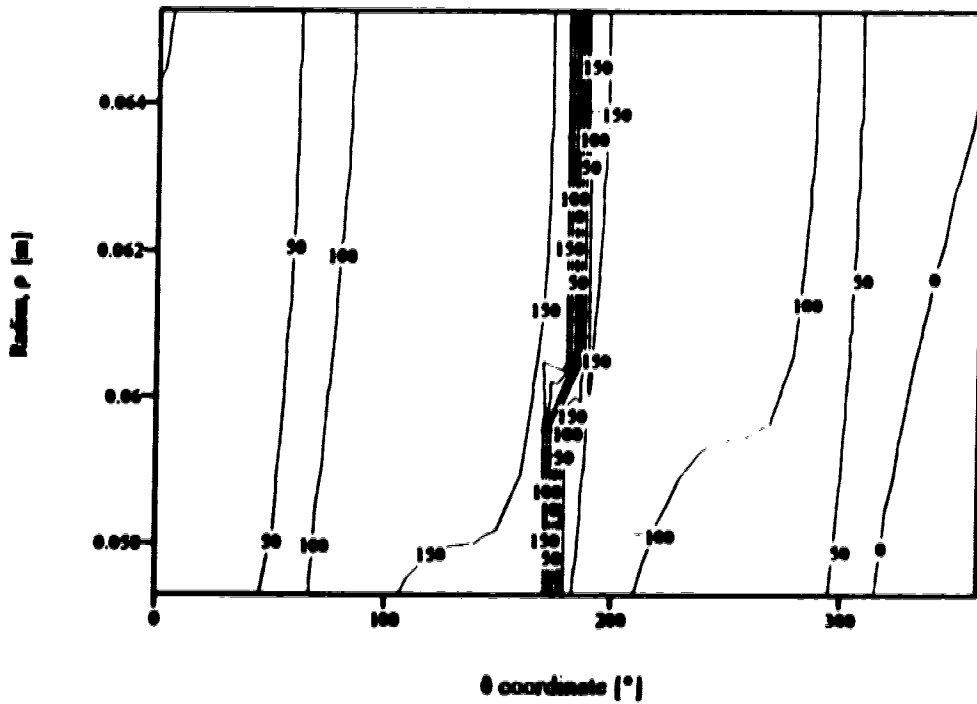


Figure 6-7b Contour plot of the phase of the current density [°] in wellbore casing 4.

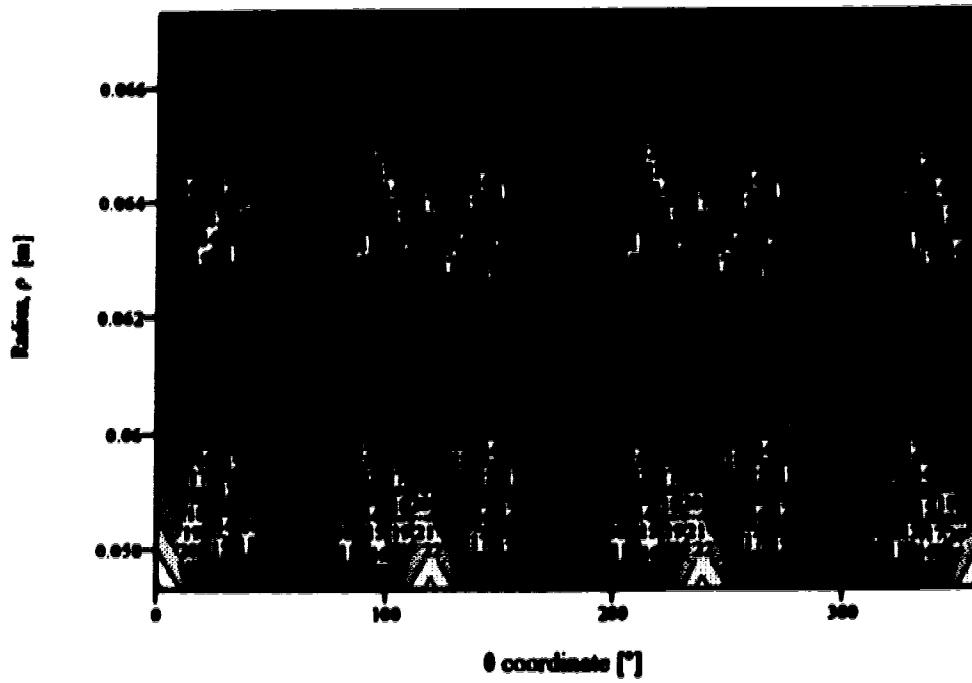


Figure 6-8a Contour plot of the magnitude of the current density [A/cm^2] in wellbore casing 5.

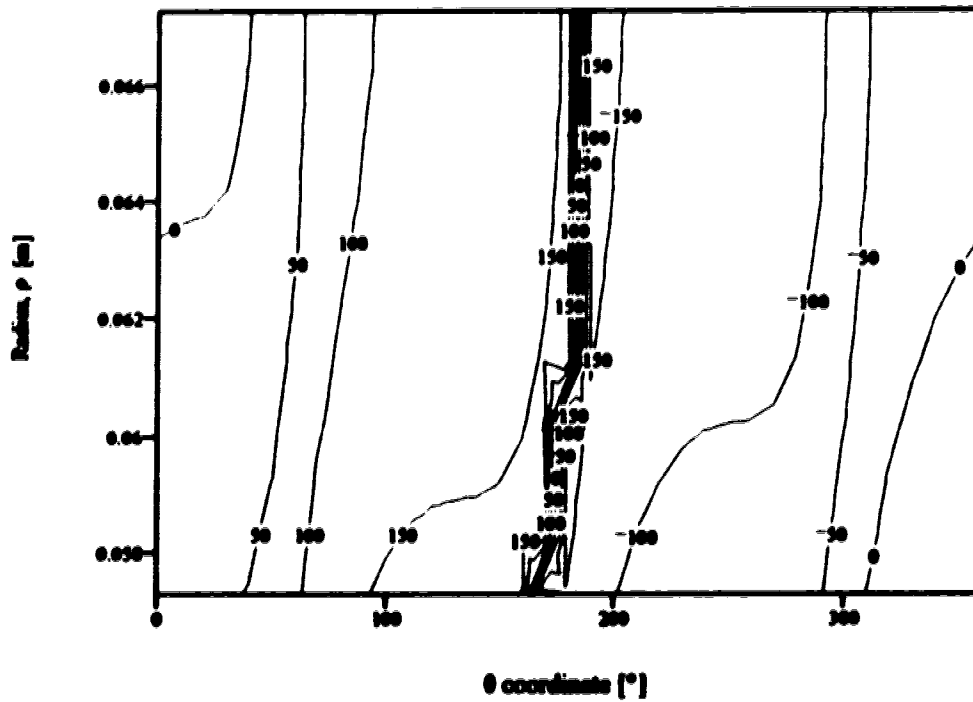


Figure 6-8b Contour plot of the phase of the current density [°] in wellbore casing 5.

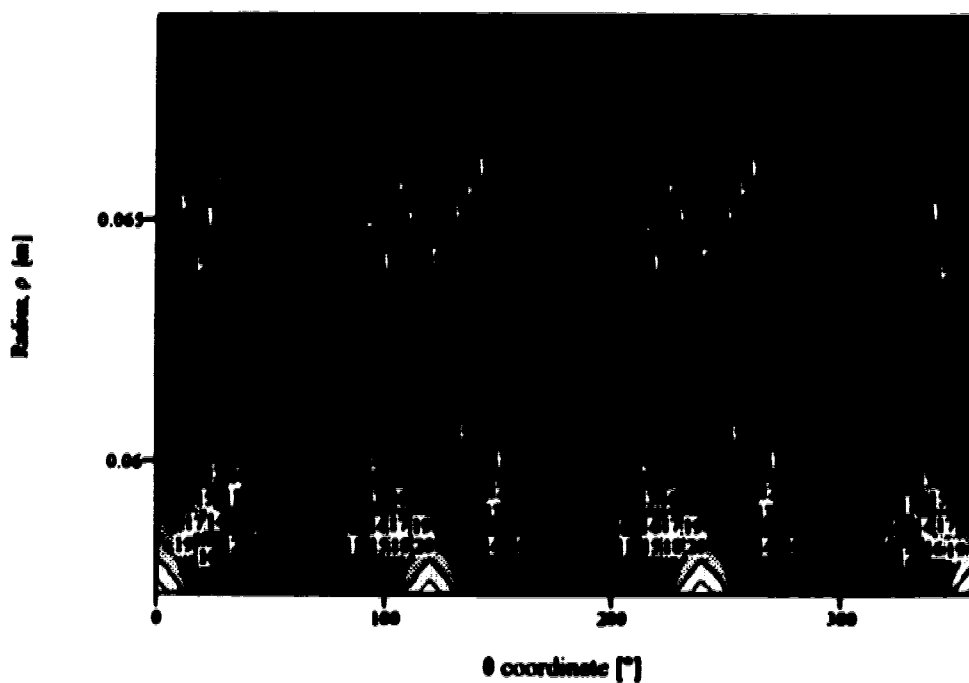


Figure 6-9a Contour plot of the magnitude of the current density [A/cm^2] in wellbore casing 6.

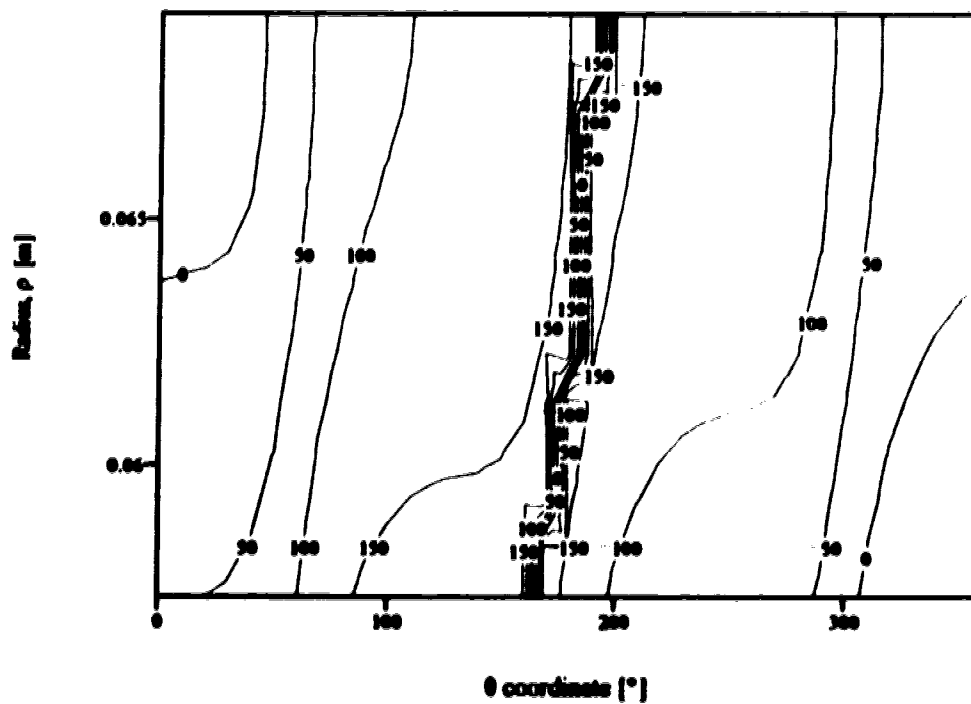


Figure 6-9b Contour plot of the phase of the current density [°] in wellbore casing 6.

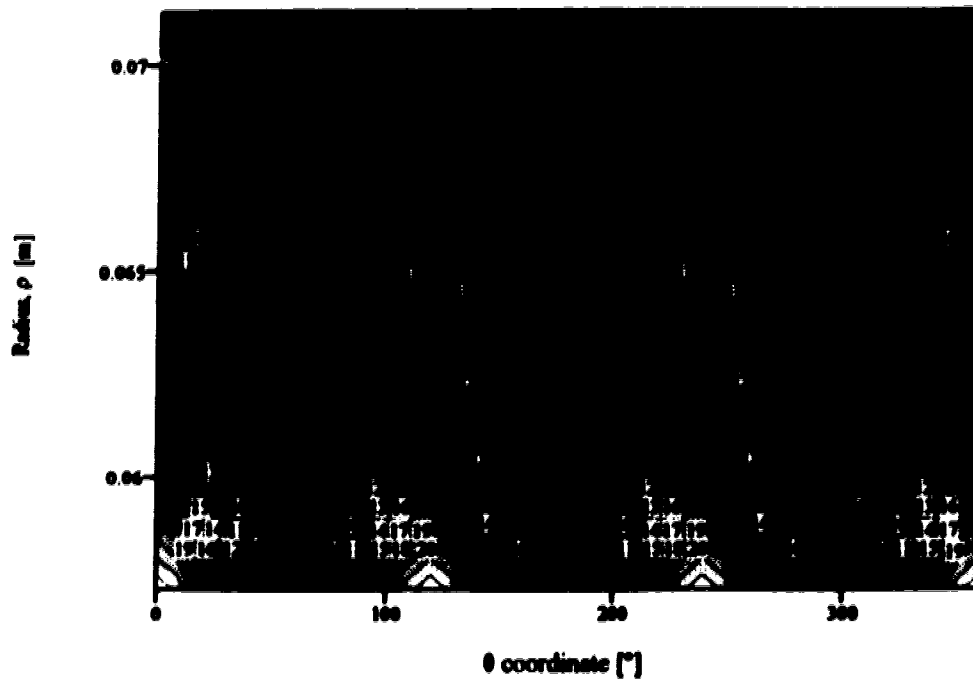


Figure 6-10a Contour plot of the magnitude of the current density [A/cm^2] in wellbore casing 7.

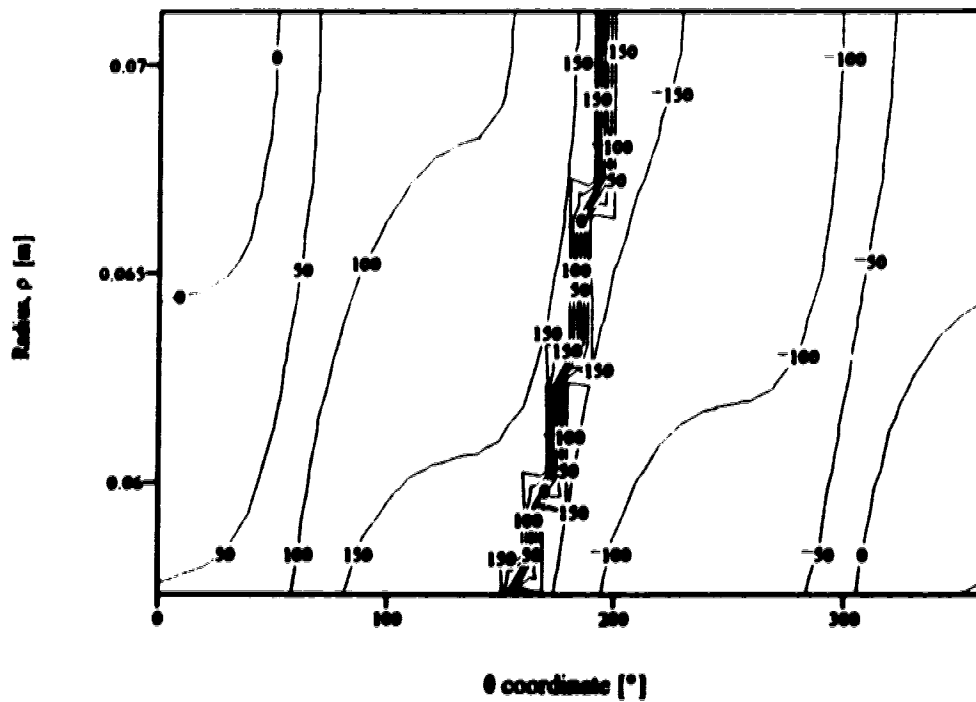


Figure 6-10b Contour plot of the phase of the current density [$^{\circ}$] in wellbore casing 7.

Once the solution for the *total* electric field in a wellbore casing is obtained, the resistive loss due to the resultant eddy current flow may be calculated. Once again, the integral from Poynting's theorem is evaluated numerically for each casing in problem 3a; the result being the eddy current loss per meter of casing. Figure 6-11 is a plot of eddy current loss as a function of casing thickness (refer to Table 6-1 for casing thicknesses).

Figure 6-11 also includes a plot of the eddy current loss as calculated by Kawasaki, et al. in reference [10]. In addition, a plot of eddy current loss calculated using Dwight's expression (7) from reference [7] is also included in Figure 6-11. Note that Dwight's expression is only valid for thin casings (less than one skin depth) with a relative permeability of unity. The plots of Kawasaki, et al. and Dwight provide a check for the FEM solutions.

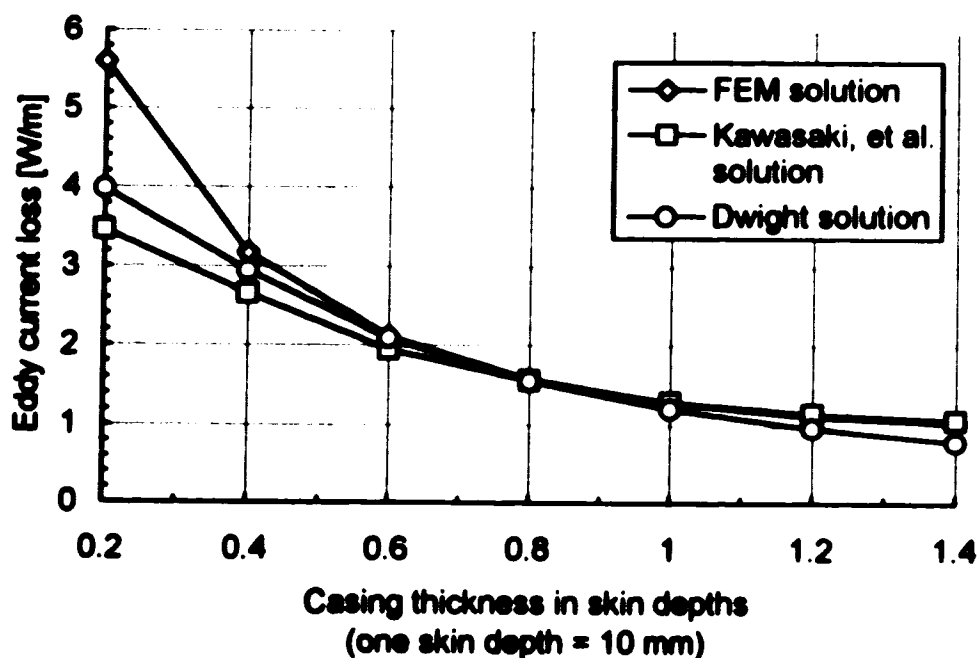


Figure 6-11. Eddy current loss in wellbore casings of various thicknesses.

From Figure 6-11, the agreement between the FEM and analytical solutions appears to be quite good. The discrepancy for casings less than 0.6 skin depths thick may be attributed to the approximate boundary condition $\vec{H}_z|_{\rho=a} = 0$. Recall from section 6.7 that no definitive conclusion was reached as to whether this boundary condition could be justified for the casings in problem 3a. However, on the basis of Figure 6-11, the

approximate boundary condition seems justified for those casings greater than 0.6 skin depths thick.

As a final check of the FEM solution for current density, the solution is integrated (numerically) over the cross sectional area of the casing. The result of this integration is the FEM solution for the *total* current in the casing of problem 3a. Theoretically, the total current induced in the casing of problem 3a should be exactly zero because the sum of the currents I_1 , I_2 and I_3 is also zero. In fact, for all casing samples, the FEM solution for I_{casing} is indeed less than 0.01% of the current in a single power cable (i.e., $I_{casing} \cong 0$).

On the basis of Figure 6-11, it is apparent that the eddy current loss decreases as casing thickness increases. This can be explained as follows: All the casings carry the same total current (i.e., $I_{casing} = 0$ as discussed in the previous paragraph). One should therefore expect $|J|$ (the magnitude of the current density) to decrease as casing thickness (and therefore cross sectional area) increases. This supposition can be confirmed if one examines the current density magnitudes plotted in Figures 6-4a to 6-10a. Since the eddy current loss *at a given point* in a casing is proportional to $|J|^2$ at that point, as $|J|$ decreases throughout the casing, so should the eddy current loss.

6.10 Finite Element Method Solutions for the Multi-Cable Problem Analyzed in Problem 3b

For each casing analyzed in problem 3b, three FEM solutions are computed using UNAFEM II. Each FEM solution yields a solution for that fraction of the total electric field in problem 3b which can be ascribed to the current in *one* of the three power cables. The three single cable solutions are superimposed to obtain the total electric field in a given casing. Note the single cable solutions are superimposed with due regard to the original, azimuthal positions of the power cables in problem 3b. Plots of the FEM solutions for the current density (σE_z) in casings 1 through 5 are shown in Figures 6-12 to 6-16.

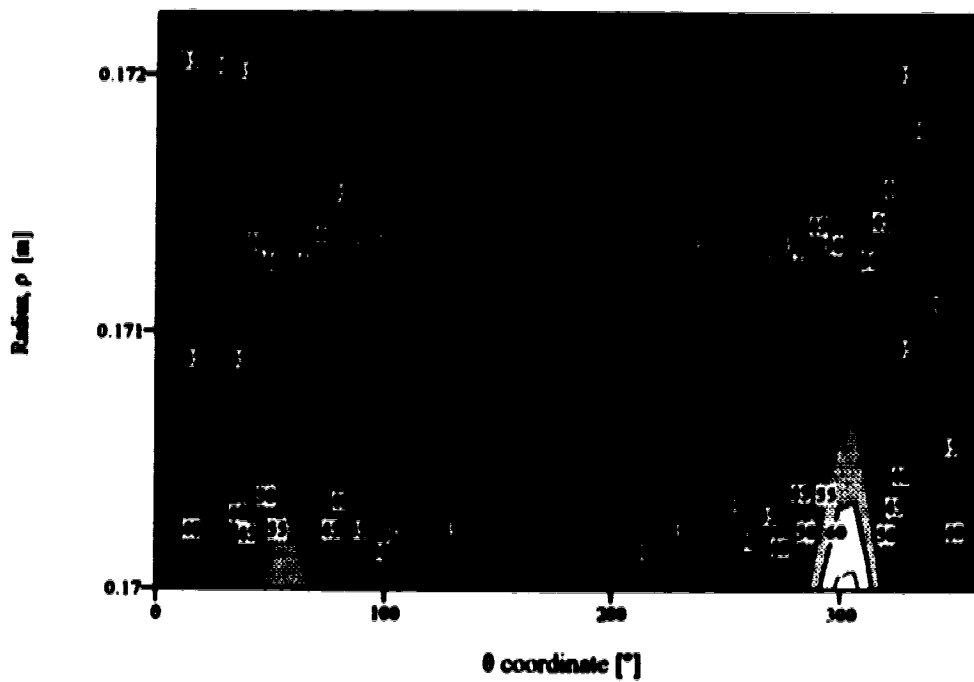


Figure 6-12a Contour plot of the magnitude of the current density [A/cm²] in wellbore casing 1.

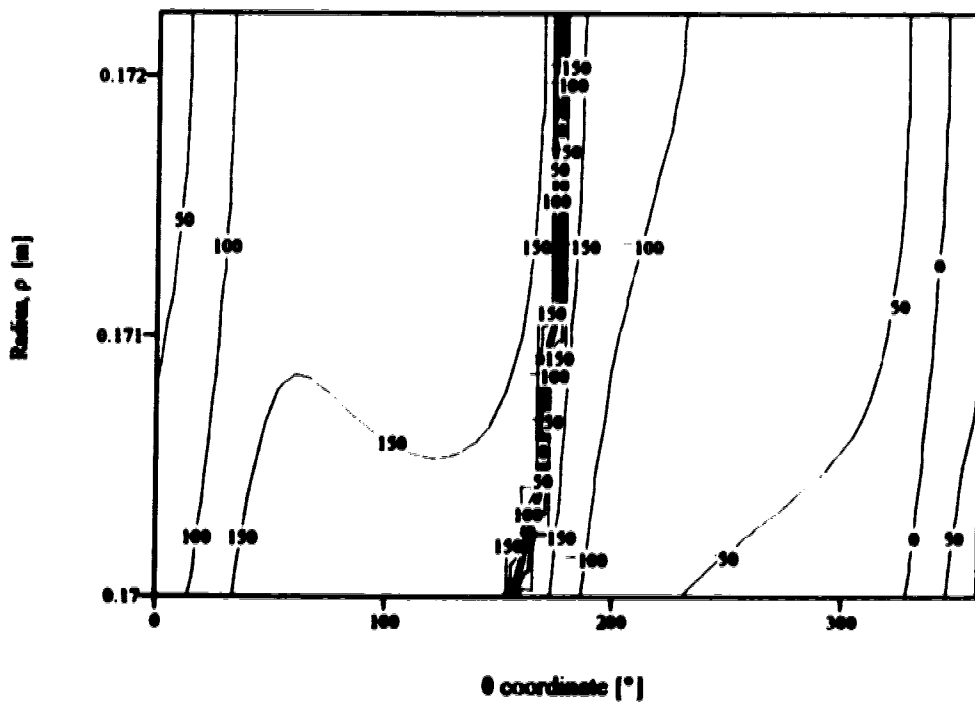


Figure 6-12b Contour plot of the phase of the current density [°] in wellbore casing 1.

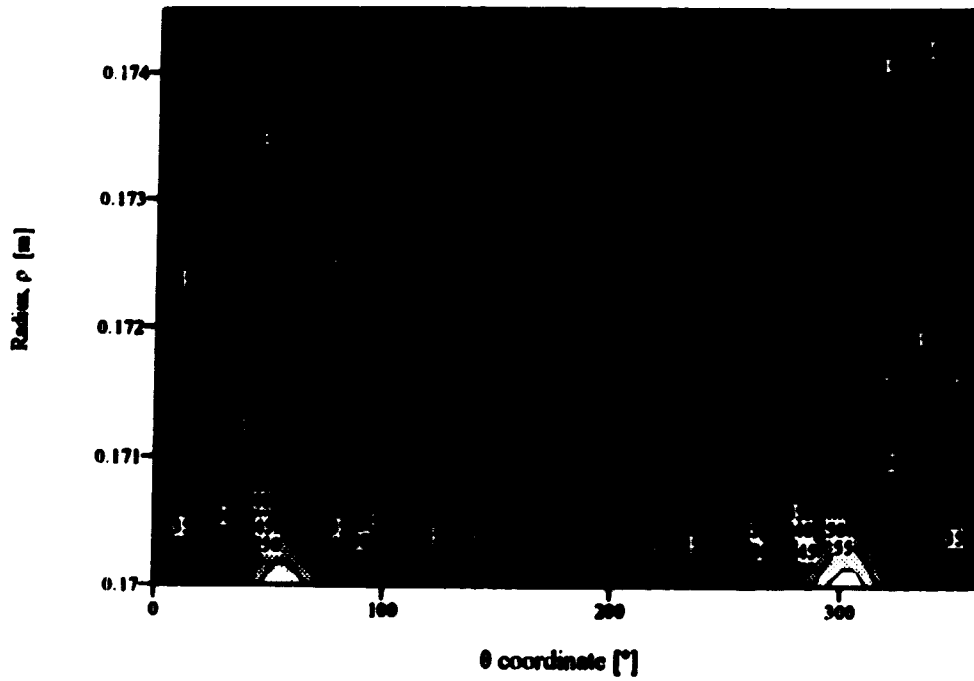


Figure 6-13a Contour plot of the magnitude of the current density [A/cm^2] in wellbore casing 2.

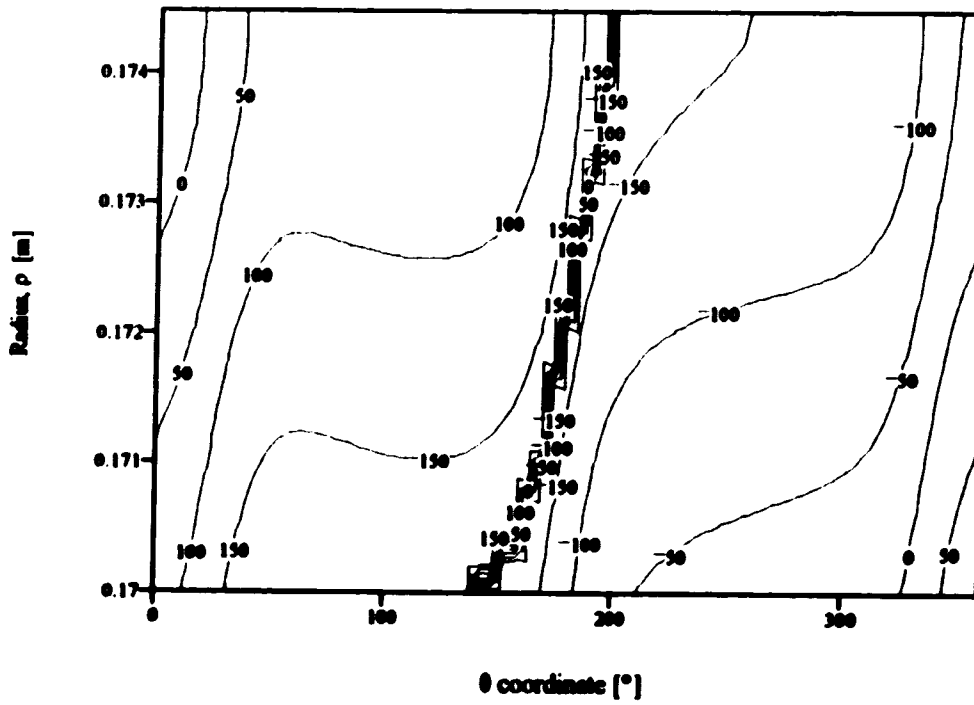


Figure 6-13b Contour plot of the phase of the current density [$^{\circ}$] in wellbore casing 2.

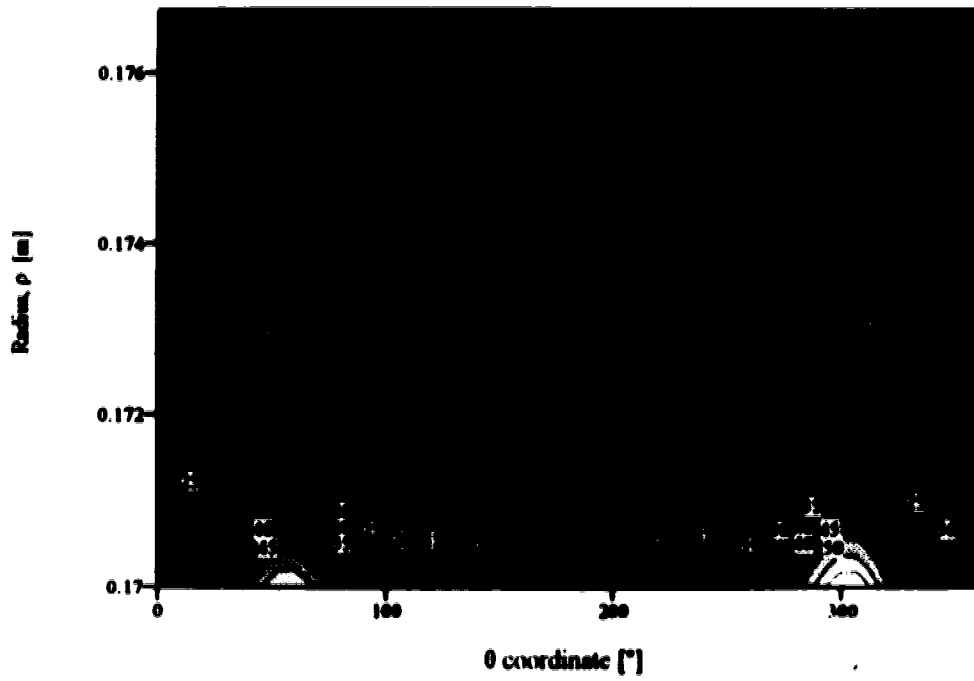


Figure 6-14a Contour plot of the magnitude of the current density [A/cm^2] in wellbore casing 3.

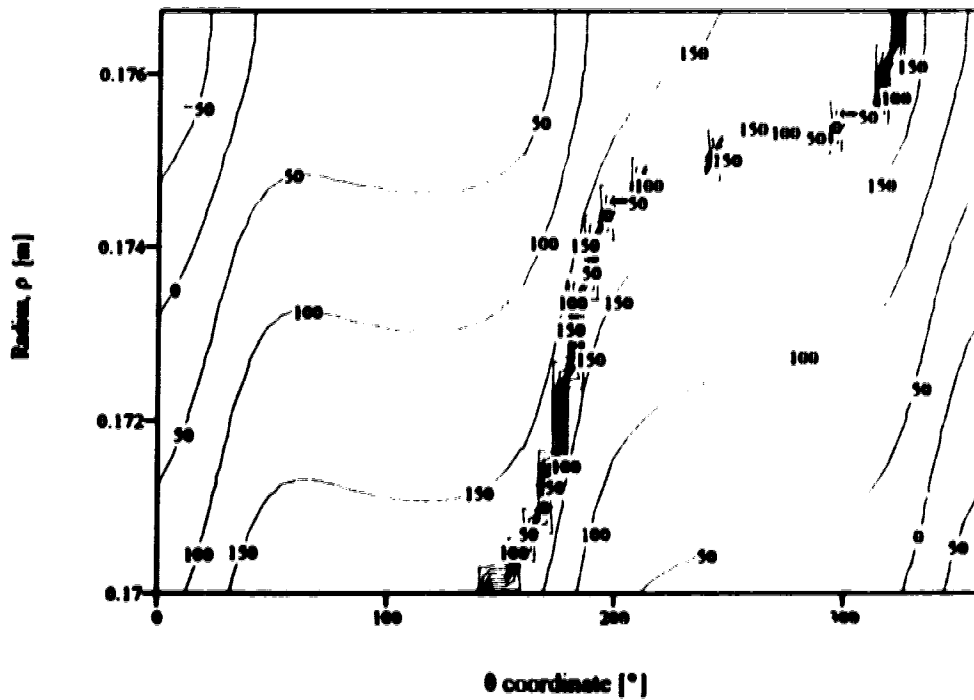


Figure 6-14b Contour plot of the phase of the current density [$^\circ$] in wellbore casing 3.

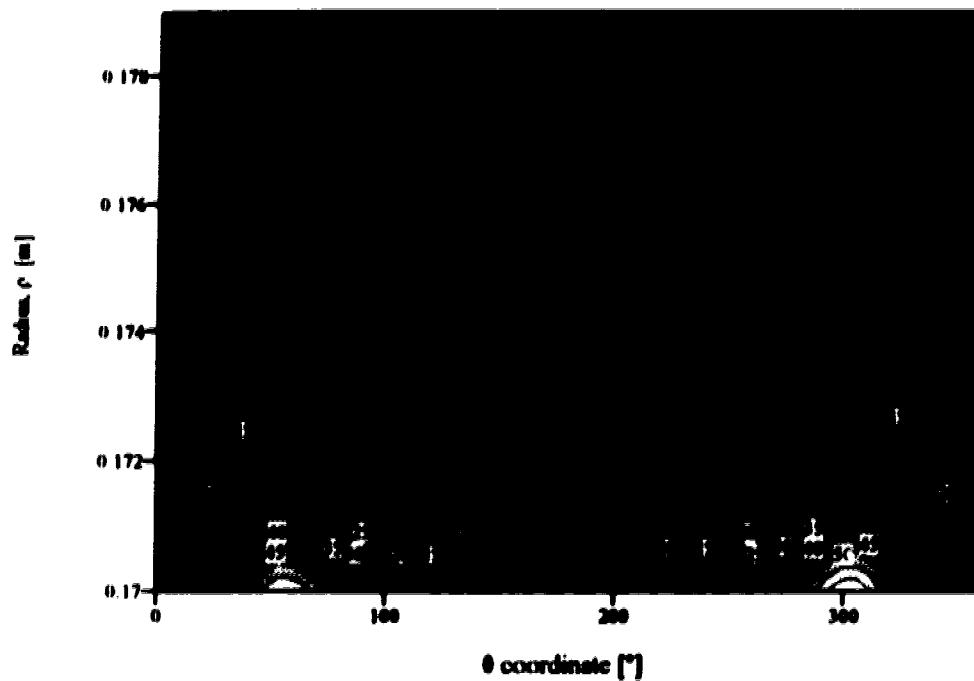


Figure 6-15a Contour plot of the magnitude of the current density [A/cm^2] in wellbore casing 4.

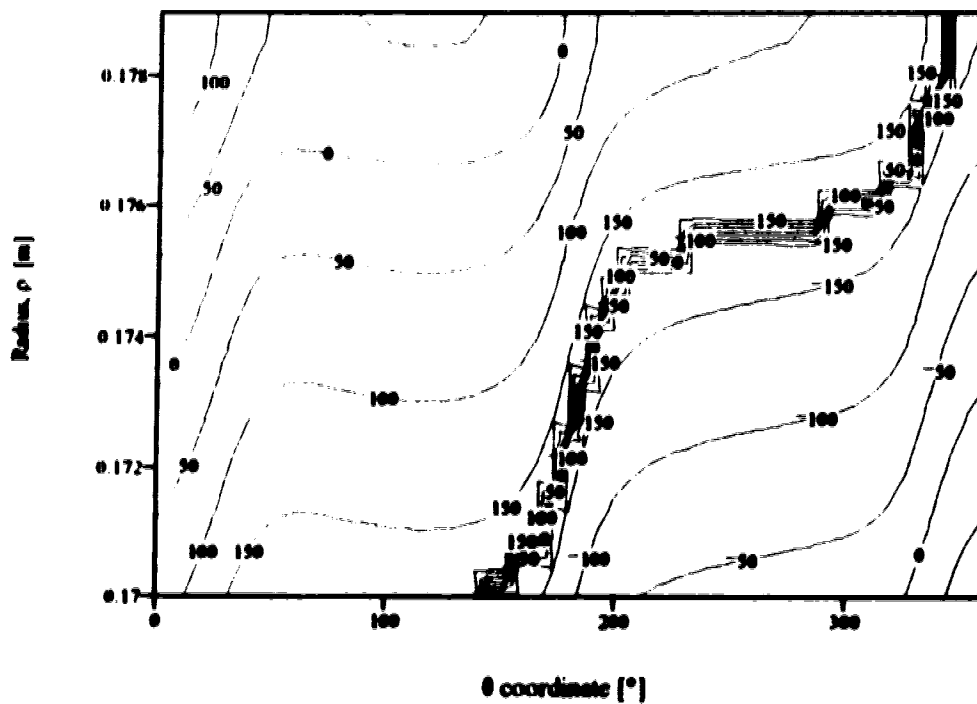


Figure 6-15b Contour plot of the phase of the current density [$^{\circ}$] in wellbore casing 4.

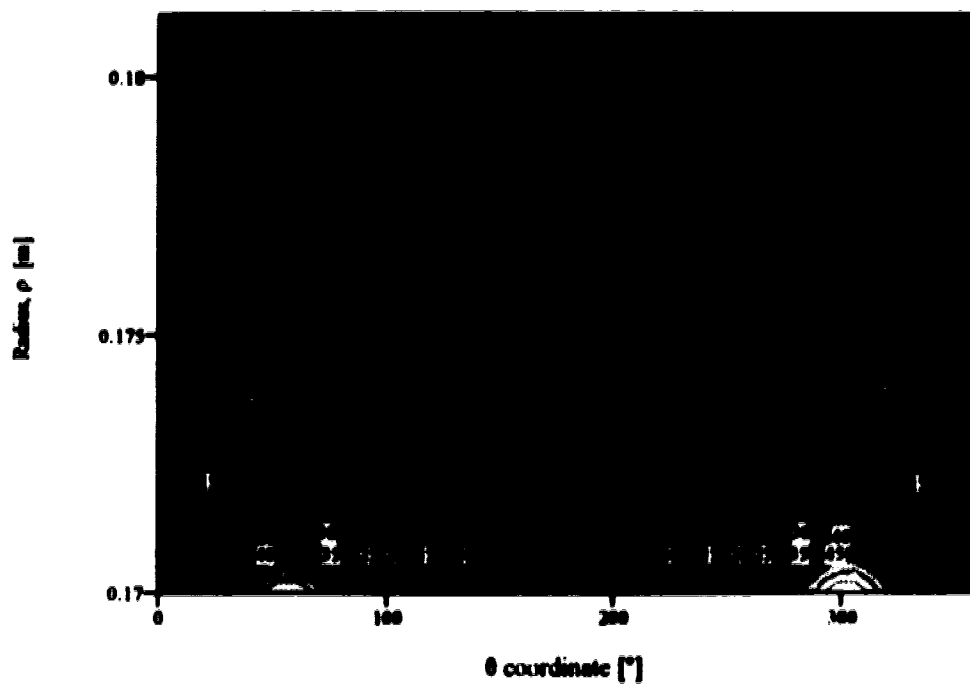


Figure 6-16a Contour plot of the magnitude of the current density [A/cm²] in wellbore casing 5.

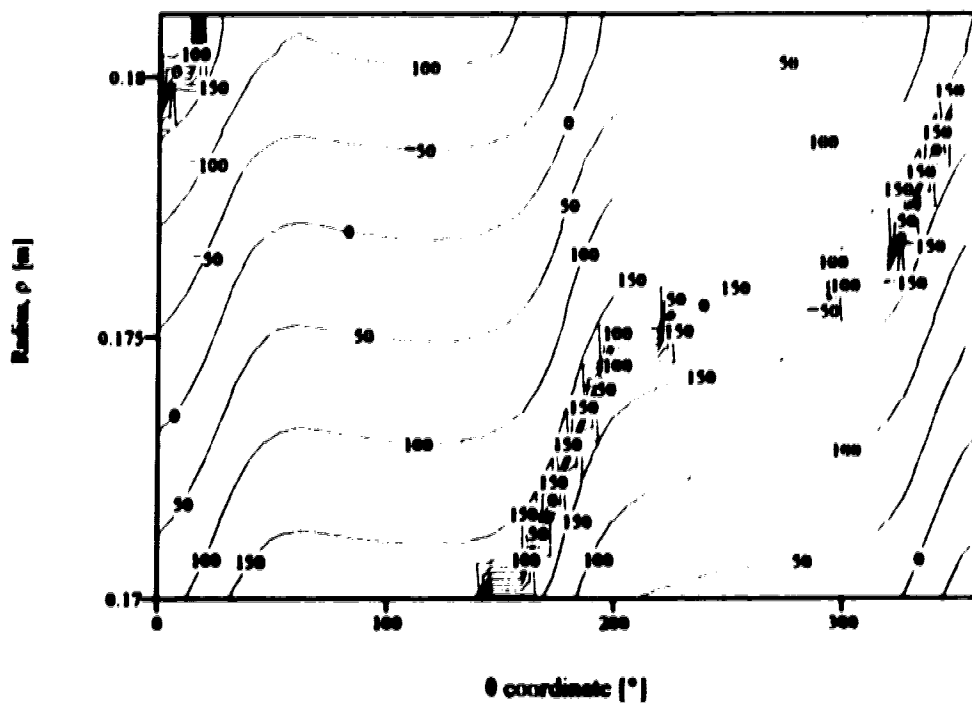


Figure 6-16b Contour plot of the phase of the current density [°] in wellbore casing 5.

Once the solution for the total electric field in a wellbore casing is obtained, the resistive loss due to the resultant eddy current flow may be calculated. The integral from Poynting's theorem is evaluated numerically for each casing in problem 3b; the result being the eddy current loss per meter of casing. Figure 6-17 is a plot of the eddy current loss as a function of casing thickness (refer to Table 6-2 for casing thicknesses).

Figure 6-17 also includes a plot of the eddy current loss as calculated by Kawasaki, et al. in reference [10]. The plot by Kawasaki, et al. provides a check for the FEM solutions.

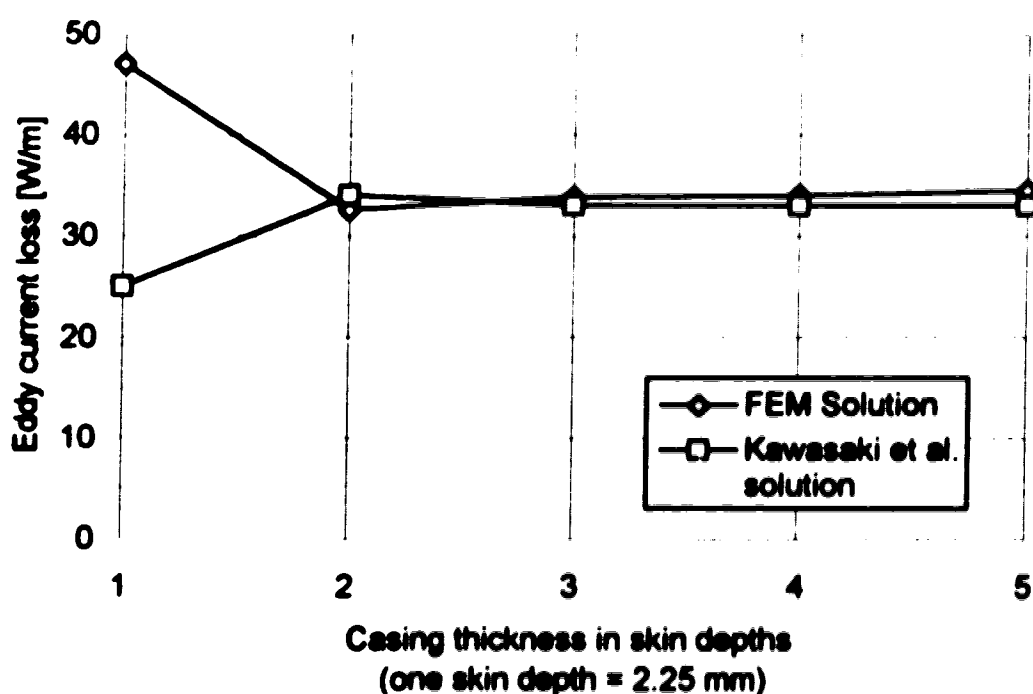


Figure 6-17 Eddy current loss in wellbore casings of various thicknesses.

From Figure 6-17, the agreement between the FEM and analytical solutions appears to be quite good. The discrepancy for casings less than two skin depths thick can be attributed to the approximate boundary condition $\hat{H}_2|_{\rho=b} = 0$. Recall from section 6.7 that the approximate boundary condition was not valid for casings less than two skin depths thick.

Also note from Figure 6-17 that the eddy current loss is essentially independent of casing thickness if the thickness is greater than two skin depths. From an examination of

the current density plots in Figures 6-13a to 6-16a, it appears the magnitude of the current density near the inner surface of the casing does not change appreciably as the casing thickness increases beyond two skin depths. The current density near the inner surface of the casing tends to be the major contributor to the eddy current loss in the casing because this is where the magnitude of the current density is greatest. Since the current density near the inner surface of the casing does not change appreciably beyond a thickness of two skin depths, the eddy current loss remains essentially constant beyond a thickness of two skin depths.

6.11 Finite Element Method Solutions for the Multi-Cable Problem Analyzed in Problem 3c

For each casing analyzed in problem 3c, three FEM solutions are computed using UNAFEM II. Each FEM solution yields a solution for that fraction of the total electric field in problem 3c which can be attributed to the current in one of the three power cables. The three single cable solutions are superimposed to obtain the total electric field in a given casing. Note the single cable solutions are superimposed with due regard to the original, azimuthal positions of the power cables in problem 3c. Plots of the FEM solutions for the current density (σE_z) in casings 1 through 5 are shown in Figures 6-18 to 6-22.

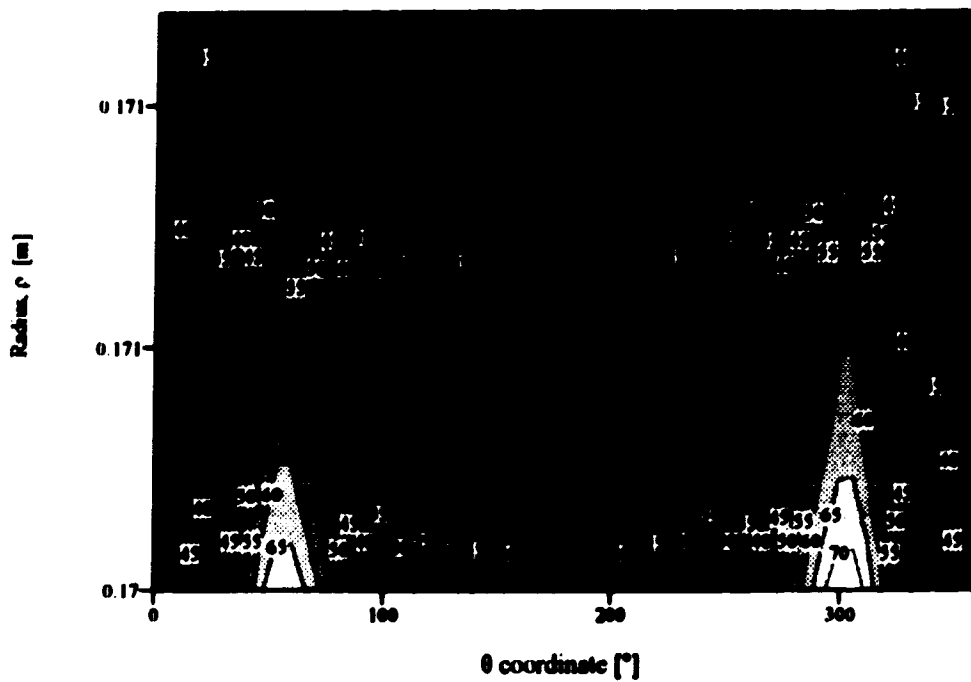


Figure 6-18a Contour plot of the magnitude of the current density [A/cm²] in wellbore casing 1.

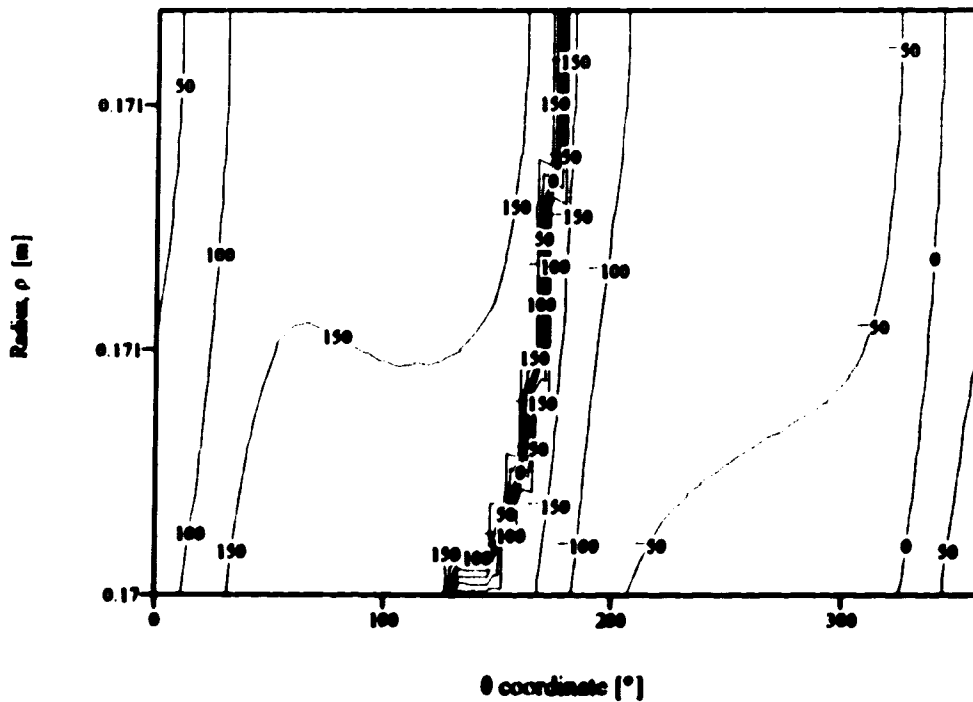


Figure 6-18b Contour plot of the phase of the current density [°] in wellbore casing 1.

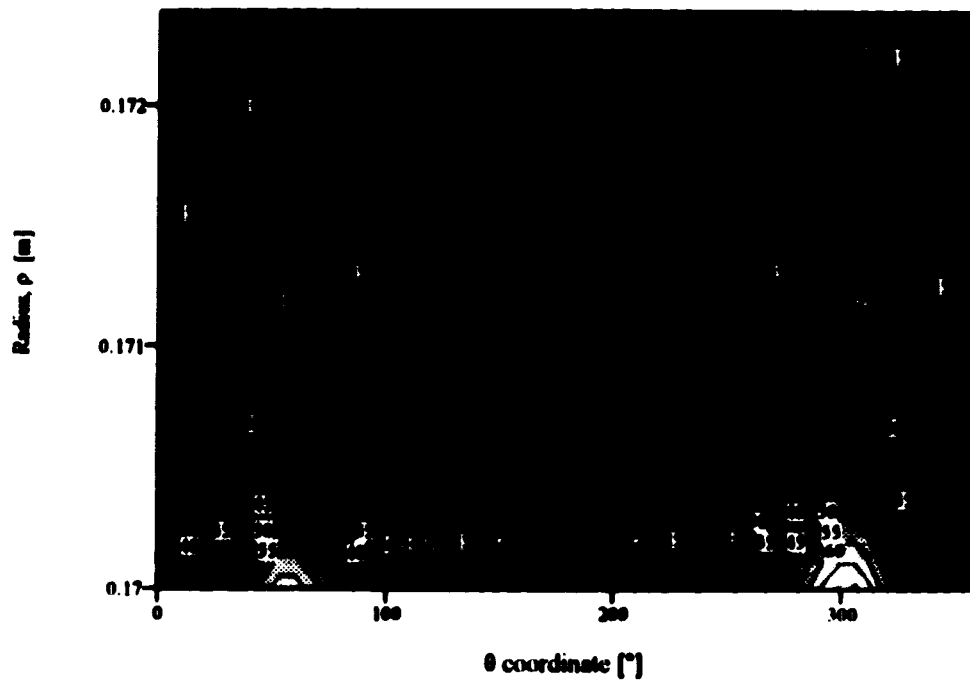


Figure 6-19a Contour plot of the magnitude of the current density [A/cm²] in wellbore casing 2.

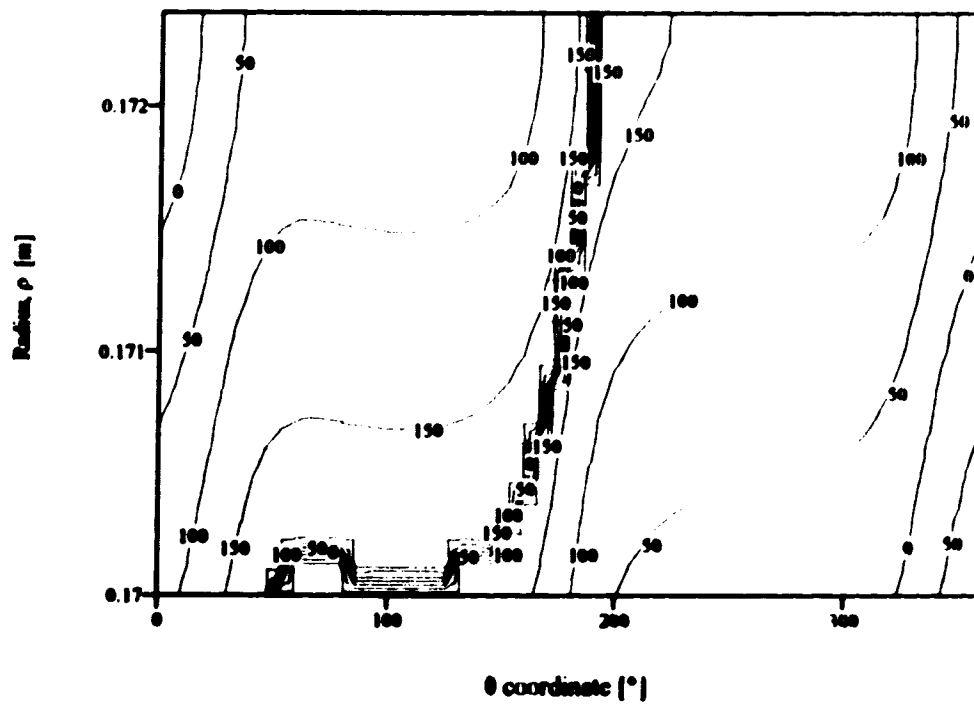


Figure 6-19b Contour plot of the phase of the current density [$^{\circ}$] in wellbore casing 2.

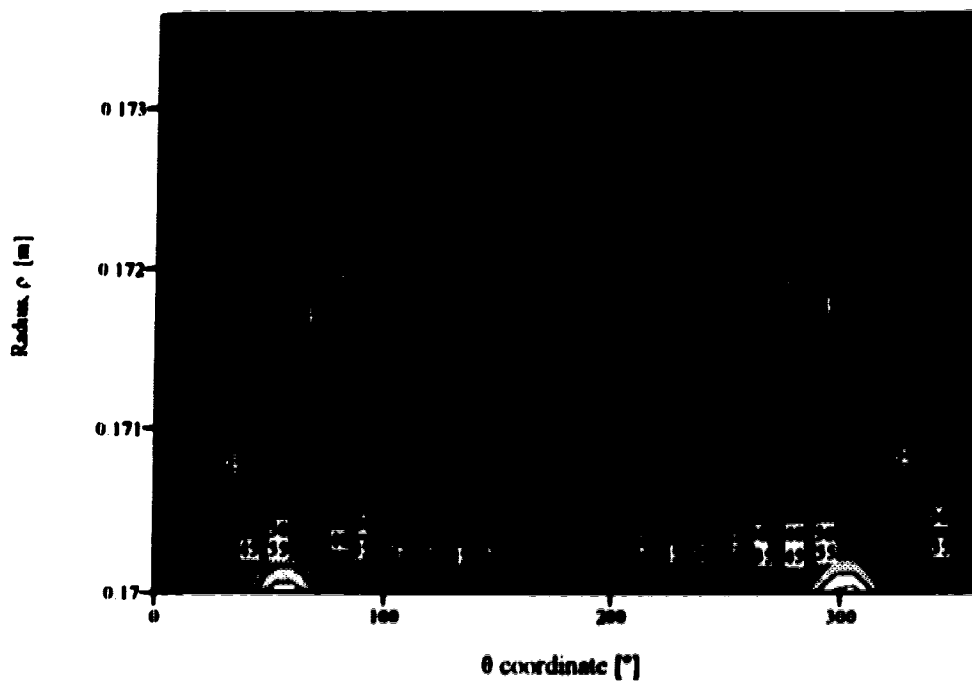


Figure 6-20a Contour plot of the magnitude of the current density [A/cm²] in wellbore casing 3.

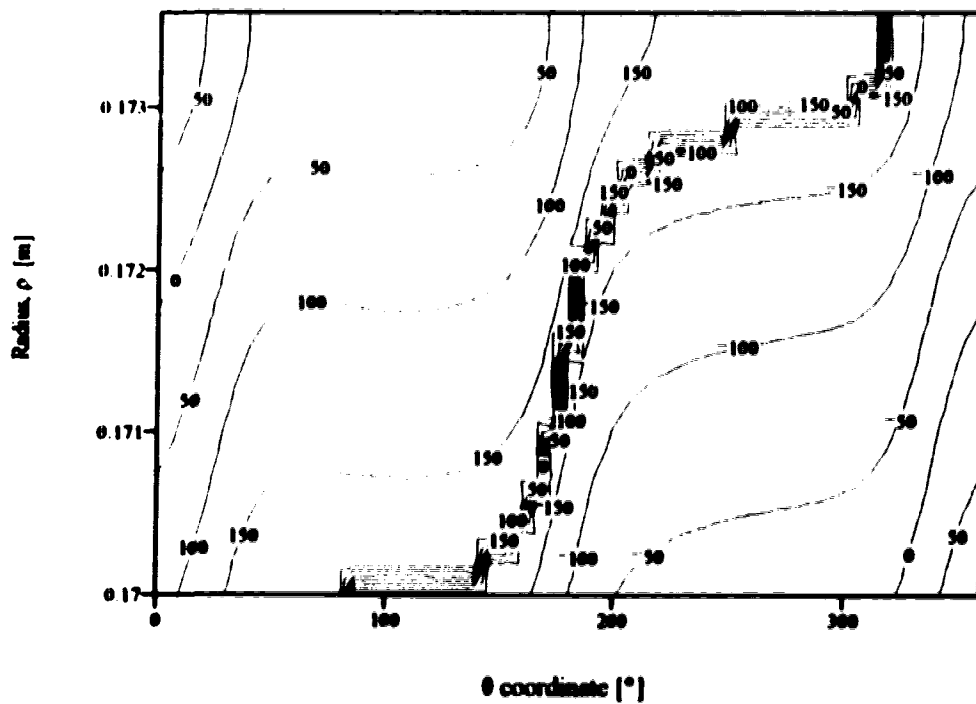


Figure 6-20b Contour plot of the phase of the current density [°] in wellbore casing 3.

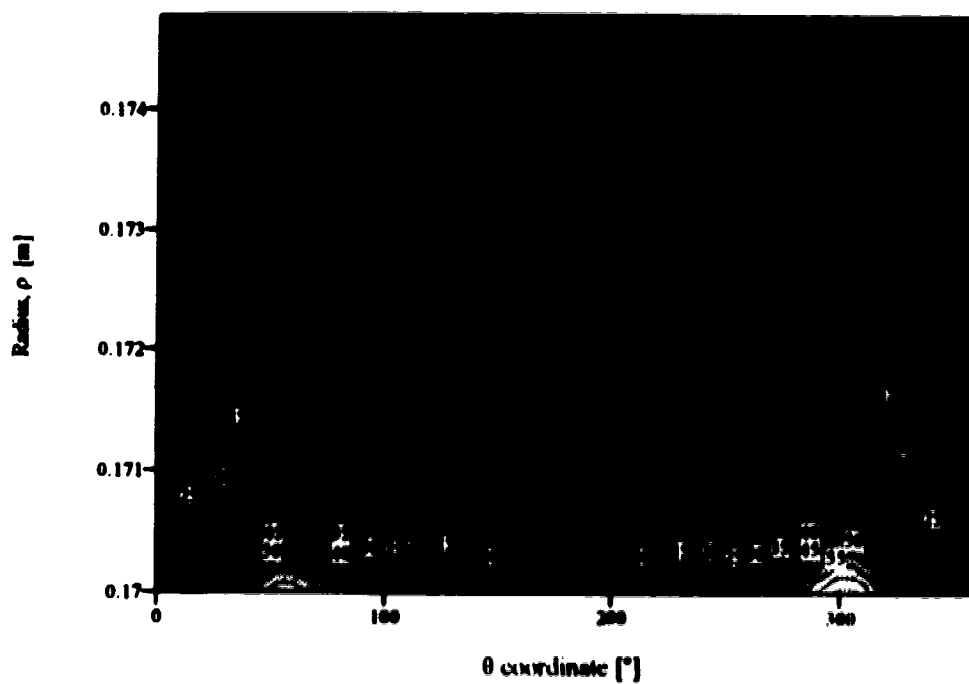


Figure 6-21a Contour plot of the magnitude of the current density [A/cm^2] in wellbore casing 4.

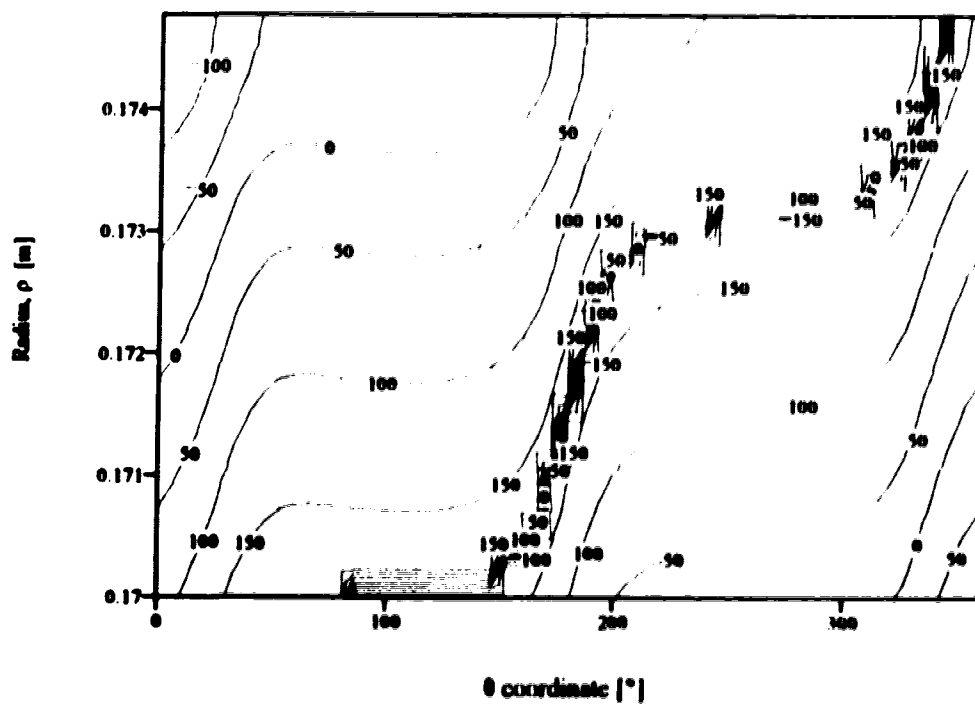


Figure 6-21b Contour plot of the phase of the current density [$^\circ$] in wellbore casing 4.

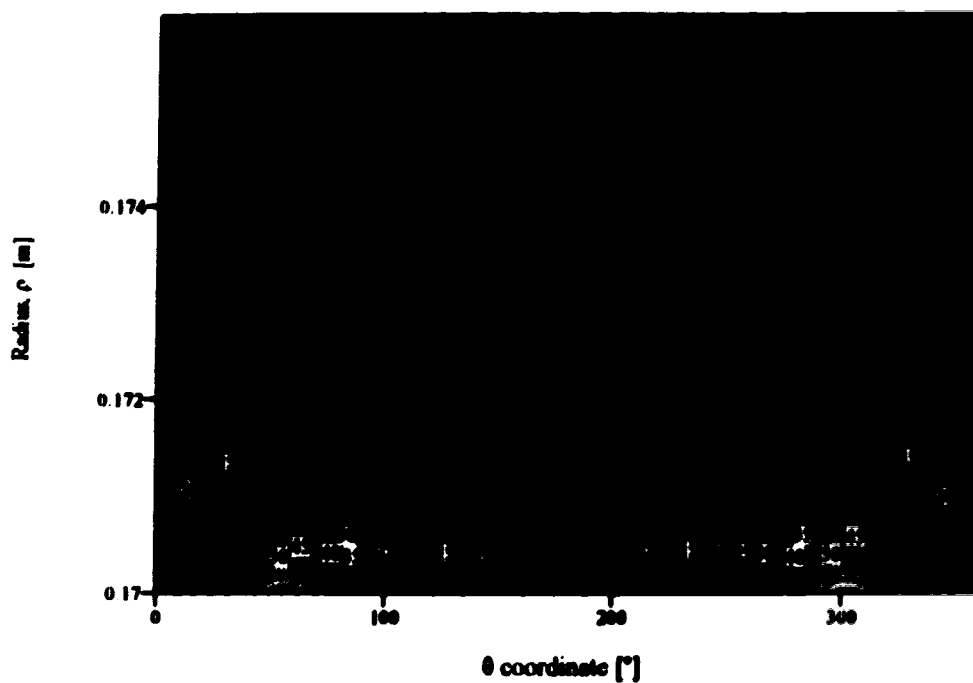


Figure 6-22a Contour plot of the magnitude of the current density [A/cm^2] in wellbore casing 5.

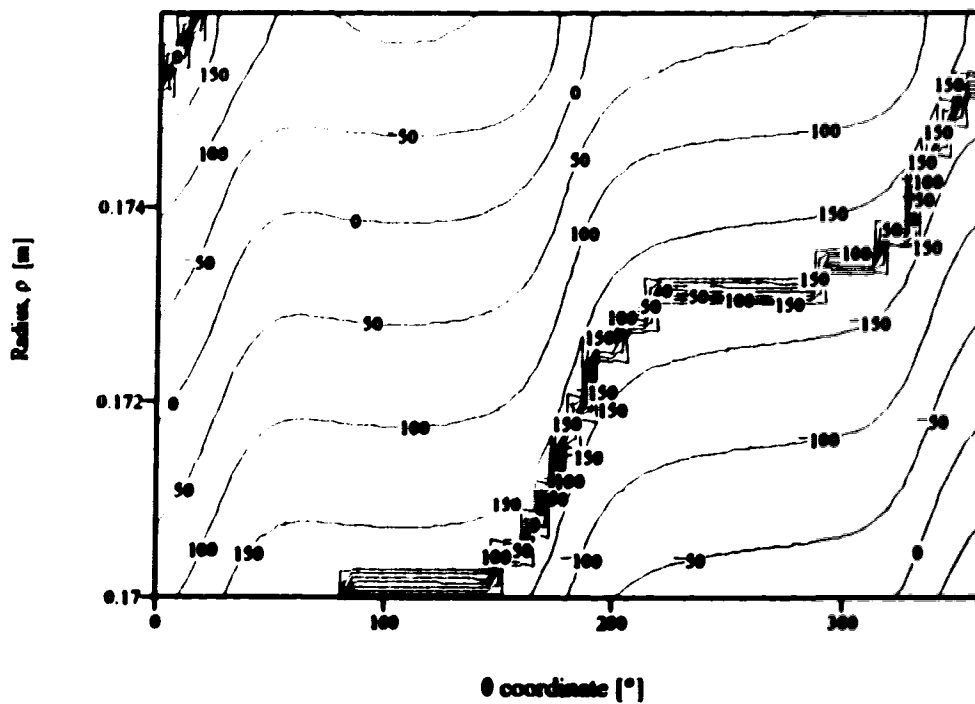


Figure 6-22b Contour plot of the phase of the current density [$^{\circ}$] in wellbore casing 5.

Once the solution for the total electric field in a wellbore casing is obtained, the resistive loss due to the resultant eddy current flow may be calculated. The integral from Poynting's theorem is evaluated numerically for each casing in problem 3c, the result being the eddy current loss per meter of casing. Figure 6-23 is a plot of the eddy current loss as a function of casing thickness (refer to Table 6-3 for casing thicknesses)

Figure 6-23 also includes a plot of the eddy current loss as calculated by Kawasaki, et al. in reference [10]. The plot by Kawasaki, et al. provides a check for the FEM solutions.

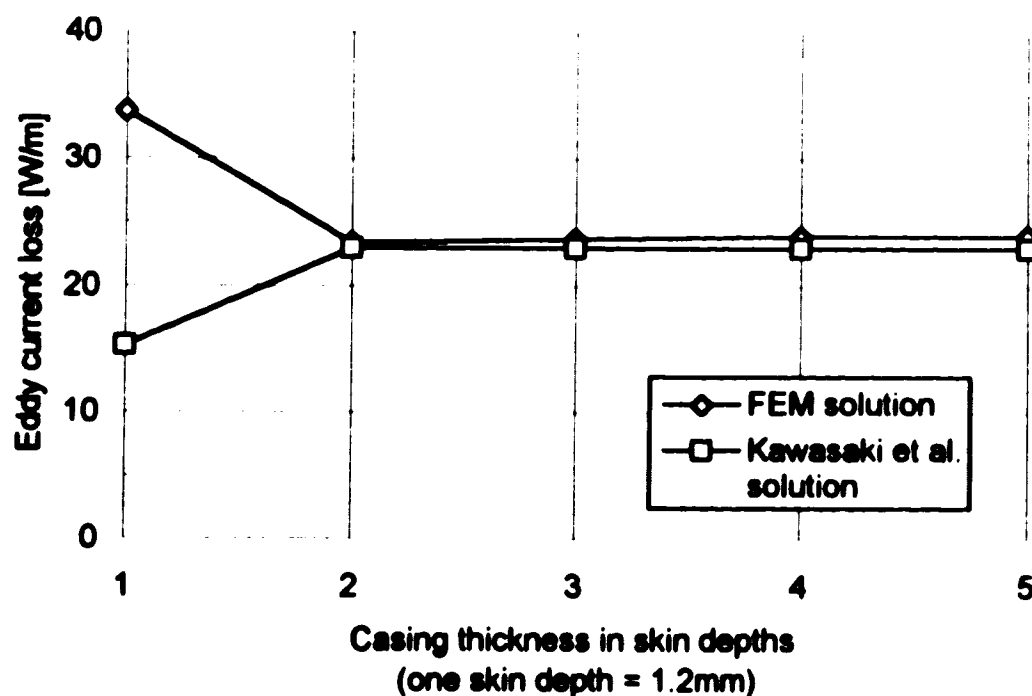


Figure 6-23 Eddy current loss in wellbore casings of various thicknesses.

From Figure 6-23, the agreement between the FEM and analytical solutions appears to be quite good. The discrepancy for casings less than two skin depths thick can be attributed to the approximate boundary condition $\vec{H}_2|_{p, s} = 0$. Recall from section 6.7 that the approximate boundary condition was not valid for casings less than two skin depths thick.

CHAPTER 7

CONCLUSION

7.1 The Finite Element Method and the Magnetic Field Boundary Condition at the Outer Wall of the Wellbore Casing

In general terms, the goal of this thesis has been to obtain numerical solutions for the eddy current distribution and eddy current losses induced in a wellbore casing. Eddy currents are induced in the wellbore casing by magnetic fields which emanate from one or more power cables situated inside the casing. The eddy current problem is modeled as a two dimensional boundary value problem consisting of three regions: (1) the air filled region inside the casing, (2) an annular region that is the casing itself, and (3) the air filled region outside the casing which extends radially to infinity. This is best illustrated in Figure 1-5.

In more specific terms, the goal of this thesis has been to prove that accurate numerical solutions for the eddy current problem can be obtained by using the finite element method. The main conclusion of this thesis is that accurate numerical solutions for the eddy current problem can be obtained by using a finite element method that models only the power cables and the casing, *provided that the magnetic field at the outer wall of the casing can be set to approximately zero*. The provision concerning the magnetic field is important because the accuracy of the FEM solution depends on the validity of this boundary condition.

For the simple one dimensional problem examined in chapter 2, analytical solutions were derived for the electromagnetic fields within the casing. After examining these analytical solutions, it was observed that the magnetic field at the outer wall of the casing is approximately zero under the following circumstances:

1. If the thickness of the wellbore casing is greater than three skin depths, or
2. If the wave impedance at the outer wall of the wellbore casing (see equation 2.33) is much greater than the intrinsic impedance of the wellbore casing (η).

Detailed physical explanations as to why the magnetic field at the outer wall of the casing is approximately zero under these two circumstances are given in sections 2.6.1.1 and 2.6.1.2, but may be summarized as follows.

For the first case, if the thickness of the wellbore casing is greater than three skin depths then incident electromagnetic waves originating at the inner wall of the casing will have decayed by a factor of approximately e^{-3} by the time they reach the outer wall of the casing. At the outer wall, portions of the waves are reflected back into the casing. As the reflected waves travel back towards the inner wall, they continue to attenuate. Compared to the magnitudes of the incident waves, the reflected waves are extremely small. Thus the effects of the reflected waves may be neglected everywhere except near the outer wall. Even at the outer wall, the field strength is only about 5% of its maximum.

For the second case, if the wave impedance at the outer wall of the wellbore casing is much greater than the intrinsic impedance of the casing then nearly all of the incident magnetic field at the outer wall is reflected back into the casing. Furthermore, the reflected field undergoes a 180° phase shift. Thus the incident and reflected magnetic fields will be nearly equal in magnitude and opposite in phase, the two fields cancel each other out and, as a result, the magnetic field at the outer wall of the casing is nearly zero.

A quick though somewhat crude method for gauging whether the approximate boundary condition is valid is to examine the magnetic shielding ratio. The magnetic shielding ratio for the simple one dimensional problem illustrated in Figure 2-1 is simply the ratio of the magnetic field at the inner wall of the wellbore casing to the field at the outer wall. The formula for the shielding ratio is given by expression (2.43). It was decided in chapter 2 that the minimum magnetic shielding ratio magnitude for which the approximation $\vec{H} = 0$ can be justified is approximately 30. For a more complicated, two dimensional problem, such as that illustrated in Figure 5-1, the solutions for the electromagnetic fields in the casing are composed of an infinite series of spatial harmonics. In this situation, the approximation $\vec{H} = 0$ is considered good if the magnetic shielding ratios for the first five harmonics of the magnetic field are greater than 30.

7.2 Proof That the Finite Element Method Can Yield Accurate Solutions for the Eddy Current Problem

Chapters 4, 5 and 6 examine wellbore casing problems of increasing complexity. Each chapter details a procedure for obtaining FEM solutions for the eddy current density and losses induced in a wellbore casing. In the numerical examples presented in these chapters, the FEM solutions for current density and resistive losses agree closely with

analytical solutions derived in chapters 2 and 3 and elsewhere in the published literature. Evidence to support this statement is given throughout this work.

For problem 1, the simple one dimensional problem analyzed in chapter 4, FEM solutions for the electric and magnetic fields in various wellbore casings were compared with exact analytical solutions derived in chapter 2. The comparisons between the FEM and analytical solutions may be seen in Figures 4-2 to 4-9. Except for the phase of the magnetic fields, the agreement between the FEM and analytical solutions is relatively good.

Also for problem 1, FEM based solutions for effective casing impedance are compared with experimentally measured values from reference [3]. Effective casing impedance is defined in (4.12) and the results of the comparison are available in Table 4-2. The results indicate a remarkably close agreement between the FEM and experimental values for effective casing impedance.

Finally, for problem 1, FEM based solutions for the resistive power loss in wellbore casings are compared with analytic solutions derived in chapter 2 and some experimentally measured values from reference [3]. The results of the comparison, available in Table 4-4, indicate good agreement between the FEM and analytic solutions.

FEM solutions were also calculated for more complex, two dimensional boundary value problems such as problem 2 in chapter 5. For problem 2, FEM solutions for the current density in various casing samples were compared with analytical solutions derived in reference [6], [9] and [13]. For the magnitude of the current density, FEM and analytic solutions were plotted together in Figures 5-3, 5-6 and 5-9. For the phase of the current density, FEM and analytic solutions were plotted together in Figures 5-4, 5-7 and 5-10. *Overall, the FEM and analytical solutions were in relatively close agreement.* There were, however, certain instances where fairly substantial discrepancies arose. The discrepancies between the FEM and analytical solutions can be attributed to the use of the approximate boundary condition, $\vec{H} = 0$, at the outer wall of the casing. The validity of this approximation was not very strong for some of the casing samples in problem 2.

The resistive losses (i.e., eddy current losses) in the various casing samples of problem 2 were also examined. FEM based solutions for the resistive losses were compared with analytical solutions derived in reference [9] and [13]. In some cases the two solutions gave very similar values; however, in one instance there was a 50% difference between the

analytic and FEM solutions. Once again, the discrepancy between the two solutions may be attributed to the inappropriate use of the approximate boundary condition $\vec{H} = 0$ at the outer wall of the casing.

Finally, in chapter 6, the general problem of multiple power cables arranged in an arbitrary configuration inside a wellbore was considered. Three different boundary value problems were solved: 3a, 3b and 3c. Each problem was distinguished by the arrangement of the power cables inside the wellbore and the electromagnetic properties of the casings.

Using the procedure outlined in section 6.3 for solving multiple cable problems, FEM solutions were computed for the electric fields inside the various wellbore casings. Employing the FEM solutions for the electric fields and Poynting's theorem, values for the resistive losses in various casing samples were obtained. These FEM based solutions for the resistive losses were compared with analytic solutions from reference [10]. The results of the comparisons, presented in Figures 6-11, 6-17 and 6-23, indicate good agreement between the FEM and analytic solutions.

7.3 Potential Areas of Further Investigation

There are several avenues of research related to the eddy current problems discussed in this thesis which appear worthy of further investigation. These potential areas of further research are outlined below.

Instead of applying the finite element method to numerically solve for the eddy currents in a wellbore casing, as was done in this thesis, the *method of moments* could be used. The method of moments is a numerical method quite different from the finite element method. Adapted by Harrington [14] for use in solving electromagnetic boundary value problems, the method of moments numerically solves for the integral equation associated with a given boundary value problem. The method of moments has a significant advantage over the finite element method in that it can readily solve problems which have an infinite domain. Thus, the exact boundary conditions on the electromagnetic fields can be used instead of the approximate boundary condition ($\vec{H} = 0$ at the outer wall of the casing) which is required for the finite element method.

In reference [13], Kriezis and Cangellaris used the method of moments to solve for the eddy currents induced in a metal shell by a single current filament located inside the shell. Their results were used as a comparison for some of the FEM solutions in chapter 5.

Their solutions for the magnitude of the current density were consistently smaller than either the FEM solutions or the (purely analytical) revised Tegopoulos and Kriezis solutions. In one instance, their solution for power loss in a wellbore casing (which was based on their eddy current solution) differed from the FEM and analytical solutions by 50%. This discrepancy deserves further investigation. In addition, reference [13] gave no results for the phase of the eddy current density. For the sake of completeness, a method of moments solution for the *phase* of the eddy current density would be desirable.

Another logical extension of the research done in this paper would be to extend the analysis of the problem from two to three dimensions. The eddy current density could be solved for analytically or numerically. In reference [13], Kriezis and Cangellaris use the method of moments to obtain a numerical solution, in three dimensions, for the current density in a metal shell of finite length and thickness. Some three dimensional, *analytic* solutions have been derived by Tegopoulos and Kriezis [21, 22]. Their solution is for the case of a single current filament situated inside (but not necessarily at the center of) an infinitely thick cylindrical, metal shell. As of yet, no purely analytical solution exists for a shell of finite length *and* thickness.

Finally, it would be advisable to obtain experimental confirmation of some or all of the above numerical and analytical solutions. From Stroemich et al. [3], some experimental data is available for the case of a single power cable situated at the center of a wellbore casing. It would be desirable to obtain measurements of eddy current loss for the situation where the power cable is off centered.

Experimental data is also available from Kawasaki et al. [10] for the situation where a steel pipe encompasses three power cables carrying a balanced, three phase current. For situations where the current inside the pipe is *unbalanced*, it would be advisable to obtain experimental results in order to verify the analytical and numerical solutions presented in this thesis.

Bibliography

1. F.E. Vermeulen, F.S. Chute, "Electromagnetic Techniques in the In-Situ Recovery of Heavy Oil", *Journal of Microwave Power*, 18(1), 1983, pp. 15-29.
2. F.S. Chute, F.E. Vermeulen, "Present and Potential Applications of Electromagnetic Heating in the In-Situ Recovery of Oil", *AOSTRA Journal of Research*, Vol. 4, No. 1, Winter 1988, pp. 19-33.
3. C.P. Stroemich, F.E. Vermeulen, F.S. Chute, E. Sumbar, "Wellbore Power Transmission For In-Situ Electrical Heating", *AOSTRA Journal of Research*, Vol. 6, No. 4, Fall 1990, pp. 273-294.
4. J. Poltz, E. Kuffel, "A Simple and Accurate Evaluation of Eddy-Current Loss in Magnetic Pipe of a Cable", *IEEE Trans. (Power Apparatus and Systems)*, Vol. 104, No.8, pp. 1951-1957.
5. J.H. Dableh, R.D. Findlay, "An Annotated Summary of Analysis and Design Techniques for Pipe-Type Cable Systems", *IEEE Trans. (Power Apparatus and Systems)*, Vol. 103, No.10, pp. 2786-2793.
6. H.B. Dwight, "Proximity Effect in Wires and Thin Tubes", *Journal of A.I.E.E.*, Vol. 42 (1923), pp. 850-859.
7. H.B. Dwight, "Proximity Effect in Cable Sheaths", *Journal of A.I.E.E.*, Vol. 50 (1931), pp. 993-998.
8. J.A. Tegopoulos, E.E. Kriezis, "Eddy Current Distribution in Cylindrical Shells of Infinite Length Due to Axial Currents; Part I: Shells of One Boundary", *IEEE Trans. (Power Apparatus and Systems)*, Vol. 90, No.3 (1971), pp. 1278-1287.
9. J.A. Tegopoulos, E.E. Kriezis, "Eddy Current Distribution in Cylindrical Shells of Infinite Length Due to Axial Currents; Part II: Shells of Finite Thickness", *IEEE Trans. (Power Apparatus and Systems)*, Vol. 90, No.3 (1971), pp. 1287-1294.
10. K. Kawasaki, M. Inami, T. Ishikawa, "Theoretical Considerations on Eddy-Current Losses in Non-Magnetic Pipes for Power Transmission Systems", *IEEE Trans. (Power Apparatus and Systems)*, Vol. 100, No.2 (1981), pp. 474-484.

11. A. Emanuel, H.C. Doepken, "Calculation of Losses in Steel Enclosures of Three Phase Bus or Cables", *IEEE Trans. (Power Apparatus and Systems)*, Vol. 93, No.2 (1974), pp. 1758-1767.
12. R. Sikora, J. Purczynski, R. Palka, S. Gratkowski, "Analysis of Electromagnetic Field and Power Losses in Three Phase Gas Insulated Cable", *IEEE Trans. (Magnetics)*, Vol. 13 (1977), pp. 1140-1142.
13. E.E. Kriezis, A.K. Cangellaris, "An Integral Equation Approach to the Problem of Eddy Currents in Cylindrical Shells of Finite Thickness with Infinite or Finite Length", *Archiv Für Electrotechnik*, Vol. 13 (1984), pp. 317-324.
14. R.F. Harrington, *Field Computation by Moment Methods*, New York: McMillan 1965.
15. J. Poltz, E. Kuffel, S.Grzybowski, M.R. Raghuvver, "Eddy-Current Losses in Pipe-Type Cable Systems", *IEEE Trans. (Power Apparatus and Systems)*, Vol. 101, No.4 (1982), pp. 825-832.
16. J. Poltz, E. Kuffel, S.Grzybowski, M.R. Raghuvver, "Models Adopted For the Calculation of Eddy Current Losses in Pipe-Type Cables", *IEEE Trans. (Magnetics)*, Vol. 17, No.6 (1981), pp. 2592-2594.
17. D.S. Burnett, *Finite Element Analysis, From Concepts to Applications*, Reading, Massachusetts, Addison-Wesley, 1988.
18. R.F. Harrington, *Time-Harmonic Electromagnetic Fields*, New York, McGraw-Hill, 1961.
19. S. Ramo, J. R. Whinnery, T. Van Duzer, *Fields and Waves in Communication Electronics*, New York, John Wiley & Sons, 1984.
20. Wolfram Research, Inc., *Mathematica, Version 2.1*, Champaign, Illinois, Wolfram Research, Inc., 1992.

21. J.A. Tegopoulos, E.E. Kriezis, "Eddy Current Distribution in Cylindrical Shells of Finite Length and One Boundary Due to Axial Currents; Part I: Cylindrical Hole with Symmetrical Excitation", IEEE Trans. (Power Apparatus and Systems), Vol. 91 (1972), pp. 1614-1616.
22. J.A. Tegopoulos, E.E. Kriezis, "Eddy Current Distribution in Cylindrical Shells of Finite Length and One Boundary Due to Axial Currents, Part II Cylindrical Hole with Non-Symmetrical Excitation", IEEE Trans. (Power Apparatus and Systems), Vol. 91 (1972), pp. 1617-1623.
23. N. W. McLachlan, *Bessel Functions for Engineers*, London, Oxford University Press, 1955.
24. M. Abramowitz, I. Stegun, (Editors), *Handbook of Mathematical Functions*, New York, Dover Publications, Inc., 1965.

APPENDIX I

Errors and Inconsistencies In the Works of Tegopoulos and Kriezis Which Relate to the Eddy Current Distribution in Cylindrical Shells of Infinite Length.

As mentioned in section 1.2.1.2, an analytical solution for the current density induced in a cylindrical metal shell by a current filament is available from the works of Tegopoulos and Kriezis. This solution for current density is derived in references [8] and [9] and is given by equation (29) in reference [9]. However, there are two minor errors in the derivation of equation (29) which affect its validity. These errors are discussed in detail in sections A1.1 and A1.2 of this appendix. In section A1.3, equation (29) is rederived after correcting for the aforementioned errors.

A1.1 The Magnetic Vector Potential of an Infinitely Long Current Filament

The first error in the derivation of equation (29) relates to the magnetic vector potential of an infinitely long current filament in unbounded space. Figure A1-1a is a two dimensional cross section of a filament of infinite length in the z direction. The filament carries a low frequency, alternating current of magnitude I .

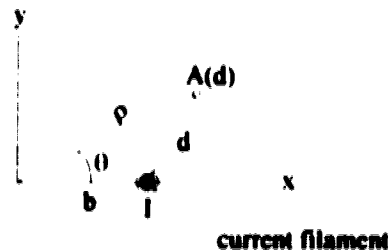


Figure A1-1 An infinitely long current filament in unbounded space.

According to equation (11) of reference [8], the vector potential of an infinitely long current filament in an air filled, unbounded region is

$$A(d) \cong \frac{\mu_0 I}{2\pi} \ln(d),$$

where d is the distance between the filament and observation point as shown in Figure A1-1a. However, equation (11) is wrong. In fact, the correct expression for the vector potential of a current filament in an air filled, unbounded region is

$$A(d) \cong -\frac{\mu_0 I}{2\pi} \ln(d). \quad (\text{A1.1})$$

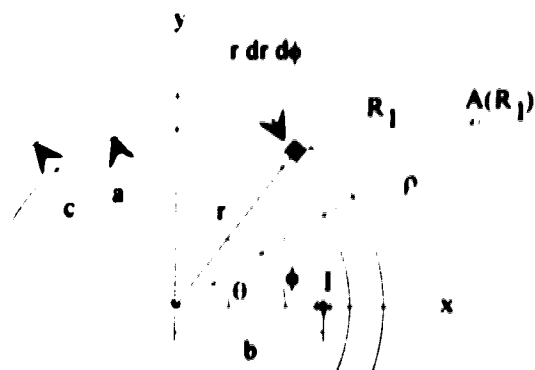


Figure A1-2 A partial cross section of an infinitely long cylindrical shell and current filament.

Consider now Figure A1-2; this is a partial cross section of an infinitely long cylindrical shell. An unknown current density flows along the length of the shell. The current density, referred to as $J(r, \phi)$, is some unknown function of r and ϕ . The current in the infinitesimal element $r dr d\phi$ is given by the term $J(r, \phi) r dr d\phi$. According to Tegopoulos and Kriezis, the vector potential (in air) due to the current element $J(r, \phi) r dr d\phi$ is

$$d^2 A = \frac{\mu_0}{2\pi} \ln(R_1) J(r, \phi) r dr d\phi,$$

where R_1 is the distance between the current element and the observation point, as shown in Figure A1-2. However the above expression, which occurs in references [8] and [9], is incorrect; once again the expression lacks a negative sign. The *correct* expression for the vector potential of the current element $J(r, \phi) r dr d\phi$ is

$$d^2 A = -\frac{\mu_0}{2\pi} \ln(R_1) J(r, \phi) r dr d\phi. \quad (\text{A1.2})$$

The consequences of the error in sign are apparent when one examines the solution for *total* current in the shell, as presented in references [8] and [9]. In reference [8], the outer radius of the shell is assumed to be infinite and the solution for current density is given by equation (34):

$$J(r, \phi) = \frac{\sqrt{j\rho l}}{2\pi a} \frac{K_0(\sqrt{j\rho r})}{K_1(\sqrt{j\rho a})} - \frac{\sqrt{j\rho l}}{\pi a} \sum_{n=1}^{\infty} \left(\frac{b}{a}\right)^n \frac{K_n(\sqrt{j\rho r}) \cos(n\phi)}{(1+\mu_n) K_n(\sqrt{j\rho a}) + \mu_n K_{n-1}(\sqrt{j\rho a})}$$

where $p = \sqrt{\mu_0 \omega / \rho}$ and μ_n is the relative magnetic permeability of the metal shell. In equation (74) of reference [8], Tegopoulos and Kriezis attempt to verify that the integral of $J(r, \phi)$ over the cross sectional area of the shell is $-I$. This would demonstrate that the total current in the problem is conserved since $I_{\text{plasma}} + I_{\text{shell}} = I - I = 0$. However, the integration in equation (74) contains an error. The integral of $J(r, \phi)$ over the cross sectional area of the shell is actually equal to $+I$. This is shown below:

$$\begin{aligned} I_{\text{shell}} &= \int_0^{2\pi} \int_a^{\infty} J(r, \phi) r dr d\phi \\ &= 2\pi \int_a^{\infty} \frac{\sqrt{j\rho l}}{2\pi a} \frac{K_0(\sqrt{j\rho r})}{K_1(\sqrt{j\rho a})} r dr \\ &= \frac{\sqrt{j\rho l}}{a} \frac{1}{K_1(\sqrt{j\rho a})} \int_a^{\infty} K_0(\sqrt{j\rho r}) r dr \\ &= \frac{\sqrt{j\rho l}}{a} \frac{1}{K_1(\sqrt{j\rho a})} \left[\frac{-r}{\sqrt{j\rho}} K_1(\sqrt{j\rho r}) \right] \\ &= \frac{\sqrt{j\rho l}}{a K_1(\sqrt{j\rho a})} \left[0 - \frac{-a}{\sqrt{j\rho}} K_1(\sqrt{j\rho a}) \right] \\ &= I \end{aligned}$$

Thus, according to the solution for current density given by equation (34) from reference [8], $I_{\text{shell}} = +I$ and current is not conserved. However, if equation (34) is rederived *after correcting for the negative sign in the expressions for magnetic vector potential*, it can be shown that I_{shell} does equal $-I$.

A similar situation arises in reference [9] where the thickness of the shell is finite. The solution for current density in a shell of finite thickness is given by equation (29) from reference [9]:

$$J(r, \phi) = -\sqrt{j} \frac{\rho l}{\pi a} \sum_{n=0}^{\infty} \delta_n^0 \frac{1}{D_n} \left(\frac{b}{a}\right)^n \left[K_{n-1}(\sqrt{j} pc) \cdot I_n(\sqrt{j} pr) + I_{n-1}(\sqrt{j} pc) \cdot K_n(\sqrt{j} pr) \right] \cos(n\phi),$$

where

$$p = \sqrt{\mu_0 \omega / \rho}$$

$$\delta_n^0 = 1/2 \text{ for } n=0 \text{ and } \delta_n^0 = 1 \text{ for } n \geq 1$$

$$D_n = I_{n+1}(\sqrt{j} pa) K_{n-1}(\sqrt{j} pc) - I_{n-1}(\sqrt{j} pc) K_{n+1}(\sqrt{j} pa).$$

The dimensions a , b and c are defined in Figure A1-2. Again, Tegopoulos and Kriezis claim that by integrating their equation (29) over the cross sectional area of the shell, the total current in the shell is found to be $-I$. Strangely, however, after their initial statement that $I_{shell} = -I$, Tegopoulos and Kriezis go on to show in appendix I of reference [9] that $I_{shell} = +I$.

It appears that the integral of equation (29) over the cross sectional area of the shell does indeed equal $+I$. This is shown below:

$$I_{shell} = \int_0^{2\pi} \int_0^c J(r, \phi) r dr d\phi$$

After integrating $J(r, \phi)$ from 0 to 2π , only the $n=0$ term of $J(r, \phi)$ remains. Therefore

$$I_{shell} = 2\pi \int_0^c \left[-\sqrt{j} \frac{\rho l}{\pi a} \frac{1}{2} \frac{K_{-1}(\sqrt{j} pc) I_0(\sqrt{j} pr) + I_{-1}(\sqrt{j} pc) K_0(\sqrt{j} pr)}{D_0} \right] r dr.$$

Given that $K_{-1}(\sqrt{j} pc) = K_1(\sqrt{j} pc)$ and $I_{-1}(\sqrt{j} pc) = I_1(\sqrt{j} pc)$,

$$I_{shell} = 2\pi \int_0^c \left[-\sqrt{j} \frac{\rho l}{\pi a} \frac{1}{2} \frac{K_1(\sqrt{j} pc) I_0(\sqrt{j} pr) + I_1(\sqrt{j} pc) K_0(\sqrt{j} pr)}{D_0} \right] r dr.$$

Rearranging terms in the above integral yields

$$I_{shell} = -\sqrt{j} \frac{\rho l}{a} \frac{1}{D_0} \left[K_1(\sqrt{j} \rho c) \int_a^c I_0(\sqrt{j} \rho r) r dr + I_1(\sqrt{j} \rho c) \int_a^c K_0(\sqrt{j} \rho r) r dr \right]$$

The modified Bessel functions in the above integral may be evaluated using the formulae

$$\int z^n I_{n-1}(z) dz = z^n I_n(z)$$

$$\int z^n K_{n-1}(z) dz = -z^n K_n(z)$$

Evaluating the integral for I_{shell} yields

$$\begin{aligned} I_{shell} &= -\sqrt{j} \frac{\rho l}{a} \frac{1}{D_0} \left[\frac{K_1(\sqrt{j} \rho c)}{\sqrt{j} \rho} \Big|_a^c I_1(\sqrt{j} \rho r) - \frac{I_1(\sqrt{j} \rho c)}{\sqrt{j} \rho} \Big|_a^c K_1(\sqrt{j} \rho r) \right] \\ &= -\frac{I}{a} \frac{1}{D_0} \left[K_1(\sqrt{j} \rho c) \left[c I_1(\sqrt{j} \rho c) - a I_1(\sqrt{j} \rho a) \right] - I_1(\sqrt{j} \rho c) \left[c K_1(\sqrt{j} \rho c) - a K_1(\sqrt{j} \rho a) \right] \right] \\ &= I \frac{1}{D_0} \left[K_1(\sqrt{j} \rho c) I_1(\sqrt{j} \rho a) - I_1(\sqrt{j} \rho c) K_1(\sqrt{j} \rho a) \right] \end{aligned}$$

From equation (26) of reference [9],

$$D_n = I_{n-1}(\sqrt{j} \rho a) K_n(\sqrt{j} \rho c) - I_n(\sqrt{j} \rho c) K_{n-1}(\sqrt{j} \rho a)$$

Therefore,

$$\begin{aligned} D_0 &= I_1(\sqrt{j} \rho a) K_1(\sqrt{j} \rho c) - I_1(\sqrt{j} \rho c) K_1(\sqrt{j} \rho a) \\ &= I_1(\sqrt{j} \rho a) K_1(\sqrt{j} \rho c) - I_1(\sqrt{j} \rho c) K_1(\sqrt{j} \rho a) \\ &= K_1(\sqrt{j} \rho c) I_1(\sqrt{j} \rho a) - I_1(\sqrt{j} \rho c) K_1(\sqrt{j} \rho a) \end{aligned}$$

Substituting the above expression for D_0 into the expression for I_{shell} yields

$$I_{shell} = I \frac{K_1(\sqrt{j} \rho c) I_1(\sqrt{j} \rho a) - I_1(\sqrt{j} \rho c) K_1(\sqrt{j} \rho a)}{K_1(\sqrt{j} \rho c) I_1(\sqrt{j} \rho a) - I_1(\sqrt{j} \rho c) K_1(\sqrt{j} \rho a)}$$

$$I_{shell} = I, \text{ Q.E.D.}$$

$I_{shell} = +I$ makes no physical sense because the total current in the problem is not conserved. The total current in the shell should be $-I$, as initially stated by Tegupankas and Kriezis. Once again, the problem can be traced to the omission of the negative sign in

Tegopoulos's original expressions for magnetic vector potential. If equation (29) is rederived after correcting for the negative sign in the expressions for vector potential, it can be shown that J_{shell} does equal $-J$.

A1.2 The Series Expansion of $\ln|r^2 + \rho^2 - 2r\rho\cos(\phi - \theta)|$

The second error in the derivation of equation (29) is directly traceable to equation (13) in reference [9]. Equation (13) is merely a series expansion of the term $\ln(R_1)$, where $R_1 = \sqrt{r^2 + \rho^2 - 2r\rho\cos(\phi - \theta)}$ and $\rho > r$. According to equation (13),

$$\ln(R_1) = \ln(r) - \sum_{m=1}^{\infty} \frac{1}{m} \left(\frac{r}{\rho}\right)^m [\cos(m\phi)\cos(m\theta) + \sin(m\phi)\sin(m\theta)], \text{ with } \rho > r.$$

In fact, the correct expansion with $\rho > r$ is

$$\ln(R_1) = \ln(\rho) - \sum_{m=1}^{\infty} \frac{1}{m} \left(\frac{r}{\rho}\right)^m [\cos(m\phi)\cos(m\theta) + \sin(m\phi)\sin(m\theta)]; \quad (\text{A1.3})$$

the argument of the natural logarithm should be ρ , not r . The fact that the zeroth order term in the expansion is $\ln(\rho)$ and *not* $\ln(r)$ immediately affects equation (14), the magnetic vector potential in the region outside the shell. This, in turn, has repercussions which affect the zeroth order term in equation (29), the solution for current density in the shell.

A1.3 Corrections to Equation (29) After Accounting for Errors in Its Original Derivation by Tegopoulos and Kriezis

The goal of this section is to rederive equation (29) in reference [9] *after correcting for the two errors which appeared in the original derivation*. The two errors are those discussed above, in sections A1.1 and A1.2.

Unless otherwise stated, the equations of Tegopoulos and Kriezis referred to in this section are from reference [9]. Wherever possible, the notation in this section is consistent with that used in the original papers by Tegopoulos and Kriezis (references [8] and [9]); the only notable difference is the use of ' $J(r, \phi)$ ' for current density instead of ' $J(r, \phi)$ '.

Equations (1) and (2) are correct as shown in reference [9]. Equation (3), the magnetic vector potential due to the current filament, should be rewritten as

$$A_1(\rho, \theta) = -\frac{\mu_0 I}{4\pi} \ln(\rho^2 + b^2 - 2\rho b \cos\theta). \quad (\text{A1.4})$$

Similarly, equation (4) should be rewritten as

$$d^2 A_{\sigma,1} = -\frac{\mu_0}{2\pi} J(r, \phi) \ln(R) r dr d\phi. \quad (\text{A1.5})$$

Equation (5) is correct as written. Equation (6) is altered by the correction to equation (4); equation (6) should be rewritten as

$$A_{\sigma,1}(\rho, \theta) = -(L_0 \bar{I}_0 + V_0 \bar{V}_0) + \sum_{n=1}^{\infty} L_n \frac{\rho^n}{n} S_{1,n} \cos(n\theta) + \sum_{n=1}^{\infty} V_n \frac{\rho^n}{n} S_{2,n} \cos(n\theta). \quad (\text{A1.6})$$

Equations (7), (8), (9) and (10) are correct as shown in reference [9]. Equation (11) is also correct, but note that $A_1(\rho, \theta)$ and $A_{\sigma,1}(\rho, \theta)$ should refer to the expressions in (A1.4) and (A1.6) respectively.

Equation (12) should be rewritten as

$$d^2 A_{\sigma,1}(\rho, \theta) = -\frac{\mu_0}{2\pi} J(r, \phi) \ln(R_1) r dr d\phi. \quad (\text{A1.7})$$

The mistake in equation (13) from reference [9] was discussed in the previous section; equation (13) should be rewritten as

$$\ln(R_1) = \ln(\rho) - \sum_{m=1}^{\infty} \frac{1}{m} \left(\frac{r}{\rho}\right)^m [\cos(m\phi) \cos(m\theta) + \sin(m\phi) \sin(m\theta)]. \quad (\text{A1.8})$$

After correcting equations (12) and (13), equation (14) needs to be reevaluated. Equation (14) is the integral of equation (12) over the cross sectional area of the shell. Equation (14) is reevaluated as follows:

$$A_{n,\theta}(\rho,\theta) = \int_0^{2\pi} \int_a^c -\frac{\mu_0}{2\pi} J(r,\phi) \ln(R_1) r dr d\phi,$$

where $J(r,\phi)$ is the general solution for current density given by equation (1) and $\ln(R_1)$ is given by (A1.3). Thus,

$$A_{n,\theta}(\rho,\theta) = -\frac{\mu_0}{2\pi} \int_0^{2\pi} \int_a^c \left(\sum_{n=0}^{\infty} [F_n I_n(\sqrt{jpr}) + C_n K_n(\sqrt{jpr})] \cos(n\phi) \right) \cdot \left(\ln(\rho) - \sum_{m=1}^{\infty} \frac{1}{m} \left(\frac{r}{\rho}\right)^m [\cos(m\phi)\cos(m\theta) + \sin(m\phi)\sin(m\theta)] \right) r dr d\phi, \quad (A1.8)$$

or

$$A_{n,\theta}(\rho,\theta) = -\frac{\mu_0}{2\pi} \int_0^{2\pi} \int_a^c \left[\ln(\rho) \sum_{n=0}^{\infty} [F_n I_n(\sqrt{jpr}) + C_n K_n(\sqrt{jpr})] \cos(n\phi) - \sum_{n=0}^{\infty} \sum_{m=1}^{\infty} \frac{1}{m} \left(\frac{r}{\rho}\right)^m [\cos(m\phi)\cos(m\theta) + \sin(m\phi)\sin(m\theta)] [F_n I_n(\sqrt{jpr}) + C_n K_n(\sqrt{jpr})] \cos(n\phi) \right] r dr d\phi \quad (A1.9)$$

Integrating (A1.9) with respect to ϕ from 0 to 2π reduces the above expression to

$$A_{n,\theta}(\rho,\theta) = -\frac{\mu_0}{2\pi} \int_a^c \left[2\pi \ln(\rho) [F_0 I_0(\sqrt{jpr}) + C_0 K_0(\sqrt{jpr})] - \pi \sum_{n=1}^{\infty} \frac{1}{n} \left(\frac{r}{\rho}\right)^n [F_n I_n(\sqrt{jpr}) + C_n K_n(\sqrt{jpr})] \cos(n\theta) \right] r dr. \quad (A1.10)$$

Equation (A1.10) may be simplified somewhat:

$$A_{n,\theta}(\rho,\theta) = -\mu_0 \ln(\rho) \left[F_0 \int_a^c I_0(\sqrt{jpr}) r dr + C_0 \int_a^c K_0(\sqrt{jpr}) r dr \right] + \frac{\mu_0}{2} \sum_{n=1}^{\infty} \frac{1}{n} \left(\frac{1}{\rho}\right)^n \left[F_n \int_a^c r^{n+1} I_n(\sqrt{jpr}) dr + C_n \int_a^c r^{n+1} K_n(\sqrt{jpr}) dr \right] \cos(n\theta). \quad (A1.11)$$

Integrating (A1.11) with respect to r from a to c yields

$$\begin{aligned}
 A_{\sigma,\sigma}(\rho,\theta) &= -\mu_0 \ln(\rho) \left[F_0 \left[\frac{r I_1(\sqrt{j\rho r})}{\sqrt{j\rho}} - C_0 \right] \frac{r K_1(\sqrt{j\rho r})}{\sqrt{j\rho}} \right] + \\
 &\quad \frac{\mu_0}{2} \sum_{n=1}^{\infty} \frac{1}{n} \left(\frac{1}{\rho} \right)^n \left[F_n \left[\frac{r^{n+1}}{\sqrt{j\rho}} I_{n+1}(\sqrt{j\rho r}) - C_n \left[\frac{r^{n+1}}{\sqrt{j\rho}} K_{n+1}(\sqrt{j\rho r}) \right] \right] \cos(n\theta) \right. \\
 &= -\mu_0 \ln(\rho) \left[\frac{F_0}{\sqrt{j\rho}} [c I_1(\sqrt{j\rho c}) - a I_1(\sqrt{j\rho a})] - \frac{C_0}{\sqrt{j\rho}} [c K_1(\sqrt{j\rho c}) - a K_1(\sqrt{j\rho a})] \right] + \\
 &\quad \frac{\mu_0}{2} \sum_{n=1}^{\infty} \frac{1}{n} \left(\frac{1}{\rho} \right)^n \left[\frac{F_n}{\sqrt{j\rho}} [c^{n+1} I_{n+1}(\sqrt{j\rho c}) - a^{n+1} I_{n+1}(\sqrt{j\rho a})] - \right. \\
 &\quad \left. \frac{C_n}{\sqrt{j\rho}} [c^{n+1} K_{n+1}(\sqrt{j\rho c}) - a^{n+1} K_{n+1}(\sqrt{j\rho a})] \right] \cos(n\theta)
 \end{aligned} \tag{A1.12}$$

$$\begin{aligned}
 A_{\sigma,\sigma}(\rho,\theta) &= -\mu_0 \ln(\rho) \left[\frac{V_0}{\sqrt{j\rho}} [c I_1(\sqrt{j\rho c}) - a I_1(\sqrt{j\rho a})] - \frac{L_0}{\sqrt{j\rho}} [c K_1(\sqrt{j\rho c}) - a K_1(\sqrt{j\rho a})] \right] + \\
 &\quad \frac{\mu_0}{2} \sum_{n=1}^{\infty} \frac{1}{n} \left(\frac{1}{\rho} \right)^n \left[\frac{V_n}{\sqrt{j\rho}} [c^{n+1} I_{n+1}(\sqrt{j\rho c}) - a^{n+1} I_{n+1}(\sqrt{j\rho a})] - \right. \\
 &\quad \left. \frac{L_n}{\sqrt{j\rho}} [c^{n+1} K_{n+1}(\sqrt{j\rho c}) - a^{n+1} K_{n+1}(\sqrt{j\rho a})] \right] \cos(n\theta)
 \end{aligned} \tag{A1.13}$$

In going from (A1.12) to (A1.13), the unknown constants F_n and C_n are renamed V_n and L_n , respectively. According to Tegopoulos and Kriezis [8], the constants are renamed because the relative terms in $A_{\sigma,\sigma}(\rho,\theta)$ correspond to the contribution of eddy currents in the air and not in the material.

Rearranging (A1.13) yields

$$\begin{aligned}
 A_{n,r}(\rho,\theta) = & \ln(\rho) \left[V_n \frac{\mu_0}{\sqrt{jp}} \left[c I_1(\sqrt{jp}\rho) - a I_1(\sqrt{jp}a) \right] + I_n \frac{\mu_0}{\sqrt{jp}} \left[a K_1(\sqrt{jp}a) - c K_1(\sqrt{jp}\rho) \right] \right] + \\
 & \sum_{n=1}^{\infty} \frac{1}{n\rho^n} \left[V_n \frac{\mu_0}{2\sqrt{jp}} \left[c^{n+1} I_{n+1}(\sqrt{jp}\rho) - a^{n+1} I_{n+1}(\sqrt{jp}a) \right] + \right. \\
 & \left. I_n \frac{\mu_0}{2\sqrt{jp}} \left[a^{n+1} K_{n+1}(\sqrt{jp}a) - c^{n+1} K_{n+1}(\sqrt{jp}\rho) \right] \right] \cos(n\theta).
 \end{aligned} \tag{A1.14}$$

The above expression for $A_{n,r}(\rho,\theta)$ can be written in a more manageable form which also corresponds to the original equation (14) in reference [9]:

$$A_{n,r}(\rho,\theta) = \ln(\rho) [I'_n Y_{20} + I_n Y_{10}] + \sum_{n=1}^{\infty} \frac{1}{n\rho^n} [I'_n Y'_{2n} + I_n Y_{1n}] \cos(n\theta) \tag{A1.15}$$

where

$$Y_{10} = \frac{\mu_0}{\sqrt{jp}} \left[a K_1(\sqrt{jp}a) - c K_1(\sqrt{jp}\rho) \right], \tag{A1.16a}$$

$$Y_{1n} = \frac{\mu_0}{2\sqrt{jp}} \left[a^{n+1} K_{n+1}(\sqrt{jp}a) - c^{n+1} K_{n+1}(\sqrt{jp}\rho) \right], \text{ for } n \geq 1, \tag{A1.16b}$$

$$Y_{20} = \frac{\mu_0}{\sqrt{jp}} \left[c I_1(\sqrt{jp}\rho) - a I_1(\sqrt{jp}a) \right], \tag{A1.17a}$$

$$\text{and } Y_{2n} = \frac{\mu_0}{2\sqrt{jp}} \left[c^{n+1} I_{n+1}(\sqrt{jp}\rho) - a^{n+1} I_{n+1}(\sqrt{jp}a) \right], \text{ for } n \geq 1. \tag{A1.17b}$$

Equation (A1.15) is, therefore, the corrected version of equation (14) from reference [9]. Equations (A1.16a) and (A1.16b) are essentially the corrections to equation (15). Similarly, equations (A1.17a) and (A1.17b) are the corrections to equation (16).

Equations (17), (18), (19) and (20) are correct as written in reference [9]. These are the boundary conditions on the normal and tangential components of the magnetic fields at the inner and outer surfaces of the shell. Using these boundary conditions, Tegopoulos and Kriezis construct a system of 4 equations with 4 unknowns. Tegopoulos and Kriezis substitute the n th terms of $B_r(\rho,\theta)$ and $H_\theta(\rho,\theta)$ into equations (17), (18), (19) and (20)

and then proceed to solve for F_n and C_n . There is one minor problem with this procedure it cannot be used to solve for F_0 and C_0 because there is no zeroth terms of $H_n(\rho, \theta)$. Thus one is left with 4 unknowns (F_0 , C_0 , L_0 and V_0) but only 2 equations, (18) and (20)

To solve for F_0 and C_0 , the continuity boundary condition for the tangential components of \vec{A} must be introduced. There are general solutions available for the z component of the vector potential in all three regions of this problem. The general solution for $A_z(\rho, \theta)$, the vector potential in the air filled region inside the shell, is given by equation (11) from reference [9]. $A_n(r, \phi)$, the solution for the vector potential in the shell itself, is given by equation (2). $A_{n,s}(\rho, \theta)$, the vector potential outside the shell is given by equation (A1.15).

At the inner surface of the shell,

$$A_z(a, \theta) = A_n(a, \phi), \quad (\text{A1.18})$$

where $A_z(\rho, \theta)$ and $A_n(r, \phi)$ are given by equations (11) and (2), respectively. Likewise, at the outer surface of the shell,

$$A_n(c, \phi) = A_{n,s}(c, \theta), \quad (\text{A1.19})$$

where $A_n(r, \phi)$ is given by equation (2) and $A_{n,s}(\rho, \theta)$ is given by equation (A1.15). Equations (18), (20), (A1.18) and (A1.19) constitute a system of 4 equations in 4 unknowns which can be used to solve for F_0 and C_0 .

Solving the systems of equations yields the following solutions for the unknown constants F_n and C_n :

$$F_0 = \sqrt{j} \frac{\rho l}{2\pi a} \frac{\left[\frac{\mu_n K_0(\sqrt{j\rho c})}{\sqrt{j\rho c \ln(c)}} + K_1(\sqrt{j\rho c}) \right]}{\left[I_1(\sqrt{j\rho a}) \left[\frac{\mu_n K_0(\sqrt{j\rho c})}{\sqrt{j\rho c \ln(c)}} + K_1(\sqrt{j\rho c}) \right] + K_1(\sqrt{j\rho a}) \left[\frac{\mu_n I_0(\sqrt{j\rho c})}{\sqrt{j\rho c \ln(c)}} + I_1(\sqrt{j\rho c}) \right] \right]} \quad (\text{A1.20a})$$

$$F_n = -\frac{1}{D_n} \sqrt{j} \frac{\rho l}{2\pi} \left[\frac{2 \left(\frac{b}{a} \right)^n}{\left(\frac{a}{b} \right)^n} \right] \left[\frac{\mu_n K_n(\sqrt{j\rho c})}{\sqrt{j\rho c}} + K_n'(\sqrt{j\rho c}) \right], \text{ for } n \geq 1 \quad (\text{A1.20b})$$

$$C_0 = \sqrt{j} \frac{\rho l}{2\pi a} \frac{\left[\frac{\mu, I_0(\sqrt{j\rho c})}{\sqrt{j\rho c \ln(c)}} - I_1(\sqrt{j\rho c}) \right]}{\left[I_1(\sqrt{j\rho a}) \left[\frac{\mu, K_0(\sqrt{j\rho c})}{\sqrt{j\rho c \ln(c)}} + K_1(\sqrt{j\rho c}) \right] + K_1(\sqrt{j\rho a}) \left[\frac{\mu, I_0(\sqrt{j\rho c})}{\sqrt{j\rho c \ln(c)}} - I_1(\sqrt{j\rho c}) \right] \right]} \quad (\text{A1.21})$$

$$C_n = \frac{1}{D_n} \sqrt{j} \frac{\rho l}{2\pi} \left(\frac{2}{a} \left(\frac{b}{a} \right)^n \right) \left[\frac{\mu, n I_n(\sqrt{j\rho c})}{\sqrt{j\rho c}} + I_{n+1}'(\sqrt{j\rho c}) \right], \quad \dots n \geq 1 \quad (\text{A1.21b})$$

where

$$D_n = \left(\frac{n[\mu, -1]}{\sqrt{j\rho a}} I_n(\sqrt{j\rho a}) - I_{n+1}(\sqrt{j\rho a}) \right) \left(\frac{n[\mu, -1]}{\sqrt{j\rho c}} K_n(\sqrt{j\rho c}) - K_{n+1}(\sqrt{j\rho c}) \right) - \left(\frac{n[\mu, -1]}{\sqrt{j\rho a}} K_n(\sqrt{j\rho a}) + K_{n+1}(\sqrt{j\rho a}) \right) \left(\frac{n[\mu, -1]}{\sqrt{j\rho c}} I_n(\sqrt{j\rho c}) + I_{n+1}(\sqrt{j\rho c}) \right) \quad (\text{A1.22})$$

Equations (A1.20) and (A1.21) represent corrections to the equations (24) and (25) from reference [9]. Equation (A1.22) is the correction to equation (26).

Having obtained solutions for F_n and C_n , it is now possible to construct the final solution for the current density in the shell. The general solution for current density was given by equation (1):

$$J(r, \phi) = \sum_{n=0}^{\infty} \left[F_n I_n(\sqrt{j\rho r}) + C_n K_n(\sqrt{j\rho r}) \right] \cos(n\phi).$$

Substituting equations (A1.20) and (A1.21) into (1) yields

$$J(r, \phi) = \sqrt{j} \frac{\rho l}{2\pi a} \left\{ \frac{\left[\frac{\mu, K_0(\sqrt{j\rho c})}{\sqrt{j\rho c \ln(c)}} + K_1(\sqrt{j\rho c}) \right] I_0(\sqrt{j\rho r}) - \left[\frac{\mu, I_0(\sqrt{j\rho c})}{\sqrt{j\rho c \ln(c)}} - I_1(\sqrt{j\rho c}) \right] K_0(\sqrt{j\rho r})}{\left[I_1(\sqrt{j\rho a}) \left[\frac{\mu, K_0(\sqrt{j\rho c})}{\sqrt{j\rho c \ln(c)}} + K_1(\sqrt{j\rho c}) \right] + K_1(\sqrt{j\rho a}) \left[\frac{\mu, I_0(\sqrt{j\rho c})}{\sqrt{j\rho c \ln(c)}} - I_1(\sqrt{j\rho c}) \right] \right]} + \sqrt{j} \frac{\rho l}{2\pi} \sum_{n=1}^{\infty} \frac{1}{D_n} \left(\frac{b}{a} \right)^n \left[- \left[\frac{n[\mu, -1] K_n(\sqrt{j\rho c})}{\sqrt{j\rho c}} - K_{n+1}(\sqrt{j\rho c}) \right] I_n(\sqrt{j\rho r}) + \left[\frac{n[\mu, -1] I_n(\sqrt{j\rho c})}{\sqrt{j\rho c}} + I_{n+1}(\sqrt{j\rho c}) \right] K_n(\sqrt{j\rho r}) \right] \cos(n\phi) \right\} \quad (\text{A1.23})$$

where D_n is given by (A1.22).

In the event that $\mu_r = 1$, (A1.23) reduces to

$$J(r, \phi) = \sqrt{j} \frac{\rho I}{2\pi a} \left(\frac{\left[\frac{K_0(\sqrt{j\rho c})}{\sqrt{j\rho c \ln(c)} + K_1(\sqrt{j\rho c})} I_0(\sqrt{j\rho r}) - \left[\frac{I_0(\sqrt{j\rho c})}{\sqrt{j\rho c \ln(c)}}, I_1(\sqrt{j\rho c}) \right] K_0(\sqrt{j\rho r}) \right]}{\left[\frac{K_0(\sqrt{j\rho c})}{\sqrt{j\rho c \ln(c)} + K_1(\sqrt{j\rho c})} I_1(\sqrt{j\rho a}) + \left[\frac{I_0(\sqrt{j\rho c})}{\sqrt{j\rho c \ln(c)}}, I_1(\sqrt{j\rho c}) \right] K_1(\sqrt{j\rho a}) \right)}, \right. \\ \left. \sqrt{j} \frac{\rho I}{\pi a} \sum_{n=1}^{\infty} \frac{1}{D_n} \left(\frac{b}{a} \right)^n \left[K_{n-1}(\sqrt{j\rho c}) I_n(\sqrt{j\rho r}) + I_{n-1}(\sqrt{j\rho c}) K_n(\sqrt{j\rho r}) \right] \cos(n\phi) \right) \quad (\text{A1.24})$$

and D_n from (A1.22) reduces to

$$D_n = I_{n-1}(\sqrt{j\rho a}) K_{n-1}(\sqrt{j\rho c}) - K_{n-1}(\sqrt{j\rho a}) I_{n-1}(\sqrt{j\rho c}), \text{ for } n > 1 \quad (\text{A1.25})$$

In summary, after correcting for the two errors in the original derivation of equation (29) (the errors discussed in sections A1.1 and A1.2), the result is equation (A1.24). Equation (A1.24) represents the correct solution for the current density in a metal shell of finite thickness with $\mu_r = 1$. Note the two main differences between (A1.24) and equation (29): first, the $n = 0$ term in (A1.24) contains several extra terms in the numerator and denominator which include the factor $\ln(c)$. The second difference between (A1.24) and (29) is the sign change in front of the $n \geq 1$ terms.

A1.4 The Return Current

In reference [9], Tegopoulos and Kriezis assumed that the return path of the filament current I was confined inside the metal shell, and therefore $I_{\text{return}} = I$. In section A1.1, it was also stated that the total current in the shell should be equal to $-I$. However, this is true only if one uses the incorrect series expansion for $\ln(r)$ given by equation (13) in reference [9]. The error in the expansion of $\ln(r)$ inadvertently leads to the boundary condition $H_{\phi}(k_2, b) = 0$. This, in turn, leads to the return current being confined within the shell. The relationship between the $H_{\phi}(k_2, b) = 0$ boundary condition and return current was discussed in more detail in section 3.3.

After the correcting for the error in the expansion of $\ln(r)$, the total current in the shell may be found by re-evaluating the integral

$$I_{shell} = \int_0^{2\pi} \int_a^c J(r, \phi) r dr d\phi.$$

Substituting the correct expression for $J(r, \phi)$ from equation (A1.24) into the integral for I_{shell} yields

$$\begin{aligned} I_{shell} &= \sqrt{j} \frac{\rho l}{a} \left(\frac{\left[\frac{K_0(\sqrt{j\rho c})}{\sqrt{j\rho c \ln(c)} + K_1(\sqrt{j\rho c}) \right] \int_a^c I_0(\sqrt{j\rho r}) r dr - \left[\frac{I_0(\sqrt{j\rho c})}{\sqrt{j\rho c \ln(c)} - I_1(\sqrt{j\rho c}) \right] \int_a^c K_0(\sqrt{j\rho r}) r dr}{\left[\frac{K_0(\sqrt{j\rho c})}{\sqrt{j\rho c \ln(c)} + K_1(\sqrt{j\rho c}) \right] I_1(\sqrt{j\rho a}) + \left[\frac{I_0(\sqrt{j\rho c})}{\sqrt{j\rho c \ln(c)} - I_1(\sqrt{j\rho c}) \right] K_1(\sqrt{j\rho a})} \right) \\ &\quad - \sqrt{j} \frac{\rho l}{a} \left(\frac{\left[\frac{K_0(\sqrt{j\rho c})}{\sqrt{j\rho c \ln(c)} + K_1(\sqrt{j\rho c}) \right] \int_a^c I_0(\sqrt{j\rho r}) r dr - \left[\frac{I_0(\sqrt{j\rho c})}{\sqrt{j\rho c \ln(c)} - I_1(\sqrt{j\rho c}) \right] \int_a^c K_0(\sqrt{j\rho r}) r dr}{\left[\frac{K_0(\sqrt{j\rho c})}{\sqrt{j\rho c \ln(c)} + K_1(\sqrt{j\rho c}) \right] I_1(\sqrt{j\rho a}) + \left[\frac{I_0(\sqrt{j\rho c})}{\sqrt{j\rho c \ln(c)} - I_1(\sqrt{j\rho c}) \right] K_1(\sqrt{j\rho a})} \right) \\ &= \sqrt{j} \frac{\rho l}{a} \left(\frac{\left[\frac{K_0(\sqrt{j\rho c})}{\sqrt{j\rho c \ln(c)} + K_1(\sqrt{j\rho c}) \right] \frac{1}{\sqrt{j\rho a}} \int_a^c I_1(\sqrt{j\rho r}) - \left[\frac{I_0(\sqrt{j\rho c})}{\sqrt{j\rho c \ln(c)} - I_1(\sqrt{j\rho c}) \right] \frac{1}{\sqrt{j\rho a}} \int_a^c K_1(\sqrt{j\rho r})}{\left[\frac{K_0(\sqrt{j\rho c})}{\sqrt{j\rho c \ln(c)} + K_1(\sqrt{j\rho c}) \right] I_1(\sqrt{j\rho a}) + \left[\frac{I_0(\sqrt{j\rho c})}{\sqrt{j\rho c \ln(c)} - I_1(\sqrt{j\rho c}) \right] K_1(\sqrt{j\rho a})} \right). \end{aligned} \quad (A1.26)$$

$$I_{shell} = \frac{j}{a} \left(\frac{\left[\frac{K_0(\sqrt{j\rho c})}{\sqrt{j\rho c \ln(c)} + K_1(\sqrt{j\rho c}) \right] [c I_1(\sqrt{j\rho c}) - a I_1(\sqrt{j\rho a})] + \left[\frac{I_0(\sqrt{j\rho c})}{\sqrt{j\rho c \ln(c)} - I_1(\sqrt{j\rho c}) \right] [c K_1(\sqrt{j\rho c}) - a K_1(\sqrt{j\rho a})]}{\left[\frac{K_0(\sqrt{j\rho c})}{\sqrt{j\rho c \ln(c)} + K_1(\sqrt{j\rho c}) \right] I_1(\sqrt{j\rho a}) + \left[\frac{I_0(\sqrt{j\rho c})}{\sqrt{j\rho c \ln(c)} - I_1(\sqrt{j\rho c}) \right] K_1(\sqrt{j\rho a})} \right) \quad (A1.27)$$

Rearranging (A1.27) yields

$$I_{shell} = -I \left(1 - \frac{c}{a} \cdot \frac{\begin{matrix} K_1(\sqrt{J\rho c}) I_0(\sqrt{J\rho c}) - \begin{bmatrix} K_1(\sqrt{J\rho c}) & 1 \\ K_0(\sqrt{J\rho c}) + \sqrt{J\rho c} \ln(c) \\ I_1(\sqrt{J\rho c}) & 1 \\ I_0(\sqrt{J\rho c}) - \sqrt{J\rho c} \ln(c) \end{bmatrix} K_0(\sqrt{J\rho c}) I_1(\sqrt{J\rho c}) \\ I_0(\sqrt{J\rho c}) K_1(\sqrt{J\rho c}) - \begin{bmatrix} K_1(\sqrt{J\rho c}) & 1 \\ K_0(\sqrt{J\rho c}) + \sqrt{J\rho c} \ln(c) \\ I_1(\sqrt{J\rho c}) & 1 \\ I_0(\sqrt{J\rho c}) - \sqrt{J\rho c} \ln(c) \end{bmatrix} K_0(\sqrt{J\rho c}) I_1(\sqrt{J\rho c}) \end{matrix}}{\begin{matrix} K_1(\sqrt{J\rho c}) & 1 \\ K_0(\sqrt{J\rho c}) + \sqrt{J\rho c} \ln(c) \\ I_1(\sqrt{J\rho c}) & 1 \\ I_0(\sqrt{J\rho c}) - \sqrt{J\rho c} \ln(c) \end{matrix}} \right) \quad (A1.28)$$

By examining (A1.28), it is obvious that $I_{shell} \neq -I$ and therefore the original assumption that the return current flows entirely within the shell is erroneous. As discussed in section 3.3, the return current is *not*, in general, confined to the shell. Instead, some of the return current also flows *outside the shell* in the form of displacement current. The relationship between the conduction current in the shell, the displacement current outside the shell and the total return current is discussed in chapter 3. *Only in the extreme case where $H_{\theta_1}(k_2 h) = 0$ is $I_{shell} = -I$.*

A1.5 The Expression for Eddy Current Loss In Reference [9]

Reference [9] also contains an expression for the resistive power loss in the metal shell due to the flow of eddy currents. The formula for loss (in W/m) is given by equation (40). However, since equation (40) was derived using equation (29) (the incorrect expression for current density), it should be re-evaluated using the correct solution for current density given by (A1.24).

Fortunately, only the $n = 0$ term of the power loss formula given by equation (40) needs to be corrected. The $n \geq 1$ terms in equation (40) are unaffected by the correction to the $n \geq 1$ terms in equation (29). This is because the only correction to the $n > 1$ terms in equation (29) was a change in sign.

The correction to the $n = 0$ term in equation (40) and the proof that the $n > 1$ terms in equation (40) are still valid is given as follows.

First, rewrite (A1.24) in the following form:

$$J(r, \phi) = \frac{\rho l}{2\pi a} \left(\frac{1+j}{\sqrt{2}} \frac{[B_0(r) - jA_0(r)]}{D_w + jD_v} \right) + \frac{\rho l}{\pi a} \sum_{n=1}^{\infty} \frac{1+j}{\sqrt{2}} \frac{[B_n(r) - jA_n(r)]}{D_w + jD_n} \left(\frac{b}{a} \right)^n \cos(n\phi), \quad (\text{A1.29})$$

where

$$A_0(r) = \text{Im} \left\{ \left[\frac{K_0(\sqrt{j\rho c})}{\sqrt{j\rho c \ln(c)}} + K_1(\sqrt{j\rho c}) \right] I_0(\sqrt{j\rho r}) - \left[\frac{I_0(\sqrt{j\rho c})}{\sqrt{j\rho c \ln(c)}} - I_1(\sqrt{j\rho c}) \right] K_0(\sqrt{j\rho r}) \right\}, \quad (\text{A1.30})$$

$$B_0(r) = \text{Re} \left\{ \left[\frac{K_0(\sqrt{j\rho c})}{\sqrt{j\rho c \ln(c)}} + K_1(\sqrt{j\rho c}) \right] I_0(\sqrt{j\rho r}) - \left[\frac{I_0(\sqrt{j\rho c})}{\sqrt{j\rho c \ln(c)}} - I_1(\sqrt{j\rho c}) \right] K_0(\sqrt{j\rho r}) \right\}, \quad (\text{A1.31})$$

$$D_w = \text{Re} \left\{ \left[\frac{K_0(\sqrt{j\rho c})}{\sqrt{j\rho c \ln(c)}} + K_1(\sqrt{j\rho c}) \right] I_1(\sqrt{j\rho a}) + \left[\frac{I_0(\sqrt{j\rho c})}{\sqrt{j\rho c \ln(c)}} - I_1(\sqrt{j\rho c}) \right] K_1(\sqrt{j\rho a}) \right\}, \quad (\text{A1.32})$$

$$D_v = \text{Im} \left\{ \left[\frac{K_0(\sqrt{j\rho c})}{\sqrt{j\rho c \ln(c)}} + K_1(\sqrt{j\rho c}) \right] I_1(\sqrt{j\rho a}) + \left[\frac{I_0(\sqrt{j\rho c})}{\sqrt{j\rho c \ln(c)}} - I_1(\sqrt{j\rho c}) \right] K_1(\sqrt{j\rho a}) \right\}, \quad (\text{A1.33})$$

$$A_n(r) = -\text{Im} \left\{ K_{n-1}(\sqrt{j\rho c}) I_n(\sqrt{j\rho r}) + I_{n-1}(\sqrt{j\rho c}) K_n(\sqrt{j\rho r}) \right\} \text{ for } n \geq 1, \quad (\text{A1.34})$$

$$B_n(r) = \text{Re} \left\{ K_{n-1}(\sqrt{j\rho c}) I_n(\sqrt{j\rho r}) + I_{n-1}(\sqrt{j\rho c}) K_n(\sqrt{j\rho r}) \right\} \text{ for } n \geq 1, \quad (\text{A1.35})$$

$$D_w = \text{Re} \left\{ I_{n-1}(\sqrt{j\rho a}) K_n(\sqrt{j\rho c}) - K_{n-1}(\sqrt{j\rho a}) I_n(\sqrt{j\rho c}) \right\} \text{ for } n \geq 1, \quad (\text{A1.36})$$

$$\text{and } D_v = \text{Im} \left\{ I_{n-1}(\sqrt{j\rho a}) K_n(\sqrt{j\rho c}) - K_{n-1}(\sqrt{j\rho a}) I_n(\sqrt{j\rho c}) \right\} \text{ for } n \geq 1. \quad (\text{A1.37})$$

A_n , B_n , D_w and D_m are given explicitly in reference [9] by equations (34), (35), (36) and (37), respectively. Equation (A1.29) may be further rewritten as

$$J(r, \phi) = \frac{pl}{2\sqrt{2}\pi a} \left(\frac{[\bar{A}_0 + j\bar{B}_0]}{|D_0|^2} \right) + \frac{pl}{\sqrt{2}\pi a} \sum_{n=1}^{\infty} \left(\frac{[A_n + jB_n]}{|D_n|^2} \right) \left(\frac{b}{a} \right)^n \cos(n\phi), \quad (\text{A1.38})$$

where

$$\bar{A}_0 = (D_w [A_0(r) + B_0(r)] - D_m [A_0(r) - B_0(r)]), \quad (\text{A1.39})$$

$$\bar{B}_0 = (-D_w [A_0(r) - B_0(r)] - D_m [A_0(r) + B_0(r)]), \quad (\text{A1.40})$$

$$|D_0|^2 = D_w^2 + D_m^2, \quad (\text{A1.41})$$

$$\bar{A}_n = (D_w [A_n(r) + B_n(r)] - D_m [A_n(r) - B_n(r)]), \quad (\text{A1.42})$$

$$\bar{B}_n = (-D_w [A_n(r) - B_n(r)] - D_m [A_n(r) + B_n(r)]), \quad (\text{A1.43})$$

and

$$|D_n|^2 = D_w^2 + D_m^2. \quad (\text{A1.44})$$

Equation (A1.38) allows for $J(r, \phi)$ to be easily separated into real and imaginary parts since \bar{A}_0 , \bar{B}_0 , \bar{A}_n and \bar{B}_n are all real.

The derivation of the formula for eddy current loss, I , begins with the integral from Poynting's theorem, given by equation (73) in reference [9]. Substituting (A1.38) into equation (73) yields

$$\begin{aligned}
 I &= \int_0^{2\pi} \int_0^1 |J(r, \phi)|^2 r dr d\phi \\
 &= \int_0^{2\pi} \int_0^1 \left| \frac{pl}{2\sqrt{2\pi a}} \left(\frac{\bar{A}_0(r) + j\bar{B}_0(r)}{|D_0|^2} \right) + \frac{pl}{\sqrt{2\pi a}} \sum_{n=1}^{\infty} \frac{1}{|D_n|^2} \left(\frac{b}{a} \right)^n [\bar{A}_n(r) + j\bar{B}_n(r)] \cos(n\phi) \right|^2 r dr d\phi \\
 &= \frac{1}{\pi} \left| \frac{pl}{\sqrt{2\pi a}} \right|^2 \int_0^{2\pi} \int_0^1 \left| \frac{1}{2} \left(\frac{\bar{A}_0(r) + j\bar{B}_0(r)}{|D_0|^2} \right) + \sum_{n=1}^{\infty} \frac{1}{|D_n|^2} \left(\frac{b}{a} \right)^n [\bar{A}_n(r) + j\bar{B}_n(r)] \cos(n\phi) \right|^2 r dr d\phi \\
 &= \frac{1}{\pi} \left| \frac{pl}{\sqrt{2\pi a}} \right|^2 \int_0^{2\pi} \int_0^1 \left[\left(\frac{1}{2} \frac{\bar{A}_0(r)}{|D_0|^2} + \sum_{n=1}^{\infty} \frac{1}{|D_n|^2} \left(\frac{b}{a} \right)^n \bar{A}_n(r) \cos(n\phi) \right)^2 + \right. \\
 &\quad \left. \left(\frac{1}{2} \frac{\bar{B}_0(r)}{|D_0|^2} + \sum_{n=1}^{\infty} \frac{1}{|D_n|^2} \left(\frac{b}{a} \right)^n \bar{B}_n(r) \cos(n\phi) \right)^2 \right] r dr d\phi \\
 &= \frac{1}{\pi} \left| \frac{pl}{\sqrt{2\pi a}} \right|^2 \int_0^{2\pi} \int_0^1 \left[\left(\frac{1}{4} \frac{[\bar{A}_0(r)]^2}{|D_0|^4} + \frac{\bar{A}_0(r)}{|D_0|^2} \sum_{n=1}^{\infty} \frac{1}{|D_n|^2} \left(\frac{b}{a} \right)^n \bar{A}_n(r) \cos(n\phi) + \left[\sum_{n=1}^{\infty} \frac{1}{|D_n|^2} \left(\frac{b}{a} \right)^n \bar{A}_n(r) \cos(n\phi) \right]^2 \right) + \right. \\
 &\quad \left. \left(\frac{1}{4} \frac{[\bar{B}_0(r)]^2}{|D_0|^4} + \frac{\bar{B}_0(r)}{|D_0|^2} \sum_{n=1}^{\infty} \frac{1}{|D_n|^2} \left(\frac{b}{a} \right)^n \bar{B}_n(r) \cos(n\phi) + \left[\sum_{n=1}^{\infty} \frac{1}{|D_n|^2} \left(\frac{b}{a} \right)^n \bar{B}_n(r) \cos(n\phi) \right]^2 \right) \right] r dr d\phi
 \end{aligned} \tag{A1.45}$$

Integrating (A1.45) with respect to ϕ from 0 to 2π yields

$$\begin{aligned}
 I &= \frac{1}{\pi} \left| \frac{pl}{\sqrt{2\pi a}} \right|^2 \int_0^1 \left[\frac{\pi [\bar{A}_0(r)]^2}{2 |D_0|^4} + \int_0^{2\pi} \left[\sum_{n=1}^{\infty} \sum_{m=1}^{\infty} \frac{1}{|D_n|^2 |D_m|^2} \left(\frac{b}{a} \right)^n \left(\frac{b}{a} \right)^m \bar{A}_n(r) \bar{A}_m(r) \cos(n\phi) \cos(m\phi) \right] d\phi + \right. \\
 &\quad \left. \frac{\pi [\bar{B}_0(r)]^2}{2 |D_0|^4} + \int_0^{2\pi} \left[\sum_{n=1}^{\infty} \sum_{m=1}^{\infty} \frac{1}{|D_n|^2 |D_m|^2} \left(\frac{b}{a} \right)^n \left(\frac{b}{a} \right)^m \bar{B}_n(r) \bar{B}_m(r) \cos(n\phi) \cos(m\phi) \right] d\phi \right] r dr \\
 &= \frac{1}{\pi} \left| \frac{pl}{\sqrt{2\pi a}} \right|^2 \int_0^1 \left[\frac{\pi [\bar{A}_0(r)]^2}{2 |D_0|^4} + \pi \sum_{n=1}^{\infty} \frac{1}{|D_n|^4} \left(\frac{b}{a} \right)^{2n} [\bar{A}_n(r)]^2 + \frac{\pi [\bar{B}_0(r)]^2}{2 |D_0|^4} + \pi \sum_{n=1}^{\infty} \frac{1}{|D_n|^4} \left(\frac{b}{a} \right)^{2n} [\bar{B}_n(r)]^2 \right] r dr \\
 &= \frac{1}{\pi} \left| \frac{pl}{\sqrt{2\pi a}} \right|^2 \int_0^1 \left[\frac{\pi [\bar{A}_0(r)]^2 + [\bar{B}_0(r)]^2}{2 |D_0|^4} + \pi \sum_{n=1}^{\infty} \frac{[\bar{A}_n(r)]^2 + [\bar{B}_n(r)]^2}{|D_n|^4} \left(\frac{b}{a} \right)^{2n} \right] r dr
 \end{aligned} \tag{A1.46}$$

From (A1.39), (A1.40) and (A1.41) it may be shown that

$$\begin{aligned}\bar{A}_0(r)^2 + \bar{B}_0(r)^2 &= (D_{0r}^2 + D_{0z}^2) [2A_0^2 + 2B_0^2] \\ &= 2(D_{0r}^2 + D_{0z}^2) [A_0^2 + B_0^2].\end{aligned}\quad (\text{A1.47a})$$

Similarly, from (A1.42), (A1.43) and (A1.44) it may be shown that

$$\begin{aligned}\bar{A}_n(r)^2 + \bar{B}_n(r)^2 &= (D_{nr}^2 + D_{nz}^2) [2A_n^2 + 2B_n^2] \\ &= 2(D_{nr}^2 + D_{nz}^2) [A_n^2 + B_n^2], \quad \text{for } n \geq 1\end{aligned}\quad (\text{A1.47b})$$

Therefore, substituting (A1.47a) and (A1.47b) into (A1.46) yields

$$\begin{aligned}L &= \frac{1}{\sigma} \left| \frac{pl}{\sqrt{2\pi a}} \right|^2 \int_a^b \left[\frac{\pi}{2} \frac{2(D_{0r}^2 + D_{0z}^2) [A_0^2(r) + B_0^2(r)]}{|D_0|^4} + \pi \sum_{n=1}^{\infty} \frac{2(D_{nr}^2 + D_{nz}^2) [A_n^2(r) + B_n^2(r)]}{|D_n|^4} \right] \left(\frac{b}{a} \right)^{2n} r dr \\ &= \frac{1}{\sigma} \left| \frac{pl}{\sqrt{2\pi a}} \right|^2 \int_a^b \left[\frac{\pi}{2} \frac{[A_0(r)^2 + B_0(r)^2]}{|D_0|^2} + \pi \sum_{n=1}^{\infty} \frac{[A_n(r)^2 + B_n(r)^2]}{|D_n|^2} \right] \left(\frac{b}{a} \right)^{2n} r dr.\end{aligned}\quad (\text{A1.48})$$

Rearranging (A1.48) somewhat yields:

$$L = \frac{1}{\sigma} \left(\frac{pl}{\pi a} \right)^2 \frac{\pi}{2} \frac{1}{|D_0|^2} \int_a^b [A_0(r)^2 + B_0(r)^2] r dr + \frac{1}{\sigma} \left(\frac{pl}{\pi a} \right)^2 \pi \sum_{n=1}^{\infty} \left(\frac{b}{a} \right)^{2n} \frac{1}{|D_n|^2} \int_a^b [A_n(r)^2 + B_n(r)^2] r dr.\quad (\text{A1.49})$$

The second term of (A1.49),

$$\frac{1}{\sigma} \left(\frac{pl}{\pi a} \right)^2 \pi \sum_{n=1}^{\infty} \left(\frac{b}{a} \right)^{2n} \frac{1}{|D_n|^2} \int_a^b [A_n(r)^2 + B_n(r)^2] r dr,$$

is correctly solved by Tegopoulos and Kriezis in reference [9], with aid from references [23] and [24]. The solution to the second term in (A1.49) is given by the $n > 1$ terms in equation (40) from reference [9].

To obtain a complete solution for the eddy current loss in the metal shell, one must also evaluate the integral $\int [A_0(r)^2 + H_0(r)^2] r dr$ in the first term of (A1.49). Substituting Kelvin functions for the modified Bessel functions in $A_0(r)$ and $B_0(r)$ (from equations (A1.30) from (A1.31), respectively) yields

$$A_0(r) = \left\{ \begin{aligned} & \left(\frac{\ker_0(\rho c) - \kei_0(\rho c)}{\sqrt{2\rho c \ln(c)}} - \ker_1(\rho c) \right) \text{ber}_0(\rho r) - \left(\frac{\ker_0(\rho c) + \kei_0(\rho c)}{\sqrt{2\rho c \ln(c)}} - \kei_1(\rho c) \right) \text{bei}_0(\rho r) + \\ & \left(\frac{\text{ber}_0(\rho c) - \text{bei}_0(\rho c)}{\sqrt{2\rho c \ln(c)}} - \text{ber}_1(\rho c) \right) \ker_0(\rho r) + \left(\frac{\text{ber}_0(\rho c) + \text{bei}_0(\rho c)}{\sqrt{2\rho c \ln(c)}} - \text{bei}_1(\rho c) \right) \kei_0(\rho r) \end{aligned} \right\} \quad (\text{A1.50})$$

$$H_0(r) = \left\{ \begin{aligned} & \left(\frac{\ker_0(\rho c) + \kei_0(\rho c)}{\sqrt{2\rho c \ln(c)}} - \kei_1(\rho c) \right) \text{ber}_0(\rho r) + \left(\frac{\ker_0(\rho c) - \kei_0(\rho c)}{\sqrt{2\rho c \ln(c)}} - \ker_1(\rho c) \right) \text{bei}_0(\rho r) + \\ & \left(\frac{\text{ber}_0(\rho c) + \text{bei}_0(\rho c)}{\sqrt{2\rho c \ln(c)}} - \text{bei}_1(\rho c) \right) \ker_0(\rho r) - \left(\frac{\text{ber}_0(\rho c) - \text{bei}_0(\rho c)}{\sqrt{2\rho c \ln(c)}} - \text{ber}_1(\rho c) \right) \kei_0(\rho r) \end{aligned} \right\} \quad (\text{A1.51})$$

Substituting (A1.50) and (A1.51) into the integral in the first term of (A1.49) yields

$$\begin{aligned}
 \int_a^c [A_0^2(r) + B_0^2(r)] r dr &= \kappa_1 \int_a^c [\text{ber}_0^2(\rho r) + \text{bei}_0^2(\rho r)] r dr + \\
 &\quad \kappa_2 \int_a^c [\text{ker}_0^2(\rho r) + \text{kei}_0^2(\rho r)] r dr + \\
 &\quad \kappa_3 \int_a^c [\text{ber}_0(\rho r) \text{ker}_0(\rho r) + \text{bei}_0(\rho r) \text{kei}_0(\rho r)] r dr + \\
 &\quad \kappa_4 \int_a^c [\text{bei}_0(\rho r) \text{ker}_0(\rho r) - \text{ber}_0(\rho r) \text{kei}_0(\rho r)] r dr, \quad (\text{A1.52})
 \end{aligned}$$

where

$$\begin{aligned}
 \kappa_1 &= \left[\left(\frac{\text{ker}_0(\rho c) - \text{kei}_0(\rho c)}{\sqrt{2\rho c \ln(c)}} - \text{ker}_1(\rho c) \right)^2 + \left(\frac{\text{ker}_0(\rho c) + \text{kei}_0(\rho c)}{\sqrt{2\rho c \ln(c)}} - \text{kei}_1(\rho c) \right)^2 \right] \\
 \kappa_2 &= \left[\left(\frac{\text{ber}_0(\rho c) - \text{bei}_0(\rho c)}{\sqrt{2\rho c \ln(c)}} - \text{ber}_1(\rho c) \right)^2 + \left(\frac{\text{ber}_0(\rho c) + \text{bei}_0(\rho c)}{\sqrt{2\rho c \ln(c)}} - \text{bei}_1(\rho c) \right)^2 \right] \\
 \kappa_3 &= -2 \left[\left(\frac{\text{ker}_0(\rho c) - \text{kei}_0(\rho c)}{\sqrt{2\rho c \ln(c)}} - \text{ker}_1(\rho c) \right) \left(\frac{\text{ber}_0(\rho c) - \text{bei}_0(\rho c)}{\sqrt{2\rho c \ln(c)}} - \text{ber}_1(\rho c) \right) + \right. \\
 &\quad \left. \left(\frac{\text{ker}_0(\rho c) + \text{kei}_0(\rho c)}{\sqrt{2\rho c \ln(c)}} - \text{kei}_1(\rho c) \right) \left(\frac{\text{ber}_0(\rho c) + \text{bei}_0(\rho c)}{\sqrt{2\rho c \ln(c)}} - \text{bei}_1(\rho c) \right) \right] \\
 \kappa_4 &= 2 \left[\left(\frac{\text{ker}_0(\rho c) + \text{kei}_0(\rho c)}{\sqrt{2\rho c \ln(c)}} - \text{kei}_1(\rho c) \right) \left(\frac{\text{ber}_0(\rho c) - \text{bei}_0(\rho c)}{\sqrt{2\rho c \ln(c)}} - \text{ber}_1(\rho c) \right) \right. \\
 &\quad \left. \left(\frac{\text{ker}_0(\rho c) - \text{kei}_0(\rho c)}{\sqrt{2\rho c \ln(c)}} - \text{ker}_1(\rho c) \right) \left(\frac{\text{ber}_0(\rho c) + \text{bei}_0(\rho c)}{\sqrt{2\rho c \ln(c)}} - \text{bei}_1(\rho c) \right) \right] \quad (\text{A1.53})
 \end{aligned}$$

Evaluating the integral in (A1.52) with the aid of references [23] and [24] yields

$$\begin{aligned}
 \int_a^c [A_n^2(r) + B_n^2(r)] r dr = & \kappa_1 \left[\frac{c}{p} T_{10}(pc) - \frac{a}{p} T_{10}(pa) \right] + \\
 & \kappa_2 \left[\frac{c}{p} T_{20}(pc) - \frac{a}{p} T_{20}(pa) \right] + \\
 & \kappa_3 \left[\frac{c}{2p} T_{30}(pc) - \frac{a}{2p} T_{30}(pa) \right] + \\
 & \kappa_4 \left[\frac{c}{2p} T_{40}(pc) - \frac{a}{2p} T_{40}(pa) \right], \quad (\text{A1.54})
 \end{aligned}$$

where

$$\begin{aligned}
 T_{10}(pr) &= [\text{ber}(pr) \text{bei}'(pr) - \text{bei}(pr) \text{ber}'(pr)] \\
 T_{20}(pr) &= [\text{ker}(pr) \text{kei}'(pr) - \text{kei}(pr) \text{ker}'(pr)] \\
 T_{30}(pr) &= \text{ker}(pr) \text{bei}'(pr) - \text{ker}'(pr) \text{bei}(pr) + \text{ber}(pr) \text{kei}'(pr) - \text{ber}'(pr) \text{kei}(pr) \\
 T_{40}(pr) &= \text{ker}'(pr) \text{ber}(pr) - \text{ker}(pr) \text{ber}'(pr) + \text{kei}'(pr) \text{bei}(pr) - \text{kei}(pr) \text{bei}'(pr).
 \end{aligned} \quad (\text{A1.55})$$

Therefore, the final solution for the eddy current loss in the metal shell (i.e., the explicit solution to equation (A1.49)) is

$$\begin{aligned}
 L = & \frac{1}{\sigma} \left(\frac{pl}{\pi a} \right)^2 \frac{\pi}{2} \frac{1}{|D_0|^2} \frac{1}{p} \left(\kappa_1 [cT_{10}(pr) - aT_{10}(prt)] + \right. \\
 & \kappa_2 [cT_{20}(pr) - aT_{20}(prt)] + \\
 & \frac{\kappa_3}{2} [cT_{30}(pr) - aT_{30}(prt)] + \\
 & \left. \frac{\kappa_4}{2} [cT_{40}(pr) - aT_{40}(prt)] \right) + \\
 & \frac{1}{\sigma} \frac{pl^2}{\pi a^2} \sum_{n=1}^{\infty} \left(\frac{b}{a} \right)^{2n} \frac{1}{|D_n|^2} \left(N_{n-1}(pr)^2 [cT_{1n}(pr) - aT_{1n}(prt)] + \right. \\
 & M_{n-1}(pr)^2 [cT_{2n}(pr) - aT_{2n}(prt)] \\
 & \Lambda_{n-1}(pr) [cT_{3n}(pr) - aT_{3n}(prt)] \\
 & \left. \Pi_{n-1}(pr) [cT_{4n}(pr) - aT_{4n}(prt)] \right), \quad (\text{A1.56})
 \end{aligned}$$

where

$|D_0|^2$ is given by (A1.32), (A1.33) and (A1.41),

κ_1 , κ_2 , κ_3 and κ_4 are given by (A1.53),

$T_{10}(pr)$, $T_{20}(pr)$, $T_{30}(pr)$ and $T_{40}(pr)$ are given by (A1.55),

D_n is given by (A1.25),

$|D_n|^2$ is given by equations (31), (36) and (37) from reference [9],

$N_n(pr)$ and $M_n(pr)$ are given by equations (40) and (64) from reference [8],

$\Lambda_n(pr)$ and $\Pi_n(pr)$ are given by equations (45) and (46) from reference [9],

and $T_{1n}(pr)$, $T_{2n}(pr)$, $T_{3n}(pr)$ and $T_{4n}(pr)$ are given by equations (41) through (44) from reference [9].

APPENDIX 2

A Limitation of the Eddy Current Loss Formula of Kawasaki, Inami and Ishikawa

The formula given by equation (7) in reference [10] is Kawasaki's, Inami's and Ishikawa's precise formula for eddy current loss in a metal pipe. This formula is supposedly valid for any multi-phase system of current filaments inside the pipe. However, upon closer examination of the derivation of equation (7), it appears the formula is only correct if the currents in the interior of the pipe sum to zero.

Kawasaki et al. begin the derivation of their loss formula with an expression for the current density induced in a metal pipe by a single current filament

$$J(r, \phi) = \sum_{n=1}^{\infty} \left[H_n I_n(\sqrt{j\rho r}) + D_n K_n(\sqrt{j\rho r}) \right] I\left(\frac{b}{a}\right)^n \cos(n\phi),$$

this is equation (1) of reference [10].

The problem in the derivation of the loss formula is best illustrated by considering an azimuthally symmetric problem (i.e., a problem where only a single current filament at the center of the pipe is present). In this case $b = 0$ and consequently the Kawasaki et al. expression for current density, equation (1), reduces to

$$J(r, \phi) = 0. \quad (\text{A2.1})$$

Thus the current density is identically zero *everywhere* in the metal pipe. If equation (1) is compared to the revised Viegopoulos and Kriezis solution for current density (equation (A1.24) in appendix 1), it is apparent that equation (1) lacks an $n = 0$ term. This is the reason that, for an azimuthally symmetric problem, $J(r, \phi) = 0$ in equation (1) and $J(r, \phi) \neq 0$ in equation (A1.24).

No definite explanation is given by Kawasaki et al. for the exclusion of the $n = 0$ term from equation (1). However, it can be inferred that the $n = 0$ term was excluded because Kawasaki et al. presumed the path of the return current to be entirely separate from the pipe. In sections 3.3 and A1.4, it was demonstrated that the $n = 0$ term in a current density solution represents a *portion* of the return current, but not the total return current. In fact, for a two dimensional boundary value problem, the path of the return current is dictated by the tangential boundary conditions on the electric and magnetic fields; *the path*

of the return current cannot be arbitrarily specified if the tangential boundary conditions are to be satisfied. Thus Kawasaki et al. cannot arbitrarily specify the return current to be separate from the pipe, nor can they simply omit the $n = 0$ term from their current density expression. In general, an $n = 0$ term representing the return current should be included in equation (1).

There is, however, one situation where the $n = 0$ term in the current density solution can be legitimately omitted. This situation arises when a *balanced*, multi-phased system of current filaments is present inside the pipe. For problems where multiple current filaments are present, the eddy current density in the pipe is found by superimposing the effects of each individual current filament. *If the filaments inside the pipe carry a balanced current (i.e., the currents sum to zero), then the $n = 0$ terms from all the single filament solutions sum to zero when they are superimposed. Thus, the $n = 0$ term in the net current density solution is identically zero everywhere in the pipe material.*

Equation (4) in reference [10] is the solution for net current density when an arbitrary number of filaments are situated in the pipe. Equation (4) was derived by superimposing the current density solutions of individual filaments in the pipe. The current density solution for an individual filament is given by equation (1). Since equation (1) does not contain an $n = 0$ term, neither does equation (4). However, equation (1) should include an $n = 0$ term and consequently so should equation (4).

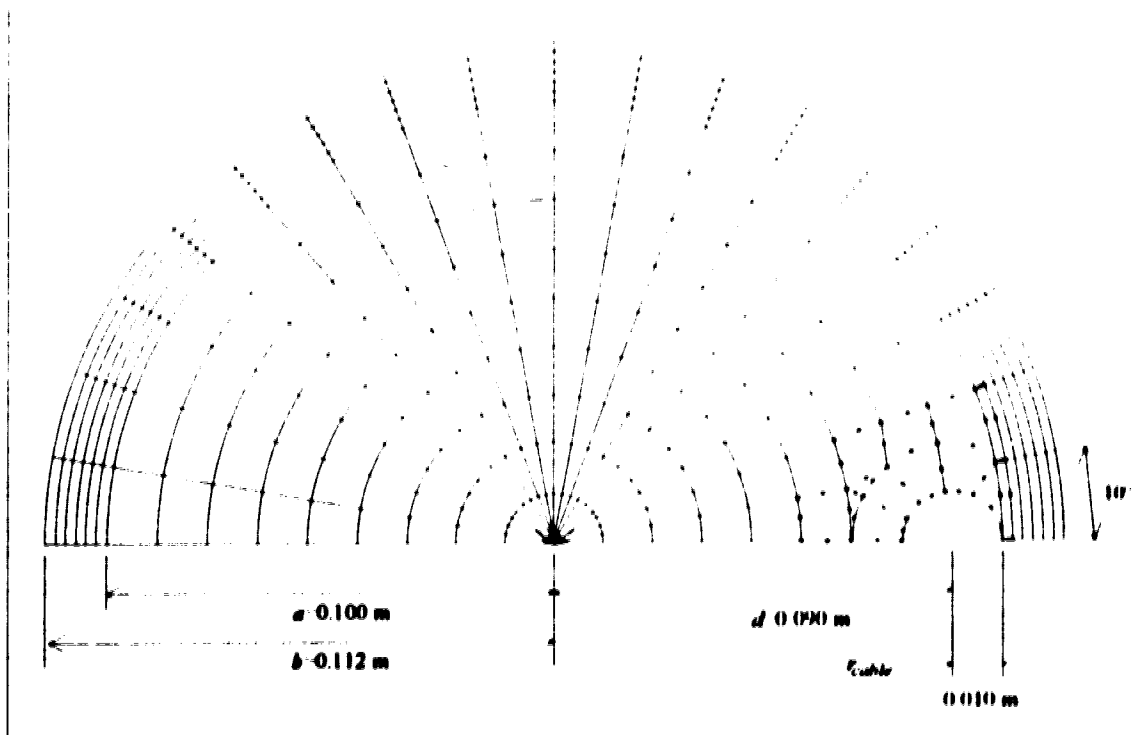
Once again, the one instance where an $n = 0$ term need not be present in equation (4) is if the filaments inside the pipe carry a balanced current. In this case equation (4) is correct as written because the $n = 0$ term (if it was present) would be identically zero; the absence of the $n = 0$ terms in the individual filament solutions makes no difference since they would sum to zero when superimposed.

Equation (7) in reference [10] is a formula for eddy current loss in a metal pipe. Equation (7) was derived directly from equation (4). Since equation (4) is only correct when the filaments inside the pipe carry a balanced current, it follows that equation (7) is also correct only when the current inside the pipe is balanced.

APPENDIX 3

The meshes used to model the domain of problem 2 for various casing samples are presented in this section.

Figure A3-1 The mesh used to model the domain of problem 2 with casing sample 1. Note that the diagram is not to scale.



The mesh shown in Figure A3-1 is constructed differently from all others in this thesis. For this first problem, the mesh design process was at a somewhat experimental stage. Each element is either a six node triangular or an eight node quadrilateral element. A more efficient, less time consuming method of mesh design was developed for later problems. Meshes for these later problems are composed of simple, four node quadrilateral elements. An example of these meshes are those depicted in Figures A3-2 and A3-3.

In spite of the large aspect ratios of some of the elements in Figures A3-2 and A3-3, this type of mesh design does not appear to adversely affect the accuracy of the FEM solutions for these two problems. FEM solutions obtained using these meshes compare favorably with corresponding analytic solutions (refer to sections 5.5.2 and 5.5.3 for details).

Figure A3-2 The mesh used to model the domain of problem 2 with casing sample 2. Note that the diagram is not to scale.

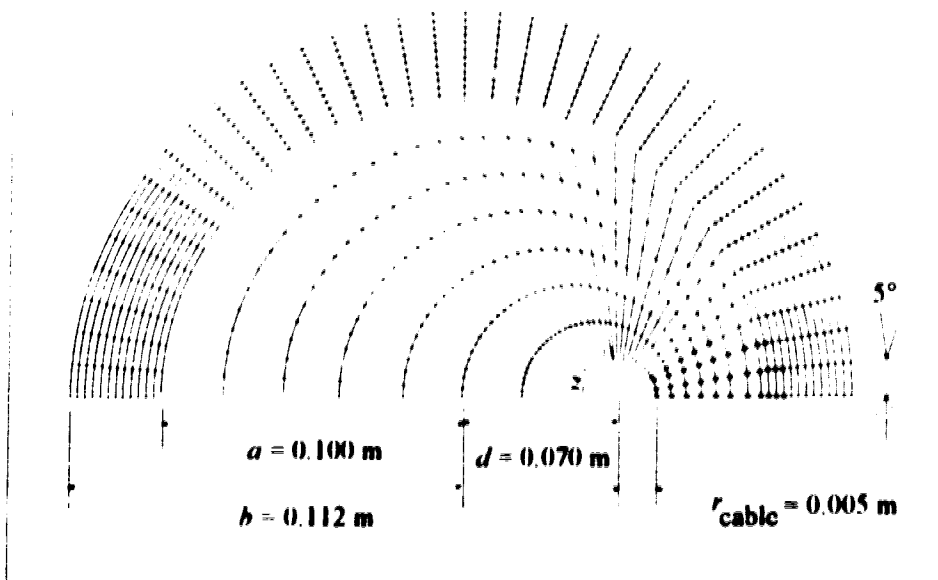
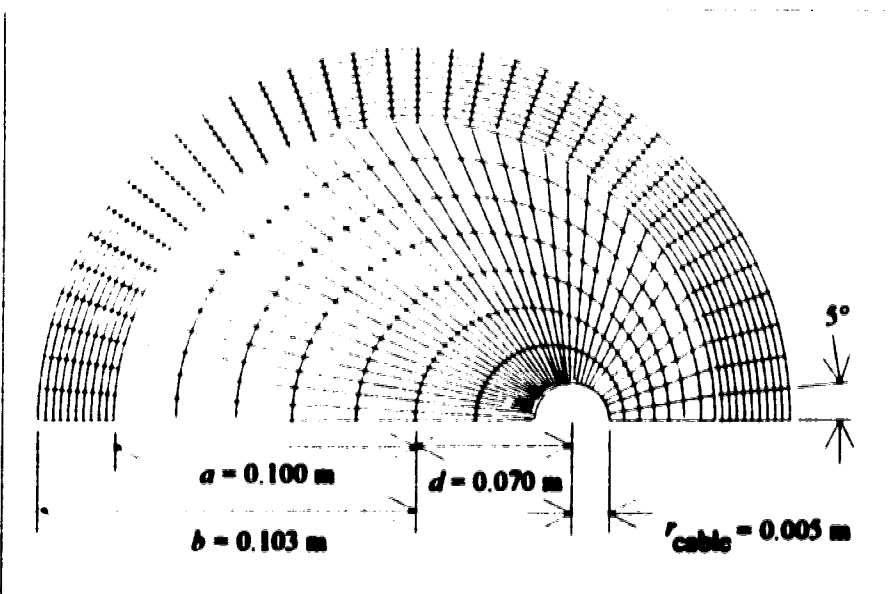


Figure A3-3 The mesh used to model the domain of problem 2 with casing sample 3. Note that the diagram is not to scale.



APPENDIX 4

The General Solutions for $E_z(\rho, \theta)$, $H_\rho(\rho, \theta)$ and $H_\theta(\rho, \theta)$ in Region 2 of Problem 2

For problem 2, the general solutions for $E_z(\rho, \theta)$, $H_\rho(\rho, \theta)$ and $H_\theta(\rho, \theta)$ in region 2 consist of an infinite series of spatial harmonics with respect to the θ coordinate. The general solutions are derived as follows.

The general solution for the electric field partial differential equation in (5.1) is

$$E_{z_2}(\rho, \theta) = \sum_{n=0}^{\infty} (A_n H_n^{(2)}(k_2 \rho) + B_n H_n^{(1)}(k_2 \rho)) (C_n \cos(n\theta) + D_n \sin(n\theta)), \quad (\text{A4.1})$$

where A_n , B_n , C_n and D_n are unknown constants. Note that the azimuthal eigenfunctions in (A4.1) satisfy the obvious boundary condition $E_z(\rho, \theta) = E_z(\rho, \theta + 2\pi)$.

The expression in (A4.1) may be further simplified by invoking the fact that problem 2 has even symmetry with respect to θ . Therefore $E_z(\rho, \theta) = E_z(\rho, -\theta)$. The general solution for the electric field in region 2 may then be written as

$$E_{z_2}(\rho, \theta) = \sum_{n=0}^{\infty} (A_n H_n^{(2)}(k_2 \rho) + B_n H_n^{(1)}(k_2 \rho)) \cos(n\theta). \quad (\text{A4.2})$$

The relationship between the electric and magnetic field components in problem 2 is as follows.

From Maxwell's equations,

$$\nabla \times \vec{E}_2 = -j\omega\mu_2 \vec{H}_2. \quad (\text{A4.3})$$

Given that there exists only a z component of the electric field, (A4.3) may be reduced to

$$\hat{a}_\rho \left(\frac{1}{\rho} \frac{\partial E_{z_2}}{\partial \theta} \right) + \hat{a}_\theta \left(\frac{\partial E_{z_2}}{\partial \rho} \right) = -j\omega\mu_2 \vec{H}_2. \quad (\text{A4.4})$$

From (A4.4) a scalar differential equation may be extracted from each of the field components

$$H_{\nu_2}(\rho, \theta) = \frac{-1}{j\omega\mu_2\rho} \frac{\partial E_{z_2}}{\partial \theta} \quad (\text{A4.5})$$

$$H_{0_2}(\rho, \theta) = \frac{1}{j\omega\mu_2} \frac{\partial E_{z_2}}{\partial \rho} \quad (\text{A4.6})$$

Equations (A4.5) and (A4.6) relate the components of the magnetic field to the electric field. Substituting the general solution for $E_{z_2}(\rho, \theta)$ from (A4.3) into (A4.5) and (A4.6) yields the general solutions for $H_{\nu_2}(\rho, \theta)$ and $H_{0_2}(\rho, \theta)$:

$$H_{\nu_2}(\rho, \theta) = \frac{1}{j\omega\mu_2\rho} \sum_{n=1}^{\infty} \left(A_n H_n^{(2)}(k_2\rho) + B_n H_n^{(1)}(k_2\rho) \right) n \sin(n\theta) \quad (\text{A4.7})$$

$$H_{0_2}(\rho, \theta) = \frac{1}{j\omega\mu_2} \sum_{n=0}^{\infty} \left(A_n \frac{\partial}{\partial \rho} H_n^{(2)}(k_2\rho) + B_n \frac{\partial}{\partial \rho} H_n^{(1)}(k_2\rho) \right) \cos(n\theta) \quad (\text{A4.8})$$

The Magnetic Shielding Ratios for Individual Spatial Harmonics of H_{ν_2} and H_{0_2}

For problem 2, a magnetic shielding ratio may be defined for individual spatial harmonics of the magnetic field in region 2. The magnetic shielding ratio for the n th harmonic of $H_{\nu_2}(\rho, \theta)$ in (A4.7) is defined as follows:

$$\frac{H_{\nu_2}(a, \theta)_n}{H_{\nu_2}(b, \theta)_n} = \frac{1}{2} \frac{b\sqrt{b}}{a\sqrt{a}} \left\{ \frac{\eta_2}{Z_1^n(k, b)} \left(e^{\mu_2(b-a)} - e^{-\mu_2(b-a)} \right) + \left(e^{\mu_2(b-a)} + e^{-\mu_2(b-a)} \right) \right\}, \quad (\text{A4.9})$$

where

$$Z_1^n(k, b) = - \frac{H_n^{(2)}(k, b)}{j\omega\mu_1 \left[\frac{d}{d\rho} H_n^{(2)}(k, \rho) \right]_{\rho=b}}$$

Similarly, the magnetic shielding ratio for the n th harmonic of $H_{0_2}(\rho, \theta)$ in (A4.8) is defined as

$$\frac{H_{0_2}(a, \theta)_n}{H_{0_2}(b, \theta)_n} = \frac{1}{2} \frac{\sqrt{b}}{\sqrt{a}} \left\{ \frac{Z_1^n(k, b)}{\eta_2} \left(e^{\mu_2(b-a)} - e^{-\mu_2(b-a)} \right) + \left(e^{\mu_2(b-a)} + e^{-\mu_2(b-a)} \right) \right\}. \quad (\text{A4.10})$$

APPENDIX 5

The meshes used to model the domain of problems 3a, 3b and 3c for various casing samples are presented in the following figures.

Figure A5-1 The mesh used to model the domain of problem 3a with casing sample 1. Note that the diagram is not to scale.

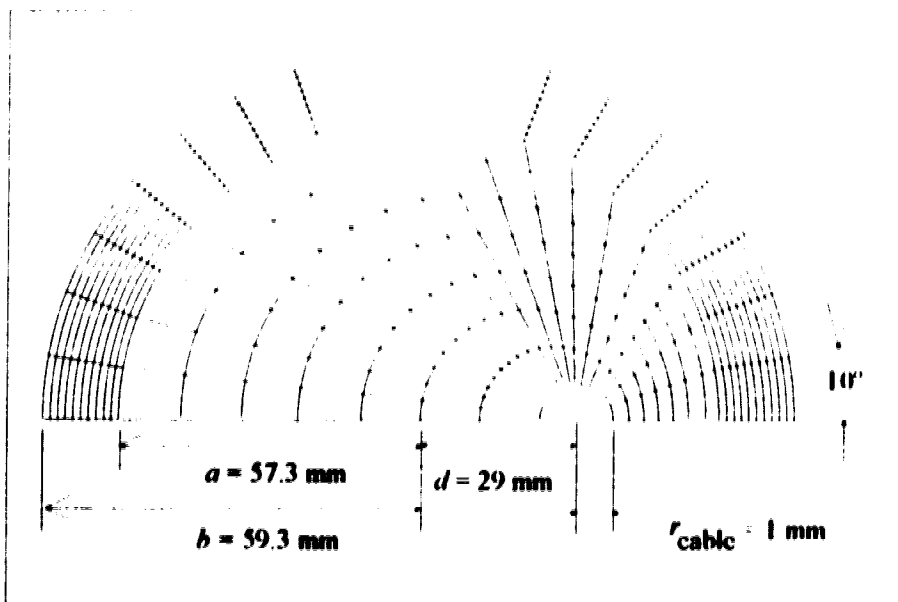


Figure A5-2 The mesh used to model the domain of problem 3a with casing sample 2. Note that the diagram is not to scale.

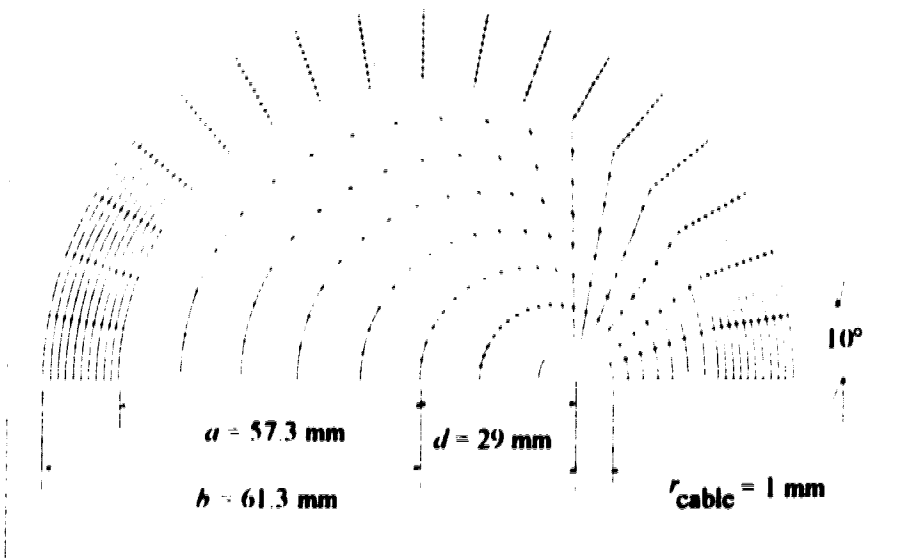


Figure A5-3 The mesh used to model the domain of problem 3a with casing sample 3. Note that the diagram is not to scale.

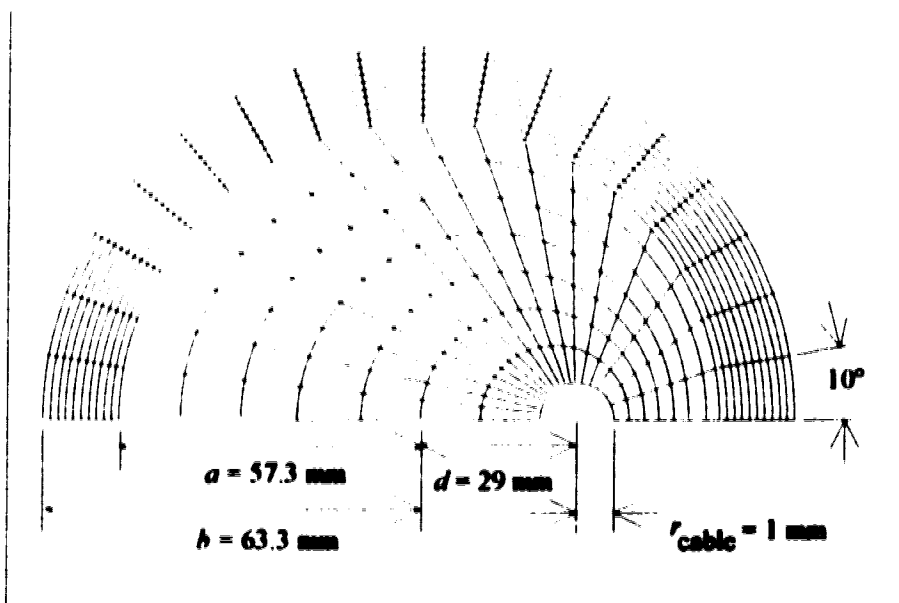


Figure A5-4 The mesh used to model the domain of problem 3a with casing sample 4
Note that the diagram is not to scale.

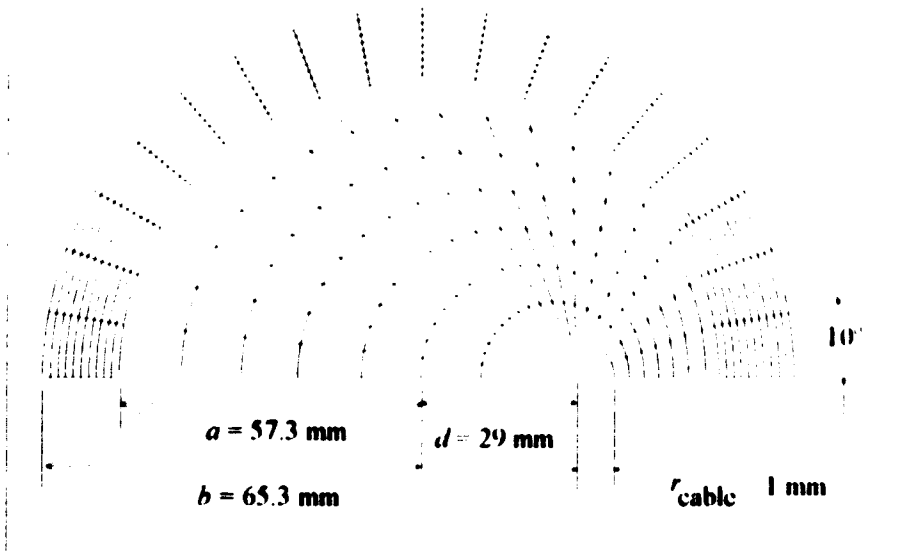


Figure A5-5 The mesh used to model the domain of problem 3a with casing sample 5
Note that the diagram is not to scale.

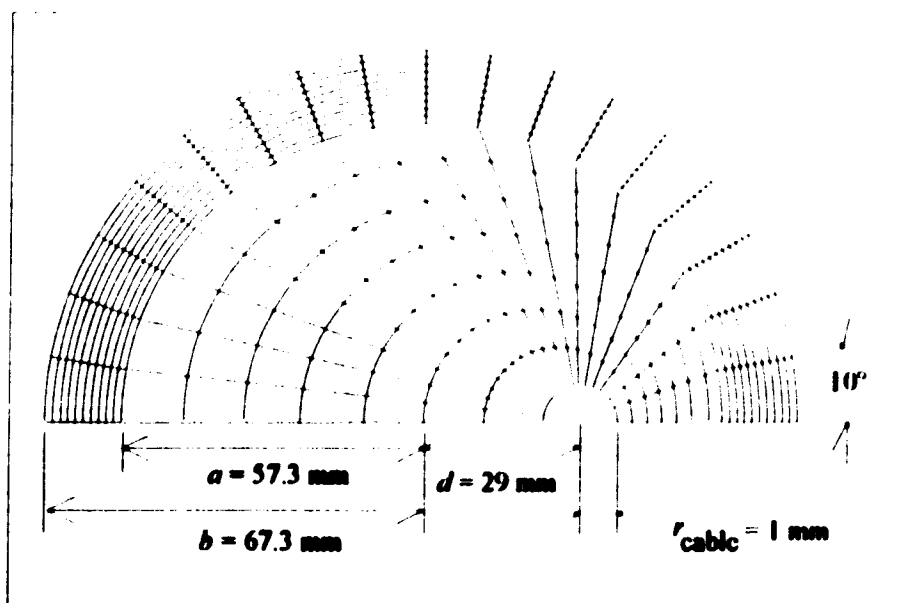


Figure A5-6 The mesh used to model the domain of problem 3a with casing sample 6. Note that the diagram is not to scale.

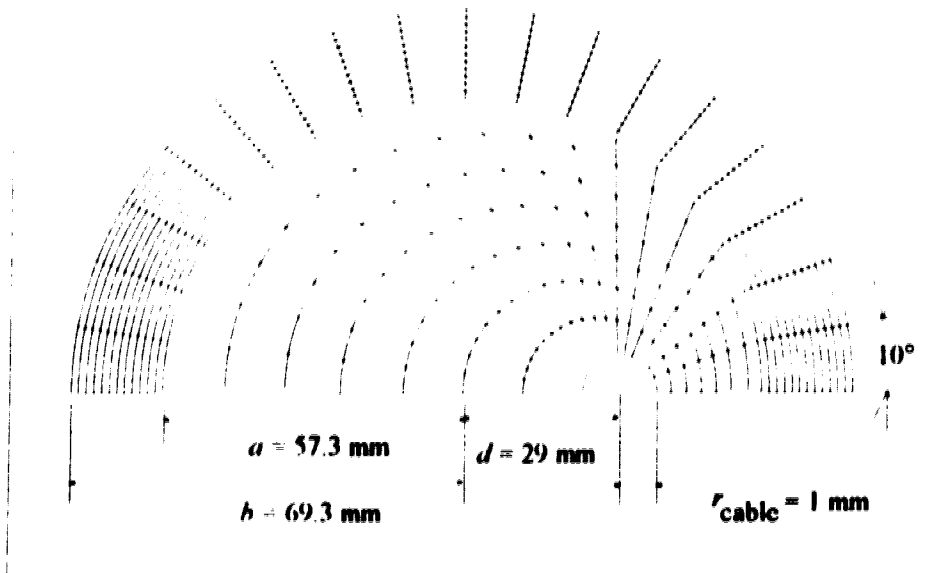


Figure A5-7 The mesh used to model the domain of problem 3a with casing sample 7. Note that the diagram is not to scale.

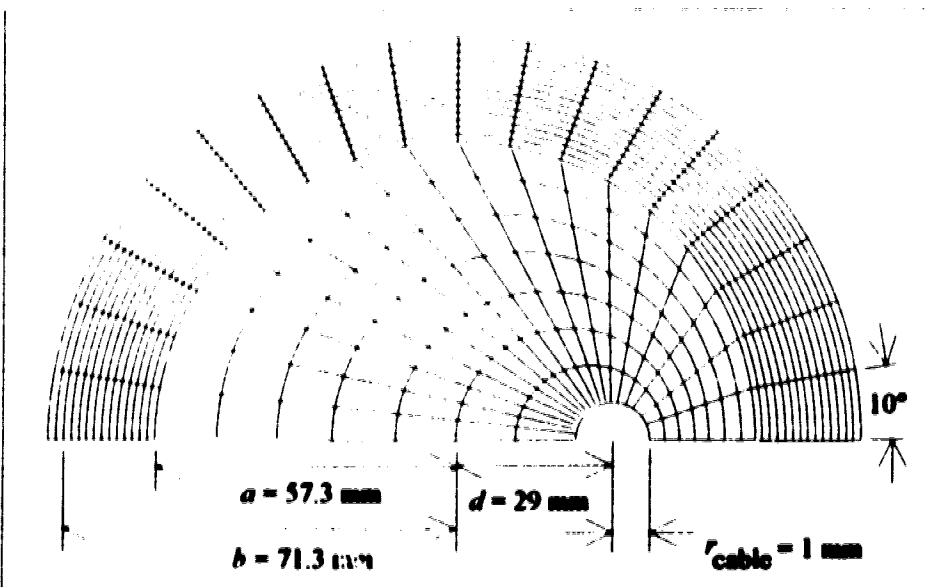


Figure A5-8 The mesh used to model the domain of problem 3b with casing sample 1
 Note that the diagram is not to scale.

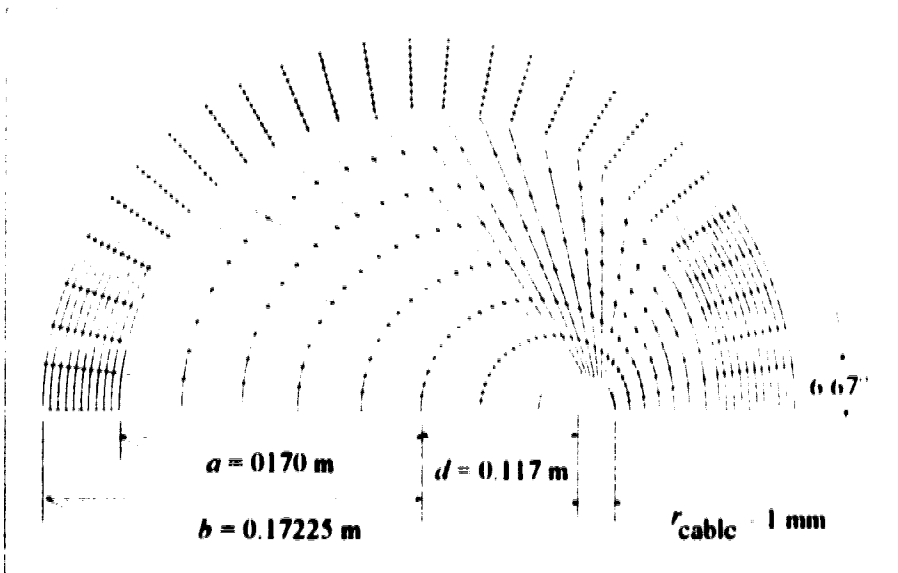


Figure A5-9 The mesh used to model the domain of problem 3b with casing sample 2
 Note that the diagram is not to scale.

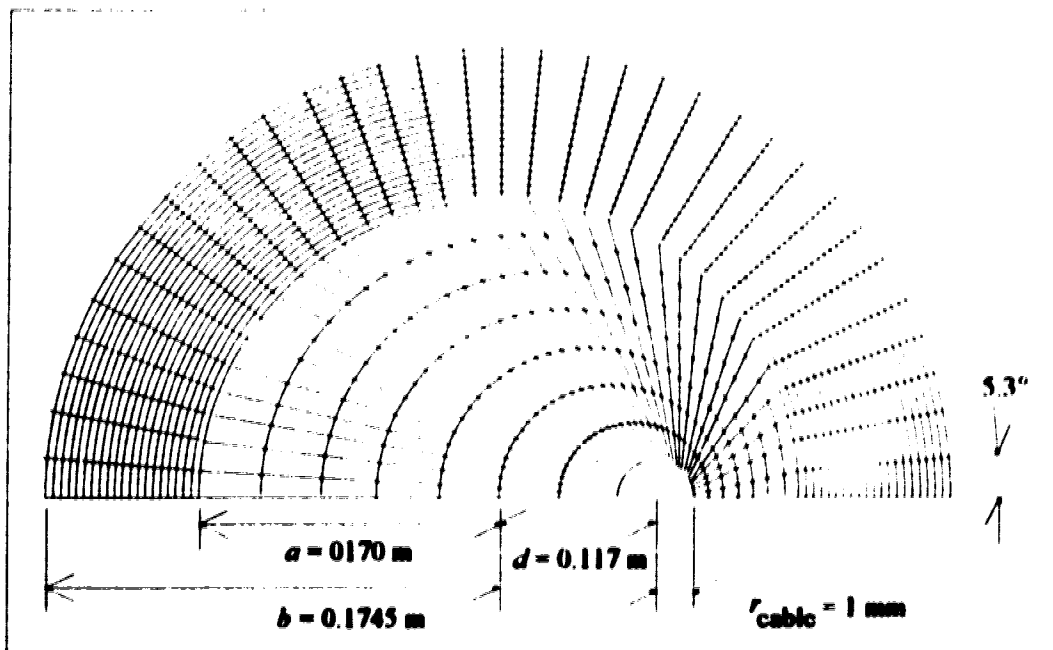


Figure A5-10 The mesh used to model the domain of problem 3b with casing sample 3. Note that the diagram is not to scale.

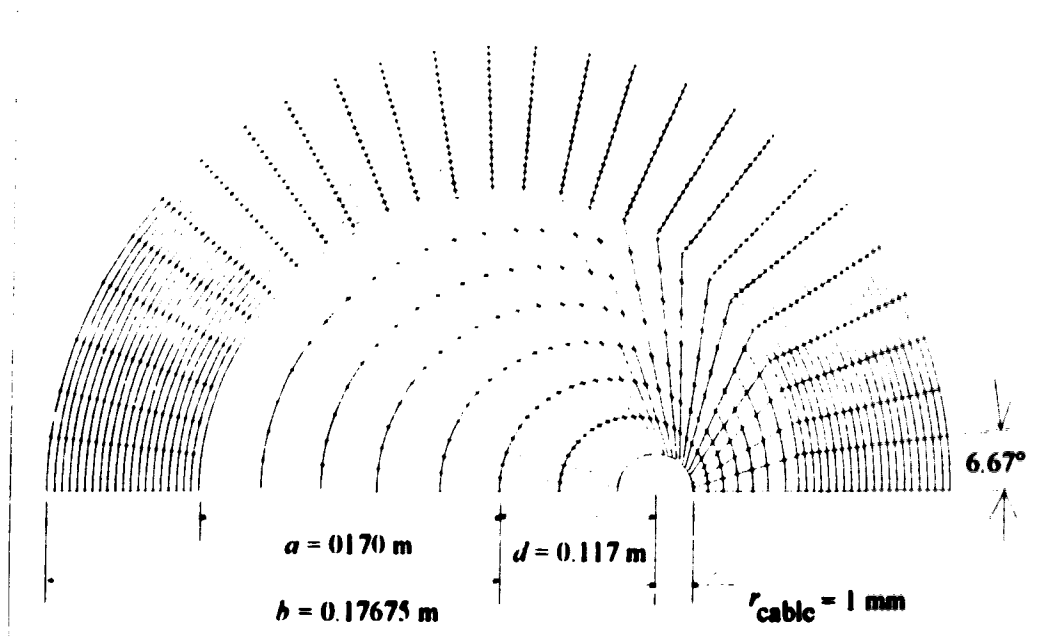


Figure A5-11 The mesh used to model the domain of problem 3b with casing sample 4. Note that the diagram is not to scale.

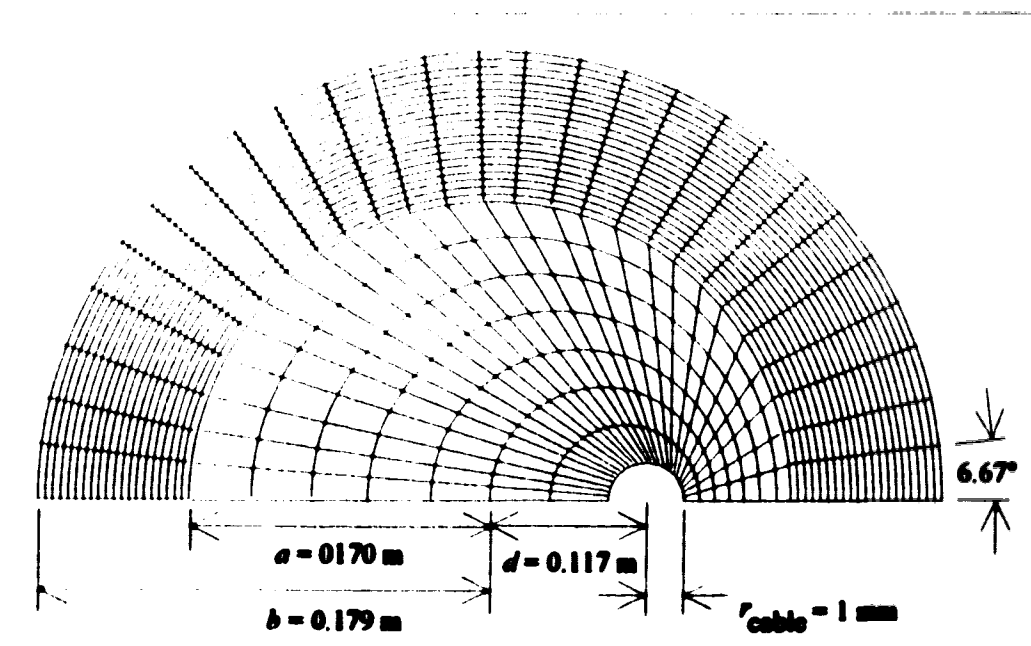


Figure A5-12 The mesh used to model the domain of problem 3b with casing sample 5
 Note that the diagram is not to scale.

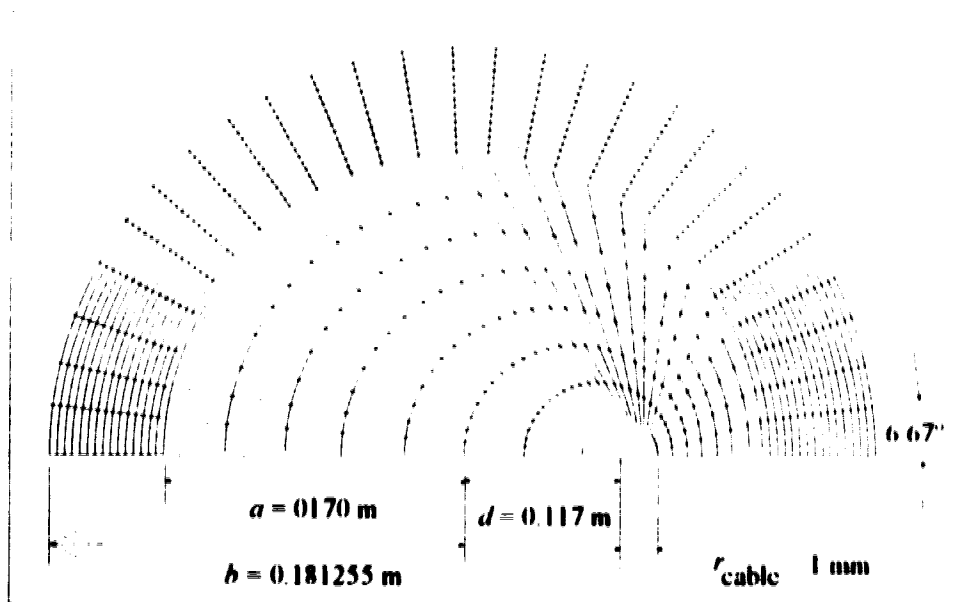


Figure A5-13 The mesh used to model the domain of problem 3c with casing sample 1
 Note that the diagram is not to scale.

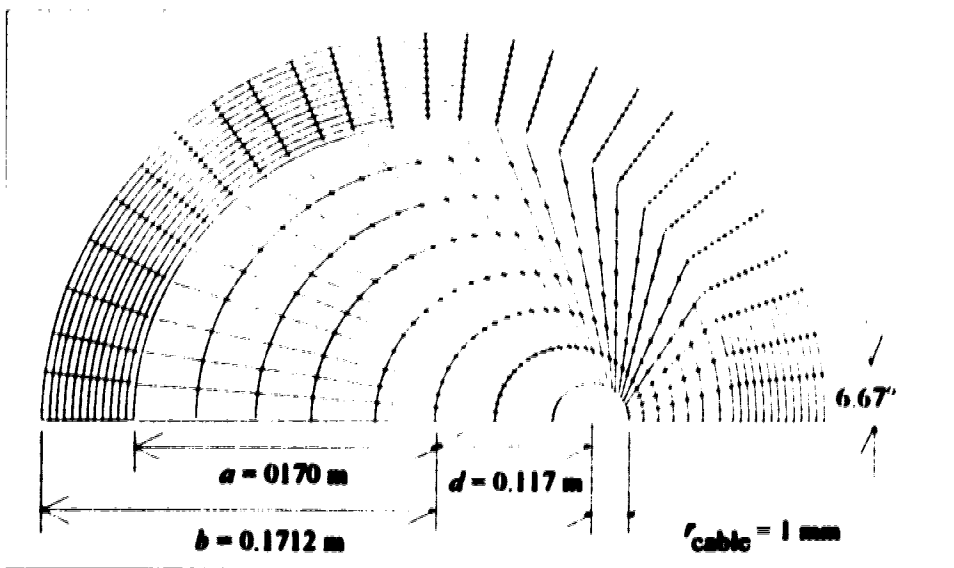


Figure A5-14 The mesh used to model the domain of problem 3c with casing sample 2. Note that the diagram is not to scale.

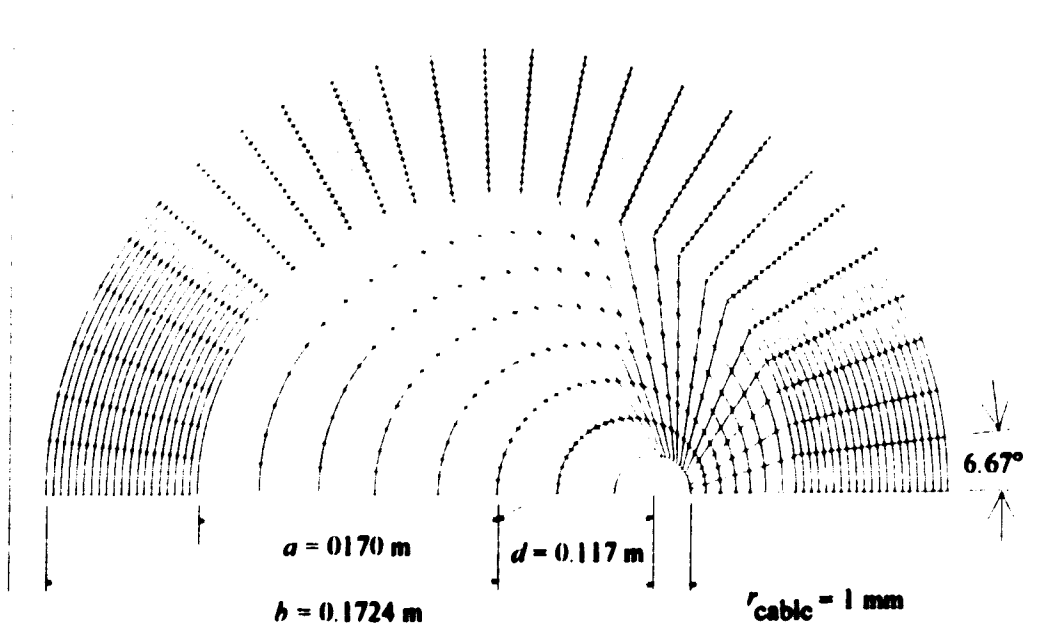


Figure A5-15 The mesh used to model the domain of problem 3c with casing sample 3. Note that the diagram is not to scale.

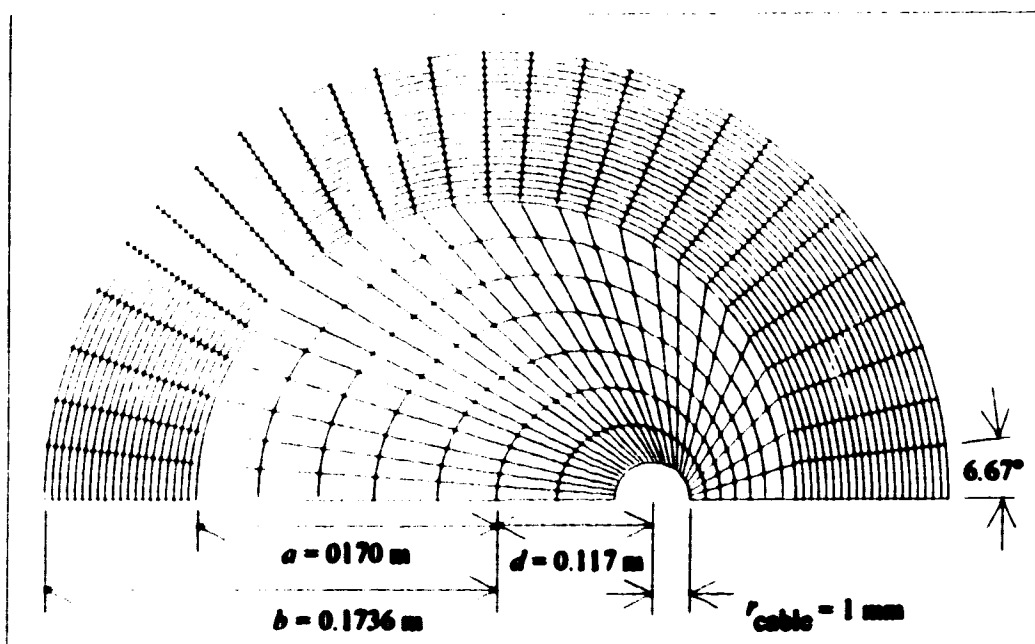


Figure A5-16 The mesh used to model the domain of problem 3c with casing sample 4
 Note that the diagram is not to scale.

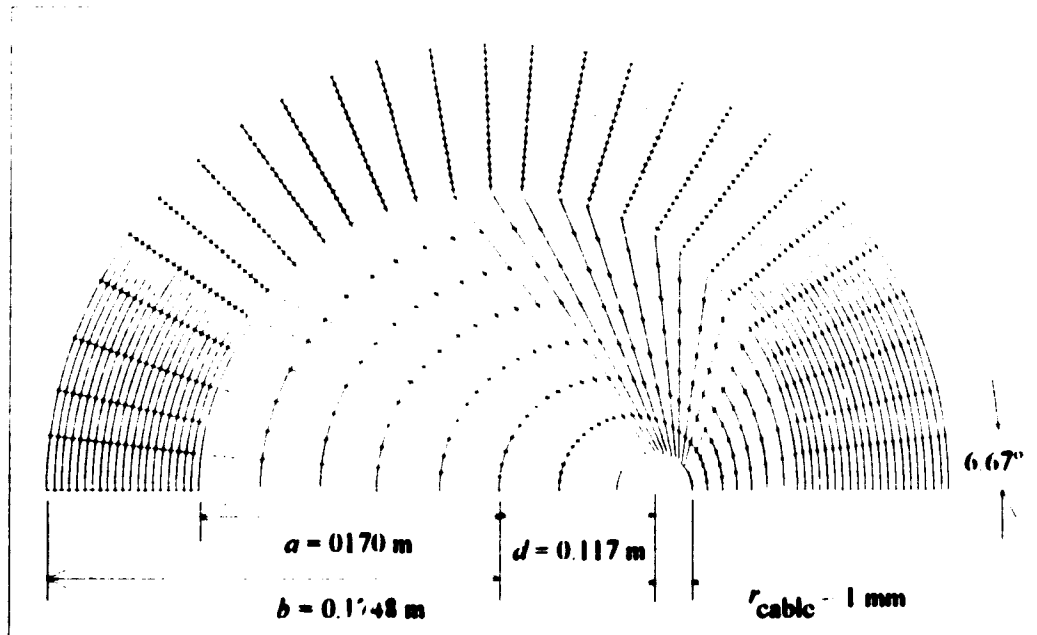


Figure A5-17 The mesh used to model the domain of problem 3c with casing sample 5.
 Note that the diagram is not to scale.

